

Aus dem
Helmholtz-Zentrum München
ABTEILUNG FÜR APOPTOSE IN HÄMATOPOIETISCHEN STAMMZELLEN



**Identifying WT1, DNMT3A and DDIT4L as dependency genes in PDX
models of acute leukemia in vivo**

Dissertation
zum Erwerb des Doctor of Philosophy (Ph.D.) an der Medizinischen Fakultät der
Ludwig-Maximilians-Universität München

vorgelegt von
Yuqiao Gao

aus
Heilongjiang / China

Jahr
2024

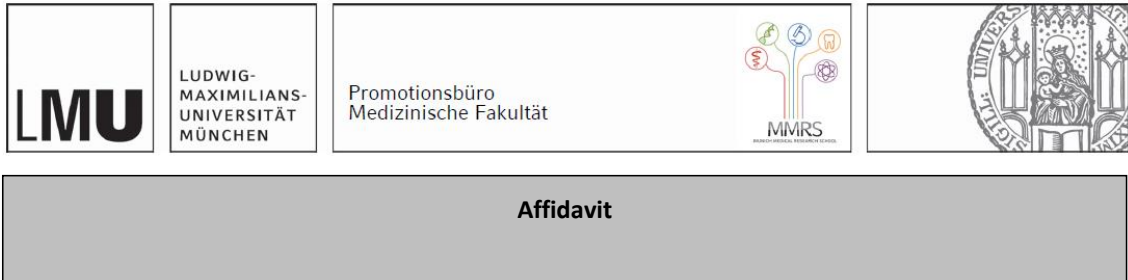
Mit Genehmigung der Medizinischen Fakultät der
Ludwig-Maximilians-Universität München

Erstes Gutachten: Prof. Dr. Irmela Jeremias
Zweites Gutachten: Priv. Doz. Ursula Zimmer-Strobl
Drittes Gutachten: Prof. Dr. Marion Subklewe
Viertes Gutachten: Prof. Dr. Dr. Michael von Bergwelt-Baildon

Dekan: Prof. Dr. med. Thomas Gudermann

Tag der mündlichen Prüfung: 15.10.2024

Affidavit



I hereby declare, that the submitted thesis entitled:

Identifying *WT1*, *DNMT3A* and *DDIT4L* as dependency genes in PDX models of acute leukemia *in vivo*

is my own work. I have only used the sources indicated and have not made unauthorized use of the services of a third party. Where the work of others has been quoted or reproduced, the source is always given.

I further declare that the dissertation presented here has not been submitted in the same or similar form to any other institution for the purpose of obtaining an academic degree.

Harbin, 2024.10.15

place, date

Yuqiao Gao

Signature doctoral candidate

Confirmation of congruency



LUDWIG-
MAXIMILIANS-
UNIVERSITÄT
MÜNCHEN

Promotionsbüro
Medizinische Fakultät



**Confirmation of congruency between printed and electronic version of
the doctoral thesis**

I hereby declare, that the submitted thesis entitled:

Identifying *WT1*, *DNMT3A* and *DDIT4L* as dependency genes in PDX models of acute leukemia *in vivo*

is congruent with the printed version both in content and format.

Harbin, 2024.10.15

place, date

Yuqiao Gao

Signature doctoral candidate

Table of Contents

Affidavit.....	3
Confirmation of congruency	4
Table of Contents.....	5
List of Abbreviations	6
List of Publications	8
1. Contribution to the publications.....	9
1.1 Contribution to paper I: <i>WT1</i> and <i>DNMT3A</i> play essential roles in the growth of certain patient AML cells in mice	9
1.2 Contribution to paper II: <i>In vivo</i> inducible reverse genetics in patients' tumors to identify individual therapeutic targets	11
2. Introductory summary	13
2.1 Acute leukemia.....	13
2.2 Current treatment of acute leukemia.....	14
2.3 Descriptive and molecular functional approaches to identify therapeutic targets	16
2.4 Reverse genomic techniques used in our studies.....	17
2.5 Patient-derived xenograft mouse models of acute leukemias.....	22
2.6 Genes studied in my projects and their dependency in AML.....	23
2.7 Summary of the studies	27
Paper I.....	29
Paper II.....	85
References.....	112
Acknowledgements	123

List of Abbreviations

ADD	ATRX-DNMT3-DNMT3L
ALL	Acute lymphoblastic leukemia
AML	Acute myeloid leukemia
<i>BCL-2</i>	B cell lymphoma-2
BCP	B-cell precursor
BM	Bone marrow
CAR	Chimeric antigen receptor
Cas9	CRISPR-associated protein 9
CEA	Carcinoembryonic antigen
CLL	Chronic lymphocytic leukemia
CNS	Central nervous system
CR	Complete remission
Cre-ER ^T	TAM-dependent Cre recombinase
CRISPR	Clustered regularly interspaced short palindromic repeats
crRNA	CRISPR RNA
<i>DDIT4L</i>	DNA-damage-inducible transcript 4-like
<i>DNMT3A</i>	De novo methyl transferase 3A
DSB	Double strand breaks
<i>DUX4</i>	Double homeobox 4
ER	Estrogen receptor
<i>ERG</i>	ETS transcription factor
FDA	US Food and Drug Administration
<i>FLT3</i>	Fms-like tyrosine kinase 3
FSHD	Facioscapulohumeral dystrophy
GDP	Guanosine diphosphate
GeCKO	Genome wide CRISPR/Cas9 knockout
gRNA	Guide RNA
GTP	Guanosine triphosphate
HDR	Homologous directed repair
HSC	Hematopoietic stem cell
HSCT	Hematopoietic stem cell transplantation
<i>IDH</i>	Isocitrate dehydrogenase
<i>IGH</i>	Immunoglobulin heavy locus
<i>KRAS</i>	Ki-ras2 Kirsten rat sarcoma viral oncogene homolog
KTS	Lysine, Serine, and Threonine

List of Abbreviations

loxP	The locus of X-over of bacteriophage P1
mi-RNA	Micro-RNA
NES	Nuclear exporter signals
NGS	Next generation sequencing
NHEJ	Non-homologous end-joining
<i>NPM1</i>	Nucleophosmin 1
NSG	NOD.Cg-Prkdc (scid) Il2rg (tm1Wjl) /SzJ
ORF	Open reading frame
PAM	Protospacer adjacent motif
PB	Peripheral blood
PDX	Patient-derived xenograft
PWWP	Pro-Trp-Trp-Pro
RalGEF	Ras-like (Ral) small GTPase
RNAi	RNA interference
R/R	Relapse/refractory
SAM	S-adenosyl methionine
sgRNA	Single-guide RNA
shRNA	Short hairpin RNA
siRNA	Small interfering RNA
TALENs	Transcription activator-like effector nucleases
TAM	Tamoxifen
TCR	T-cell receptor
tracrRNA	Transactivating CRISPR RNA
<i>WT1</i>	Wilms' tumor 1
ZFNs	Zinc-finger nucleases

List of Publications

1. Ghalandary M*, **Gao Y***, Amend D, Kutkaite G, Vick B, Spiekermann K, Rothenberg-Thurley M, Metzeler KH, Marcinek A, Subklewe M, Menden MP, Jurinovic V, Bahrami E, Jeremias I. *WT1* and *DNMT3A* play essential roles in the growth of certain patient AML cells in mice. *Blood*. 2023 Feb 23;141(8):955-960.
2. Carlet M, Völse K, Vergalli J, Becker M, Herold T, Arner A, Senft D, Jurinovic V, Liu WH, **Gao Y**, Dill V, Fehse B, Baldus CD, Bastian L, Lenk L, Schewe DM, Bagnoli JW, Vick B, Schmid JP, Wilhelm A, Marschalek R, Jost PJ, Miething C, Riecken K, Schmidt-Supprian M, Binder V, Jeremias I. In vivo inducible reverse genetics in patients' tumors to identify individual therapeutic targets. *Nature Communications*. 2021 Sep 27;12(1):5655.

1. Contribution to the publications

1.1 Contribution to paper I: *WT1* and *DNMT3A* play essential roles in the growth of certain patient AML cells in mice

In this project, we studied patient-derived xenograft (PDX) models and performed serial CRISPR/CRISPR-associated protein 9 (Cas9) knockout (KO) studies in mice. We found that *WT1* and *DNMT3A* were essential in certain PDX models of acute myeloid leukemia (AML) in mice *in vivo* and were dispensable for AML PDX cells or AML cell lines *in vitro*. By further studying the *WT1* and *DNMT3A* dependency for stem cell function, we found that knocking out either *WT1* or *DNMT3A* reduced leukemia-initiating cell number, impeded the re-engraftment of PDX cells into secondary recipient mice, and decreased the cell homing capacity into murine bone marrow. Finally, we observed that knocking out *WT1* contributed to a certain enhancement of the anti-tumor effect of Cytarabine. In summary, our findings revealed that *WT1* and *DNMT3A* are crucial dependency genes in certain AML PDX models *in vivo*, suggesting their potential as novel therapeutic targets to treat patients suffering from AML.

This paper has been published with shared first authorship because the other first author and the author of this dissertation generated most of the data in close collaboration and contributed equally to this project. Of note, following the maternity leave of the other first author starting before first submission of the article, the author of this dissertation took over all the tasks of a single first author during the 6-month revision phase of the manuscript.

Our lab had previously established an *in vivo* CRISPR/Cas9 dropout screen in acute lymphoblastic leukemia (ALL) PDX models. To transfer the technique to AML PDX models, the author of this dissertation performed an *in vivo* CRISPR/Cas9 dropout screen in the Cas9-negative AML-356 PDX model as one important quality control which showed favorable Gini index and sgRNA read counts correlation score (supplementary Figure 2A). Next, the author of this dissertation performed an *in vivo* CRISPR/Cas9 dropout screen in the Cas9-positive AML-346 PDX model (Figure 1B, supplemental Figure 2B, supplemental Table 6-8). About half of the genes that were included in the library dropped out, including common essential genes and known hematopoietic system essential genes, which were significantly depleted. Based on these findings and the results from the CRISPR/Cas9 dropout screens performed by the other first author in four additional AML PDX models (supplemental Table 1), *WT1* and *DNMT3A*, whose roles in oncogenesis are poorly understood, were chosen for further investigation.

To validate these candidate genes selected from the dropout screens, the other first author decided to perform single KO experiments using competitive assays where all cell populations can be studied under identical conditions within the same mouse. To allow for this competitive approach, each cell population needs to be labelled with a different fluorochrome. Firstly, the author of this dissertation generated non-targeting (NT) sgRNA subsets each carrying one of four different fluorochromes and then performed quality control competitive assays *in vivo* in AML-356 and *in vitro* in OCI-AML3. In more detail, cells were lentivirally transduced with the respective fluorochrome-coupled NT-sgRNAs and after puromycin enriching the cells,

cells carrying the different fluorochromes were mixed in equal parts. For the *in vivo* experiment, the mixtures of transduced AML-356 cells were injected into donor mice and for the *in vitro* part mixtures of transduced OCI-AML3 cells were kept in culture (supplementary Figure 5). The author of this dissertation harvested the AML-356 bone marrow cells from the mice upon development of advanced leukemia and the OCI-AML3 cells on day 31 after mixing. The distribution of NT-sgRNA subsets was measured using flow cytometry. The results showed no significant difference between input and output in NT-sgRNA subsets with different fluorochromes, indicating that different fluorochromes do not affect cell growth *in vivo* and *in vitro*. From these important controls we conclude that the growth of KO cells in the *in vivo* competitive assays is not influenced by the different fluorochromes. Subsequently, the author of this dissertation performed an *in vivo* competitive validation assay for *WT1* and *DNMT3A* in AML-388 (three out of six mice; the other three mice were included in the experiment performed by the other first author) and AML-393 (Figure 2A). *WT1* and *DNMT3A* showed an *in vivo* dependency in AML-388 but not in AML-393. Together with the results from the other validation assays performed by the other first author in three additional PDX samples, our results showed that *WT1* and *DNMT3A* were essential in certain PDX models *in vivo* (Figure 2B). Contrasting this finding of essentiality *in vivo*, analysis of data published on DepMap by the author of this dissertation revealed that *DNMT3A* was not essential *in vitro* in most of the AML cell lines available (supplementary Figure 6). Meanwhile, the author of this dissertation generated seven different Cas9-positive AML cell lines (two additional Cas9-positive AML cell lines were generated by the other first author and one of the co-authors) and performed *in vitro* competitive assays for *WT1* and *DNMT3A* in all nine cell lines (supplementary Figure 8-9). Reproducing the data published on DepMap, cells with *WT1* or *DNMT3A* KO had no significant growth disadvantage in these nine AML cell lines and *WT1* and *DNMT3A* showed no dependency in all AML cell lines studied, whether with or without mutation. Using THP-1 cells with single KO of the genes of interest, the author of this dissertation checked the gene editing efficiency by Western blot or TIDE analysis (supplementary Figure 4B and 7A-B). The Western blot showed significant loss of NPM1, KRAS, or WT1 protein in THP-1 *NPM1*, *KRAS* or *WT1* KOs. TIDE analysis showed a gene editing efficiency of more than 80% in *DNMT3A* KOs, which is generally considered as acceptable. Additionally, the author of this dissertation generated *WT1* and *DNMT3A* single KOs in AML-346 and AML-388 cells for immunophenotyping (supplementary Figure 10). The co-author performed immunophenotyping and analyzed the results, which showed that the respective KOs do not significantly impact the expression of the analyzed marker proteins. Furthermore, the author of this dissertation performed an *in vivo* and *in vitro* parallel competitive assay for *WT1* and *DNMT3A* in AML-346 (Figure 2C). To our surprise, the growth disadvantages of *WT1* KO or *DNMT3A* KO were restricted to *in vivo* environments but not observed *in vitro* in AML-346, suggesting that *in vivo* approaches were required to reveal certain dependencies in AML. Then, the other first author and the author of this dissertation prepared the sample for transcriptomic analyses together (Figure 2D, supplementary Figure 11). The data, which were analyzed by co-authors, showed that cell apoptosis and oxidative phosphorylation regulation accompanied the KO of *WT1* or *DNMT3A*.

To further study *WT1* and *DNMT3A* gene essentiality in leukemia stem cells, the author of this dissertation performed several *in vivo* experiments. First, the author of this dissertation performed a homing assay via intravenous injection and interfemoral injection of *WT1* KO cells in AML-346 and AML-388 PDX models

(supplementary Figure 13). *WT1* KO cells displayed early *in vivo* growth disadvantages, suggesting that loss of *WT1* reduced the capacity of AML-346 and AML-388 cells to home to the bone marrow environment upon intrafemoral or intravenous cell injection. Second, the author of this dissertation performed a kinetic *in vivo* competitive validation assay for *WT1* and *DNMT3A* in the AML-346 PDX model (supplementary Figure 14). *WT1* KO cells already exhibited growth disadvantages at an early stage of leukemia. Together with the results in AML-388 (performed by the other first author), we demonstrated that knocking out *WT1* impaired tumor-niche interaction. Third, the author of this dissertation performed an *in vivo* competitive re-transplantation assay with *WT1* and *DNMT3A* KO cells in AML-346 (supplementary Figure 15C-D). Therefore, *WT1* and *DNMT3A* KO cells isolated from recipient mice at the end point of the first competitive assay were re-injected into secondary recipient mice and the bone marrow cells were harvested at advanced leukemia stage and analyzed by flow cytometry. The results showed reduced engraftment capacity of AML-346 cells with *WT1* or *DNMT3A* KO. Based on this finding, the author of this dissertation further performed an *in vivo* competitive limiting dilution transplantation assay for *WT1* and *DNMT3A* in the AML-346 PDX model (Figure 2E). This experiment showed that KO of either *WT1* or *DNMT3A* reduced the number of stem cell surrogates, indicating an essential role of *WT1* and *DNMT3A* in leukemia stem cell survival.

To sum up, our technique allows studying gene dependencies in PDX models *in vivo*. *WT1* and *DNMT3A* have been identified as new dependencies in certain AML PDX cells in mice.

1.2 Contribution to paper II: *In vivo* inducible reverse genetics in patients' tumors to identify individual therapeutic targets

In this study, we established the first inducible system for gene knockdown *in vivo* in PDX acute leukemia (AL) models worldwide using a Cre-ER^{T2}-loxP-based RNAi-mediated gene silencing system. This system could induce a partial inhibition of a target gene, which closely mimics the clinical situation, as the treatment of individual patients with drugs or compounds induces a partial inhibition of their target proteins. First, we used *MCL1* as an exemplary target and proved that our newly established inducible knockdown system enabled studying sample-specific vulnerabilities. Next, we successfully identified a leukemia-maintaining ability of the *MLL-AF4* breakpoint product in established PDX ALL models bearing the *MLL-AF4* translocation and of *DUX4* in PDX ALL models bearing a *DUX4* translocation. Ultimately, we identified the *DUX4* downstream mediator *DDIT4L* as a therapeutic target in *DUX4* rearranged ALL. We established an *in vivo* inducible knockdown system as a valuable tool that allows individualized functional genomics studies in PDX AL models *in vivo*.

In this study, the author of this dissertation was one of the two PhD students additionally supporting the revision process of the paper and listed as a co-author in a middle position. The author of this dissertation contributed to several experiments.

To examine the effect of *MCL1* knockdown on apoptotic cell death, the author of this dissertation performed apoptosis staining three days post Tamoxifen (TAM) administration with sh*MCL1* cells and shCTRL cells in the AML-388, ALL-199, and ALL-265 PDX models (Figure S2e). The results showed a higher apoptosis

rate (Annexin V + percentage) in sh*MCL1* cells compared to the shCTRL cells after TAM administration for three days in the AML-388 PDX model suggesting that silencing *MCL1* in AML-388 induces rapid cell death. However, this effect was not observed in ALL-199 and ALL-265.

Based on the apoptotic cell death only observed in sh*MCL1* AML-388 but neither in ALL-199 nor ALL-265, we asked whether this correlates with the response to *MCL1* inhibition. We then performed *MCL1* inhibition treatment with S63845 in PDX AML-388 and ALL-199. The author of this dissertation harvested the spleen from mice 31 days after injection, helped co-first author to take images (Figure 2f), weighed the spleen (Figure S3h), harvested the spleen cells by Ficoll density gradient centrifugation and measured the percentage of PDX cells in the spleen by flow cytometry (Figure S2i). The author of this dissertation and co-first author also harvested bone marrow cells and measured the percentage of PDX cells in the bone marrow. The author of this dissertation observed that AML-388 mice treated with *MCL1* inhibitor S63845 had smaller size and weight of spleens than the PBS-treated control group and similar spleen sizes and weights compared to the healthy donor. However, the spleen size and weight showed no significant difference between the S63845 treated and control groups in ALL-199. Additionally, inhibiting *MCL1* using S63845 reduced the percentage of PDX cells in the spleen and bone marrow in AML-388 but not in ALL-199. Taken together, S63845 reduced the leukemic burden in the AML-388 PDX model but had no effect in the ALL-199 PDX model. Of note, this finding recapitulated the effect observed in the inducible knock-down system.

From the gene set enrichment analysis in sh*DUX4* ALL-811 cells and two published datasets, we identified a set of genes that was downregulated in *DUX4* knockdown PDX cells. To further verify the relevance of the detected genes for tumor maintenance in *DUX4*-rearranged samples, we tested the role of one gene, *DDIT4L*. The author of this dissertation extracted mRNA from cells of the *DUX4* rearranged PDX sample transduced with either shCTRL or sh*DUX4*, and performed qPCR to determine *DDIT4L* relative mRNA expression level (Figure 3g). The results showed that *DUX4*-rearranged samples transduced with sh*DUX4* had lower relative *DDIT4L* mRNA expression compared to controls indicating *DDIT4L* is downregulated in *DUX4* knockdown *DUX4*-rearranged cells. Furthermore, the author of this dissertation performed *DDIT4L* inducible knockdown in Nalm6 cells, harvested cells seven days post TAM, extracted RNA, performed qPCR, and analyzed relative *DDIT4L* mRNA expression level (Figure 3h). The result showed that inducible knockdown of *DDIT4L* in Nalm6 cells significantly reduces relative *DDIT4L* mRNA expression. Ultimately, to examine whether *DDIT4L* is a vulnerability in *DUX4-IGH* rearranged ALL, the author of this dissertation generated shCTRL and sh*DDIT4L* Nalm6 cells (Figure 3i) for a competitive *in vivo* assay. The co-first author prepared the mixture of these two populations for injection into recipient mice. The author of this dissertation harvested the bone marrow cells 15 days after TAM administration, performed MACS® Cell Separation to purify mouse cells, and measured samples by flow cytometry. The co-first author analyzed the data. We observed that inducible knockdown of *DDIT4L* significantly diminished leukemic growth within two weeks *in vivo*. This indicates that the downregulation of *DDIT4L* mediated the growth inhibitory effects observed in the sh*DUX4* population. To sum up, we identified *DDIT4L* as a therapeutic vulnerability in the *DUX4-IGH* subtype of B-ALL.

2. Introductory summary

2.1 Acute leukemia

Acute leukemia is a heterogeneous hematologic malignancy first described by Rudolf Virchow, a German pathologist in the 19th century¹. It is characterized by abnormal stem cell differentiation and proliferation, mainly caused by chromosomal abnormalities and genetic alterations. These immature malignant cells, called “blasts”, accumulate primarily in bone marrow (BM), peripheral blood, and extramedullary sites². This pathologic process leads to severe effects and typical clinical symptoms like bleeding, recurrent infections, and anemias in patients. The acute leukemia blasts proliferate rapidly without treatment, resulting in high mortality rates and poor prognosis³. Acute leukemia can be categorized into two main types: acute myeloid leukemia (AML) and acute lymphoblastic leukemia (ALL). This classification is based on the clonal proliferation derived from different progenitor lineages⁴.

AML is a myeloid clonal disorder originating from progenitor cells of the myeloid line. Its diagnosis typically involves the accumulation of more than 20% myeloid blasts in both the peripheral blood (PB) and BM. It is present mainly in adults, especially in people older than 55 years, and constitutes over 80% of adult leukemia cases.⁵ The prognosis of AML patients is influenced by factors such as age, genetic and molecular abnormalities, initial treatment response, and minimal residual disease. The annual incidence rate of pediatric AML is relatively low and is approximated to be around 1-2 cases per million children⁶. Furthermore, the outcome is worse upon age increase. Patients under 50 years old exhibit a 60% long-term survival rate, while those aged between 50 to 64 years have a 37% survival rate. For patients older than 65 years, the survival rate drops to less than 10%.^{7,8}

ALL is caused by lymphoblasts which proliferate and invade the BM, and tumorigenesis is usually triggered by driver gene mutations and exposure to physical or chemical radiation. It stands as the most common childhood leukemia, exhibiting a peak incidence between one year and four years of age and around a 75% incidence rate in individuals under 20 years old. Moreover, the prognosis for these patients has shown remarkable improvement over the past 50 years, with a long-term survival rate exceeding 90%⁹. In contrast, in adults, only about 20% of patients with acute leukemia are diagnosed with ALL. These patients are typically older than 50, and they often face a dramatically low 5-year survival rate, averaging around 25%. Moreover, the outcomes are more severe according to age, blood account at diagnosis, cytogenetic and or molecular abnormalities, and treatment response.^{10,11}

As acute leukemias are heterogeneous diseases, long-term survival rates in older patients above 50 years are worse than in younger patients, and precision assessment and treatment strategies for each patient are crucial and urgently needed to improve clinical outcomes.

2.2 Current treatment of acute leukemia

Treatment for acute leukemia commonly entails a combination of chemotherapy, radiation therapy, and stem cell transplantation, depending on the subtype of leukemia, the age of the patient, overall health, and individual factors.

Therapeutic approaches have been expanded upon the rapid development in molecular biology and the dramatic improvement in the understanding of pathophysiology. Targeted therapies, immunotherapies, and novel agents bring personalized treatment options for patients and considerable improvement in patients' outcomes.

2.2.1 Current treatments in acute myeloid leukemia

Treatment decisions are generally based on risk stratification, patient tolerance, and treatment response status. According to the National Comprehensive Cancer Network Guidelines or European Leukemia Net, there are three risk categories for AML: favorable, intermediate, and adverse. This classification is determined based on validated cytogenetics and molecular abnormalities¹². The AML treatment generally contains initial induction chemotherapy followed by consolidation therapy¹³. In addition, targeted therapy and immunotherapy could also be the choice for specific patients to gain better outcomes.¹⁴

Initial induction chemotherapy for AML is referred to as the “7+3” chemotherapy strategy. Patients receive cytarabine for seven days and consecutively taking anthracycline for three days. This regimen has been in use and remained unchanged for more than 40 years¹⁵. It results in a complete remission (CR) rate ranging from 60 to 85% and a five-year overall survival rate of around 40% for patients under 60 years¹⁶. For patients above 60 years old, around 50% of patients achieve CR, and only around 10% of patients are cured after this standard intensive treatment¹⁶. Currently, several studies attempt to optimize the dose of cytarabine and anthracycline, as seen in drugs like CPX-351, which contains five parts cytarabine for every one part daunorubicin^{17,18}, or incorporating a third drug, such as Gemtuzumab ozogamicin, to enhance treatment response^{19,20}.

Consolidation therapy is essentially recommended after patients achieve CR with induction chemotherapy to prevent relapse either by intensive chemotherapy (high dose or intermediate dose of cytarabine) or hematopoietic stem cell transplantation (HSCT). In patients under 60 years old, the most frequently used regimen is high dose cytarabine and could achieve around 50% long-term survival. For patients above 60 years old, only a small proportion of favorable group patients can benefit from intensive therapy²¹. HSCT is still an effective therapeutic approach to gain long-term survival in 20% poor-risk or intermediate-risk AML patients²². For high-risk patients, HSCT reduced the relapse frequency compared to chemotherapy alone. Moreover, HSCT provides the best chance for patients who failed the primary induction chemotherapy or developed a relapse stage to cure²³.

As approaches have advanced dramatically over the last years, several novel therapeutic options exist for acute leukemia patients. Due to the growing recognition of genomic heterogeneity in AML, molecular targeted therapy has been developed rapidly and achieved significant efficacy²⁴. Targeted therapy still has

significant potential, and there is a need to identify new treatment targets to promote the current therapeutic strategies. Hypomethylating agents such as azacytidine and decitabine provide better treatment options for older, “unfit” patients who cannot tolerate standard chemotherapy²⁵. Venetoclax, an oral B cell lymphoma-2 (*BCL-2*) inhibitor, was initially applied in chronic lymphocytic leukemia (CLL) and provides an effective response to pre-treated CLL patients; it also shows a better efficacy in older AML patients in the VIALE-A trial²⁶⁻²⁸. The combination therapy containing the BCL-2 inhibitor and hypomethylating agents (such as low dose cytarabine) has even become the first-line therapy for older patients who cannot tolerate chemotherapy and gives a better efficacy and fewer side effects²⁸. Midostaurin and Gilteritinib are Fms-like tyrosine kinase 3 (*FLT3*) inhibitors. They are also recommended in the clinic for *FLT3-ITD* AML patients²⁹⁻³¹. Ivosidenib and Enasidenib are isocitrate dehydrogenase (*IDH*) inhibitors. They target *IDH1/2* mutations. Relapsed/refractory (R/R) AML patients tolerate them well and gain higher CR rates when using them as single agents^{32,33}.

Immunotherapy approaches, such as chimeric antigen receptor (CAR) T-cell therapy (including anti-CD123, anti-CD33, and anti-CD70), natural killer cell therapy, bi-specific T-cell engagers (BiTEs), and checkpoint inhibitors, are currently undervalued and may find success in the minimal residual disease-positive remission stage or during early salvage³⁴⁻³⁷. The development of immunotherapy for AML continues to pose challenges due to the heterogeneity feature, the absence of specific target antigen, or concerns about anticipated toxicity.

2.2.2 Current treatments in acute lymphoblastic leukemia

The treatment strategy for ALL is complex and precisely targeted according to age, leukemia subtype, cytological features, genetic and molecular abnormalities, and further prognostic factors.

Typically, there are four phases for ALL treatments¹⁰. The first phase is the induction therapy based on a combination regimen, which typically consists of glucocorticoid, vincristine, L-asparaginase, and an anthracycline, aiming to eliminate leukemia blasts in the BM and to bring the patients into the remission stage³⁸. The second phase is consolidation therapy. Patients receive cytarabine, high-dose methotrexate, vincristine, asparaginase, mercaptopurine, and glucocorticoids every two weeks for over three months to completely eradicate the leukemia burden and prevent relapse³⁹. The following phase is intensification therapy, which encompasses a regimen analogous to that used during induction therapy⁴⁰. The last phase is the long-term maintenance therapy, which lasts for 2-3 years, including mercaptopurine, methotrexate and glucocorticoids, with or without vincristine^{41,42}.

Moreover, central nervous system (CNS) prophylaxis is recommended to avert CNS relapse in patients with high leukocyte count at diagnosis, poor induction treatment response, or T-ALL⁴³⁻⁴⁵. HSCT is suitable for patients presenting high-risk factors and minimal residual disease and could help patients restore a normal hematopoietic system⁴⁶⁻⁴⁸.

Targeted therapy for ALL has achieved considerable progress over the last decades^{49,50}. The application of first-generation tyrosine kinase inhibitor (TKI), Imatinib, combined with chemotherapy showed promisingly more than 90% CR rate and up to 50% 5-year overall survival in Philadelphia chromosome-positive

(Ph+) ALL patients⁵¹. However, a large proportion of patients suffered from relapse^{52,53}. Therefore, the second and third generation TKIs, such as Dasatinib and Ponatinib, are substituted to overcome the resistance to Imatinib⁵⁴. The utilization of a *BCL2* inhibitor, Venetoclax, combined with chemotherapy resulted in a 60% CR rate among 13 R/R T-ALL patients⁵⁵. A phase I study applied the combination therapy using 600mg Venetoclax and achieved a 90% (9/10) CR rate without detectable MRD in newly diagnosed older patients⁵⁶. Gamma secretase inhibitors (GSI), Crenigacestat and BMS-906024, can target the NOTCH1 pathway and synergistically induce T-ALL cell death combined with steroids; however, they showed severe diarrhea⁵⁷. Selumetinib, a *MEK1/2* inhibitor, was applied together with dexamethasone in a phase I/II trial in R/R ALL patients. The result showed that this combination therapy may bridge patients to CAR T-cell therapy⁵⁸. Monoclonal antibodies, such as Rituximab (an anti-CD20 monoclonal antibody), Blinatumomab (an anti-CD19 monoclonal antibody and a bispecific anti-T-cell receptor), Inotuzumab ozogamicin (an anti-CD22 monoclonal antibody), showed remarkable results and were approved for clinical use by the US Food and Drug Administration (FDA) for patients expressing corresponding biomarkers⁵⁹⁻⁶⁵. More monoclonal antibodies are under investigation.

CAR T-cell therapy targeting CD19 antigen is a promising strategy endorsed by the FDA and could achieve more than 80% CR rate with MRD negativity in R/R B-cell ALL patients⁶⁶. However, immune escape exists because tumor cells downregulate expression of the target antigen. Therefore, novel CAR T-cell therapy, CD19 and CD22 dual targeting therapy, has been established to overcome tumor cell escape⁶⁷. For T-cell ALL, the development of CAR T-cell therapy was much slower because of the challenge of omitting long term eradication of normal T-cells as an adverse effect. Nevertheless, CD5 and CD7 are currently under exploration as viable targets in CAR T-cell therapy, mainly before stem cell transplantation⁶⁸⁻⁷⁰.

2.3 Descriptive and molecular functional approaches to identify therapeutic targets

In recent years, deciphering human genomic and molecular pathogenesis has rapidly progressed, improving clinical diagnostic accuracy and patient outcomes^{14,71}. However, the therapeutic landscape of many cancers, including AML, remains challenging^{14,72}. For example, although AML patients gain benefits from updated risk stratification, chemotherapy, and bone marrow transplantation, the CR rates are around 30% in all AML patients and only 15% in older AML patients, who also have a worse overall survival^{14,73}. As the mainstream treatments have not changed for decades, identifying new therapeutic strategies, such as novel targeted therapies, is imperative for enhancing subsets of patients' clinical outcomes.

The development and maintenance of cancer hinge on genes and proteins essential for cancer cell growth and survival. Therefore, genes that are essential for cancer could be putative cancer therapeutic targets to develop additional therapeutic strategies for increasing long-term survival.

The landscape of essential genes for cancer has been gradually completed through the development of descriptive high-throughput sequencing technologies and related bioinformatics approaches in the past 20 years⁷⁴⁻⁷⁶. A better understanding of the gene dependency map boosted the identification of cancer targets

and facilitated the progression of cancer therapies to the next level, precision medicine⁷⁷. Recently, studies integrated big data such as pan-cancer genome and transcriptome to decipher single lesions, vulnerabilities, or complex aberration patterns using cell lines, primary cells, and patient-derived cells. Based on this, these studies identified robust targetable biomarkers and achieved the translation from basic science into clinical practice⁷⁷.

On the other side, functional genomics has complemented descriptive efforts, and one example of systematically analyzing essential genes in cancer is the establishment of a Cancer Dependency Map⁷⁸. The group developed an analytical framework, called DEMETER, to integrate 501 genome wide dropout screens performed in a wide diversity of cancer types and identified 769 genes differentially required within certain lineage subtypes⁷⁸. These results can be used for cancer dependency prediction and be subsequently investigated as potential cancer therapeutic targets⁷⁹.

One of the best examples of precision medicine is the detection of the chromosomal translocation, BCR-ABL, determined by genetic and karyotypic analysis in chronic myeloid leukemia (CML) and the subsequent discovery of the tyrosine kinase inhibitor (TKI), Imatinib, emerging from thousands of compounds^{80,81}. The identification of BCR-ABL and the application of Imatinib has brought remarkable clinical benefits, significantly increasing the long-term survival rate from 6% to nearly 90% in CML patients, and remains a paradigm for gene dependency investigation and targeted therapy application^{82,83}.

Moreover, BCL-2 has been demonstrated as an essential gene in hematopoietic malignancies over the last decades⁸⁴. Venetoclax (ABT-199), a promising selective *BCL-2* inhibitor, has received approval from the FDA for CLL and AML patient treatment²⁸. In many instances, combination therapy, Venetoclax plus anti-CD20 antibody, is now established as a standard regimen for R/R CLL patients⁸⁵. More clinical trials with combination therapy in AML are underway or about to begin.

2.4 Reverse genomic techniques used in our studies

The lab where I performed my PhD performs several reverse genetic approaches with the aim to identify and characterize genes with essential function for leukemia growth, mainly gene editing for gene knockout (KO) and RNA interference for gene knockdown.

Genome editing approaches have evolved from Zinc-finger nucleases (ZFNs) and transcription activator-like effector nucleases (TALENs) to clustered regularly interspaced short palindromic repeats (CRISPR)/CRISPR-associated (Cas) protein 9 system⁸⁶. By targeting specific DNA sequences with a small guide RNA (gRNA), the CRISPR/Cas9 system is a highly effective, relatively straightforward, and low-cost technique for gene modification⁸⁷. RNA interference (RNAi) functions as a gene regulatory mechanism that could downregulate gene expression on RNA expression level by small molecules of interfering RNA⁸⁸. Today, CRISPR/Cas9 and RNAi have emerged as powerful genetic approaches to identify individual or whole genome cancer dependencies⁸⁹.

2.4.1 CRISPR/Cas9 mediated knockout

CRISPR was first observed in bacterial and archaeal genomes in 1987 and given its name in 2002^{90,91}. It protects against plasmid transfer and pathogenic phage infection by excising nucleic acids by gRNA-localized Cas enzymes⁹². The CRISPR/Cas system comprises three main types (type I, II, III), differentiated by variant nucleic acid recognition mechanisms⁹³. The Type II system is the most commonly used genome editing tool relying on a single RNA-directed protein for specific DNA recognition and cleavage⁹⁴. CRISPR/Cas9, originating from the *Streptococcus pyogenes* strain, belongs to the Type II system and comprises two main components: the Cas9 protein and gRNA^{87,95}. The Cas9 is characterized by two ribonuclease structural domains, a RuvC-like nuclease and an HNH nuclease domain. These domains facilitate the cleavage of the DNA strand, introducing targeted double-strand breaks (DSBs) in genomic DNA^{96,97}. The Cas9 protein is guided to a precise genomic locus by a 20nt chimeric single-guide RNA (sgRNA) paired with a 5'-NGG protospacer adjacent motif (PAM)⁹⁵. After DSB formation, DSBs are repaired through either non-homologous end-joining (NHEJ) or homology-directed repair (HDR), leading to genomic modifications such as knockout, knock-in, and point mutation of target genes^{98,99}.

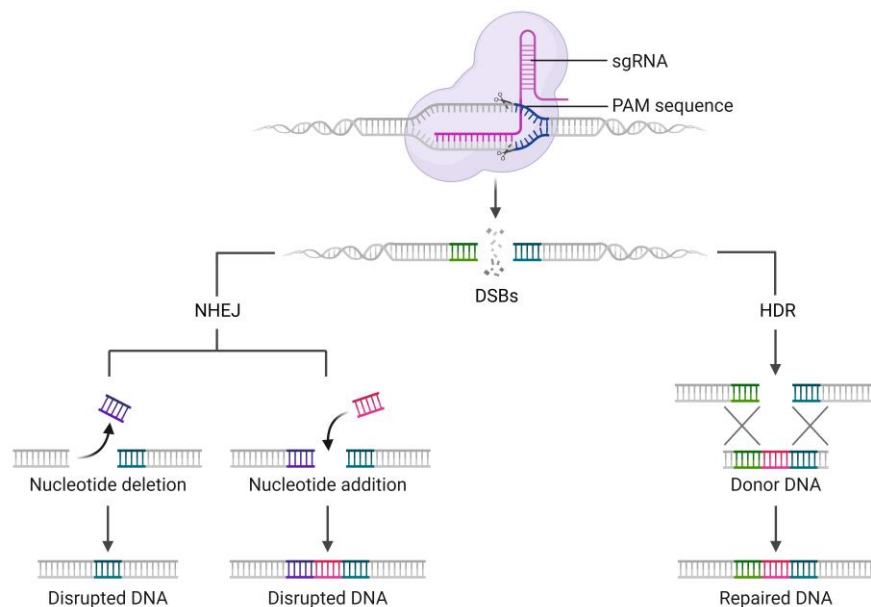


Figure 1. Schematic of CRISPR/Cas9 gene editing. The Cas9 complex, directed by a single-guide RNA (sgRNA), discriminates a specified sequence denoted as the protospacer, contingent upon the existence of a Protospacer Adjacent Motif (PAM). The binding of Cas9 elicits the induction of a double-stranded DNA break (DSB), thereby instigating downstream processes of non-homologous end-joining (NHEJ) or homology-directed repair (HDR). These processes can result in mutations or precise gene modifications, respectively.

In 2013, Zhang et al. achieved the first induction of accurate cleavage at endogenous genomic loci in both human and murine cells via CRISPR/Cas9 directed by short RNAs¹⁰⁰. In the same year, Church et al. optimized the CRISPR gene editing system by expressing CRISPR RNA (crRNA) - transactivating CRISPR RNA (tracrRNA) fusion transcripts – referred to as sgRNA and verified the modification function of the CRISPR/Cas9 system in human cells¹⁰¹. Since then, CRISPR/Cas9 has been widely used in individual gene functionality studies. Moreover, CRISPR/Cas9 has been applied in broader fields such as genome-wide screening and clinical applications.

In 2014, the first whole genome wide CRISPR/Cas9 dropout (GeCKO) screens were successfully performed in human cancer cell lines and identified essential genes, including genes consistent with the previously validated studies and novel hits¹⁰². Since then, GeCKO screening has been widely utilized for identifying gene dependencies in cancer. Our group recently implemented CRISPR/Cas9 screening in patient-derived xenograft (PDX) mouse model *in vivo*¹⁰³. This involved establishing a Cas9-positive PDX mouse model, utilizing the CLUE pipeline for CRISPR/Cas9 library design, and applying the MAGeCK algorithm for the analysis of next-generation sequencing (NGS) data^{104,105}. Through *in vivo* competitive assays targeting each identified candidate from the CRISPR/Cas9 screening, we pinpointed *WT1*, *DNMT3A*, and *ADAM10* as essential genes for acute leukemias.

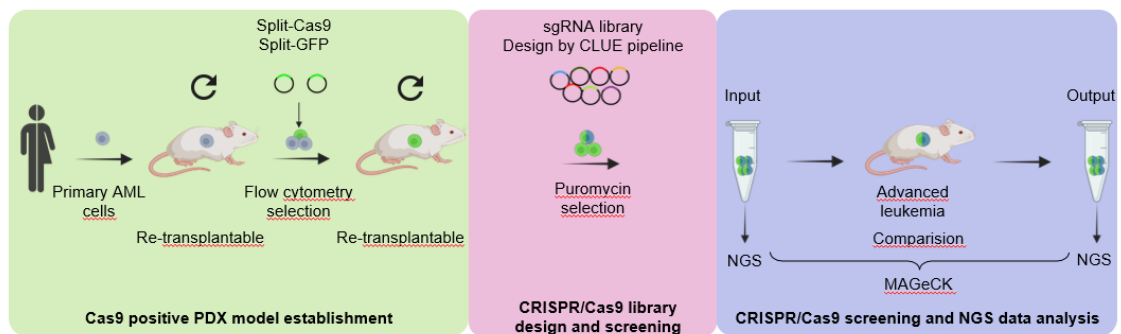


Figure2. Schematic of customized CRISPR/Cas9 library screen using PDX models. Establishing a PDX model stably expressing Cas9 involves utilizing primary leukemic cells, followed by the introduction of the split Cas9 construct together with GFP marker using lentiviruses and subsequent enrichment of Cas9-positive cells by gating GFP via flow cytometry. In a second step, a specialized sgRNA library, designed through the CLUE platform, is lentivirally transduced into Cas9-positive PDX cells and further enriched via puromycin selection. Next-generation sequencing (NGS) PCR is conducted comparing cells from pre-injection with those at an advanced leukemia stage, with the results being analyzed using the MAGeCK platform.

CRISPR has been used to improve the safety and effectiveness of engineered T cells in T-cell receptor (TCR) therapy, which has been approved by the FDA and shown to be effective and well tolerated in clinical trials¹⁰⁶. CRISPR is used to knock out the genes encoding TCR chains and PD-1, significantly strengthening tumor growth inhibition capacity¹⁰⁷.

Although CRISPR has been widely used in molecular biology and has made promising progress, the off-target effects from the mismatches between sgRNA and nontarget consistently occur and influence the specificity of target activity¹⁰⁸. More accurately modified Cas9 subtypes and using better targeted sgRNA

are under investigation to overcome this issue and will broaden the application of CRISPR in medicine and biotechnology.

2.4.2 Inducible RNAi using the Cre-ER^{T2}-loxP system

RNA interference (RNAi) is an additional functional genomic tool which reduces expression of a defined gene's mRNA and uses a cognate double-stranded RNA to trigger precise cleavage of the mRNA transcript⁸⁸.

RNAi is shown to be naturally induced by micro-RNA (mi-RNA), precursor mi-RNA (pre-miRNA), or primary mi-RNA (pri-miRNA) in a variety of eukaryotic cells, encompassing animals, plants, fungi, and some protozoa¹⁰⁹. The miRNA is first transcribed by polymerase II as pri-miRNA. Then, Drosha, an RNase III enzyme, acts upon the pri-miRNA, leading to the generation of a pre-miRNA hairpin structure¹¹⁰. Afterwards, Exportin5, the nuclear export factor, conveys the pre-miRNA from the nucleus into the cytoplasm¹¹¹. Following nuclear export, the pre-miRNA is processed in the cytoplasm by Dicer, an RNase III enzyme. Dicer cleaves the pre-miRNA hairpin loop, resulting in the formation of a double-stranded miRNA¹¹². Subsequently, this miRNA engages with the RNA induced silencing complex (RISC) and serves as a single-stranded RNA to interact with target mRNAs¹¹³. Achieving artificial gene silencing is feasible through the delivery of small interfering RNA (siRNA), short hairpin RNA (shRNA), or shRNA-mir into cells using transfection or electroporation¹¹³. siRNA mimicking the natural miRNA could directly interact with RISC, achieving gene silencing. shRNA resembling the pre-miRNA could be transcribed by RNase III enzyme and generate double-stranded miRNA. shRNA-mir is comparable to pri-miRNA and could be expressed from polymerase II.

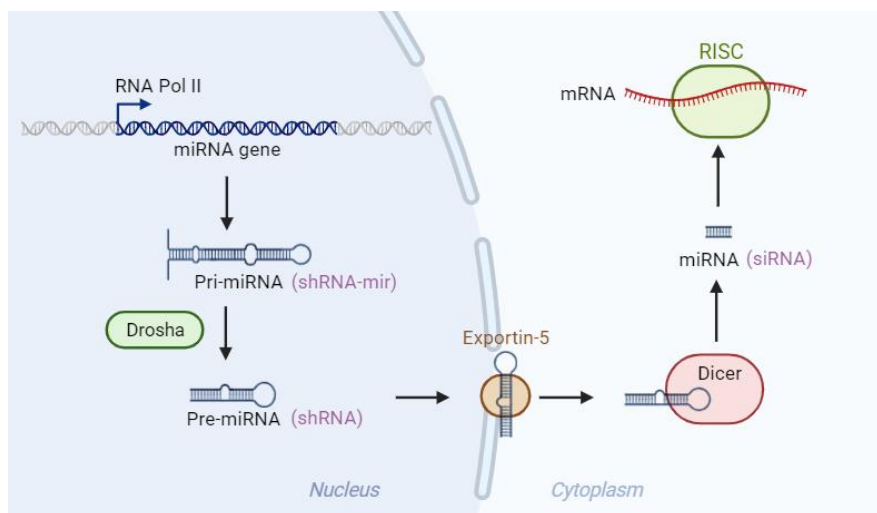


Figure3. Schematics of RNAi mediated gene silencing. First, miRNA is first transcribed by polymerase II (Pol II) as pri-miRNA. Then, Drosha acts upon the pri-miRNA, leading to pre-miRNA generation. Subsequently, Exportin-5 transports the pre-miRNA into the cytoplasm. Afterwards, Dicer cleaves the pre-miRNA hairpin loop, yielding a double-stranded miRNA. This miRNA engages with the RNA-induced silencing complex (RISC), incorporating as a single-strand RNA to target complementary mRNA. Entry sites for artificial gene silencing utilizing shRNA-mir, shRNAs, and siRNAs are highlighted in purple.

In general, RNAi is a cheap and fast process to induce gene silencing. However, challenges exist in gaining a stable perturbation of gene expression using siRNAs or avoiding cytotoxicity using shRNA¹¹⁴. The newly developed lentiviral vector allows for the incorporation of shRNA sequences within the miR-30 sequence, forming the shRNA-miR-30 cassette. This cassette enables to achieve long-term and effective integration into the genome.¹¹⁵ To increase shRNA-miR-30 knockdown efficiency, the EcoRI restriction site was optimized and re-located into the shRNA non-conserved region to increase the shRNA expression, and the miR-30 hairpin was extended to 118 nucleotides with additional restriction sites, which allow for the incorporation of multiple hairpins to achieve shRNA concatemerization¹¹⁵.

In order to inhibit the gene expression at specific time points, especially for *in vivo* studies, inducible RNAi systems were generated, including Cre-loxP¹¹⁶. Cre, a 38KDa recombinase protein, interacts with specific chromosomal sites at the locus of X-over of bacteriophage P1 (loxP) sites (loxP-2272 and 5171). LoxP sites consist of 34 bp and serve as Cre recognition and recombination loci¹¹⁷. When loxP sites are oriented in parallel, Cre-mediated recombination leads to the irreversible deletion of the intervening DNA sequence, resulting in the permanent deletion of a specific genomic segment. In contrast, when loxP sites are positioned in an opposite direction, Cre triggers a reversible rearrangement of the DNA sequence between them, enabling the redirection of the DNA sequence in the opposite orientation following subsequent recombination events¹¹⁸.

Furthermore, a mutated estrogen receptor (ER) responding to Tamoxifen (TAM) is introduced into the Cre-loxP system to generate a TAM-dependent Cre recombinase (Cre-ER^T)¹¹⁹. Without TAM exposure, Cre-ER^T remains inert and associates with heat shock protein 90 (Hsp90) within the cytoplasm. In the presence of TAM, TAM binds to Cre-ER^T, prompting the translocation of Cre-ER^T into the nucleus instead of forming a complex with Hsp90. To this extent, TAM-induced activation of Cre-ER^T allows for the precise regulation of target gene expression directed by loxP sites at specific time points¹²⁰. Later, the Cre ligand-binding domain was modified with a triple mutation to increase TAM sensitivity, resulting in Cre-ER^{T2}¹²¹. For *in vivo* use of the system, mice can be treated with TAM for gene induction.

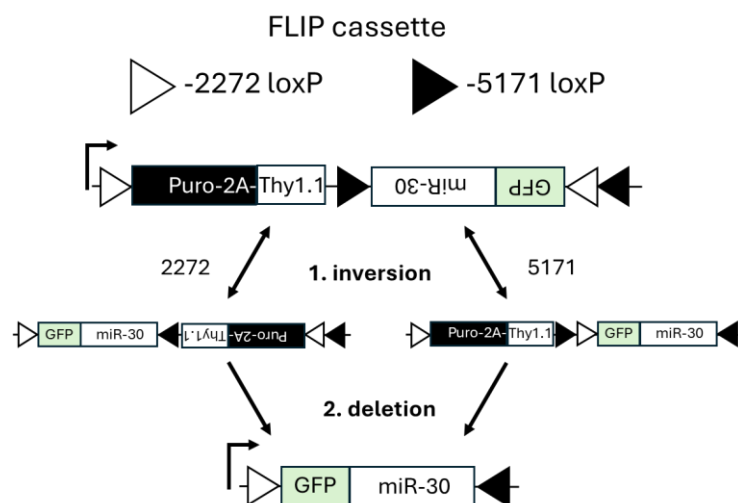


Figure4. Schematics of Cre-ER^{T2} mediated inducible knockdown system. The construct depicted consists of a puromycin resistance gene (Puro-2A) and the surface marker Thy1.1 in the sense orientation, with GFP and a miR-30 cassette in the antisense orientation. Two mutated loxP sites (loxP-2272 and 5171) enable stable, irreversible recombination through a two-step mechanism. Initially, Cre-

ER^{T2} induces a reversible inversion, generating two distinct intermediate constructs. Subsequently, the puromycin resistance gene and Thy1.1 surface marker are excised via the flanked loxP sites, resulting in the expression of GFP and the miR-30 cassette upon Cre-ER^{T2} activation. Adapted from Stern et al.¹²²

For inducible knockdown, we used the system established by Stern et al. and adapted it for use in PDX cells *in vivo*¹²². Before, the system had been mainly used to study genes essential for cells *in vitro*. To visualize and enrich transgenic cells, Stern et al. cloned the reporter genes under the same promoter as the shRNA so that reporter genes are expressed exclusively after induction and indicate expression of the shRNA¹²². The construct from Stern et al. harbors a puromycin resistance gene and the surface marker Thy1.1, both positioned adjacent to distinct loxP sites in the forward direction. Additionally, green fluorescent protein (GFP) and the miR-30 RNAi sequence are situated in the reverse orientation, with two loxP sites located next to them and oriented oppositely to the initial pair. The irreversible recombination initiating expression of the shRNA is achieved through a two-step process: firstly, Cre-ER^{T2} initiates a reversible inversion, resulting in one of two possible intermediate constructs. Following this, the subsequent recombination removes the puromycin resistance region, Thy1.1 and a loxP site. This prevents the original construct from reverting and initiates the expression of GFP and the shRNA (Fig. 4). Stern et al. coined this process 'flipping'¹²².

2.5 Patient-derived xenograft mouse models of acute leukemias

Pre-clinical cancer studies often rely on tumor models. Tumor cell lines, primary cells, animal models, and patient-derived xenograft (PDX) models are commonly used tools¹²³. Tumor cell lines, one of the most accessible tumor models to handle and culture, are widely used for basic and preclinical cancer research. However, as technical drawback especially in acute leukemias, establishing cell lines comes at the price of genetic and transcriptional changes and lack of tumor-microenvironment interaction¹²⁴. Primary tumor cells are derived directly from patient tissues and could better reflect the heterogeneity and tumor-microenvironment interaction than cell lines, although with a limited lifespan in *in vitro* culture, which is particularly short in primary acute leukemia cells¹²⁵. Genetically engineered mouse models are the other commonly employed animal models primarily utilized for molecular and functional *in vivo* characterization of genetic lesions in murine tumors. However, mouse models might not correctly mimic human conditions¹²⁶. As a result, it is still a major challenge to determine essential genetic lesions in a patient's tumor cell *in vivo*.

The orthotopic PDX mouse model represents a highly relevant preclinical surrogate and can closely mimic the clinical situation, allowing the study of individual patient's tumor cells in the *in vivo* environment¹²⁷. The PDX model is established by transplanting primary tumor cells from patients into immunocompromised NOD.Cg-Prkdc (scid) Il2rg (tm1Wjl) /SzJ (NSG) mice¹²⁷. The NSG mouse is an excellent xenograft recipient, especially for human hematopoietic stem cell engraftment¹²⁸. The patient's leukemia cells collected from human BM aspiration or PB are injected into NSG mice where they establish an orthotopic tumor as acute leukemia PDX models. The acute leukemia PDX cells can then be harvested from mouse BM or spleen in PDX models for further serial re-transplantation¹²⁹. The engraftment capacity of a primary leukemia sample and the chance of generating a PDX model thereof depends on the prognosis of the corresponding patient, with poor clinical outcome associated with a better engraftment ability and higher

chances to generate a PDX model¹³⁰. As acute leukemias are heterogeneous diseases, the PDX model is the best available model, which provides a more clinically relevant individual context and enables the investigation of reproducible gene functionality studies *in vivo*¹³¹⁻¹³⁸. To better monitor the tumor progression *in vivo*, our lab has pioneered bioluminescence *in vivo* imaging (BLI) by integrating a luciferase reporter gene into the PDX cells, enabling the reliable and repetitive quantification of leukemic burden in living mice^{139,140}. Imaging advanced the sensitivity and feasibility of following up leukemia progression, monitoring minimal residual disease, and quantifying treatment response. Thus, the PDX model, combined with *in vivo* bioluminescence imaging represents a valuable tool in studying leukemia biology and can be applied in preclinical treatment trials.

2.6 Genes studied in my projects and their dependency in AML

Exploration of gene dependencies has witnessed significant strides in recent decades, advancing through clinical and preclinical studies. Identification of genes deemed essential to cancer, facilitated by clinical and genome-wide screening, culminates in their validation as putative therapeutic targets. Subsequently, these genes may be intricately linked to potential drugs, paving the way for novel cancer therapies.

2.6.1 *KRAS*

The *KRAS* gene (Ki-ras2; Kirsten rat sarcoma viral oncogene homolog) is situated on chromosome 12p12 with 7 exons and encodes one of the small *RAS* superfamily proteins, which belongs to a subset of small GTP-binding proteins^{141,142}. *KRAS* protein participates in intracellular signal transduction and converts the nucleotide guanosine diphosphate (GDP) into guanosine triphosphate (GTP)¹⁴³. While *KRAS* protein binds to GTP in its active state, it transmits signals from activated growth factor receptors, thereby affecting downstream signaling pathways¹⁴⁴.

KRAS is a commonly mutated oncogene. Mutations in *KRAS* are located near the GTP binding site, impeding GTP hydrolysis, and consequently leading to *RAS* molecules' permanent activation¹⁴⁵. It profoundly affects cancer cell invasion, adhesion, and carcinoembryonic antigen (CEA) expression. *KRAS* mutations have been detected in more than 80% of pancreatic carcinomas, about 40% of colon carcinomas, and around 40% in *MLL*-positive B-precursor ALL¹⁴⁶⁻¹⁴⁸. The mutant subtypes of *KRAS* are predominantly categorized into seven distinct types¹⁴⁹. From a clinical perspective, *KRAS* mutants present compelling potential therapeutic targets. Specific *KRAS* (G12C) inhibitors showed benefits in many patients with *KRAS* mutations¹⁵⁰. Sotorasib, a selective *KRAS*(G12C) inhibitor, exhibited around 10% to 30% overall response rates in advanced colorectal cancer harboring the *KRAS* G12C mutation in a phase 1 study¹⁵¹. In AML, a study with 56 patients observed that a high frequency of *KRAS* mutations co-occur with *MLL* fusions. In addition, individuals with *MLL*-AML carrying a *KRAS* mutation had a significantly poorer prognosis¹⁵². Unfortunately, there are no clinical or pre-clinical studies demonstrating the effectiveness of *KRAS* inhibitors in hematologic malignancies¹⁵².

2.6.2 *NPM1*

Nucleophosmin 1 (*NPM1*) gene is located on chromosome 5q35, comprises 12 exons, and encodes a ubiquitous nucleus-cytoplasmic shuttling protein primarily found in the nucleolus^{153,154}. *NPM1* protein is involved in multiple cellular processes, including genomic stability maintenance, and DNA damage response¹⁵⁵.

NPM1 consists of three domains: a central region that enables histone binding, an N-terminus, and a C-terminus. The amino-terminal core region is located at the N-terminus and is crucial for partner interactions to build up the nucleolus structure. The N-terminus has two nuclear exporter signals (NES)¹⁵⁶. *XPO1*, a primary karyopherin protein, facilitates nuclear export. Together with *XPO1*, NES is essential in localizing *NPM1* from the nucleoplasm to the cytoplasm¹⁵⁷. In collaboration with *XPO1*, known *NPM1* mutations result in enhancing nuclear exportation and inactivating the function of mutant *NPM1*¹⁵⁸. The C-terminus is stabilized by Phe268, Phe276, Trp288, and Trp290. Mutants of Trp288 and/or Trp290 cause the *NPM1c* variant which shows an aberrant delocalization of *NPM1* to the cytoplasm, e.g., in AML, severely altering protein function¹⁵⁹. The mutated *NPM1* C-terminus protein could be targeted and degraded by a small molecule, Avrainvillamide, which shows vigorous activity in decreasing the proliferation of *NPM1*-mutated cell in an AML PDX model¹⁶⁰.

NPM1 mutations are the most prevalent genetic aberrations in AML, occurring in approximately 30% of adult AML and much less frequently in childhood AML with approximately 5%¹⁶¹. Recent research shows that the overexpression of *HOX* genes associated with stem cell signature is facilitated by *NPM1* mutations, leading to an arrest of differentiation of AML cells through nuclear re-localization or targeted degradation^{157,161,162}. The *XPO1* inhibitor, Selinexor, could correct the delocalization of mutant *NPM1* and benefit AML patients with *NPM1* mutations¹⁶³. Newly diagnosed AML patients harboring *NPM1* mutations are now considered as a distinct subgroup¹⁶⁴. Patients with isolated *NPM1* mutations belong to the favorable risk group and show high response rates. However, this prognostic impact is significantly affected and converted into poor prognosis if *NPM1* mutations co-occur with *DNMT3A* mutations or *FLT3* mutations in AML^{161,165}. The prognostic relevance of *NPM1* mutations regarding response to different therapies in R/R AML patients is still under investigation¹⁶⁶.

2.6.3 *DNMT3A*

The de novo methyl transferase 3A (*DNMT3A*) is located on chromosome 2p23.3 and is coded by 23 exons expressed in two isoforms, *DNMT3A1* and *DNMT3A2*^{167,168}. *DNMT3A* consists of three domains¹⁶⁷. The Pro-Trp-Trp-Pro (PWWP) domain is involved in specific DNA recognition and binding. The ATRX-DNMT3-DNMT3L (ADD) domain mediates protein-protein interactions. The methyltransferase (MTase) domain is also called the S-adenosyl methionine (SAM)-dependent methyltransferase C5-type domain and catalyzes cytosine methylation in DNA. There are 219 extra amino acids in the long isoform *DNMT3A1*, which has increased DNA binding affinity and methylation activity¹⁶⁷.

DNMT3A mutations exist in more than 30% of karyotypically normal AML patients and could be detected in early leukemogenesis¹⁶⁹. The main types of *DNMT3A* mutations are nonsense, frameshift, and missense

alterations located within the MTase domain and thus induce the loss of *DNMT3A* function¹⁷⁰. Codon R882 is a hot spot mutation site with around 60% prevalence. The most prevalent mutation in R882 is R882H, which has been demonstrated to exert a dominant-negative effect on unmutated *DNMT3A*, resulting in reduced MTase activity¹⁷¹. The hypomethylation of hematopoietic stem cell (HSC)-related genes is thought to enhance self-renewal capacity in stem cell, reduce differentiation, and is involved in leukemogenesis¹⁷². Comparing to wild-type *DNMT3A* AML patients, patients harboring the *DNMT3A* R882H mutation have worse outcomes¹⁷³. Furthermore, *DNMT3A* mutations frequently coexist with *NPM1* mutations, *FLT3-ITD*, and *IDH1/2*, associated with shorter overall survival in AML patients¹⁷⁴.

DNMT3A mutant AML patients benefit from approved therapies, including dose-intensified anthracyclines during induction and low-dose cladribine with hypomethylating agents in older age groups such as *HDAC* inhibitors combined with azacytidine in a phase III trial^{175,176}. Moreover, treatments targeting co-occurring genetic alterations like BTK inhibitors, *FLT3* inhibitors, *BRD4* inhibitors, and BET inhibitors have become new choices for AML patients in the last five years²⁴. Furthermore, novel agents harnessing structural alterations in mutant *DNMT3A* protein as selective agents are under investigation¹⁷⁷.

2.6.4 *WT1*

Wilms' tumor 1 (*WT1*) gene was initially recognized as a predisposition gene for familial Wilms tumor in 1990¹⁷⁸. It is located on chromosome 11p13 and contains ten exons¹⁷⁹. The *WT1* gene encodes a transcription factor involved in RNA and protein interactions. It has four zinc-fingers motifs at the C-terminus and a DNA binding domain at the N-terminus¹⁸⁰. The *WT1* protein has four predominant isoforms derived from two splicing events: exon 5 splicing gives rise to two isoforms with or without a 17 amino acid insertion, exon 9 splicing at 3' end causes two isoforms with or without three amino acids including Lysine, Serine, and Threonine (KTS)¹⁸¹. The isoform without KTS insertion has more vital DNA binding activity and transcriptional activity, while the isoform containing KTS insertion has additional functions involving post-transcriptional processes¹⁸². Studies have shown that the differential expression of various *WT1* isoforms might be associated with different prognosis in AML patients^{183,184}.

WT1 is a crucial regulator involved in cell survival, growth and differentiation processes¹⁸⁵. The expression of *WT1* could be detected in CD34+ cells in normal hematopoiesis¹⁸⁶. Overexpression of *WT1* has been demonstrated in primary AML patients and AML cell lines. It is related to treatment resistance, higher incidence of relapse, and poor prognostic outcomes¹⁸⁷. Further studies characterized the contribution of *WT1* in leukemogenesis and found that *WT1* overexpression led to rapid leukemia development but was not required for leukemia propagation¹⁸⁷. However, the role of *WT1* overexpression in established leukemias remains unprecise.

Around 10% of AML patients harbor *WT1* mutations, which is correlated with younger age, and co-occurring with *CEBPA* mutation and *FLT3-ITD*¹⁸⁸. The major type of *WT1* mutation is a nonsense mutation, leading to the production of a truncated protein either expressed or degraded¹⁸⁹. The clinical significance of *WT1* mutations in AML patients is contradictory. One cohort containing more than 400 AML individuals

(without acute promyelocytic leukemia) showed that patients with *WT1* mutations had a worse overall survival, lower relapse-free survival rates, and higher chemotherapy resistance¹⁹⁰. However, another study showed that *WT1* mutations were unrelated to overall survival and relapse-free survival in patients treated with high-dose cytarabine¹⁹¹. More studies are needed to comprehend the effect of *WT1* mutational background on patient outcomes.

The assessment of therapies for individuals with AML overexpressing wildtype or mutated *WT1* is underway as the WT1 protein is also used as surface protein for immunotherapies. Peptide vaccines exhibit noteworthy responses, eliciting heightened frequencies of *WT1*-specific T-cells without eliciting autoimmune reactions¹⁹². Moreover, the monoclonal antibody, RMF-peptide-MHC-specific T-cell bispecific antibody, was studied in AML cell lines and primary cells in both *in vivo* and *in vitro* settings and showed effective killing capacity¹⁹³. Furthermore, this antibody is currently undergoing a phase I trial for R/R AML¹⁹³. These novel treatment strategies indicate the major potential of *WT1* as attractive surface molecule for immunotherapies.

2.6.5 *DUX4*

The double homeobox 4 (*DUX4*) gene is located at chromosome 4q within a D4Z4 repeat array and comprises 3 exons¹⁹⁴. Within each D4Z4 repeat lies an open reading frame (ORF) of *DUX4* and thus a highly variable copy number exists between individuals, ranging from 11 to 150, discernible on chromosome 4 and 10¹⁹⁵. The *DUX4* gene encodes double homeoboxes and acts as a transcriptional programmer, regulating the cleavage-stage transcriptional platform and the zygotic genome, and is silenced in most somatic tissues¹⁹⁶. *DUX4* might become activated in pathogenic conditions due to changes in chromatin packing¹⁹⁷.

The misexpression of *DUX4* has been proven to be associated with facioscapulohumeral dystrophy (FSHD), while *DUX4* rearrangements are detected in around 7% of B-cell ALL patients and result in a truncated *DUX4* protein overexpression^{198,199}. The truncated *DUX4* protein binds to the ETS transcription factor (ERG) or immunoglobulin heavy locus (IGH) intragenic region and deregulates their transactivation²⁰⁰. In patients with *DUX4* rearrangements, the predominant cases were found to harbor a *DUX4-IGH* fusion. The *DUX4-IGH* fusion has been found to impair mouse pro-B cell differentiation and elicit leukemic transformation²⁰⁰. Nalm6 harbors the *IGH-DUX4* translocation and knocking down *DUX4-IGH* in Nalm6 cells induced a growth disadvantage²⁰¹. *DUX4* rearranged ALL is identified as a new oncogenic subtype of B-cell precursor (BCP)-ALL and shows lower early treatment response rate, but favorable long-term outcome, even in patients with *IKZF1* deletions²⁰². Children with *DUX4*-rearranged B-ALL exhibit high overall survival rates and low relapse rates²⁰³. The typical clinical genetic alternation diagnosis is based on karyotyping, FISH, and RT-PCR. However, *DUX4* fusions are not detectable by fusion transcript assay²⁰⁴, while targeted RNA sequencing might improve its diagnosis in ALL.

2.6.6 *DDIT4L*

DNA-damage-inducible transcript 4-like (*DDIT4L*), also known as *REDD2* and *RTP801L*, is a protein-coding gene in human cells located in chromosome 4,²⁰⁵. *DDIT4L* is involved in the mTOR signaling

pathway and is implicated in cell death under hypoxic conditions²⁰⁵. In mouse bone marrow cells, *DDIT4L* could interact with the critical hematopoietic transcription factor, IRF-1, and regulate cell growth and apoptosis²⁰⁶. *DDIT4L* overexpression was shown to promote autophagy in cardiomyocytes under pathological stress²⁰⁷. In melanoma, *DDIT4L* promoter methylation was detected and analyzed by genome-wide methylation-sensitive representation difference analysis, and the hypermethylation of *DDIT4L* was mostly detected in advanced-stage tumors²⁰⁸, while studies on *DDIT4L* in leukemia are entirely lacking.

2.7 Summary of the studies

Acute leukemia is a heterogeneous hematologic malignancy which is characterized by abnormal stem cell differentiation and proliferation driven by chromosomal abnormalities and genetic alterations. Unfortunately, patients with acute leukemia in certain subgroups still have a very poor prognosis and novel treatment options are urgently needed.

Dependency genes are genes which play an essential role for cell growth and survival. Molecular targeting of these dependencies, for example via CRISPR/Cas9 KO reduces tumor cell viability and tumor burden. T respective proteins transcribed from a dependency gene represent an attractive therapeutic target as its inhibition by a drug might also kill cancer cells. As higher problem connecting the publications, this thesis work aimed to identify new dependency genes in acute leukemia in order to allow developing new therapeutic drugs to treat acute leukemia patients.

In the present work, the author searched for new gene dependencies which might allow novel treatment options for acute leukemias. The author used the orthotopic PDX mouse model, which is a clinically relevant surrogate for human AML, enabling the study of individual patient tumor cells *in vivo*. The author applied reverse genomic techniques, such as CRISPR/Cas9-mediated knockout (Publication I) and RNAi-mediated knockdown (Publication II), to determine genes indispensable for leukemia growth and survival.

2.7.1 Publication I: *WT1* and *DNMT3A* play essential roles in the growth of certain patient AML cells in mice

Several genes recurrently mutated in AML were shown to be responsible for both leukemogenesis as well as for keeping established tumors alive and growing. In this study, we aimed to identify additional yet unknown dependency genes within the genes recurrently mutated in AML, which represent putative therapeutic vulnerabilities.

The author of this dissertation successfully performed CRISPR/Cas9 library screens in AML PDX models *in vivo*, which allowed us to investigate dependency genes in a more patient-related background and in an *in vivo* environment. By generating single KOs and performing *in vivo* competitive validation assays in AML PDX cells and AML cell lines either *in vivo* or *in vitro*, the author of this dissertation, together with the other first author, has identified *WT1* and *DNMT3A* as previously unknown dependency genes in AML, with a dependency restricted to a subset of AML samples and to the *in vivo* setting and thus overlooked by previous *in vitro* studies. Additionally, in homing assays, *WT1* and *DNMT3A* KO leukemia stem cells presented engraftment disadvantages in early stage of leukemia *in vivo*, which indicated an impaired leukemia

stem cell homing capacity. This suggested that *WT1* and *DNMT3A* were essential for stem cell homing to the bone marrow niche. In re-transplantation assays, *WT1* and *DNMT3A* KO cells harvested from first recipient mice showed decreased engrafted cell numbers in secondary recipient mice. In LDFA assay, *WT1* KOs had a lower number of leukemia stem cells which allowed engraftment of PDX cells *in vivo*; these results demonstrated the dependency AML PDX stem cells on *WT1* and *DNMT3A* *in vivo*. In summary, *WT1* and *DNMT3A* may represent future therapeutic targets for selected AML patients.

2.7.2 Publication II: *In vivo* inducible reverse genetics in patients' tumors to identify individual therapeutic targets

In this study, we aimed to prove whether genes characterized as dependency genes in cell lines *in vitro* would also display a dependency function in PDX models *in vivo*. We established the first worldwide inducible system for gene knockdown *in vivo* in PDX acute leukemia models using a Cre-ER^{T2}-loxP-based RNAi-mediated gene silencing system. It could induce a partial inhibition of a target gene, which closely mimics the clinical situation, as the treatment of individual patients with drugs or compounds induces a partial inhibition of their target proteins.

Using *in vivo* inducible RNA interference, the author of this dissertation observed higher apoptosis rate in sh*MCL1* AML-388 cells, but not in sh*MCL1* ALL-199 and ALL-265. The author of this dissertation observed smaller and lighter spleens, and less number of human cells in the spleen after *MCL1* inhibitor treatment in AML-388 mice but not in ALL-199 mice. Together with the bone marrow data generated by co-first author, we found that *MCL1* dependency was observed in AML-388, but not ALL-199 and ALL-265, such that the dependency on the *MCL1* gene as shown by knockdown experiments was associated with sensitivity to *in vivo* treatment with the *MCL1* inhibitor. We verified *MCL1* dependency using the inducible system we established. Furthermore, the author of this dissertation applied *DUX4* and *DDIT4L* inducible knockdown in *DUX4-IGH* rearranged PDX ALL-811 and NALM6 cells and found lower relative *DDIT4L* mRNA levels in sh*DUX4* cells and sh*DDIT4L* cells compared to controls. Taken together, we identified *DDIT4L* as a novel dependency gene in *DUX4-IGH* rearranged ALL.

To sum up, the author of this dissertation used reverse genetic approaches such as gene knockout and gene knockdown to identify gene dependencies in PDX models of acute leukemias *in vivo* and thereby novel therapeutic targets which broadened the treatment possibility of acute leukemia patients.

Paper I

novo acute lymphoblastic leukemia, but outcomes are comparable in transplanted patients. *Haematologica*. 2018;103(10):1662-1668.

11. Saygin C, Kishtagari A, Cassaday RD, et al. Therapy-related acute lymphoblastic leukemia is a distinct entity with adverse genetic features and clinical outcomes. *Blood Adv*. 2019;3(24):4228-4237.
12. Furstenau M, Fink AM, Schilhabel A, et al. B-cell acute lymphoblastic leukemia in patients with chronic lymphocytic leukemia treated with lenalidomide. *Blood*. 2021;137(16):2267-2271.
13. Aldoss I, Capelletti M, Park J, et al. Acute lymphoblastic leukemia as a clonally unrelated second primary malignancy after multiple myeloma. *Leukemia*. 2019;33(1):266-270.
14. Tan M, Fong R, Lo M, Young R. Lenalidomide and secondary acute lymphoblastic leukemia: a case series. *Hematol Oncol*. 2017;35(1):130-134.
15. Sperling AS, Guerra VA, Kennedy JA, et al. Lenalidomide promotes the development of TP53-mutated therapy-related myeloid neoplasms. *Blood*. 2022;140(16):1753-1763.
16. Iriyama N, Tokuhira M, Takaku T, et al. Incidences and outcomes of therapy-related chronic myeloid leukemia in the era of tyrosine kinase inhibitors: Surveillance of the CML cooperative study group. *Leuk Res*. 2017;54:55-58.
17. Yang LH, Su P, Luedke C, et al. Chronic myeloid leukemia following treatment for primary neoplasms or other medical conditions. *Am J Clin Pathol*. 2018;150(3):246-258.
18. Waller CF, Fetscher S, Lange W. Treatment-related chronic myelogenous leukemia. *Ann Hematol*. 1999;78(8):341-354.
19. Curtis RE, Boice JD Jr, Stovall M, et al. Risk of leukemia after chemotherapy and radiation treatment for breast cancer. *N Engl J Med*. 1992;326(26):1745-1751.
20. Nandakumar A, Davis S, Moolgavkar S, Witherspoon RP, Schwartz SM. Myeloid leukaemia following therapy for a first primary cancer. *Br J Cancer*. 1991;63(5):782-788.
21. Curtis RE, Boice JD Jr, Stovall M, Flannery JT, Moloney WC. Leukemia risk following radiotherapy for breast cancer. *J Clin Oncol*. 1989;7(1):21-29.
22. Subari S, Patnaik M, Alfakara D, et al. Patients with therapy-related CMML have shorter median overall survival than those with de novo CMML: mayo clinic long-term follow-up experience. *Clin Lymphoma Myeloma Leuk*. 2015;15(9):546-549.
23. Takahashi K, Pemmaraju N, Strati P, et al. Clinical characteristics and outcomes of therapy-related chronic myelomonocytic leukemia. *Blood*. 2013;122(16):2807-2811. quiz 2920.
24. Does GM, Curtis RE, Linet MS, Morton LM. Cause-specific mortality following polycythemia vera, essential thrombocythemia, and primary myelofibrosis in the US population, 2001-2017. *Am J Hematol*. 2021;96(12):E451-E454.
25. McNerney ME, Godley LA, Le Beau MM. Therapy-related myeloid neoplasms: when genetics and environment collide. *Nat Rev Cancer*. 2017;17(9):513-527.

<https://doi.org/10.1182/blood.2022018051>

TO THE EDITOR:

WT1 and *DNMT3A* play essential roles in the growth of certain patient AML cells in mice

Maryam Ghalandary,^{1,*} Yuqiao Gao,^{1,*} Diana Amend,¹ Ginte Kutkaite,^{2,3} Binje Vick,^{1,4} Karsten Spiekermann,⁵ Maja Rothenberg-Thurley,⁵ Klaus H. Metzeler,^{5,6} Anetta Marcinek,⁵ Marion Subklewe,⁵ Michael P. Menden,^{2,3,7} Vindi Jurinovic,¹ Ehsan Bahrami,¹ and Irmela Jeremias^{1,4,8}

¹Research Unit Apoptosis in Hematopoietic Stem Cells and ²Institute of Computational Biology, Helmholtz Zentrum München, German Research Center for Environmental Health, Munich, Germany; ³Department of Biology, Ludwig-Maximilians University Munich, Martinsried, Germany; ⁴German Cancer Consortium, Partner Site Munich, Munich, Germany; ⁵Laboratory for Leukemia Diagnostics, Department of Medicine III, University Hospital, Ludwig Maximilians University, Munich, Germany; ⁶Department of Hematology and Cell Therapy, University Hospital Leipzig, Leipzig, Germany; ⁷German Centre for Diabetes Research, Neuherberg, Germany; and ⁸Department of Pediatrics, University Hospital, Ludwig Maximilians University, Munich, Germany

Patients with acute myeloid leukemia (AML) experience poor prognosis, and precision oncology represents an attractive therapeutic option, applying targeted therapies against so-called dependencies.¹⁻⁴ Dependencies are essential components required for cell growth and survival; they represent attractive therapeutic targets as their inhibition reduces tumor burden.¹⁻⁴

Many genes recurrently mutated in AML contribute to oncogenesis,^{5,6} which may imply a role as dependency and allow precision therapy, based on genetic profiling. Examples already in routine clinical practice include AML with mutated FMS related receptor tyrosine kinase 3 treated with midostaurin and AML with mutated isocitrate dehydrogenase responding to ivosidenib.² Herein, we asked whether additional recurrently mutated genes might represent dependencies in established AML.

Previous efforts to identify dependencies used established cell lines, including large-scale functional genomic screens; *WT1* and

DNMT3A were shown to be dispensable in AML cell lines.⁷ As a limitation, cell lines might acquire nonphysiologic alterations, and discrepant results have been described (eg, between cell lines and organoids).^{8,9} To approximate the clinical situation, we studied patient-derived xenograft (PDX) models^{10,11} and mimicked the complex in vivo situation by performing CRISPR/CRISPR associated protein 9 (Cas9) knockout (KO) studies in mice. Using this highly patient-related in vivo approach, we identified *WT1* and *DNMT3A* as yet unknown dependencies in a subset of patients' AML tumor cells.

From our toolbox of serially transplantable AML xenografts,¹² models derived from 7 patients were selected for the study (supplemental Tables 1-3, available on the *Blood* website). Genetically engineered PDX (GEPDX) models were generated that stably expressed recombinant Cas9 (supplemental Figure 1A).

We had recently established in vivo CRISPR/Cas9 dropout screens in GEPDX models of acute lymphoblastic leukemia¹³; herein, we transferred the technique to AML, which resulted in favorable quality controls (Figure 1A; supplemental Figure 2A). The 34 most frequently mutated genes in AML were studied, restricted to gain-of-function or change-of-function mutations.⁵ A library was designed containing 5 single-guide RNAs per target gene, together with positive and negative controls (supplemental Tables 4 and 5); the library was cloned into a lentiviral vector that coexpressed recombinant markers to enrich successfully transduced cells, using our custom library multiplexed cloning (CLUE) technique (supplemental Figures 1 and 2A; supplemental Tables 3 and 4).¹⁴

A CRISPR/Cas9 dropout screen was performed with 5 GEPDX models. KO resulted in dropout in about half of all genes from the screen, albeit to varying degrees, and most KO induced similar effects across the PDX samples (Figure 1B; supplemental Figure 2B; supplemental Tables 6-8). Confirming the robustness of our technical approach, genes with known common essential function or genes required for the hematopoietic system were strongly depleted in the KO screen. Among them, *NPM1* was a dropout hit and served as a positive control, as it is known to have a broad essential function in malignant cells (Figure 1B).⁷ Another expected hit was *KRAS*, which is one of the genes most frequently mutated across all cancers and known to represent a dependency in numerous tumor types, including AML.^{15,16}

Hits from dropout screens require validation, and single-KO experiments were performed as competitive in vivo assays where all cell populations are studied under identical conditions within the same mouse, giving robust results at low resources.¹⁸ Recombinant fluorochromes enabled an unbiased differentiation of cell populations by flow cytometry (Figure 1C-D; supplemental Figure 3). For each gene of interest as well as for nontargeting controls, 3 different, highly efficient single-guide RNAs were tested in 3 independent mixtures (supplemental Figures 4 and 5). From the 7 PDX models studied, up to 5 PDX models gave reliable results for each gene.

NPM1 was included as a positive control, and KO of *NPM1* completely eliminated AML GEPDX cells in all GEPDX models tested in vivo (Figure 1E). *KRAS* was studied in PDX models carrying mutant *KRAS* at variant allele frequencies of either 0 or close to 0.5, avoiding intrasample heterogeneity. *KRAS* KO revealed a strong dropout in all GEPDX models studied, which was significantly more pronounced in *KRAS*^{mutant} PDX models than *KRAS*^{wildtype} PDX models (Figure 1F; supplemental Figure 6). Thus, our PDX models strengthen previously published data showing that *KRAS* represents a dependency and attractive therapeutic target in AML, especially in tumors carrying a *KRAS* mutation.¹⁶

Next, we examined 2 genes with poorly defined roles in oncogenes and for which we had suitable PDX models with appropriate variant allele frequencies at hand (supplemental Table 1). Although data on *WT1* as an oncogene are controversial,^{19,20} *DNMT3A* mainly represents a tumor suppressor, required for hematopoietic differentiation.²¹⁻²⁴

Reproducing published data with our own tools,⁷ we found no evidence that either *WT1* or *DNMT3A* might play a role as dependencies in AML cell lines, with trends toward slightly increased proliferation rates on gene KO (supplemental Figures 7-9; supplemental Table 1). In contrast and surprisingly, in in vivo GEPDX models, we discovered a pronounced dropout of either of both genes on KO in certain PDX models (Figure 2A). Thus, *WT1* and *DNMT3A* represent dependencies in a subset of PDX AML models in vivo, indicating an obvious discrepancy with their function in cell lines in vitro (Figure 2B), without any meaningful impact on the immunophenotype (supplemental Figure 10). PDX models showed dropout of *WT1* or *DNMT3A* exclusively in the in vivo environment on which PDX cells depend as opposed to cell lines, suggesting that in vivo approaches are required to unmask certain dependencies in AML (Figure 2C). There was no correlation between dependency on *DNMT3A* and presence of a somatic hot spot mutation in *DNMT3A* in the GEPDX models (supplemental Figure 6D). In the transcriptome, KO of *WT1* or *DNMT3A* was accompanied by regulation of biological processes, such as apoptosis and oxidative phosphorylation (Figure 2D; supplemental Figure 11).

When characterizing in vivo essentiality in more detail, we found that KO of *WT1* induced a certain increase in the antitumor effect of cytarabine, an important drug in routine treatment of AML (supplemental Figure 12). *WT1* KO reduced the capacity of AML-346 cells to home to the bone marrow environment on either intrafemoral or intravenous cell injection followed by early in vivo growth disadvantage, suggesting an impaired tumor-niche interaction (supplemental Figures 13 and 14). KO of either *WT1* or *DNMT3A* reduced the numbers of leukemia-initiating cells in competitive limiting dilution transplantation assays and prevented reengraftment of AML-346 cells into secondary recipient mice, with and without prior cell enrichment, indicating that stem cell surrogates were depleted on *WT1* or *DNMT3A* KO (Figure 2E; supplemental Figure 15). Taken together, our data reveal that *WT1* and *DNMT3A* represent dependencies in a subset of AML GEPDX models in vivo, suggesting that they might represent therapeutic targets.

Our study identified *WT1* and *DNMT3A* as dependencies in a subset of patient AML PDX samples growing in vivo, although less pronounced and less frequent compared with *KRAS*. KO of *WT1* and *DNMT3A* impaired PDX AML growth in vivo, attenuated the tumor-niche interaction, eradicated AML stem cells, and increased treatment response.

Although cell lines did not reveal the phenotype, PDX models proved valuable tools to identify dependency on *WT1* and *DNMT3A* and might more closely resemble patient's tumors.^{10,11} Our technique now allows studying gene dependencies in patient PDX models in vivo (eg, to personalize pharmacologic precision therapy). Our data encourage testing additional genes recurrently mutated in AML for their essentiality in PDX models in vivo (eg, additional dropout candidates from our screens).

The essential function of *WT1* identified herein fits with its previously described oncogenic function,¹⁹ whereas different

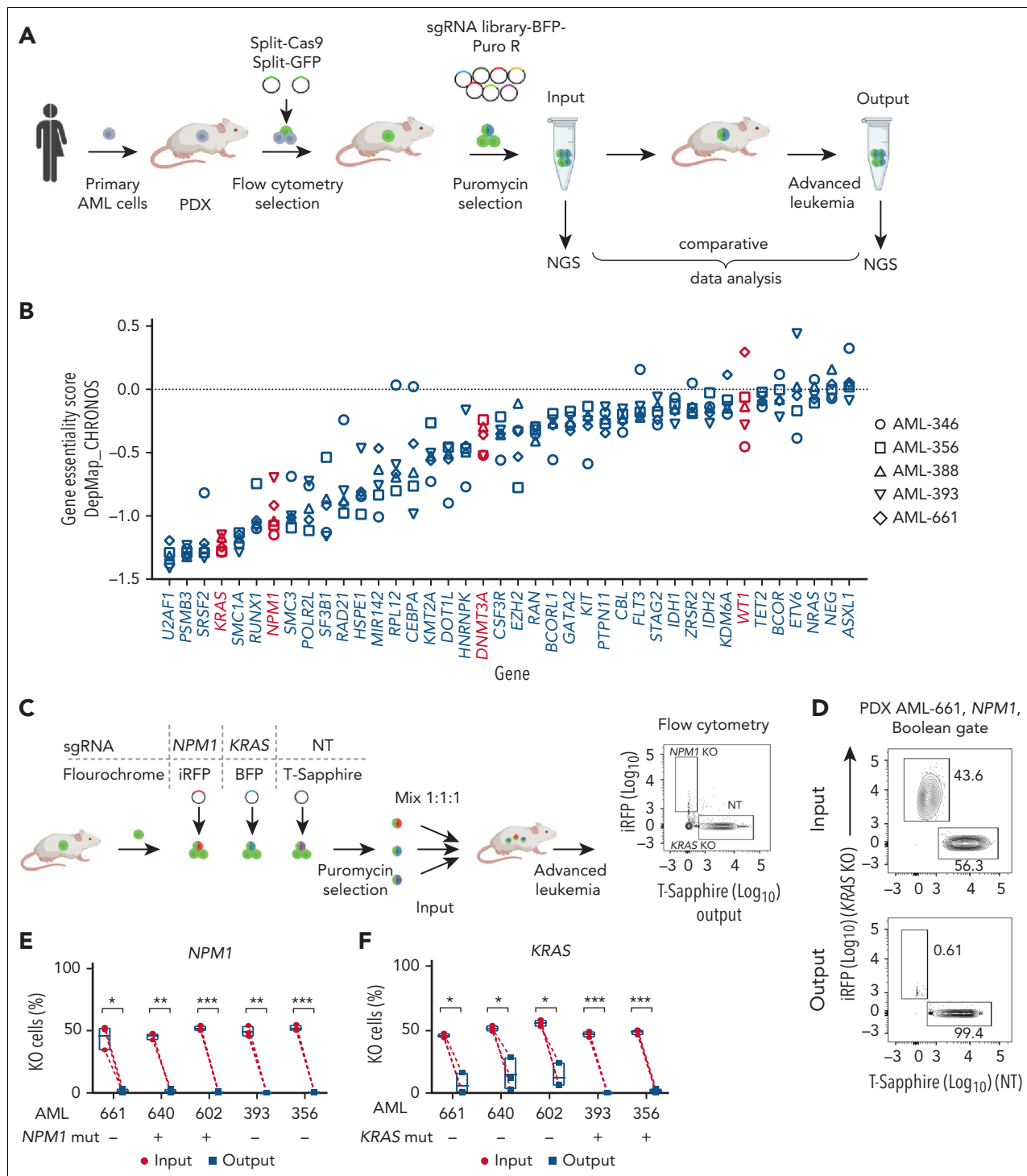


Figure 1. PDX models depend on *KRAS* and *NPM1* for in vivo growth. (A) Experimental procedure for CRISPR/Cas9 in vivo screens performed with PDX models. Serially transplantable AML PDX models were established from primary patient AML cells and lentivirally transduced to express a split version of Cas9 together with a single-guide RNA (sgRNA) library (see supplemental Figure 1 for constructs). Transgenic cells were enriched by flow cytometry (Cas9–green fluorescent protein [GFP]) and puromycin selection (sgRNA library). Except for the input control aliquot, cells were injected into groups of mice and recovered from the mice at advanced leukemia stage (output). Next-generation sequencing (NGS) was performed and analyzed using the DepMap_CHRONOS, Lin et al.,¹⁷ MAGeCK algorithm to compare sgRNA distribution between input and output. (B) CRISPR/Cas9 in vivo dropout screens were performed in 5 PDX AML models using the library of 34 genes recurrently mutated in AML; gene essentiality scores were calculated using the DepMap_CHRONOS algorithm (see supplemental Figure 2 for quality controls). (C) Experimental procedure for competitive in vivo assays for single-hit validation. sgRNAs targeting either *KRAS* or *NPM1* or nontargeting (NT) sgRNAs (n = 3 per gene) were cloned into the sgRNA construct together with the appropriate fluorochromes and transduced into Cas9–GFP–expressing PDX cells. After puromycin selection, 3 subpopulations (*KRAS* KO, *NPM1* KO, and NT sgRNA) were mixed at a 1:1:1 ratio as an input. Three replicate mixtures, each containing different sgRNAs, were transplanted into one mouse each (9 different sgRNAs per experiment in 3 replicate mice) and recovered at advanced disease stage (output). The distribution of the subpopulations was analyzed by flow cytometry (see supplemental Figure 3 for the step-by-step analysis and supplemental Figures 4 and 5 for quality controls). Blue fluorescent protein (BFP). (D) Representative flow cytometry plots for *KRAS* KO1 and NT-1 in AML-661, using Boolean gating. (E and F) Quantitative summaries of the knockout effects for *NPM1* (E) and *KRAS* (F) in all PDX models studied. Each dot represents the percentage of gene of interest KO population from a single mouse, with related sgRNAs linked by a dotted line. Bar plots indicate mean, minimum, and maximum. The results of a 2-tailed paired t-test are shown if they were significant: **P* < .05, ***P* < .01, and ****P* < .001.

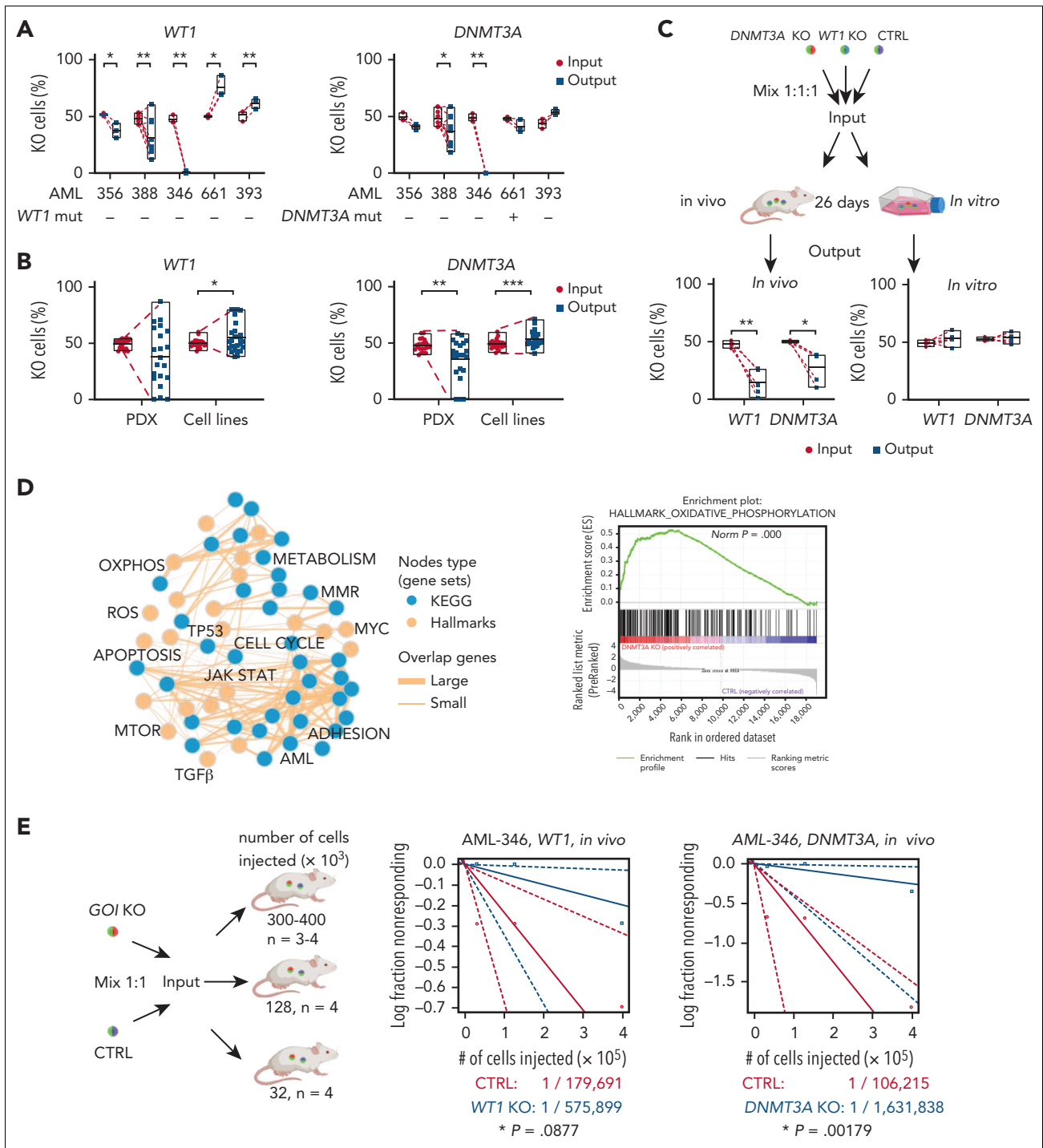


Figure 2. Certain PDX models depend on WT1 and DNMT3A for in vivo growth. (A) Competitive in vivo assays were performed, analyzed, and depicted as in Figure 1C,D, except that WT1 and DNMT3A were studied (see supplemental Figure 6 for quality controls). (B) Comparing gene dependency in PDX models vs cell lines. Raw data from Figure 2A and supplemental Figures 8 and 9 are summarized using a single dot for each single KO of each PDX model or cell line. For each PDX model or cell line, 3 single-guide RNAs (sgRNAs) per gene were studied. Results of an unpaired t-test are shown if they were significant (* $P < .05$, ** $P < .01$, and *** $P < .001$). (C) Comparing behavior of PDX cells with KO in vitro vs in vivo. Experiment with AML-346 cells was performed, analyzed, and depicted as in Figure 2A, except that the incubation time was 26 days and an aliquot of cells was kept in vitro (* $P < .05$, ** $P < .01$, and *** $P < .001$). (D) Transcriptomes of AML-356, AML-388, AML-661, and AML-346 cells with DNMT3A knockdown were compared with nontargeting (NT) control (raw and complementary data in supplemental Figure 10). Gene enrichment map shows gene overlap (lines) in gene sets of hallmarks (orange nodes) and Kyoto Encyclopedia of Genes and Genomes (KEGG) (blue nodes) pathways. Node size is proportional to the number of genes in each set; the proportion of shared genes between gene sets is depicted by the thickness of the line between nodes. Enrichment plot shows the genes differentially regulated in the hallmark oxidative phosphorylation on KO of DNMT3A (normalized enrichment score [NES] = 2.1537; $P < .001$; adjusted P [false discovery rate q -value] < 0.001). (E) Limiting dilution transplantation assay. PDX AML-346 cells were transduced with sgRNAs against WT1 or DNMT3A or control (CTRL), enriched, mixed in a 1:1 ratio for WT1:CTRL or DNMT3A:CTRL, and injected into 4 mice each at 400 000, 128 000, or 32 000 cells per mouse (WT1, $n = 12$; and DNMT3A, $n = 11$ mice). After 14 weeks, bone marrow was analyzed by flow cytometry, and data were analyzed using the ELDA software. Mean (solid lines) and 95% confidence interval (CI; dashed line) are depicted.

phenotypes between different PDX models might mirror conflicting data on *WT1* obtained during leukemogenesis.^{19,20}

For *DNMT3A*, a prevailing tumor suppressor function was described,²¹⁻²³ making a dependency function unlikely. Amid complexity, a tumor-supportive function of mutant *DNMT3A* was reported in specific AML subsets (eg, AML driven by a partial tandem duplication in *KMT2A*).²⁵ AML-388 harbors a *KMT2A-AFDN* translocation (supplemental Table 2), indicating that *KMT2A*-driven AML might preferably depend on *DNMT3A*.

Taken together, our molecular PDX AML in vivo studies allowed identifying *WT1* and *DNMT3A* as dependencies and putative therapeutic targets in defined subsets of AML, warranting further evaluation.

Acknowledgments

The authors thank Martin Becker for helping to perform the CRISPR Cas9 screens; Lucas E. Wange and Wolfgang Enard (LMU München) for the measuring transcriptome; Jan Philipp Schmid for help with the limiting dilution transplantation assay; Katharina Hunt for helping with in vivo experiments; Helmut Blum, Stefan Krebs, and the LaFuGa team (LMU München) for sequencing; Markus Brielmeier and his team (Research Unit Comparative Medicine, Helmholtz Zentrum München) for providing animal care services; Daniela Senft for discussion; Liliana Mura, Fabian Klein, Maik Fritschle, Annette Frank, and Miriam Krekel for excellent technical assistance; and Stephanie Hoffmann for laboratory management assistance.

This project received funding from the European Research Council under the European Union's Horizon 2020 research and innovation programme (Consolidator Grant no. 681524 [I.J.] and Starting Grant no. 950293 [M.P.M.]); a Mildred Scheel Professorship by German Cancer Aid (I.J.); Bettina Bräu Stiftung and Helmut Legerlotz Stiftung (I.J.); and the China Scholarship Council (CSC no. 202108080142) (Y.G.).

Authorship

Contribution: M.G. and Y.G. designed and performed experiments and designed figures; D.A. performed CLUE cloning; G.K. and M.P.M. analyzed DepMap data; B.V. established patient-derived xenograft models and in vivo chemotherapy protocols; K.S. provided primary acute myeloid leukemia samples; A.M. and M.S. performed immunophenotype assay; M.R.-T. and K.H.M. performed panel sequencing; E.B. and V.J. analyzed the single-cell RNA barcoding and sequencing data; and I.J. designed the study, guided the experiments, and wrote the manuscript, with the help of all authors.

Conflict-of-interest disclosure: M.P.M. is a former employee at AstraZeneca, academically collaborates with AstraZeneca, GSK, and Roche, and receives funding from GSK and Roche. The remaining authors declare no competing financial interests.

ORCID profiles: G.K., [0000-0002-2918-294X](https://orcid.org/0000-0002-2918-294X); B.V., [0000-0003-1956-2778](https://orcid.org/0000-0003-1956-2778); K.S., [0000-0002-5139-4957](https://orcid.org/0000-0002-5139-4957); K.H.M., [0000-0003-3920-7490](https://orcid.org/0000-0003-3920-7490); M.S., [0000-0003-3905-0251](https://orcid.org/0000-0003-3905-0251); M.P.M., [0000-0003-0267-5792](https://orcid.org/0000-0003-0267-5792); E.B., [0000-0002-1672-5503](https://orcid.org/0000-0002-1672-5503); I.J., [0000-0003-1773-7677](https://orcid.org/0000-0003-1773-7677).

Correspondence: Irmela Jeremias, Helmholtz Center Munich, Feodor-Lynen-Str 21, 81377 Munich, Germany; email: irmela.jeremias@helmholtz-muenchen.de.

Footnotes

Submitted 23 March 2022; accepted 25 September 2022; prepublished online on *Blood* First Edition 18 October 2022.

*M.G. and Y.G. contributed equally to this study.

Transcriptome data generated in this study are publicly available in Gene Expression Omnibus at (GSE215836). Whole exome sequencing raw data generated in this study are not publicly available because of information that could compromise patient privacy or consent but are available on reasonable request from the corresponding author.

The online version of this article contains a data supplement.

REFERENCES

1. Kantarjian H, Kadia T, DiNardo C, et al. Acute myeloid leukemia: current progress and future directions. *Blood Cancer J*. 2021;11(2):41.
2. Short NJ, Konopleva M, Kadia TM, et al. Advances in the treatment of acute myeloid leukemia: new drugs and new challenges. *Cancer Discov*. 2020;10(4):506-525.
3. Park JJH, Hsu G, Siden EG, Thorlund K, Mills EJ. An overview of precision oncology basket and umbrella trials for clinicians. *CA Cancer J Clin*. 2020;70(2):125-137.
4. Lin A, Sheltzer JM. Discovering and validating cancer genetic dependencies: approaches and pitfalls. *Nat Rev Genet*. 2020;21(11):671-682.
5. Metzeler KH, Herold T, Rothenberg-Thurley M, et al. Spectrum and prognostic relevance of driver gene mutations in acute myeloid leukemia. *Blood*. 2016;128(5):686-698.
6. Mardis ER, Ding L, Dooling DJ, et al. Recurring mutations found by sequencing an acute myeloid leukemia genome. *N Engl J Med*. 2009;361(11):1058-1066.
7. Dempster JM, Pacini C, Pantel S, et al. Agreement between two large pan-cancer CRISPR-Cas9 gene dependency data sets. *Nat Commun*. 2019;10(1):5817.
8. Ben-David U, Siranosian B, Ha G, et al. Genetic and transcriptional evolution alters cancer cell line drug response. *Nature*. 2018;560(7718):325-330.
9. Unger C, Kramer N, Walzl A, Scherzer M, Hengstschlager M, Dolznig H. Modeling human carcinomas: physiologically relevant 3D models to improve anti-cancer drug development. *Adv Drug Deliv Rev*. 2014;79-80:50-67.
10. Woo XY, Giordano J, Srivastava A, et al. Conservation of copy number profiles during engraftment and passaging of patient-derived cancer xenografts. *Nat Genet*. 2021;53(1):86-99.
11. Ben-David U, Beroukhim R, Golub TR. Genomic evolution of cancer models: perils and opportunities. *Nat Rev Cancer*. 2019;19(2):97-109.
12. Vick B, Rothenberg M, Sandhofer N, et al. An advanced preclinical mouse model for acute myeloid leukemia using patients' cells of various genetic subgroups and in vivo bioluminescence imaging. *PLoS One*. 2015;10(3):e0120925.
13. Bahrami E, Becker M, Wirth AK, et al. A CRISPR/Cas9 library screen in patients' leukemia cells in vivo [abstract]. *Blood*. 2019;134(suppl 1):Abstract 3945.
14. Li W, Xu H, Xiao T, et al. MAGECK enables robust identification of essential genes from genome-scale CRISPR/Cas9 knockout screens. *Genome Biol*. 2014;15(12):554.
15. Asimgil H, Ertetik U, Cevik NC, et al. Targeting the undruggable oncogenic KRAS: the dawn of hope. *JCI Insight*. 2022;7(1):e153688.
16. Wang T, Yu H, Hughes NW, et al. Gene essentiality profiling reveals gene networks and synthetic lethal interactions with oncogenic Ras. *Cell*. 2017;168(5):890-903.e815.
17. Lin S, Scheidegger NK, et al. An In Vivo CRISPR Screening Platform for Prioritizing Therapeutic Targets in AML. *Cancer Discov*. 2022;12(2):432-449.

18. Liu WH, Mrozek-Gorska P, Wirth AK, et al. Inducible transgene expression in PDX models in vivo identifies KLF4 as a therapeutic target for B-ALL. *Biomark Res.* 2020;8:46.
19. Rampal R, Figueroa ME. Wilms tumor 1 mutations in the pathogenesis of acute myeloid leukemia. *Haematologica.* 2016;101(6):672-679.
20. Pronier E, Bowman RL, Ahn J, et al. Genetic and epigenetic evolution as a contributor to WT1-mutant leukemogenesis. *Blood.* 2018;132(12):1265-1278.
21. Mayle A, Yang L, Rodriguez B, et al. Dnmt3a loss predisposes murine hematopoietic stem cells to malignant transformation. *Blood.* 2015;125(4):629-638.
22. Celik H, Mallaney C, Kothari A, et al. Enforced differentiation of Dnmt3a-null bone marrow leads to failure with c-Kit mutations driving leukemic transformation. *Blood.* 2015;125(4):619-628.
23. Huang YH, Chen CW, Sundaramurthy V, et al. Systematic profiling of DNMT3A variants reveals protein instability mediated by the DCAF8 E3 ubiquitin ligase adaptor. *Cancer Discov.* 2022;12(1):220-235.
24. Challen GA, Sun D, Jeong M, et al. Dnmt3a is essential for hematopoietic stem cell differentiation. *Nat Genet.* 2011;44(1):23-31.
25. Bera R, Chiu MC, Huang YJ, Huang G, Lee YS, Shih LY. DNMT3A mutants provide proliferating advantage with augmentation of self-renewal activity in the pathogenesis of AML in KMT2A-PTD-positive leukemic cells. *Oncogenesis.* 2020;9(2):7.

<https://doi.org/10.1182/blood.2022016411>

© 2023 by The American Society of Hematology

***WT1* and *DNMT3A* play essential roles
in the growth of certain patient AML cells in mice**

Maryam Ghalandary^{1*}, Yuqiao Gao^{1*}, Diana Amend¹, Ginte Kutkaite^{2,3}, Binje Vick¹, Karsten Spiekermann⁴, Maja Rothenberg-Thurley⁴, Klaus H. Metzeler^{4,5}, Anetta Marcinek⁴, Marion Subklewe⁴, Michael P. Menden^{2,3,6}, Vindi Jurinovic¹, Ehsan Bahrami¹, Irmela Jeremias^{1,7,8,#}

This file contains:

Supplemental Methods

Supplemental Tables (8)

Supplemental Figures (15)

Supplemental Methods

Ethical Statement

Patient samples of adult AML patients were obtained from the Department of Internal Medicine III, Ludwig-Maximilians-Universität, Munich, Germany. Specimens were collected for diagnostic purposes before the start of treatment. Written informed consent was obtained from all patients. The study was performed in accordance with the ethical standards of the responsible committee on human experimentation (written approval by Ethikkommission des Klinikums der Ludwig-Maximilians-Universität Munich, number 068–08 and 222–10) and with the Helsinki Declaration of 1975, as revised in 2000. Pediatric samples AML-346 and AML-356 were established at University Children's Hospital Tuebingen¹.

Animal trials were performed following the current ethical standards of the official committee on animal experimentation (written approval by Regierung von Oberbayern, tierversuche@reg-ob.bayern.de; ROB-55.2Vet2532.Vet_02–16-7, ROB-55.2Vet-2532.Vet_03–16-56, ROB-55.2-2532.Vet_02-20-159, ROB-55.2-2532.Vet_03-21-9 and ROB-55.2-2532.Vet_02-20-221). Work on genetic engineering was approved by Regierung von Oberbayern (written approvals 55-8791-8.549.1460, 55-8791-8.549.1562, 55.1-8791-8.549.2261, 2721, 2722, 2723, 2864).

Patient derived xenograft mouse model of AML

Female and male immunocompromised NOD.Cg-*Prkdc^{scid} Il2rg^{tm1Wjl}*/SzJ (The Jackson Laboratory, Bar Harbour, ME, USA) age 6-20 weeks were used in all *in vivo* studies. Animals were kept under specified pathogen-free (SPF) conditions with a 12/12 hour light cycle, a temperature of 20-24°C and 45-65% humidity according to Annex A of the European Convention 2007/526 EC. Hygiene monitoring was carried out at least quarterly in accordance with the current FELASA recommendation. The cages were constantly filled with structural enrichment and the animals had unlimited access to food and water.

Generation of serially transplantable PDX AML samples and genetic modification by lentiviral transduction was performed as described previously²⁻⁴. In brief, PDX cells were transplanted into mice by injection of 1×10^5 – 1×10^7 cells into the tail vein. Tumor outgrowth was monitored by in vivo bioluminescence imaging (BLI) for cells expressing enhanced firefly luciferase and flow cytometric blood measurements as previously described². PDX cells were reisolated from murine bone marrow and spleen in cases of splenomegaly and either used for transduction or re-transplantation as whole bone marrow cells or were viably frozen. Accuracy of sample identity was regularly verified by repetitive fingerprinting using PCR of mitochondrial DNA⁵.

Cell culture

AML PDX models were cultivated in StemPro-34 medium (Thermo Fisher Scientific Waltham, MA, USA) supplemented with 1% L-Glutamin, 1% Penicillin/Streptomycin (both Gibco), 10 ng/ml rhFLT3L (R&D Systems, Minneapolis, MN, USA), 10 ng/ml rhSCF, 10 ng/ml rhTPO, and 10 ng/ml rhIL3 (all Peprotech, Rocky Hill, NJ, USA) medium⁶.

AML cell lines: HL60, THP-1, MV4-11 and MOLM-13 were cultivated in RPMI-1640 medium supplemented with 1% L-Glutamin and 10% FBS (all Gibco, USA). KMOE-2, SKM-1 and PL-21 were cultivated in RPMI-1640 medium supplemented with 1% L-Glutamin and 20% FBS. OCI-AML3 was cultivated in alpha-MEM medium (Gibco, USA) supplemented with 1% L-Glutamin and 20% FBS. SIG-M5 was cultivated in IMEM medium (Gibco, USA) supplemented with 1% L-Glutamin and 10% FBS. All cell lines were obtained from DSMZ (Braunschweig, Germany), and were repetitively tested negative for mycoplasma contamination (myco kit).

Cells were cultivated at 37°C in the presence of 5% CO₂.

Lentivirus production and transduction

Lentiviruses were produced using third-generation packaging plasmids pMDLg/pRRE, pRSV-Rev and pMD2-G as described⁷. Virus titration was estimated by transducing cell

lines followed by flow cytometric analysis of transgenic marker. For transduction, cells were mixed with virus particles in the presence of 8 µg/ml polybrene (Sigma-Aldrich).

Generation of Cas9-expressing PDX AML samples and cell lines

Cas9-expressing PDX AML models or cell lines were generated by transduction with lentiviral particles expressing a split version of Cas9 protein. Transductions were performed at low multiplicity of infection (MOI) to ensure that transduced cells were mainly single integrants. Cas9 is reconstituted by the fusion of each half via intein moieties and can be traced by the expression of the GFP marker using flow cytometry. Cas9-GFP-positive cells were enriched 72 hours after transduction by sorting on a FACSAria (BD) and were either re-transplanted into new recipient mice for expansion of transgenic PDX cells and generating latter passages, or expanded *in vitro* for AML transgenic cell lines.

Targeted-sequencing of Cas9-expressing PDX AML samples

Cas9-expressing PDX AML cells were sorted on a FACSAria (BD) and enriched for GFP-positive population. Sequencing of 68 genes recurrently mutated in myeloid malignancies was performed using a targeted amplicon-based enrichment assay (Haloplex, Agilent, Boeblingen, Germany) as previously described ⁸.

sgRNA library design and cloning

The customized sgRNA library targeting 34 genes recurrently mutated in AML was designed using the CLUE (www.crispr-clue.de) platform and cloned into a lentiviral vector with five different sgRNAs per target gene, plus positive and negative controls as previously described ⁷. The lists of genes and sequences of sgRNAs are provided in supplementary Table S2-3. The vector contained a mTagBFP fluorochoime for flow cytometric analysis of transduction efficiency and a puromycin resistance marker for selection of transduced cells.

CRISPR/Cas9 screening and bioinformatic analysis

PDX cells *in vivo*: A total of 10×10^6 Cas9-expressing PDX AML cells, freshly isolated from donor mice bone marrow, were transduced with the sgRNA library lentiviral particles at a low MOI. Cells were cultured in a StemPro-34 medium supplemented as described above. 72 hours after transduction, transduction efficiency was measured by mTagBFP expression level to quality control for a maximum transduction efficiency of around 30% to achieve mainly integration of a single sgRNA per cell. Cells were enriched 72h after transduction by puromycin selection at a 1.5 - 3 $\mu\text{g}/\text{mL}$ concentration for 2-6 days. A fraction of transduced cells and puromycin-enriched cells were collected as input controls. Enriched PDX cells were injected into the tail vein of NSG mice and the animals sacrificed at advanced leukemic disease. PDX cells were re-isolated from bones and spleen in cases of splenomegaly. Screens were performed in triplicates.

Cell lines *in vitro*: A total of 3×10^6 Cas9-expressing AML cells were transduced with the sgRNA library lentiviral particles at a low MOI. 72 hours post transduction, transduction efficiency was measured by mTagBFP expression level, and transduced cells were enriched using puromycin selection at 1.5 - 2 $\mu\text{g}/\text{ml}$ for 2-4 days. A fraction of puromycin-enriched cells were collected as input controls. The rest of the enriched cells were kept in culture and harvested 25 days post-transduction. Screens were performed in triplicates.

Genomic DNA was obtained from 10^6 cells using the Qiagen DNA mini kit (51306, Qiagen, Netherlands) according to the manufacturer's instructions. sgRNA barcodes were PCR amplified and submitted for standard sequencing as described before ⁷. The sgRNAs distribution and relative abundance between input and output samples were determined and analyzed using the DepMap_CHRONOS, Lin et al. ⁹ and MAGeCK algorithm¹⁰.

For all calculations negative control 7 was filtered out. For Lin et al. method and DepMap_CHRONOS, we used the following genes as common essentials, *HNRNPK*, *SF3B1*, *SMC1A*, *SMC3*, *SRSF2*, *U2AF1*, *HSPE1*, *POLR2L*, *PSMB3*, *RAN* and *RPL12*.

To calculate simplistic gene depletion scores we have used method described in publication by Lin et al. Briefly, we have normalized sgRNA counts to the total reads per million of all negative control guide RNAs. Following the normalization, we have averaged the values between replicates (n=3 for each AML model). The fold-change of each sgRNA was calculated in relation to the input and log2 transformed. Final depletion score was calculated as follows, $-1 * (\text{sgRNA_LFC} - \text{median}(\text{negative_controls_LFC})) / (\text{median}(\text{common_essentials_LFC}) - \text{median}(\text{negative_controls_LFC}))$. The median sgRNA score was selected to represent final gene depletion score.

For CHRONOS derived gene effect scores, we employed the algorithm as described in Dempster et al.¹¹. We have used all default parameters except of `cell_efficacy_guide_quantile` which we have adjusted to 0.3 to account for a small screening library. The derived scores were normalised for common essential genes to have a median score of -1 and other nonessential genes to have a median of 0.

To control proper library presentation *in vivo*, Cas9 negative AML-661 and AML-356 were screened with the same sgRNA library as quality controls. Here, each sgRNA was analyzed as a barcode to exploit whether the entire library was restorable in tested PDX models. The experimental setting was the same as described above.

Immunoblotting

1X10⁶ cells were lysed in lysis buffer (#9803, Cell Signaling Technology, Boston, USA) supplemented with 1:200 Phenylmethylsulfonyl fluoride (PMSF, 8553, Cell Signaling Technologies, USA) on ice for 30 min. The lysates were cleared by centrifugation at 13,000 g at 4°C for 3 min. Protein concentrations were normalized by Bradford quantification and an equal amount of cell lysates were subjected to SDS-PAGE under reducing conditions. Proteins were transferred onto polyvinylidene difluoride (PVDF) membranes using the Trans-Blot Turbo Transfer System (Bio-Rad). Membranes were blocked in 5% skimmed milk. The primary antibodies used were anti-KRAS (H00003845-M02, Novus Biologicals, 1:1000), anti-NPM1 (47354, Novus Biologicals, 1:1000), anti-

WT1 (ab89901, Abcam, 1:500), and anti-beta-actin (sc-47778, Santa Cruz Biotechnology, 1:3000). The secondary antibodies were as follows, Anti-mouse IgG, HRP-linked Antibody (7076, Cell Signaling Technology, 1:1000) and Anti-rabbit IgG, HRP-linked Antibody (7074, Cell Signaling Technology, 1:1000). Chemiluminescence signal was detected using chemiluminescent substrate (Thermo Fisher Scientific) with the Fusion Fx chemiluminescent imaging system.

Assessment of genome editing efficiency

DNMT3A gene knockout efficiency was evaluated using Tracking of Indels by Decomposition (TIDE) analysis. A total of 1×10^6 cells were harvested 2 weeks after transduction. Genomic DNA was obtained using the Qiagen DNA mini kit (51306, Qiagen, Netherlands) according to the manufacturer's instructions. Specific primers were designed according to the requirements of TIDE analysis (<http://shinyapps.datacurators.nl/tide/>) and ordered from Sigma-Aldrich company (St. Louis, MO). *DNMT3A* sgRNA1 forward primer: 5'-CTCCCTGGCCTTGTTCTCAG-3', reverse primer: 5'-CCACACACTCCACGCAAAG-3'; *DNMT3A* sgRNA2 forward primer: 5'-CTCCTCTCCCTTCCCCACAG-3', reverse primer: 5'-CCCTCACCTGTAGCGATTCC-3'; *DNMT3A* sgRNA3 forward primer: 5'-TTTCAAGGGGTCAAGCCCAG-3', reverse primer: 5'-AGCAGACCTTTAGCCACGAC-3'.

50 ng gDNA was used for amplifying sgRNA targeting locus by polymerase chain reaction (PCR). gDNA was initially denatured at 95°C for 30 seconds and followed with 35 cycles' denaturation at 95°C for 10 sec, annealing at 62°C for 30 sec and extension at 72°C for 30 sec; and finally extended at 72°C for 10 min.

DNA fragments were separated by agarose gel electrophoresis, purified by gel clean-up kit (740986.20, Macherey-Nagel, Germany), and sent for standard Sanger sequencing. The sequence traces were analyzed by the TIDE algorithm (available at <http://shinyapps.datacurators.nl/tide/>).

Cloning of targeting sgRNAs in sgRNA expression vectors encoding different fluorochrome markers

A set of 3 sgRNAs each targeting either *WT1*, *NPM1*, *DNMT3A*, or *KRAS* and non-targeting sgRNAs were selected from the screening library. The oligos were ordered from Sigma-Aldrich (St. Louis, MO) company with the following overhangs:

Forward oligo: 5'-TCCCGN20(Target)-3'

Reverse oligo: 5'-AAACN20(Target)-3'

Golden gate cloning strategy was used for cloning of sgRNAs into expression vectors encoding different fluorochrome markers. Annealing of oligos was performed by mixing 2 μ l of forward (100 μ M) and 2 μ l of reverse (100 μ M) oligos with 2 μ l T4 DNA ligase buffer (EI0012, Thermo Fischer Scientific, USA) and 14 μ l H₂O and incubation at 95 °C for 5 minutes ramping down to 25 °C at 0.1 °C/sec in a thermocycler. The expression vectors were linearized using FastDigest Bpil (isoschizomer of BbsI, Thermo Scientific) by digesting 500 ng of each plasmid with 0.5 μ l FD Bpil enzyme at 37°C for 10 min. Golden gate cloning was performed with 2 μ l of each annealed oligoes diluted 1/500 and with 100 ng predigested expression vector together with 2 μ l of T4 ligase buffer (EI0012, Thermo Scientific, USA), 1 μ l FastDigest Bpil (FD1014, Thermo Scientific, USA), 1 μ l T4 Ligase (EI0012, Thermo Scientific, USA), and brought to a total volume of 20 μ l with water. The reaction condition in a thermocycler was as follows: 3 min at 37 °C followed by 10 min at 16°C for 20 cycles and a final step of 5 min at 55°C and 5 min 80°C. 2.5 μ l of the reaction was transformed into chemically competent DH5 α and plated on LB agar containing 100 μ g/ml ampicillin. The next day, the colonies were harvested in LB medium and incubated overnight at 37 °C and 220 rpm shaking. DNA was isolated using the NucleoBond® Xtra Midi kit (740410-100, Macherey-Nagel, Germany) according to the manufacturer's instructions.

***In vivo* competitive assay**

In vivo competitive assays were performed as previously described¹². Cas9-expressing PDX cells were freshly harvested from donor mice bone marrow or spleen and then transduced with lentiviral vectors expressing sgRNAs targeting either *WT1*, *NPM1*, *DNMT3A*, or *KRAS* or non-targeting (NT) sgRNAs as control. The sgRNA vectors encoding gene-targeting or NT sgRNAs expressed different fluorochrome markers as depicted in printed Figure 1C, enabling monitoring cell proliferation for more than one gene of interest and distinction of each population. *KRAS* KOs (iRFP) and *NPM1* KOs (mTagBFP) were mixed with NT subsets (T-Sapphire) as one group and *WT1* KOs(mTagBFP), *DNMT3A* KOs (iRFP), and NT subsets (T-Sapphire) as the second group. For PDX AML-640 for the first group, since the percentage of *KRAS* KO cells was below 10%, *KRAS* KO competitive assay was repeated with the second group by cloning *KRAS* targeting sgRNAs into a construct expressing mCherry. Cells were enriched 72 h after transduction by puromycin selection at a 1.5 - 3 µg/mL concentration for 2-6 days. Enriched transgenic cells expressing each gene-targeting sgRNAs were mixed in a 1:1:1 ratio with NT subsets and injected into NSG mice. Mice were sacrificed at an advanced leukemic stage. The relative proportion of each population was analyzed in input mix and output cells from leukemic animals by flow cytometry from whole bone marrow cells. Analysis of each KO population together with the control group was performed using FlowJo's Boolean gating option. Output mix was analyzed in PDX cells reisolated from bone marrow; for AML-346, PDX cells were reisolated from spleen in 2 of 3 mice.

The experiments were considered conclusive when either depletion or enrichment was observed in the KO population for all 3 tested sgRNAs; in case of conflicting results, the PDX sample was excluded from further analysis.

***In vitro* competitive assay**

Cas9-expressing AML cell lines were transduced with lentiviral vectors expressing either *WT1*, *DNMT3A* sgRNAs, or NT sgRNAs. The constructs encoding gene-targeting or NT sgRNAs expressed different fluorochrome markers, as mentioned above. Cells were

enriched 72 h after transduction by puromycin selection at a 1.5 - 3 $\mu\text{g}/\text{mL}$ concentration for 2-6 days, mixed in a 1:1 ratio with NT controls after enrichment and kept in culture. The experiment was performed in triplicates, with each replicate containing different sgRNAs. The distribution of each population was measured by flow cytometry every four days from mixing day (day 0) to 28 days after mixing. The relative proportion of each population was analyzed by FlowJo.

Non-targeting control assay *in vivo* and *in vitro*

One NT sgRNA used in the *in vivo* and *in vitro* competitive assay was cloned into four kinds of lentiviral constructs expressing 4 corresponding fluorochromes used in the *in vivo* and *in vitro* competitive assay. Cas9-transgenic cells (either Cas9-expressing bone marrow PDX cells or Cas9-expressing AML cell lines) were transduced with these NT lentiviral particles. NT _1 (mTagBFP), NT_2 (iRFP), NT_3 (mCherry) and NT_4 (T-Sapphire) and enriched 72 h after transduction by puromycin selection at a 1.5 - 3 $\mu\text{g}/\text{mL}$ concentration for 2-6 days. 4 populations were mixed in a 1:1:1:1 ratio and either kept in culture (AML cell lines) or injected into NSG mice (PDX cells). The relative proportion of each population was analyzed in input mix and output cells from leukemic animals by fluorochrome-dependent flow cytometry. For AML cell lines, the mixture was cultured *in vitro* for 24 days and measured by flow cytometry as an output.

Flow cytometry analysis

According to the corresponding fluorochrome in every cell population, cells were analyzed on BD LSRFortessa™ X-20 Cell Analyzer (BD Biosciences) or sorted on a BD FACS ARIA™ II SORP Flow Cytometer Cell Sorter (BD Biosciences). The flow cytometry data was analyzed with FlowJo software (v10.6.2, Tree Star, Ashland, OR, USA).

To quantify percentage of single KO populations, NT control cells had to account for a minimum of 10% of all PDX cells retrieved from the mouse. A direct comparison between every single knockout population (e.g., either *NPM1* or *KRAS*) versus control cells was

obtained by restricting analysis to 2 cell populations using “Boolean” gating (see Figures S4).

Comparing intrafemoral with intravenous cell injection

Cas9-expressing PDX donor cells were isolated from BM and spleen of advanced leukemia stage donor mice and transduced with lentiviral vectors expressing either *WT1* or NT sgRNAs marked by different fluorochromes. A single of 2 different sgRNAs (sgRNA-2) was used. After puromycin enrichment of transgenic cells, *WT1* KO and CTRL populations were mixed in a 1:1 ratio. For intrafemoral injection, 8×10^5 cells were injected per mouse (n=3) and human cells analysed from the injected femur; for intravenous injection, 10×10^6 cells were injected per mouse (n=3) and the entire bone marrow was analysed. Mice were sacrificed three days after injection and human cells enriched by MACS using a mouse cell depletion kit (Miltenyi). The distribution of *WT1* KO and CTRL population were analyzed by flow cytometry. Experiments were performed once with AML-346 and twice with AML-388.

Analysis of leukemic cells engraftment and cell proliferation kinetics

Cas9-expressing PDX cells were transduced with lentiviral vectors expressing either *WT1*, *DNMT3A*, or NT sgRNAs marked by different fluorochromes. A single of 3 different sgRNAs (sgRNA-2) was used. After puromycin enrichment of transgenic cells, mixing was performed in a 1:1:1 ratio between all three populations and 9×10^6 cells injected into NSG mice. The experiment was performed in triplicates. 1, 3, 5, and 8 days post-injection in AML388, and 3, 5, and 8 days post-injection in AML346, the animals were sacrificed and human cells were enriched from murine bone marrow by negative selection using mouse cell depletion kit (Miltenyi) with 400-600ul beads per mouse. The relative proportion of each population was analyzed in input mix and output cells from leukemic animals by flow cytometry.

***In vivo* chemotherapy trial**

Cas9 and enhanced firefly luciferase-expressing AML-388 PDX cells were transduced with lentiviral vectors expressing sgRNA targeting *WT1*, *DNMT3A*, or NT sgRNAs marked with different fluorochromes. A single of 3 different sgRNAs (sgRNA-2) was used. After puromycin enrichment of transgenic cells, mixing was performed at a 1:1:1 ratio between all three populations and cells injected into mice (n=8). Tumor burden was regularly examined using BLI. When tumor burden reached total flux of around $\sim 1e9$ Photons/second, mice were treated with cytarabine (200 mg/kg dissolved in PBS, i.p.; Cell Pharma GmbH, Bad Vilbel, Germany) or PBS. The drug was administered two times a week, and therapy continued for 2.5 weeks. Two days after the last drug administration, animals were sacrificed, and the relative proportion of each population of the leukemic cells within the bone marrow was examined by flow cytometry as described above.

Investigating *WT1* and *DNMT3A* knockouts re-engraftment capacity

From the output samples of AML-346 *in vivo* competitive assays, whole bone marrow cells were re-isolated at advanced stage leukemia, cell populations were quantified using flow cytometry and 2×10^6 cells re-injected into the secondary recipient mice (n=3). In a variant of this assay, cells were re-isolated after 26 days *in vivo*, re-enriched to a 1:1 ratio for KO:CTRL cells by flow cytometry and re-inject into the secondary recipient mice (*WT1* KO n=3, cell number injected= 13400 (sgRNA2); *DNMT3A* KO n=7, cell number injected= 13400 (sgRNA3), 20000 (sgRNA2), 26700 (sgRNA1)). The secondary recipient mice were sacrificed at advanced leukemic stage. BM cells were harvested and the distribution of each population was determined using flow cytometry.

LDTA assay

Freshly isolated Cas9 and T-sapphire expressing PDX cells were transduced with lentiviral vectors expressing sgRNA targeting *WT1* (mTag-BFP), *DNMT3A* (iRFP), or NT (mTag-BFP or iRFP) sgRNAs marked with different fluorochromes. After flow cytometry

enrichment of transgenic cells, *WT1* / *DNMT3A* KO and CTRL cells were mixed in a 1:1 ratio and injected into groups of NSG mice at different cell numbers. Engraftment and tumor growth were monitored via blood measurement. As soon as engraftment was observed in the group injected with the highest cell number, all mice were sacrificed, PDX cells were isolated from the BM and the distribution of the cell populations analyzed via flow cytometry followed by analysis on FlowJo Software (FlowJo™ Software, version 10.7, Ashland, USA). For positive engraftment, a threshold of 0.2% of the population of interest in the BM was defined. LIC frequency was calculated using the ELDA software (<http://bioinf.wehi.edu.au/software/elda/index.html>)

Immunophenotype staining

PDX cells were phenotypically analyzed by multiparameter flow cytometry (CytoFLEX flow cytometer, Beckman Coulter). Staining antibodies against CD33 (PerCP-Cy5.5, Clone WM53, 303414 Biolegend), GPR56 (PE, Clone 4C3, 391903 Biolegend), CD44 (PE/Dazzle™ 594, Clone BJ18, 338821 Biolegend), CD14 (PE/Cy7, Clone 63D3, 367112 Biolegend), CD11b (APC, Clone ICRF44, 301310 Biolegend), CD45 (APC/Cy7, Clone HI30, 304014 Biolegend), CD45 (APC, Clone HI30, 304011 Biolegend), CD90 (BV650, Clone 5E10, 328143 Biolegend), CD123 (PerCp-Cy5.5, Clone 6H6, 306015 Biolegend), CD45RA (PE, Clone HI100, 304107 Biolegend), CD38 (PE/ Dazzle™ 594, Clone HB-7, 356630 Biolegend), MICA/MICB (PE/Cy7, Clone 6D4, 320917 Biolegend) and CD34 (APC/Cy7, Clone 581, 343513 Biolegend) were used. Dead and living cells were discriminated by Zombie UV™ Fixable Viability Kit according to the manufacturer's recommendations (423107, Biolegend). Gating strategy to assess the percentage of positive cells can be depicted in S10. Analysis was performed on *WT1* KO, *DNMT3A* KO and CTRL on two PDX (AML-346 and AML-388) samples with three different gRNAs, each.

Transcriptional profiling and data analysis

AML-356, AML-388, and AML-661 single *WT1* and *DNMT3A* KOs and control subsets from the output samples of in vivo competitive assay were enriched by sorting on a FACSAria (BD Biosciences) and lysed in RLT Plus buffer (Qiagen). In AML-346, since the KO populations were completely depleted in the in vivo competitive assay, freshly isolated Cas9-expressing PDX cells were transduced with lentiviral vectors expressing *WT1*, *DNMT3A*, or NT sgRNAs and samples were taken for further analysis after puromycin enrichment.

Lysates containing 20,000 cells in RLT Plus buffer (Qiagen) were subjected to the prime-seq method^{13 14} prime-seq is a three prime counting method that introduces a sample specific barcode sequence and unique molecular identifiers (UMI) for accurate quantification of gene expression. In addition direct lysis and isolation of RNA using SPRI beads was used here. Sequencing library preparation was performed using a modified NEBNext Ultra II Fs protocol. A full step-by-step protocol can be found on protocols.io (<https://www.protocols.io/view/prime-seq-s9veh66>).

Illumina paired end sequencing was performed on a NextSeq1000 instrument, where the first read was 28 bases long and covered the sample barcode (12 bases) and UMI (16 bases), and the second read was 93 bases long and was used to identify the gene. Raw data was demultiplexed based on unique i5 and i7 indices using deML¹⁵ and further processed using the zUMIs pipeline (2.9.6,¹⁶) with STAR (2.6, ¹⁷). Reads were mapped to a concatenated human and mouse genome (hg38,mm10) with Gencode gene annotations (v35, vM25). Mouse mapping reads were treated as contamination from the mouse model and discarded for further analysis.

The raw gene expression counts were preprocessed with the R package edgeR (3.30.3). Genes with ≤ 1 count per million in more than 2/3 of samples were excluded from the analysis. The differential gene expression analysis was done with the R package limma (3.44.3). Genes with a *p*-value of ≤ 0.01 and $|\log \text{fold change}| > 1$ are displayed in the heatmaps. The heatmaps were generated with the R-package ComplexHeatmap (2.6.2).

A preranked gene set enrichment analysis (GSEA) was done with the software GSEA (<http://www.broad.mit.edu/gsea/>)¹⁸. The ranking metric was calculated from the output of the differential gene expression analysis as $-\log_{10}(p\text{-value}) \cdot \text{sign}(\log \text{fold change})$. The tested pathway databases were hallmark gene sets, KEGG pathways, gene ontology (GO) gene sets and oncogenic signature gene sets. Pathways with an adjusted p-value of 0.05 were considered significant.

Enriched gene-sets of KEGG and Hallmarks were graphically organized into a map network, where each gene set is a node and edges represent gene similarity between sets. The Cytoscape network software v.3.9.0¹⁹ and the plugin “Enrichment Map” were used to visualize the network. Node color refers to the set types (KEGG in blue and Hallmarks in orange). Node size is proportional to the total number of genes belonging to the corresponding gene-set. Edge thickness is proportional to the overlap score.

DepMap data analysis

DepMap data release 21Q3 was used for generating gene essentiality score scatter plots.

Statistics

Statistical analyses were performed using GraphPad Prism 7 software (Graphpad Prism, La Jolla, CA, USA). Statistical tests and the number of replicates were mentioned in the associated figure legends. MAGeCK count (Galaxy Version 0.5.9.2.4) and MAGeCKs test (Galaxy Version 0.5.9.2.1) was used for calculating the sgRNAs distribution and calculating the p values.

Data presentation

Graphics were created using BioRender.com.

Data Availability Statement

Transcriptome data generated in this study are publicly available in Gene Expression Omnibus (GEO) (GSE215836). Whole Exome Sequencing raw data generated in this study are not publicly available due to information that could compromise patient privacy or consent but are available upon reasonable request from the corresponding author.

Literature

1. Woiterski J, Ebinger M, Witte KE, et al. Engraftment of low numbers of pediatric acute lymphoid and myeloid leukemias into NOD/SCID/IL2R γ mice reflects individual leukemogenecity and highly correlates with clinical outcome. *Int J Cancer*. 2013;133(7):1547-1556.
2. Vick B, Rothenberg M, Sandhofer N, et al. An advanced preclinical mouse model for acute myeloid leukemia using patients' cells of various genetic subgroups and in vivo bioluminescence imaging. *PLoS One*. 2015;10(3):e0120925.
3. Ebinger S, Zeller C, Carlet M, et al. Plasticity in growth behavior of patients' acute myeloid leukemia stem cells growing in mice. *Haematologica*. 2020;105(12):2855-2860.
4. Ebinger S, Ozdemir EZ, Ziegenhain C, et al. Characterization of Rare, Dormant, and Therapy-Resistant Cells in Acute Lymphoblastic Leukemia. *Cancer Cell*. 2016;30(6):849-862.
5. Hutter G, Nickenig C, Garritsen H, et al. Use of polymorphisms in the noncoding region of the human mitochondrial genome to identify potential contamination of human leukemia-lymphoma cell lines. *Hematol J*. 2004;5(1):61-68.
6. Wermke M, Camgoz A, Paszkowski-Rogacz M, et al. RNAi profiling of primary human AML cells identifies ROCK1 as a therapeutic target and nominates fasudil as an antileukemic drug. *Blood*. 2015;125(24):3760-3768.
7. Becker M, Noll-Puchta H, Amend D, et al. CLUE: a bioinformatic and wet-lab pipeline for multiplexed cloning of custom sgRNA libraries. *Nucleic Acids Res*. 2020;48(13):e78.
8. Metzeler KH, Herold T, Rothenberg-Thurley M, et al. Spectrum and prognostic relevance of driver gene mutations in acute myeloid leukemia. *Blood*. 2016;128(5):686-698.
9. Lin S, Larrue C, Scheidegger NK, et al. An In Vivo CRISPR Screening Platform for Prioritizing Therapeutic Targets in AML. *Cancer Discov*. 2022;12(2):432-449.
10. Li W, Xu H, Xiao T, et al. MAGeCK enables robust identification of essential genes from genome-scale CRISPR/Cas9 knockout screens. *Genome Biol*. 2014;15(12):554.
11. Dempster JM, Boyle I, Vazquez F, et al. Chronos: a cell population dynamics model of CRISPR experiments that improves inference of gene fitness effects. *Genome Biol*. 2021;22(1):343.
12. Liu WH, Mrozek-Gorska P, Wirth AK, et al. Inducible transgene expression in PDX models in vivo identifies KLF4 as a therapeutic target for B-ALL. *Biomark Res*. 2020;8:46.
13. Holgersen EM, Gandhi S, Zhou Y, et al. Transcriptome-Wide Off-Target Effects of Steric-Blocking Oligonucleotides. *Nucleic Acid Ther*. 2021;31(6):392-403.
14. Janjic A, Wange LE, Bagnoli JW, et al. Prime-seq, efficient and powerful bulk RNA sequencing. *Genome Biol*. 2022;23(1):88.
15. Renaud G, Stenzel U, Maricic T, Wiebe V, Kelso J. deML: robust demultiplexing of Illumina sequences using a likelihood-based approach. *Bioinformatics*. 2015;31(5):770-772.
16. Parekh S, Ziegenhain C, Vieth B, Enard W, Hellmann I. zUMIs - A fast and flexible pipeline to process RNA sequencing data with UMIs. *Gigascience*. 2018;7(6).
17. Dobin A, Davis CA, Schlesinger F, et al. STAR: ultrafast universal RNA-seq aligner. *Bioinformatics*. 2013;29(1):15-21.

18. Subramanian A, Tamayo P, Mootha VK, et al. Gene set enrichment analysis: a knowledge-based approach for interpreting genome-wide expression profiles. *Proc Natl Acad Sci U S A*. 2005;102(43):15545-15550.
19. Shannon P, Markiel A, Ozier O, et al. Cytoscape: a software environment for integrated models of biomolecular interaction networks. *Genome Res*. 2003;13(11):2498-2504.

Table S1 Characteristics of PDX models

PDX	Disease stage	Diagnosis age [years]	Sex	Cytogenetics	Mutations and gene fusions	Reference
AML-346	R1	1	f	Interst. 5q Del, interst. 13q Del	None identified within panel	1, 2, 3, 4, 5
AML-356	R1	5	m	ND	U2AF1, KRAS	1, 4, 6
AML-388	ID	57	m	KMT2A/AFDN	KRAS	3, 4, 5, 7, 8, 9, 10
AML-393	R1	47	f	KMT2A/MLLT10	BCOR, KRAS	1, 3, 4, 5, 7, 8, 9, 10, 11, 12, 13, 14, 15
AML-602	R1	40	f	complex	DNMT3A, NPM1, FLT3-ITD, TET2, JAK3, CEBPA	10, 16
AML-640	ID, primary refractory	79	m	t(11;15)(p1?1;q?22)	NPM1, FLT3-ITD, IDH1	17
AML-661	R2	54	f	del7q (7q21.13 q36.3); del6p (6p25.3 p21.1)	DNMT3A, RUNX1, ETV6, PTPN11, BCOR, EZH2	4, 18, 19, 20

ID=initial diagnosis; R1= first relapse, R2= second relapse;m = male; f = female;

- Vick, Rothenberg, Sandhöfer et al., An advanced preclinical mouse model for acute myeloid leukemia using patients' cells of various genetic subgroups and in vivo bioluminescence imaging. *PLoS One*. 2015
- Krupka et al., Blockade of the PD-1/PD-L1 axis augments lysis of AML cells by the CD33/CD3 BiTE antibody construct AMG 330: reversing a T-cell-induced immune escape mechanism. *Leukemia*. 2016
- Heckl et al., Frequent and reliable engraftment of certain adult primary acute lymphoblastic leukemias in mice. *Leuk Lymphoma*. 2019
- Ebinger et al., Plasticity in growth behavior of patients' acute myeloid leukemia stem cells growing in mice. *Haematologica*. 2020
- Meißner et al., Small molecule inhibitors of the mitochondrial ClpXP protease possess cytostatic potential and re-sensitize chemo-resistant cancers. *Sci Rep*. 2021
- Habringer et al., Dual Targeting of Acute Leukemia and Supporting Niche by CXCR4-Directed Theranostics. *Theranostics*. 2018
- Jensen et al., Requirement for LIM kinases in acute myeloid leukemia. *Leukemia*. 2020
- Yankova et al., Small-molecule inhibition of METTL3 as a strategy against myeloid leukaemia. *Nature* 2021
- Carlet et al., In vivo inducible reverse genetics in patients' tumors to identify individual therapeutic targets. *Nat Commun*. 2021
- Janjic et al., Prime-seq, efficient and powerful bulk RNA-sequencing. *bioRxiv* 2021.09.27.459575.
- Sandhöfer et al., Dual PI3K/mTOR inhibition shows antileukemic activity in MLL-rearranged acute myeloid leukemia. *Leukemia*. 2015
- Tzelepis et al., SRPK1 maintains acute myeloid leukemia through effects on isoform usage of epigenetic regulators including BRD4. *Nat Commun*. 2018
- Koczian et al., Targeting the endoplasmic reticulum-mitochondria interface sensitizes leukemia cells to cytostatics. *Haematologica*. 2019
- Stief et al., Loss of KDM6A confers drug resistance in acute myeloid leukemia. *Leukemia*. 2020
- Chen et al., A JAK/STAT-mediated inflammatory signaling cascade drives oncogenesis in AF10-rearranged AML. *Blood*. 2021
- Garz et al., Azacitidine combined with the selective FLT3 kinase inhibitor crenolanib disrupts stromal protection and inhibits expansion of residual leukemia-initiating cells in FLT3-ITD AML with concurrent epigenetic mutations. *Oncotarget*. 2017
- Reiter et al., Tyrosine kinase inhibition increases the cell surface localization of FLT3-ITD and enhances FLT3-directed immunotherapy of acute myeloid leukemia. *Leukemia*. 2018
- Kempf et al., Loss-of-function mutations in the histone methyltransferase EZH2 promote chemotherapy resistance in AML. *Sci Rep*. 2021
- Sun et al., RSPO2 inhibits BMP signaling to promote self-renewal in acute myeloid leukemia. *Cell Rep*. 2021
- Zeller et al., Adverse stem cell clones within a single patient's tumor predict clinical outcome in AML patients. *Journal of Hematology and Oncology*. 2022

Table S2 AML-specific mutations in PDX models and AML cell lines

PDX	Gene	Variant *	VAF (%)**
AML-602	<i>NPM1</i>	NM_002520.6:c.863_864insCCTG p.(Trp288Cysfs*12)	51
	<i>TET2</i>	NM_001127208.2:c.4106C>G, p.(Ser1369*)	27
	<i>TET2</i>	NM_001127208.2:c.840dup, p.(Asn281*)	39
	<i>CEBPA</i>	NM_004364.4:c.783dup, p.(Asp262Argfs*59)	43
	<i>DNMT3A</i>	NM_175629.2:c.1122+1G>A, p.(=?)	51
	<i>FLT3-ITD</i>	51nt	51
AML-356	<i>U2AF1</i>	NM_001025203.1:c.101C>A, p.(Ser34Tyr)	52
	<i>KRAS</i>	NM_033360.3:c.436G>A, p.(Ala146Thr)	48
AML-388	<i>KRAS</i>	NM_033360.3:c.183A>C, p.(Gln61His)	45
AML-661	<i>DNMT3A</i>	NM_175629.2:c.2644C>A p.(Arg882Ser)	52
	<i>RUNX1</i>	NM_001754.4:c.408T>G p.(Asn136Lys)	48
	<i>PTPN11</i>	NM_002834.4:c.181G>C p.(Asp61His)	54
	<i>ETV6</i>	NM_001987.4:c.641C>T p.(Pro214Leu)	53
	<i>BCOR</i>	NM_001123385.2:c.2048delC p.(Pro683Glnfs*32)	51
	<i>EZH2</i>	NM_004456.5:c.2075C>G p.(Ala692Gly)	99
AML-393	<i>KRAS</i>	NM_033360.4:c.35G>C (p.Gly12Ala)	47
	<i>BCOR</i>	NM_001123385.1:c.3035_3038delCCGC p.(Pro1012Leufs*8)	51
AML-640	<i>NPM1</i>	NM_002520.6:c.860_863dup p.(Trp288Cysfs*12)	54
	<i>IDH1</i>	NM_005896.3: c.395G>A p.(Arg132His)	52
	<i>FLT3-ITD</i>	60nt	55
	<i>FLT3-ITD</i>	84nt	55
AML-346	-	no variant detected	
AML cell lines	Gene	Variants according to https://web.expasy.org/cellosaurus/ ***	VAF (%)
HL60	<i>CDKN2A</i>	NM_000439.5:c.238C>T(p.Arg80Ter)	100
	<i>NRAS</i>	NM_002524.5:c.182A>T(p.Gln61Leu)	48
	<i>TP53</i>	Gene deletion	No data
KMOE-2	<i>NRAS</i>	NM_002524.5:c.182A>G(p.Gln61Arg)	No data
	<i>TP53</i>	NM_000546.6:c.814G>A(p.Val272Met)	No data
MOLM-13	<i>FLT3-ITD</i>	Internal tandem duplication	53
MV4-11	<i>FLT3-ITD</i>	Internal tandem duplication	93
OCI-AML3	<i>DNMT3A</i>	NM_022552.5:c.2644C>T(p.Arg882Cys)	50
	<i>NRAS</i>	NM_002524.5:c.182A>T(p.Gln61Leu)	99
	<i>NPM1</i>	NM_002520.7:c.860_863dupTCTG(p.Trp288Cysfs*12)	40
PL-21	<i>FLT3-ITD</i>	Internal tandem duplication	No data
	<i>KRAS</i>	NM_033360.4:c.437C>T (p.Ala146Val)	70
	<i>TP53</i>	NM_000546.6:c.107delC(p.Pro36fs*8)	99
SIG-M5	<i>DNMT3A</i>	NM_022552.5:c.2644C>T(p.Arg882Cys)	No data
SKM-1	<i>ASXL1</i>	NM_015338.5:c.1773C>A(p.Tyr591Ter)	99
	<i>BCORL1</i>	NM_001379451.1:c.4619-1G>A(NA)	100
	<i>KRAS</i>	NM_033360.4:c.351A>C (p.Lys117Asn)	100
	<i>TP53</i>	NM_000546.6:c.743G>A (p.Arg248Gln)	99
	<i>WT1</i>	NM_024426.6: (p.PVS95fs) frame shift depletion	39
THP-1	<i>NRAS</i>	NM_002524.5:c.35G>A (p.Gly12Asp)	69
	<i>TP53</i>	NM_000546.6:c.520_545del26(p.Arg174fs*3)	92

* Variants of PDX were determined by panel sequencing.

**Variant allele frequency (VAF) were determined by panel sequencing.

*** variants of cell lines were got from <https://web.expasy.org/cellosaurus/>.

Table S3 Mutations present in PDX models and AML cell lines

	JAK2	TP53	FLT3	NRAS	EP300	KRAS	DNMT3A	RAD21	NPM1	PTEN	PTPN11	WT1	KMT2A	BCOR1L	KIT	TET2	CEBPA	U2AF1	RUNX1	BCOR	ETV6	EZH2	IDH1	CDKN2A	ASXL1
PDX*	AML-356					X												X							
	AML-388					X																			
	AML-661						X				X								X	X	X	X			
	AML-393					X														X					
	AML-346																								
	AML-640			X						X														X	
	AML-602			X			X		X								X	X							
cell line**	MV4-11		X																						
	THP-1		X	X																					
	OCI-AML3				X		X		X																
	MOLM-13			X																					
	HL60		X	X																					X
	KMOE-2		X	X																					
	PL-21		X	X		X																			
	SIG-M5						X																		
	SKM-1		X				X								X										X

* Mutations of PDX were determined by panel sequencing.

** Mutations of cell lines were from <https://web.expasy.org/cellosaurus/>

Table S4 Genes studied together with their chromosomal locations and genetic alterations in PDX AML models

Gene	Chromosomal location	PDX sample genetic alteration	PDX sample chromosomal alteration
<i>NRAS</i>	1p13.2		
<i>CSF3R</i>	1p34.3		
<i>KRAS</i>	2p12.1	AML-356, AML-388, AML-393	
<i>DNMT3A</i>	2p23.3	AML-661, AML-602	
<i>HSPE1</i>	2q33.1		
<i>SF3B1</i>	2q33.1		
<i>IDH1</i>	2q34	AML-640	
<i>GATA2</i>	3q21.3		
<i>KIT</i>	4q12		
<i>TET2</i>	4q24	AML-602	
<i>NPM1</i>	5q35.1	AML-602, AML-640	Eventually AML-346
<i>EZH2</i>	7q36.1	AML-661	AML-661
<i>RAD21</i>	8q24.11		
<i>HNRNPK</i>	9q21.32		
<i>RPL12</i>	9q33.3		
<i>SMC3</i>	10q25.2		
<i>WT1</i>	11p13		
<i>POLR2L</i>	11p15.5		
<i>CBL</i>	11q23.3		
<i>KMT2A</i>	11q23.3		
<i>ETV6</i>	12p13.2	AML-661	
<i>PTPN11</i>	12q24.13	AML-661	
<i>RAN</i>	12q24.33		
<i>FLT3</i>	13q12.2	AML-602, AML-640	Eventually AML-346
<i>IDH2</i>	15q26.1		
<i>PSMB3</i>	17q12		
<i>MIR142</i>	17q22		
<i>SRSF2</i>	17q25.1		
<i>DOT1L</i>	19p13.3		
<i>CEBPA</i>	19q13.11	AML-602	
<i>ASXL1</i>	20q11.21		
<i>U2AF1</i>	21q22.3	AML-356	
<i>RUNX1</i>	21q22.12	AML-661	
<i>KDM6A</i>	Xp11.3		
<i>BCOR</i>	Xp11.4	AML-661, AML-393	
<i>SMC1A</i>	Xp11.22		
<i>ZRSR2</i>	Xp22.2		
<i>STAG2</i>	Xq25		
<i>BCORL1</i>	Xq26.1		

Table S5 Sequences of sgRNAs used and results of the CRISPR/Cas9 dropout screen

sgRNA_ID	Sequence	Gene
ASXL1-1	GAAGGAGCGCACGTGGGCCG	ASXL1
ASXL1-2	ACAGGAGTCAGAACAAGCAG	ASXL1
ASXL1-3	GGACAAACAGAAGAAGAAGA	ASXL1
ASXL1-4	GAGAGTTGATCAGGGCACGG	ASXL1
ASXL1-5	GATACGACAGGAAATGGAGA	ASXL1
BCOR-1	GAATCCCTTGAACCACAACG	BCOR
BCOR-2	GACTGGGCTCAGAGAAAGGT	BCOR
BCOR-3	GCTGCCACAAGCACTCTAGG	BCOR
BCOR-4	GAATACACCCGAGACAGTGG	BCOR
BCOR-5	TGTAGCCACAGCAGAAGCGC	BCOR
BCORL1-1	GGGGCGAGTGA AAAATGGAGA	BCORL1
BCORL1-2	GCAGCTCCAGCCACAAGCCA	BCORL1
BCORL1-3	GAGCTCACGGCAGTTGGAAG	BCORL1
BCORL1-4	GA ACTGGAGTCCCTGTGGAG	BCORL1
BCORL1-5	GGACAGATAGGGGCTGGCAG	BCORL1
DNMT3A-1(KO1)	GGACACCAGCAGCTCTGCTG	DNMT3A
DNMT3A-2	GCACCACGGCACGGAAGGTG	DNMT3A
DNMT3A-3	GGGGACTTGGAGATCACCGC	DNMT3A
DNMT3A-4(KO2)	GCGGAGTGAGCCCCAGCCAG	DNMT3A
DNMT3A-5(KO3)	GGACTCACCCGCTTCTGCAG	DNMT3A
KRAS-1	CCAGTACATGAGGACTGGGG	KRAS
KRAS-2	GTAGTTGGAGCTGGTGGCGT	KRAS
KRAS-3(KO1)	AAGAGGAGTACAGTGCAATG	KRAS
KRAS-4(KO2)	GGACTCTGAAGATGTACCTA	KRAS
KRAS-5(KO3)	AGTAGACACAAAACAGGCTC	KRAS
NEG-1(NT_1)	TGTGTTAGCCGAGATCTCTG	NEG
NEG-2(NT_2)	TGTTCTACTTTTCAAGTTAA	NEG
NEG-3(NT_3)	TGTTTTGCATGTTGCATAGG	NEG
NEG-4	TTAACGCCTTATTTTTATGT	NEG
NEG-5	TTAACTCGAACGCTCGAAAG	NEG
NEG-6	TTAATTTGGGTGGGCCCTGC	NEG
NEG-7	CAGGTTTGCACGCATAGCTA	NEG
NEG-8	CCTCCGTGCTAACGCGGACG	NEG
NEG-9	CCTGTCGCTATCGTTAGAGA	NEG
NEG-10	CGACCCGGAGGATGAGATGT	NEG
NPM1-1(KO1)	TCACAGGTCAGTTTAGGGGC	NPM1
NPM1-2	AGGTGGTAGCAAGGTTCCAC	NPM1
NPM1-3(KO2)	TCTCCCTTCTAGGTTTCCCT	NPM1
NPM1-4(KO3)	ATTAGTGACAGCACTTAGT	NPM1
NPM1-5	GTTGCACATTGTTGAAGCAG	NPM1
WT1-1(KO1)	GGTGTGGCAGCCATAGACCG	WT1
WT1-2(KO2)	GCTGCCGGTGCAGCTGTCCG	WT1
WT1-3	GTATTGGGCTCCGCAGAGGA	WT1
WT1-4	GATGCCGACCGTACAAGAGT	WT1
WT1-5(KO3)	ACTTCAAGGACTGTGAACGA	WT1
⋮	⋮	⋮
⋮	⋮	⋮

First lines of the supplement Excel file listing all sgRNAs sequences; sgRNAs used in experiments beyond the screen are marked with grey background.

Table S6 Gene essentiality score of CRISPR/Cas9 dropout screens as analysed by DepMap_CHRONOS.

DepMap_CHRONOS_ Normalized gene essentiality score	AML-346	AML-356	AML-388	AML-393	AML-661
<i>U2AF1</i>	-1.37662	-1.28929	-1.31494	-1.41232	-1.19405
<i>PSMB3</i>	-1.25859	-1.29115	-1.32068	-1.23249	-1.31156
<i>SRSF2</i>	-0.81706	-1.28989	-1.25282	-1.33242	-1.21662
<i>KRAS</i>	-1.28646	-1.2787	-1.16865	-1.15076	-1.24595
<i>SMC1A</i>	-1.22308	-1.13244	-1.17284	-1.28689	-1.14629
<i>RUNX1</i>	-1.10006	-0.74413	-1.05826	-1.08588	-1.03588
<i>NPM1</i>	-1.14865	-1.07334	-1.04046	-0.69791	-0.91572
<i>SMC3</i>	-0.68685	-1.0939	-1.02207	-1	-1.01288
<i>POLR2L</i>	-0.76202	-1.11428	-0.93927	-0.72661	-1.02923
<i>SF3B1</i>	-1.12951	-0.53644	-0.86359	-1.16118	-0.91607
<i>RAD21</i>	-0.23966	-0.97762	-0.87823	-0.80096	-0.89746
<i>HSPE1</i>	-0.84582	-0.98639	-0.82655	-0.46506	-0.80913
<i>MIR142</i>	-1.00735	-0.83319	-0.63139	-0.75925	-0.46608
<i>RPL12</i>	0.035905	-0.8008	-0.69227	-0.59416	-0.6641
<i>CEBPA</i>	0.022287	-0.76296	-0.65582	-0.98492	-0.42848
<i>KMT2A</i>	-0.7274	-0.26375	-0.52593	-0.50437	-0.56183
<i>DOT1L</i>	-0.89784	-0.45441	-0.5097	-0.46346	-0.55127
<i>HNRNPK</i>	-0.76938	-0.46651	-0.49466	-0.16355	-0.44666
<i>DNMT3A</i>	-0.5199	-0.24005	-0.29501	-0.52326	-0.35812
<i>CSF3R</i>	-0.55843	-0.21538	-0.35629	-0.3221	-0.35085
<i>EZH2</i>	-0.32349	-0.77517	-0.10901	-0.33493	-0.5309
<i>RAN</i>	-0.29374	-0.31841	-0.40673	-0.29558	-0.36441
<i>BCORL1</i>	-0.55482	-0.18972	-0.26761	-0.24063	-0.28194
<i>GATA2</i>	-0.28393	-0.17215	-0.25973	-0.21667	-0.32645
<i>KIT</i>	-0.58695	-0.13375	-0.20769	-0.24548	-0.28729
<i>PTPN11</i>	-0.18314	-0.26907	-0.23528	-0.1378	-0.34488
<i>CBL</i>	-0.33829	-0.19536	-0.22864	-0.15495	-0.25034
<i>FLT3</i>	0.157594	-0.17908	-0.21941	-0.13316	-0.20687
<i>STAG2</i>	-0.28012	-0.17562	-0.13086	-0.05958	-0.23904
<i>IDH1</i>	-0.06452	-0.11423	-0.155	-0.2747	-0.16957
<i>ZRSR2</i>	0.050975	-0.18884	-0.17368	-0.15051	-0.13767
<i>IDH2</i>	-0.13624	-0.02646	-0.14493	-0.26815	-0.18578
<i>KDM6A</i>	-0.19475	-0.08265	-0.14672	-0.13468	0.116084
<i>WT1</i>	-0.45214	-0.0605	-0.13453	-0.27946	0.295726
<i>TET2</i>	-0.13597	-0.02068	-0.08403	-0.05364	-0.09295
<i>BCOR</i>	0.118741	-0.00135	-0.07773	-0.2178	-0.08939
<i>ETV6</i>	-0.38554	-0.16721	0.021916	0.440408	-0.04958
<i>NRAS</i>	0.078747	-0.10691	0.02283	-0.04767	-0.07603
<i>NEG</i>	-0.07006	0	0.159276	-0.06875	0.042338
<i>ASXL1</i>	0.32576	0.02103	0.040081	-0.08673	0.055513

Table S7 Gene essentiality score of CRISPR/Cas9 dropout screens as analysed by Lin et al.

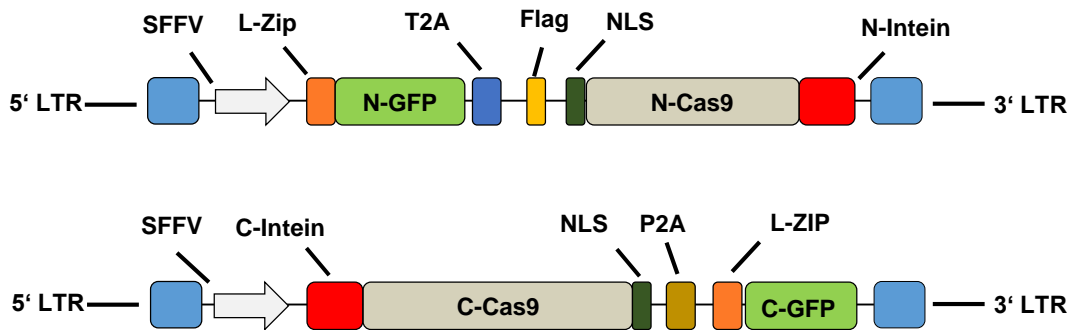
Lin, Shan et al. _ gene essentiality score	AML-346	AML-356	AML-388	AML-393	AML-661
<i>POLR2L</i>	-1.5692	-1.69838	-1.006762919	-2.08497	-1.38318
<i>PSMB3</i>	-1.41696	-1.66995	-1.540977903	-0.93885	-1.44967
<i>U2AF1</i>	-0.97354	-1.33914	-1.267626092	-1.51349	-1.11488
<i>SRSF2</i>	-1.38745	-1.26157	-1.413046778	-1.16692	-1.19196
<i>RUNX1</i>	-1.3137	-0.70571	-1.193550017	-1.04535	-1.22842
<i>KRAS</i>	-2.68042	#NUM!	-1.023416577	-0.68671	-1.13702
<i>RAD21</i>	-0.82632	-1.64835	-1.040465667	-0.50043	-1.47456
<i>SMC3</i>	-0.21478	-0.98136	-1.314272559	-1.03833	-1.34416
<i>CEBPA</i>	1.621838	-0.96764	-1.123921169	-1.68431	-0.12936
<i>NPM1</i>	-1.16602	-0.9651	-1.059589121	-0.38598	-0.75346
<i>SMC1A</i>	-1.26798	-0.87058	-1.02862213	-0.64742	-0.93642
<i>SF3B1</i>	-0.85482	-0.29391	-0.7699974	#NUM!	-0.87895
<i>RAN</i>	-0.80644	-0.65382	-0.653824449	-0.90112	-1.15394
<i>RPL12</i>	1.431594	-0.80297	-1.100220194	-0.71252	-1.27501
<i>HSPE1</i>	-1.257	-1.0664	-0.722478531	-0.66481	-0.7351
<i>EZH2</i>	-0.69339	-0.87788	0.049412062	0.25026	-0.95415
<i>KMT2A</i>	-0.61774	-0.25914	-0.707744713	-0.71683	-0.61626
<i>DOT1L</i>	-0.7697	-0.37652	-0.432881097	0.100558	-0.55926
<i>STAG2</i>	-0.57639	-0.20363	-0.42691786	0.054666	-0.41493
<i>GATA2</i>	-0.43964	-0.07132	-0.40145661	0.025721	-0.60884
<i>MIR142</i>	-1.27954	-0.81943	-0.384379018	-0.38354	-0.01541
<i>HNRNPK</i>	-0.98077	-0.38294	-0.45567748	0.335676	-0.36148
<i>PTPN11</i>	0.978504	-0.33105	-0.416354241	-0.33784	-0.98803
<i>FLT3</i>	1.701393	-0.31607	-0.713583636	-0.12671	-0.50136
<i>CBL</i>	-0.26517	-0.22183	-0.309807544	-0.84356	-0.41076
<i>DNMT3A</i>	0.590651	-0.20312	-0.280723441	-0.43143	-0.26304
<i>IDH2</i>	0.695956	0.010594	-0.308473637	-0.22696	-0.40147
<i>BCORL1</i>	0.106589	-0.15966	-0.214293387	-0.2661	-0.22433
<i>KIT</i>	-0.71808	0.015894	-0.193139979	-0.07362	-0.22602
<i>IDH1</i>	0.367774	-0.08031	-0.238039489	-0.18734	-0.18871
<i>BCOR</i>	0.193248	-0.18557	-0.253559357	-0.68262	-0.17859
<i>NRAS</i>	0.422523	-0.21876	-0.159717348	0.12054	-0.19893
<i>CSF3R</i>	0.774383	-0.10523	-0.400189764	-0.10588	-0.26671
<i>ZRSR2</i>	0.810849	-0.23522	-0.531009257	-0.06204	-0.10351
<i>TET2</i>	0.323361	-0.10225	-0.515669844	0.147029	-0.52178
<i>ASXL1</i>	-0.68702	-0.07187	-0.129086898	0.073383	-0.09676
<i>ETV6</i>	-0.46725	-0.12629	-0.049316223	0.832108	0.035122
<i>KDM6A</i>	0.286418	0.001605	-0.275162964	-0.12415	0.409581
<i>WT1</i>	0.334503	0.044185	-0.18656338	-0.27728	0.884145

Table S8 Gene depletion score of CRISPR/Cas9 dropout screen as analysed by MAGECK

MAGECK_depletion score	AML-346	AML-356	AML-388	AML-393	AML-661
<i>POLR2L</i>	0.002699	0.00021	0.000183	0.000615	0.000615
<i>SRSF2</i>	0.003947	0.000679	0.003219	0.00868	0.01981
<i>RUNX1</i>	0.10255	0.29981	0.003966	0.005669	0.000441
<i>SMC1A</i>	0.006885	0.00316	0.005289	0.19168	0.006496
<i>RPL12</i>	0.62682	0.006944	0.017417	0.009934	0.002844
<i>PSMB3</i>	0.11261	0.009346	0.010166	0.006944	0.016052
<i>RAD21</i>	0.36138	0.010817	0.009568	0.31047	0.00076
<i>CEBPA</i>	0.97752	0.002844	0.012195	0.00047	0.88441
<i>SMC3</i>	0.012195	0.003681	0.014352	0.006885	0.036929
<i>U2AF1</i>	0.02143	0.003412	0.002699	0.016207	0.044068
<i>RAN</i>	0.00648	0.028345	0.12773	0.12073	0.012195
<i>HSPE1</i>	0.010817	0.0399	0.037329	0.38269	0.15857
<i>KRAS</i>	0.1068	0.003966	0.05997	0.12493	0.005385
<i>NPM1</i>	0.26717	0.00459	0.029502	0.086664	0.29153
<i>SF3B1</i>	0.36851	0.35097	0.098415	0.003412	0.069214
<i>KMT2A</i>	0.18219	0.68716	0.14614	0.20099	0.62746
<i>EZH2</i>	0.29003	0.054296	0.99603	0.96473	0.027741
<i>MIR142</i>	0.011295	0.29153	0.17297	0.39489	0.99209
<i>FLT3</i>	0.45771	0.32639	0.1068	0.47256	0.28989
<i>DOT1L</i>	0.059791	0.36851	0.14948	0.45457	0.49485
<i>HNRNPK</i>	0.23219	0.45771	0.41319	0.45771	0.37832
<i>STAG2</i>	0.45457	0.94669	0.42224	0.96301	0.34228
<i>TET2</i>	0.54204	0.87998	0.62746	0.83369	0.60951
<i>PTPN11</i>	0.96951	0.71893	0.72659	0.73428	0.031339
<i>GATA2</i>	0.66219	0.9443	0.74266	0.93103	0.31659
<i>CBL</i>	0.33366	0.83369	0.76317	0.27521	0.949
<i>NEG_</i>	-	0.90441	0.88971	-	0.81127
<i>ZRSR2</i>	0.89287	0.97977	0.39519	0.67062	0.98282
<i>CSF3R</i>	0.73428	0.91868	0.96638	0.72659	0.97506
<i>DNMT3A</i>	0.96122	0.92192	0.9724	0.44438	0.52449
<i>KDM6A</i>	0.39302	0.92809	0.93926	0.88441	1
<i>IDH1</i>	0.95744	0.73428	0.97977	0.94182	0.93386
<i>BCORL1</i>	0.37736	0.98851	0.92506	0.95337	0.95544
<i>BCOR</i>	0.73414	0.96638	0.95744	0.17831	0.99043
<i>KIT</i>	0.57253	0.99433	0.99684	0.97506	0.94182
<i>IDH2</i>	0.43131	0.99684	0.99043	0.91188	0.97752
<i>NRAS</i>	0.37236	0.97867	0.99897	0.90831	0.97867
<i>ASXL1</i>	0.31047	0.99603	0.98918	0.95544	0.98185
<i>ETV6</i>	0.49485	0.99393	0.99932	1	0.98918
<i>WT1</i>	0.93103	1	0.99751	0.35097	1
<i>NEG</i>	0.76975	0.99999	0.99997	0.99971	1

Figure S1 Lentiviral constructs

A Scheme of the split-Cas9 / split-GFP constructs



B Scheme of the sgRNA expression construct

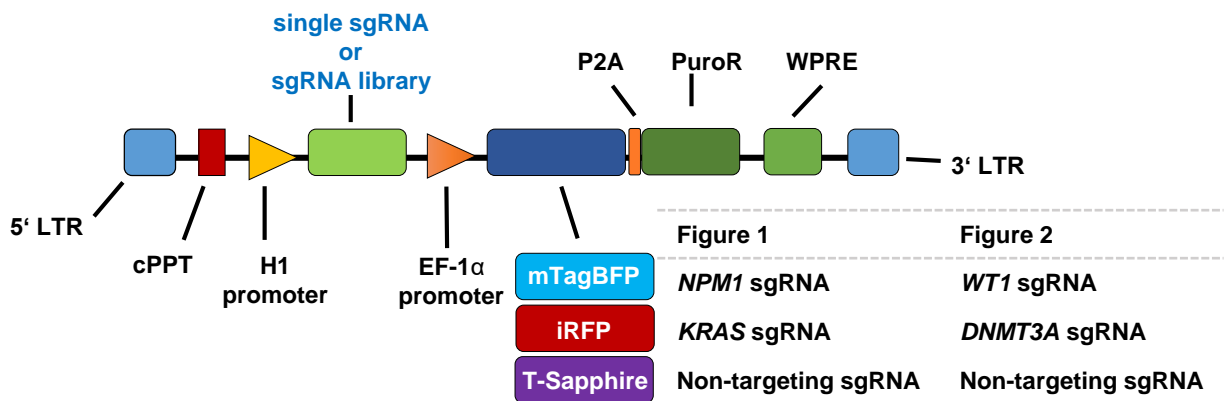


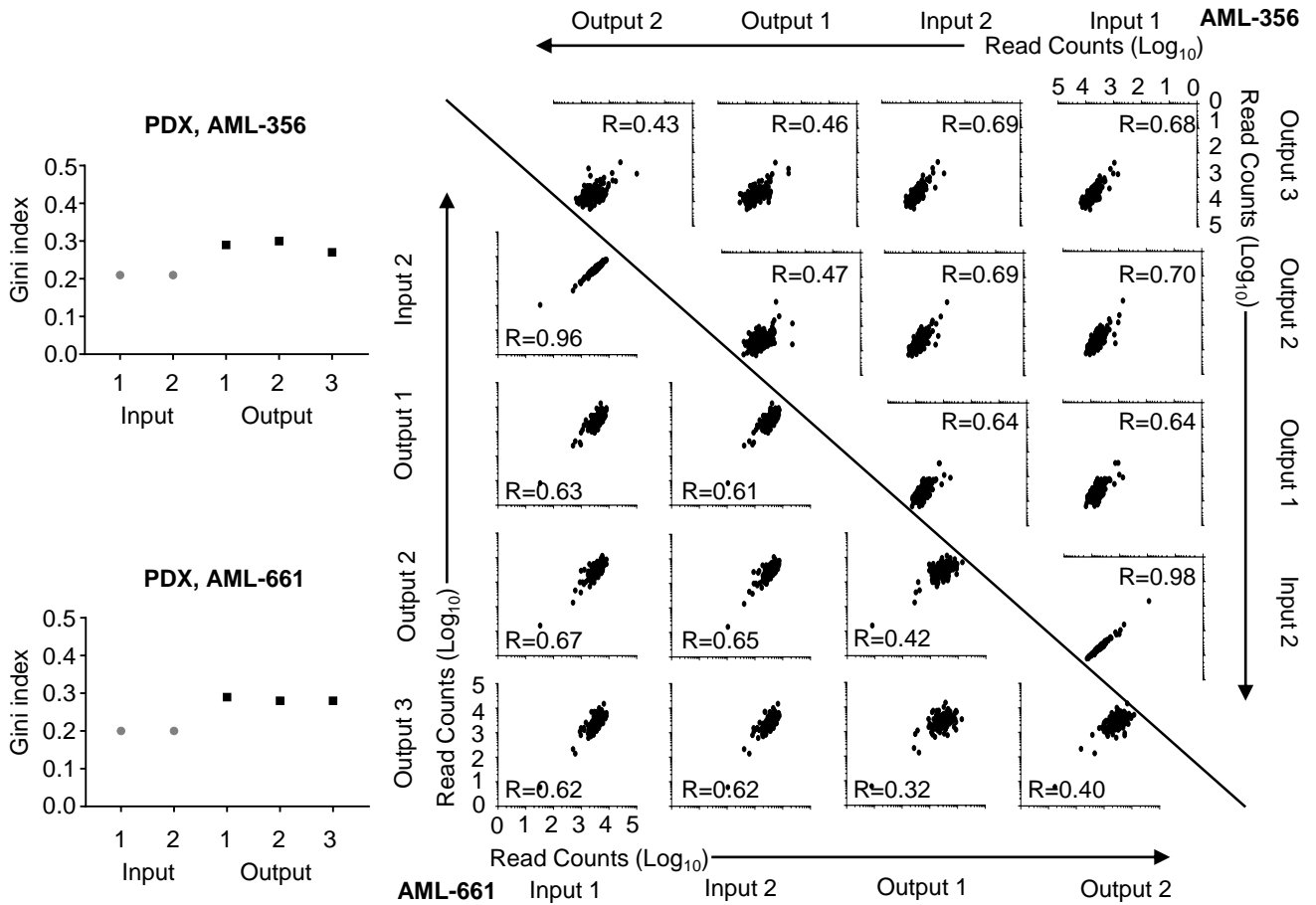
Figure S1. Lentiviral constructs

A Scheme of the split-Cas9 / split-GFP constructs. SFFV, spleen focus-forming virus promoter; L-Zip, leucine zipper; GFP, green fluorescent protein; P2A and T2A, 2A peptides derived from porcine teschovirus-1 and thosea asigna virus; NLS, nuclear localization signal; Cas9, CRISPR associated protein 9; N-GFP/C-GFP or N-Intein/C-Intein or N-Cas9/C-Cas9, N/C-terminal part of the GFP or /Intein or Cas9 coding sequence, respectively.

B Scheme of the sgRNA expression construct. sgRNA, single guide RNA; LTR, long terminal repeat; cPPT, central polypurine tract; EF-1 α , elongation factor-1 α short promoter; mTagBFP, monomeric tag blue fluorescent protein; iRFP, near-infrared fluorescent protein; T-Sapphire, T-Sapphire fluorescent protein; mCherry, mCherry fluorescent protein; PuroR, puromycin resistance gene; WPRE, woodchuck hepatitis virus posttranscriptional regulatory element.

Figure S2 CRISPR/Cas9 screen in PDX models *in vivo*

A Quality controls in Cas9 negative PDX models



B PDX CRISPR/Cas9 *in vivo* screen

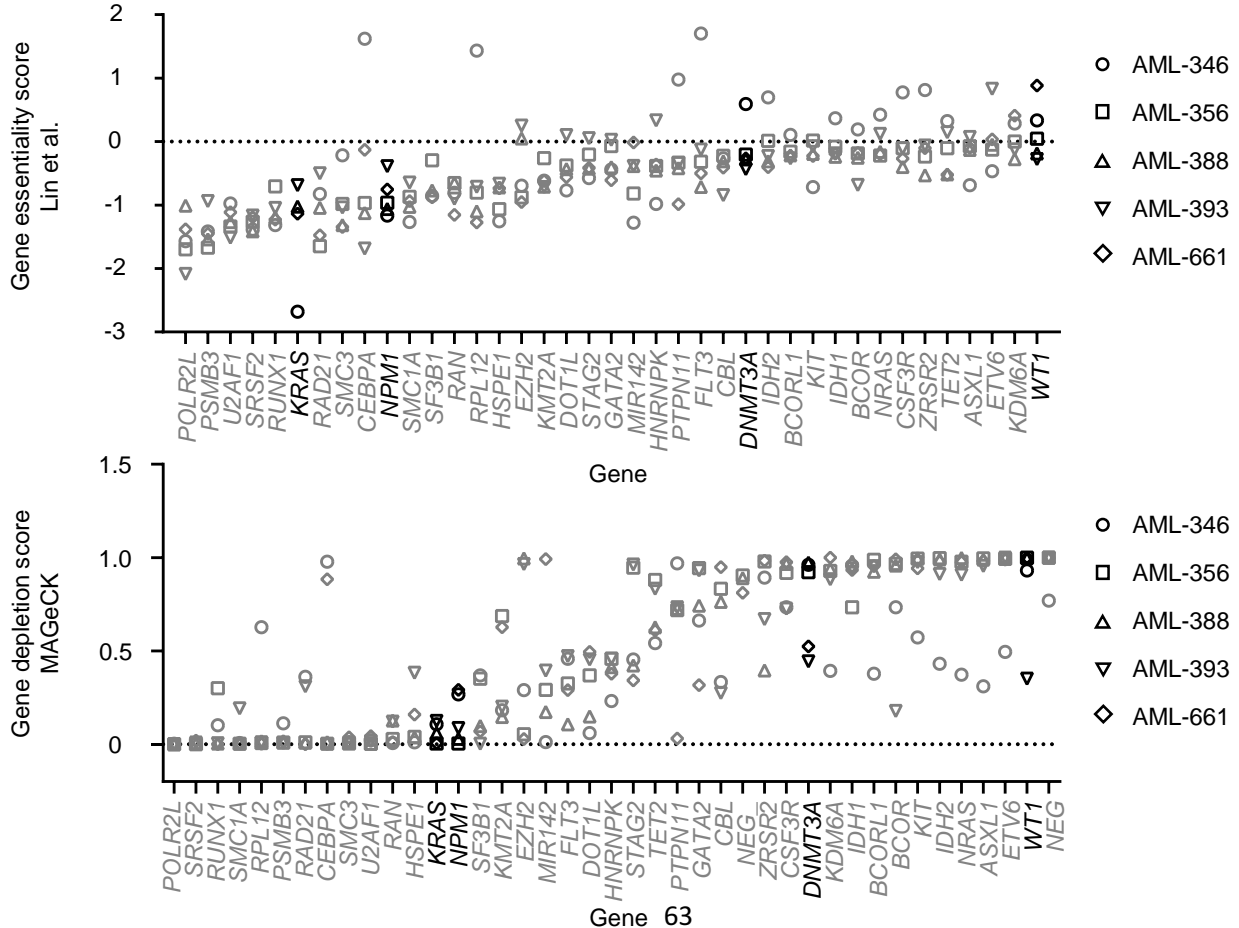


Figure S2. CRISPR/Cas9 dropout screen in PDX models *in vivo*.

A Quality controls. The experiment was performed as described in Figure 1A,B, except that Cas9 negative PDX cells were used so that no DNA editing took place; input 1 was harvested 1 day post-transduction, input 2 was harvested after puromycin selection and outputs 1-3 were harvested from 3 replicate mice. Gini indices were analyzed with custom Python scripts. The correlation of sgRNA read counts were analyzed by Pearson R.

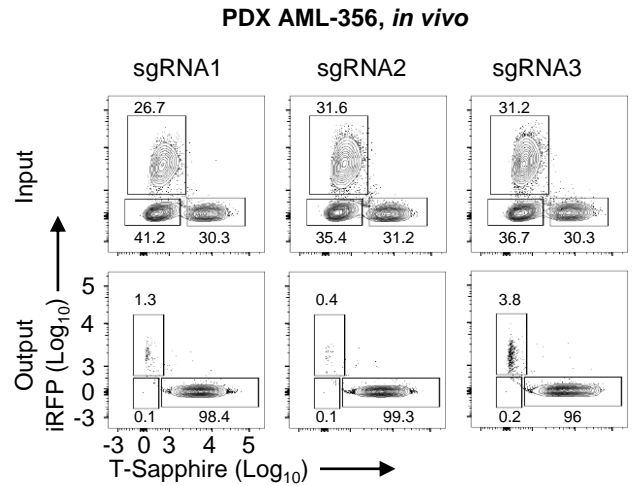
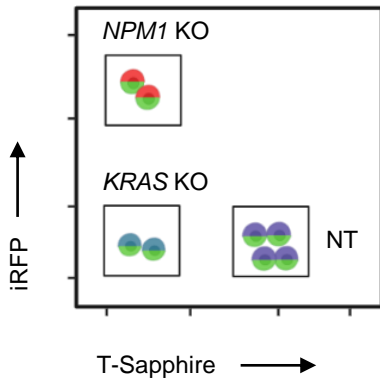
B Experiment from Figure 1C, with data analysed according to Lin et al.^[1] or the MAGeCK algorithm^[2].

[1] Lin S, Larrue C, Scheidegger NK, et al. An In Vivo CRISPR Screening Platform for Prioritizing Therapeutic Targets in AML. *Cancer Discov.* 2022.

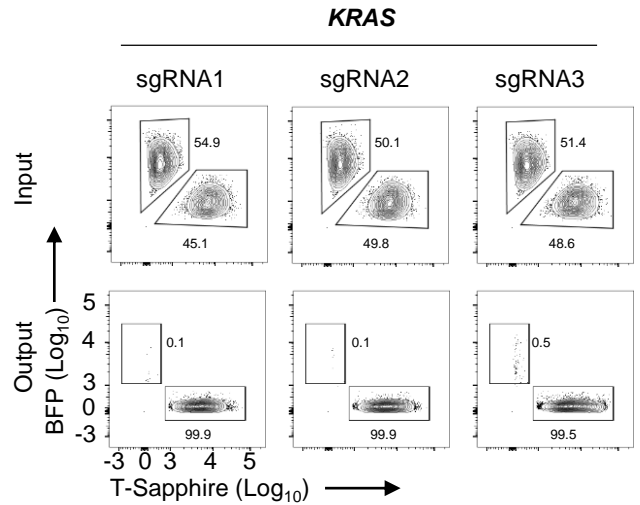
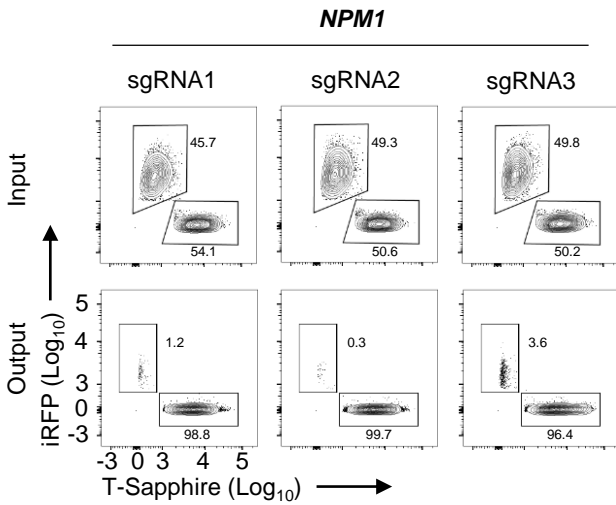
[2] Li W, Xu H, Xiao T, et al. MAGeCK enables robust identification of essential genes from genome-scale CRISPR/Cas9 knockout screens. *Genome Biol.* 2014.

Figure S3 Step-by-step analysis of flow cytometric data from *in vivo* competitive knockout experiments

A Raw data of all 3 populations



B 2 populations using Boolean gates



C Quantification and statistics

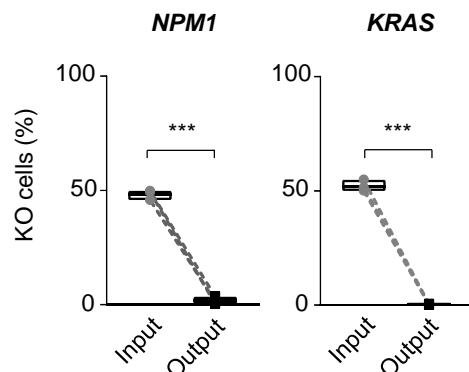


Figure S3. Step-by-step analysis of flow cytometric data from *in vivo* competitive knockout experiments

Additional data from AML-356 as in Figure 1C,D for AML-661.

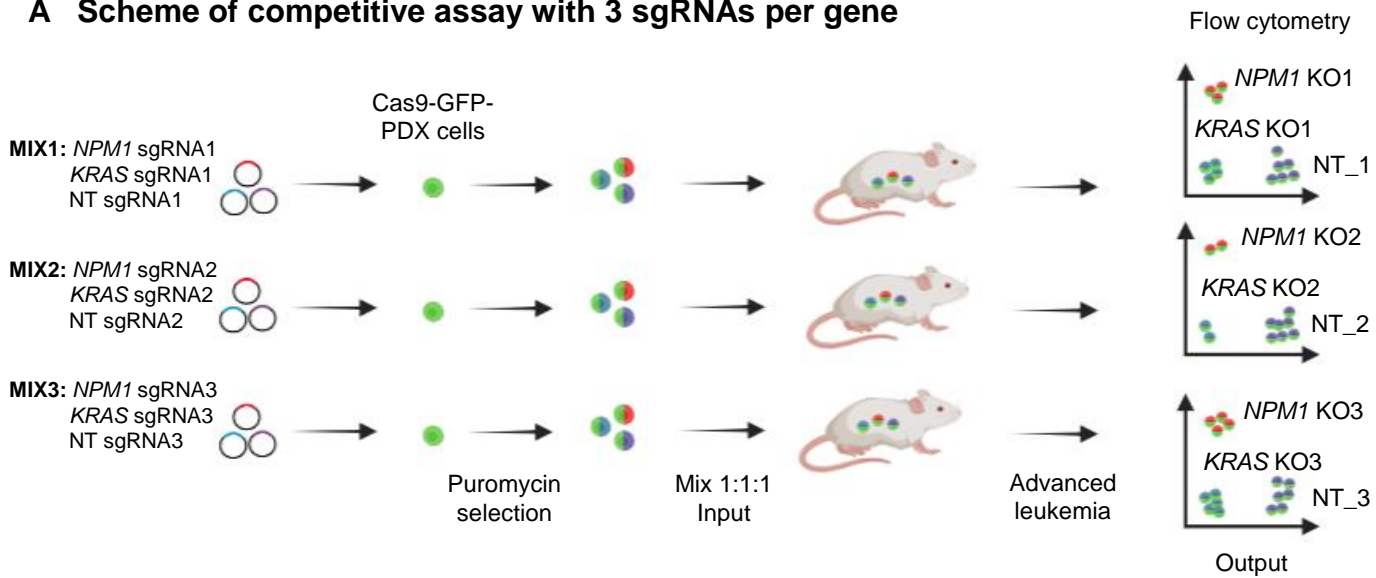
A Flow cytometry schematic view and raw data of the entire population of PDX cells; co-expression of recombinant fluorochromes (Figure S1B) allowed separating the 3 subpopulations, namely *NPM1* KO, *KRAS* KO and NT (non-targeting).

B From data in A, Boolean gates were set in FlowJo to analyze each knockout population (either *NPM1* KO or *KRAS* KO) separately and in direct comparison to the NT population.

C From data in B, statistical analyses were performed. Input and output data are linked by a dotted line containing the same sgRNA. Each output dot represents a single mouse. Bar plots indicate mean, minimum and maximum. *P*-values were calculated by paired two-tailed t-test (***) $p < 0.001$.

Figure S4 *In vivo* competitive assay using 3 replicate sgRNAs per gene in 3 replicate mixtures

A Scheme of competitive assay with 3 sgRNAs per gene



B Quality controls for knockout of *NPM1* and *KRAS* using 3 different sgRNAs

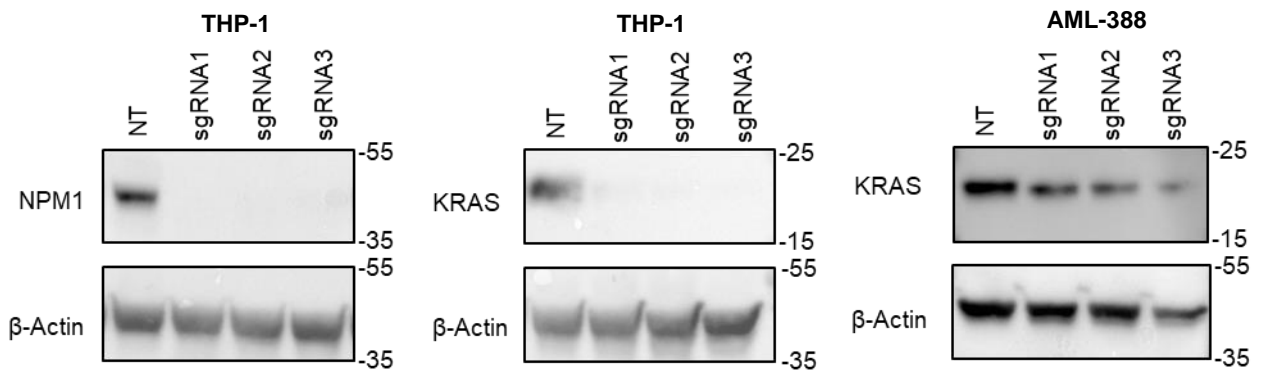


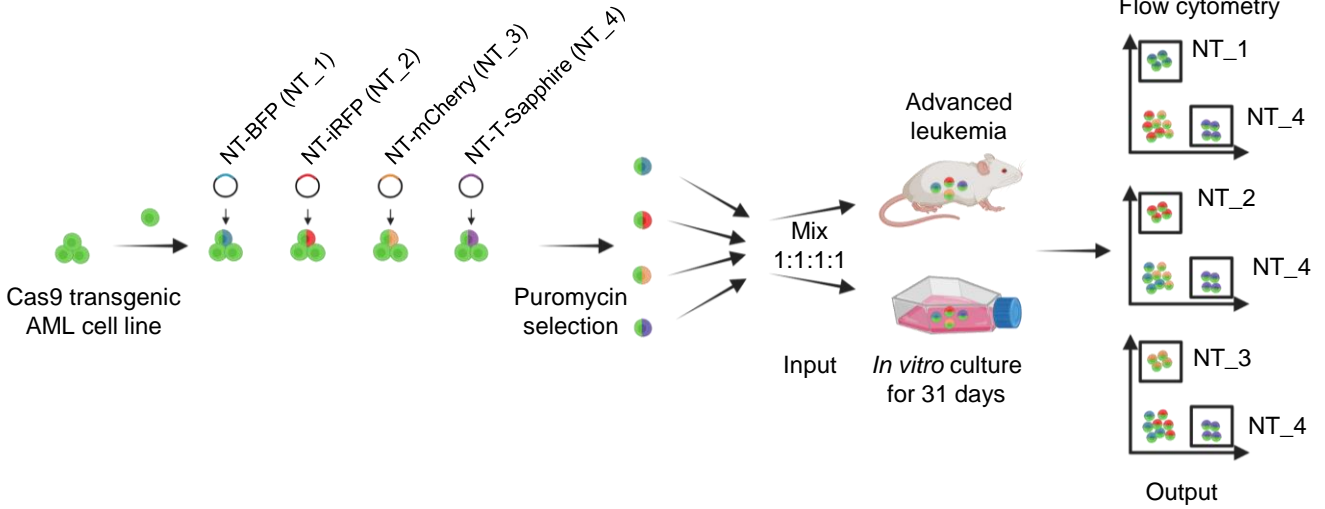
Figure S4. *In vivo* competitive assay using 3 replicate sgRNAs per gene in 3 replicate mixtures

A Complementary scheme to Figure 1C. Experiments depicted in Figure 1C were performed with 3 replicate mice, each mouse receiving a different sgRNA each for knockout of each *KRAS*, *NPM1* and NT subsets. Thus, a total of 9 different sgRNAs was injected into a total of 3 mice for each experiment and PDX model.

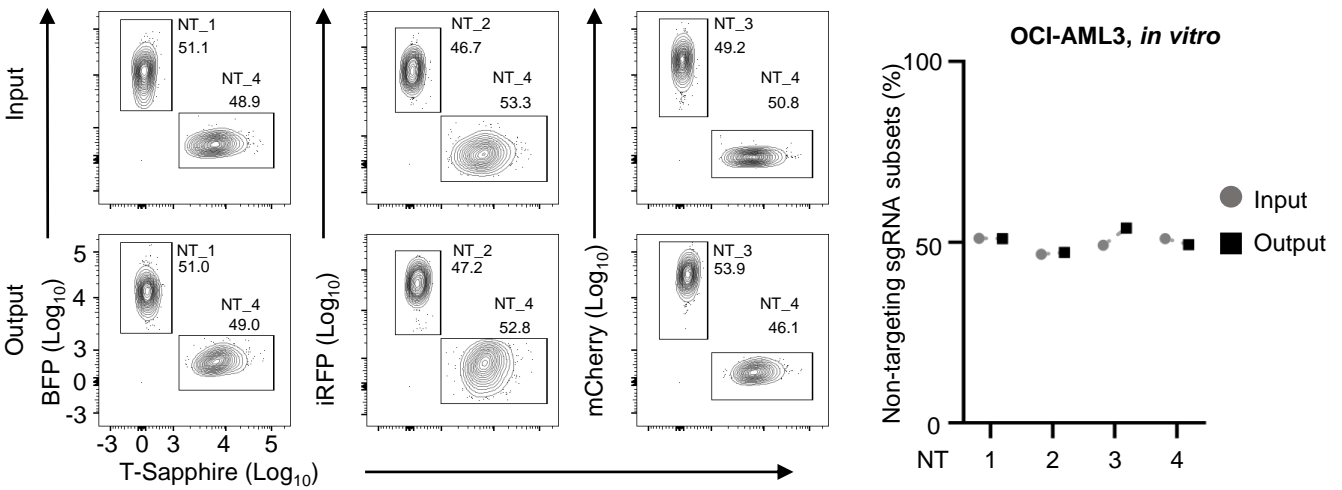
B Quality control of sgRNAs targeting *NPM1* and *KRAS*. Western Blot on THP-1 cells and AML-388 PDX cells transduced with either a nontargeting (NT) sgRNA or one of the 3 different sgRNAs targeting either *NPM1* or *KRAS*. 1×10^6 cells from each knockout population were harvested 14 days after transduction. β -Actin served as loading control.

Figure S5 Quality controls using nontargeting sgRNAs

A Scheme of competitive assay with nontargeting sgRNAs



B *In vitro* competitive assay with nontargeting sgRNA subsets in a cell line



C *In vivo* competitive assay with nontargeting sgRNA subsets in a PDX model

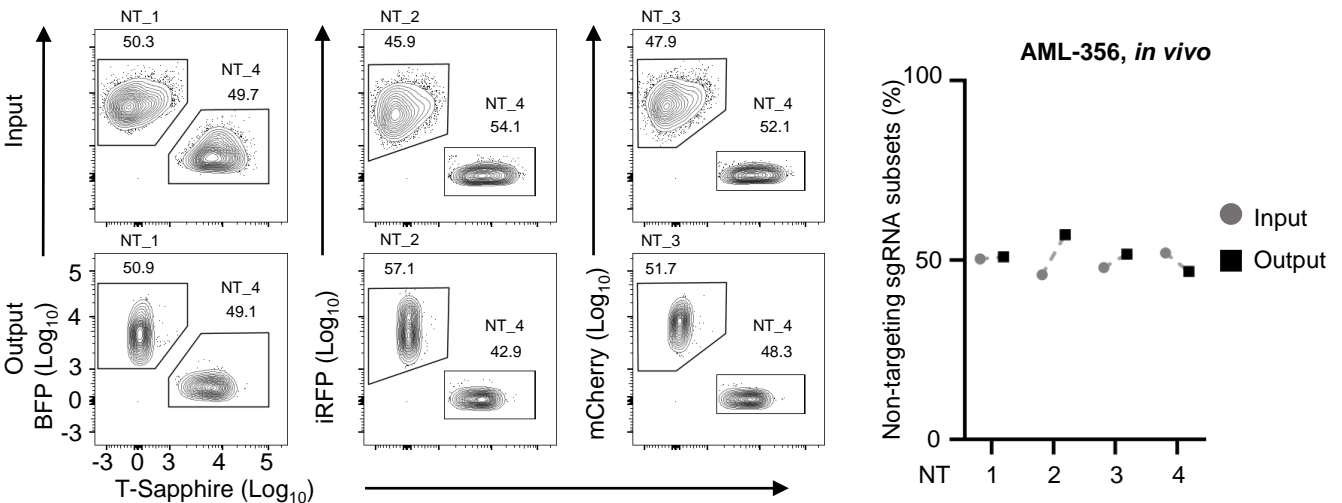


Figure S5 ff

Figure S5. Quality control using nontargeting sgRNAs

Complement to Figure 1C,D to exclude putative bias by the fluorochromes.

A **Scheme of experiments *in vivo* and *in vitro*.** Four different fluorochromes were cloned into the construct containing the same nontargeting (NT) sgRNA, namely NT-BFP (NT_1), NT-iRFP (NT_2), NT-mCherry (NT_3) and NT-T-sapphire (NT_4). AML PDX cells and cell lines were lentivirally transduced. After puromycin selection, all four populations were mixed at a 1:1:1:1 ratio. PDX or cell line mixture was injected into mouse or kept in vitro culture. The distribution of non-targeting subsets was measured when mice were in advanced leukemia or on day 31 post-transduction.

B, C NT sgRNA subsets *in vitro* (B) and *in vivo* (C) competitive assay was performed on OCI-AML3 cells and AML-356. Data were step-by-step analyzed as described in Figure S4. Left flow cytometry plots show data gating NT_4 subset with one of the other three NT sgRNA subsets by using Boolean gate strategy in FlowJo. Right show a quantitative summary for all NT populations. Each dot represents a single NT population, with input and output data linked by a dotted line.

Figure S6 Presence of a hot spot mutation increases gene dependency in *KRAS*, but not in *DNMT3A*

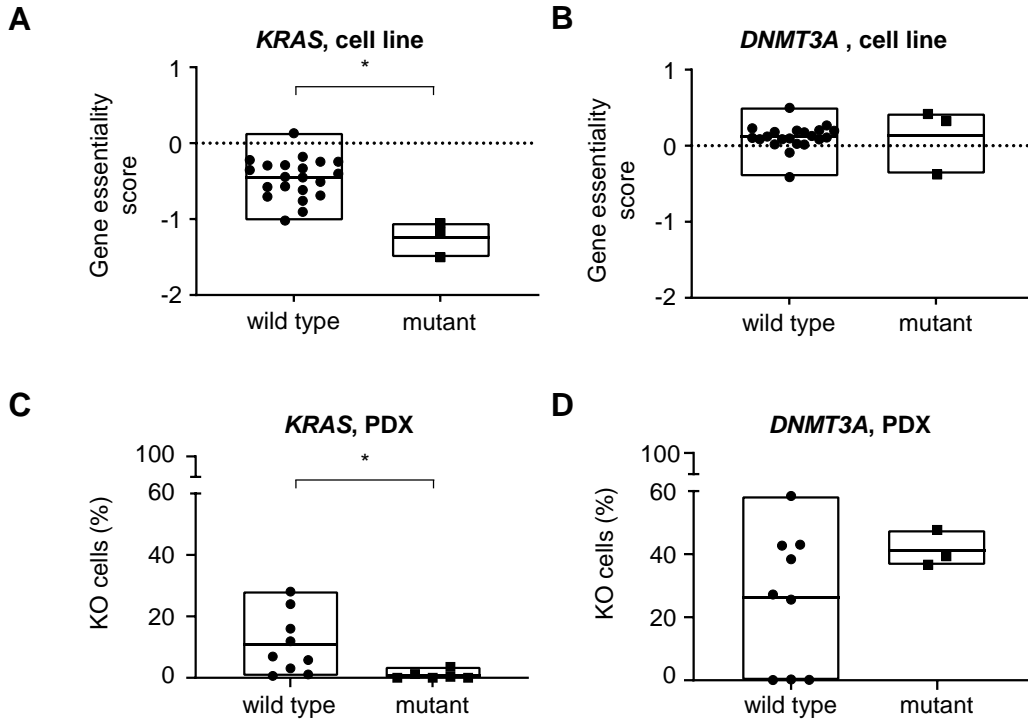


Figure S6. Presence of a hot spot mutation increases gene dependency in *KRAS*, but not in *DNMT3A*

A,B Gene essentiality score of *KRAS* and *DNMT3A* in wild type and mutated AML cell lines were taken from DepMap Public 21Q3. Data from a total of 24 AML cell lines were available; each dot represents the score of one AML cell line.

C,D Summary data of *KRAS* or *DNMT3A* knockouts from Figure 1D and 2A, separated according to the presence or absence of a mutation in either *KRAS* or *DNMT3A*. Each dot represents an output of single knockout.

Results from statistical analyses by two-tailed paired t-test are shown if they were significant. * $p < 0.05$ and ** $p < 0.01$, *** $p < 0.001$.

Figure S7 Quality control for *DNMT3A* and *WT1* knockout

A

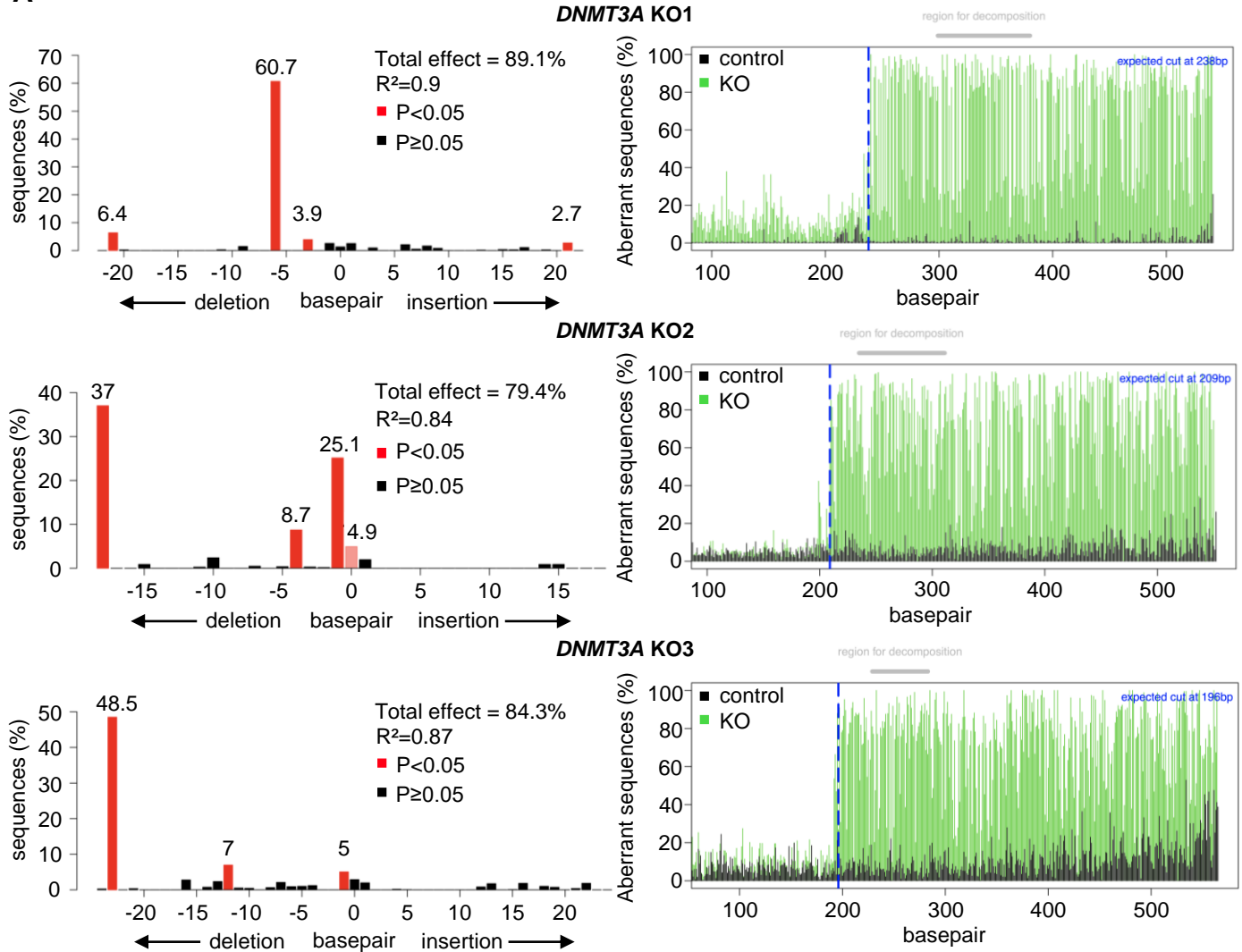
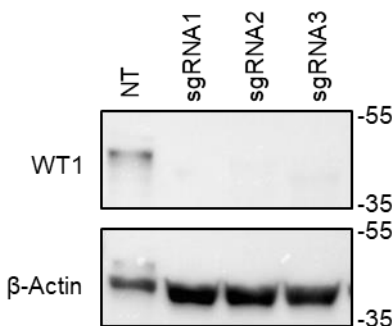


Figure S7. Quality control for *DNMT3A* and *WT1* knockout

B

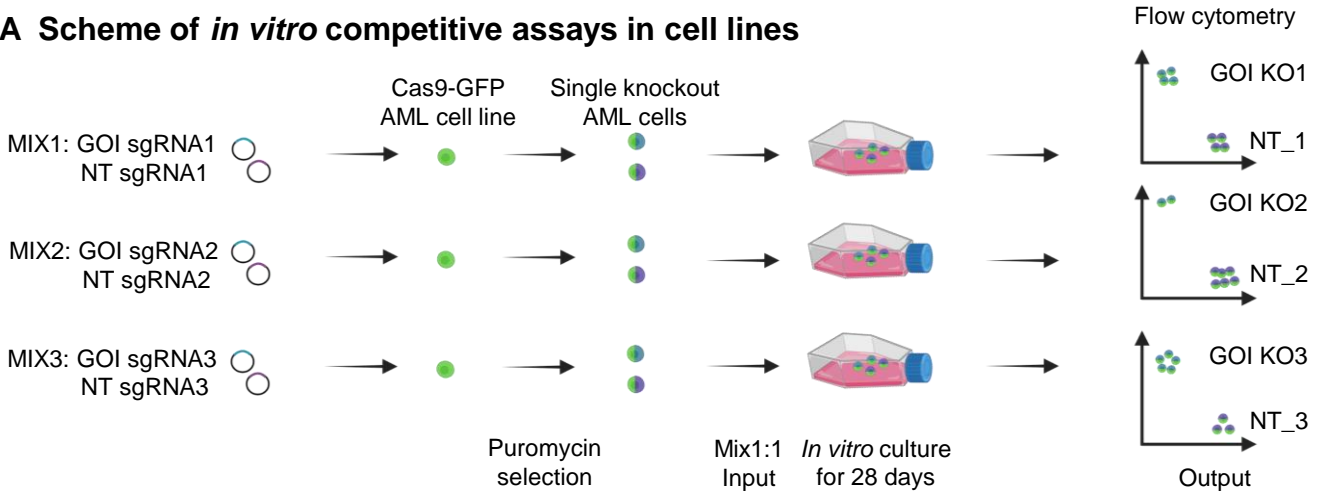


A Gene editing efficiency of *DNMT3A* analyzed by TIDE analysis. THP-1 cells were transduced with 3 different sgRNAs targeting *DNMT3A* and knockout efficiency measured 14 days after transduction by tracking of indels using decomposition (TIDE) analysis. The left panel shows the DNA modification percentage by each *DNMT3A* sgRNA. In the right panel, *DNMT3A* knockout reads getting from Sanger sequencing are shown in green, non-targeting cell reads in black and the blue dashed line indicates the break site.

B Efficient depletion of *WT1* by distinct sgRNAs. Western Blot was performed identically as Figure S3B to quality control of *WT1* KO. 1×10^6 cells from each *WT1* knockout population in THP-1 were harvested 14 days after transduction. β -Actin served as loading control.

Figure S8 Both *WT1* and *DNMT3A* lack an essential function in AML cell lines

A Scheme of *in vitro* competitive assays in cell lines



B *WT1* lacks essential function in AML cell lines *in vitro*

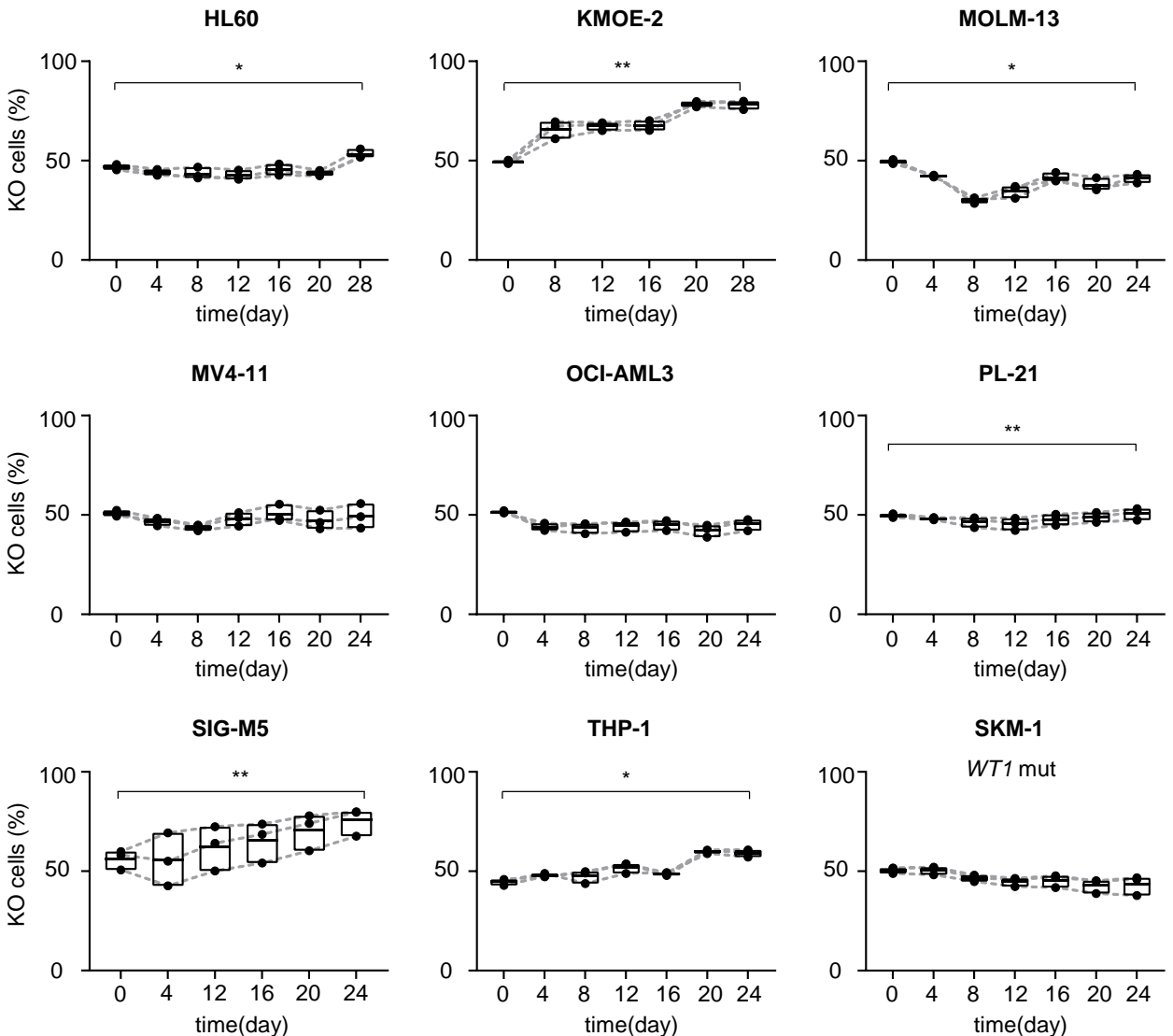


Figure S8 ff

C *DNMT3A* lacks essential function in AML cell lines *in vitro*

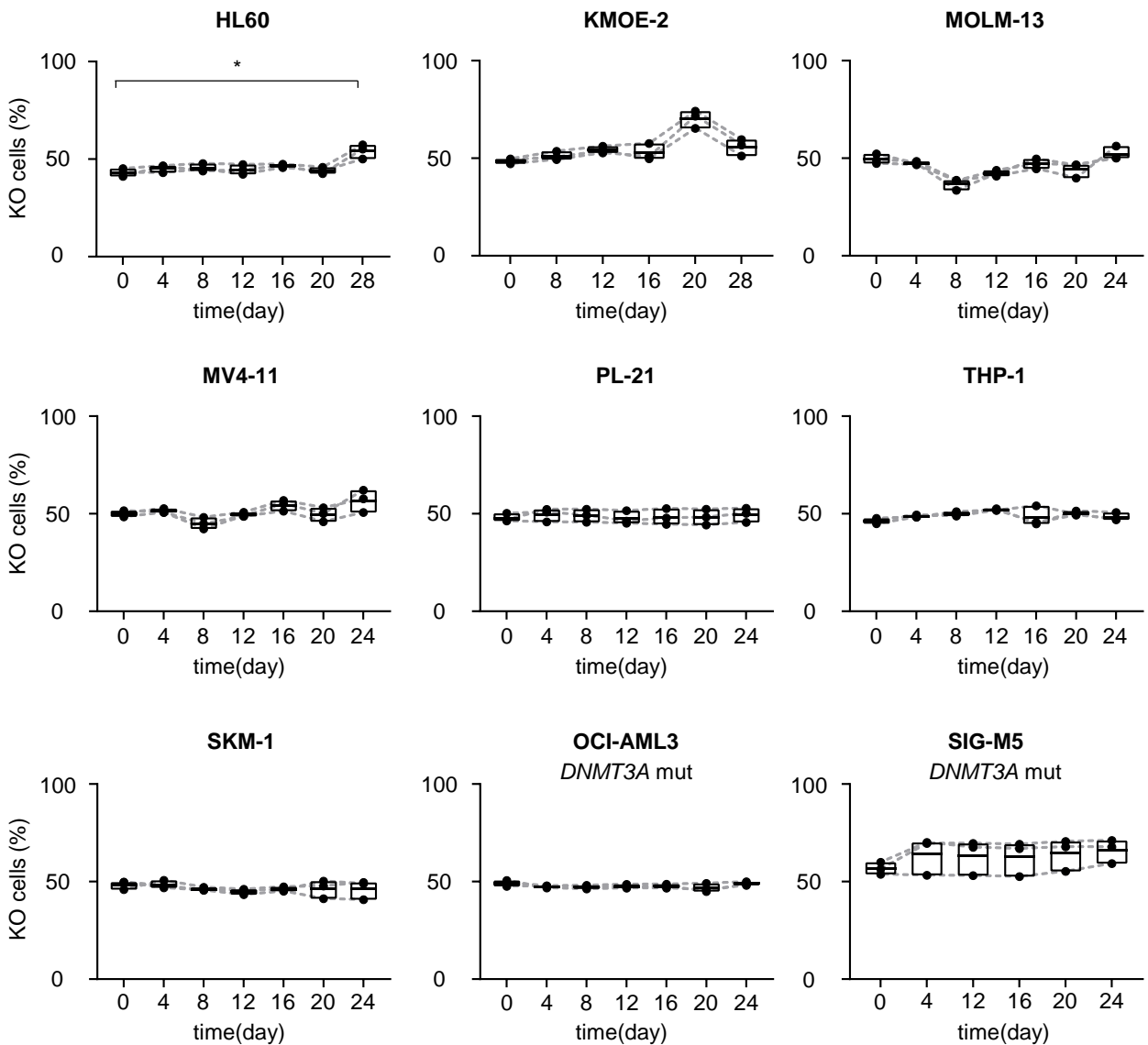


Figure S8. Both *WT1* and *DNMT3A* lack an essential function in AML cell lines

A Scheme of competitive assays in cell lines *in vitro*. Cas9-transgenic cell lines were transduced with a sgRNA targeting *WT1* or *DNMT3A* or a NT sgRNA, expressing different fluorescent markers to discriminate the populations by flow cytometry, related to Figure 1C and Figure S1B. After cells were enriched by puromycin selection, *WT1* or *DNMT3A* knockout cells were mixed with control cells at a 1:1 ratio and cultured *in vitro* for 28 days. The distribution of the mixture was measured by flow cytometry at the beginning and every four days. The experiment was performed in triplicates using three different sgRNAs per gene. GOI, gene of interest.

B,C *WT1* (B) and *DNMT3A* (C) lack essential function in AML cell lines *in vitro*. Experiments on 9 AML cell lines were performed as described in A; data were analyzed and depicted as described in Figure S4. Each dot represents a single output, with related sgRNAs linked by a dotted line. Bar plots indicate mean, minimum and maximum percentage of knockout populations. Results from statistical analyses by two-tailed paired t-test are shown if they were significant. * $p < 0.05$, ** $p < 0.01$, *** $p < 0.001$.

Figure S9 Summary: Both *WT1* and *DNMT3A* lack an essential function in AML cell lines

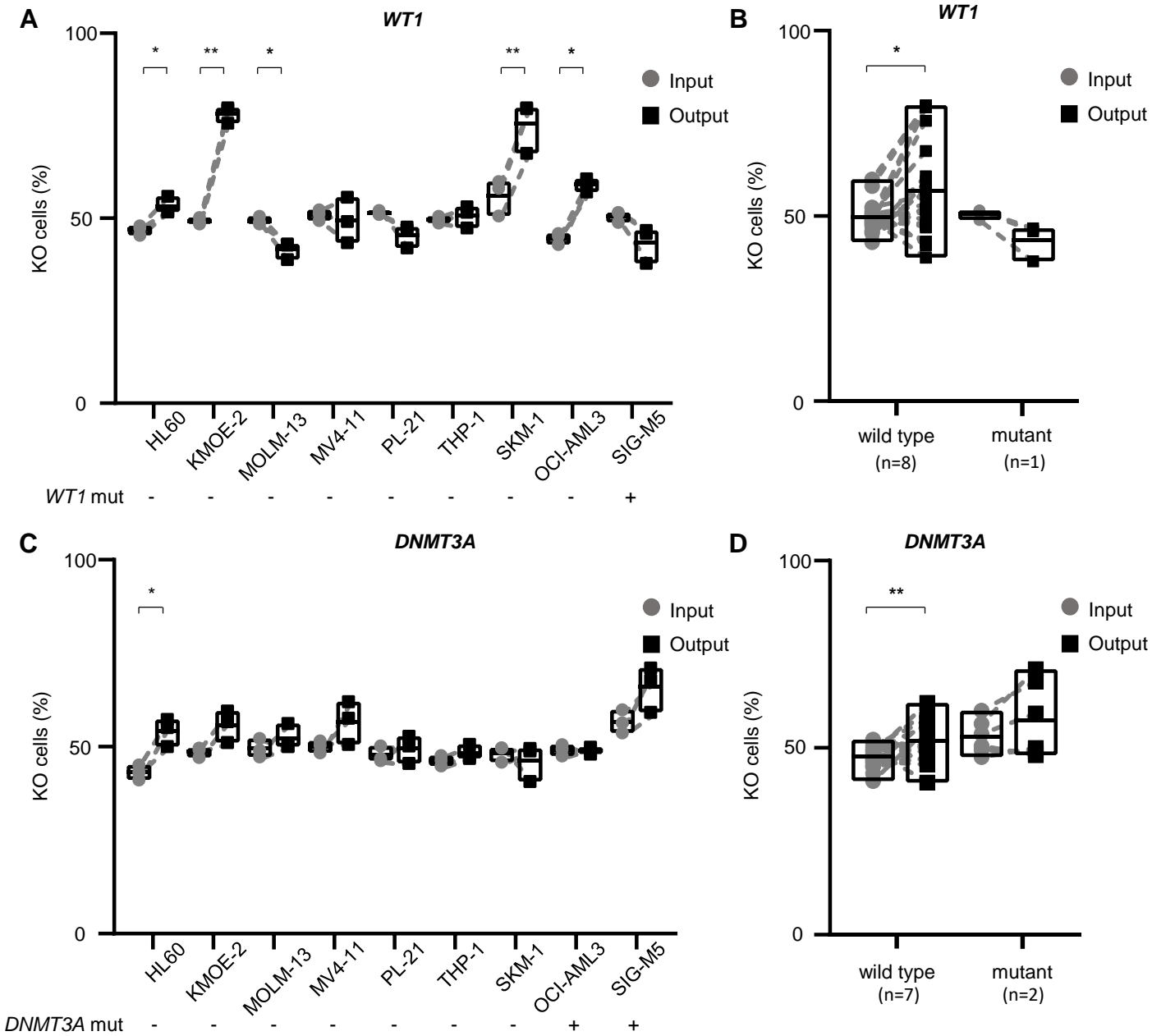


Figure S9. Summary: Both *WT1* and *DNMT3A* lack an essential function in AML cell lines

A,C Summary data from Figure S7, depicted as in Figure 1D; n=3.

B,D Summary of data from Figure S7A or S7C, respectively, separated according to the presence or absence of a mutation in either *WT1* or *DNMT3A*, respectively.

Bar plots indicate mean, minimum and maximum percentage of input or output knockout populations. Results from statistical analyses by two-tailed paired t-test are shown if they were significant. * $p < 0.05$ and ** $p < 0.01$, *** $p < 0.001$. Grey dashed lines linked the dots representing the same knockout.

Fig S10. Immunophenotype of PDX AML cells after KO of *WT1* or *DNMT3A*

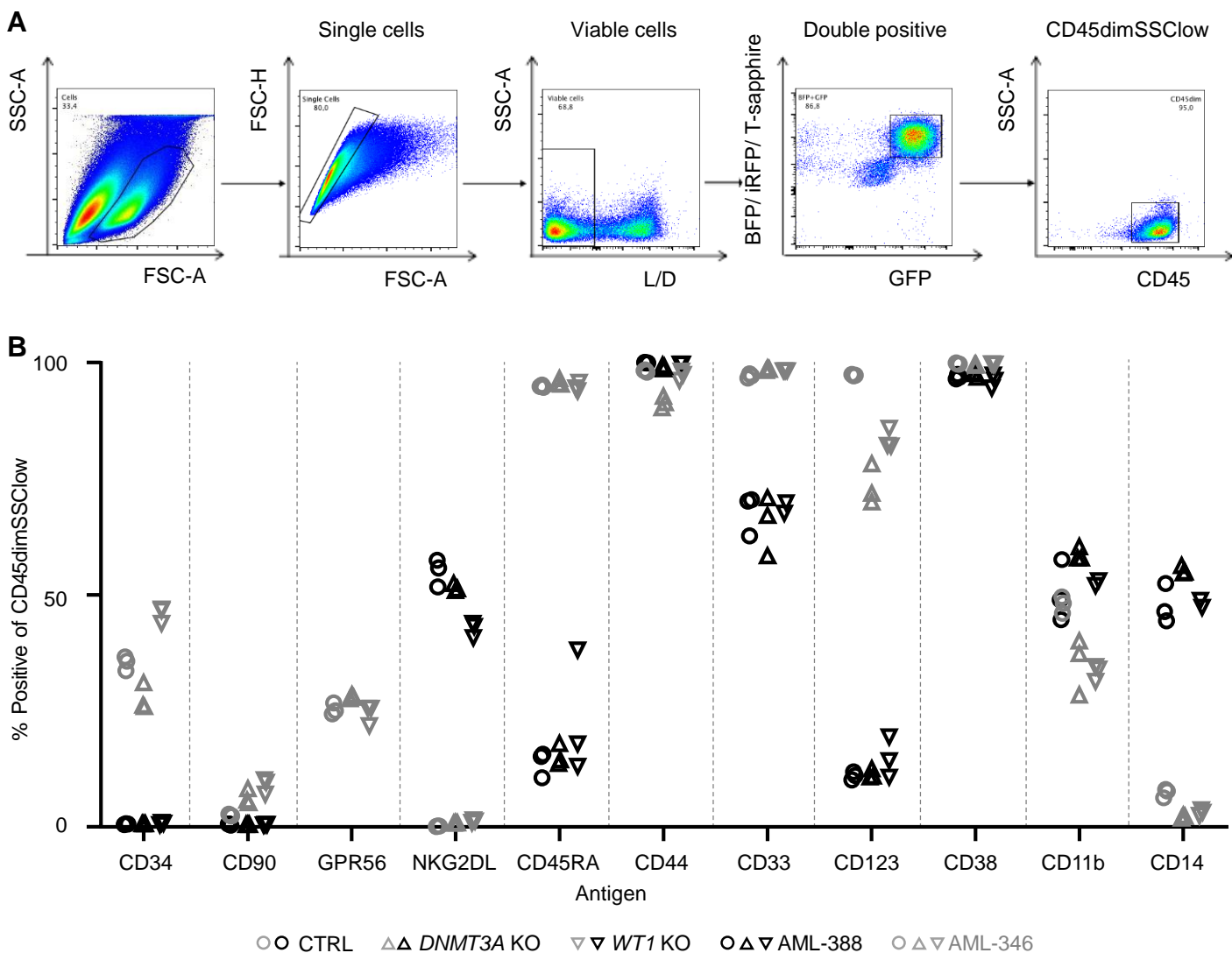


Fig S10. Immunophenotype of PDX AML cells after KO of *WT1* or *DNMT3A*

A Gating strategy to quantify antigen expression on single, living, GFP+mTag-BFP/ iRFP/ T-Sapphire+ and CD45dimSSCLOW cells.

B Antigen expression of CD34, CD90, GPR56, NKG2DL (MICA/MICB), CD45RA, CD44, CD33, CD123, CD38, CD11b and CD14 on control as well as *DNMT3A* and *WT1* knock outs for AML-346 (grey) and AML-388 (black) (n=3-6).

Figure S11 Knockout of *WT1* or *DNMT3A* alter gene expression in biological processes like cell death

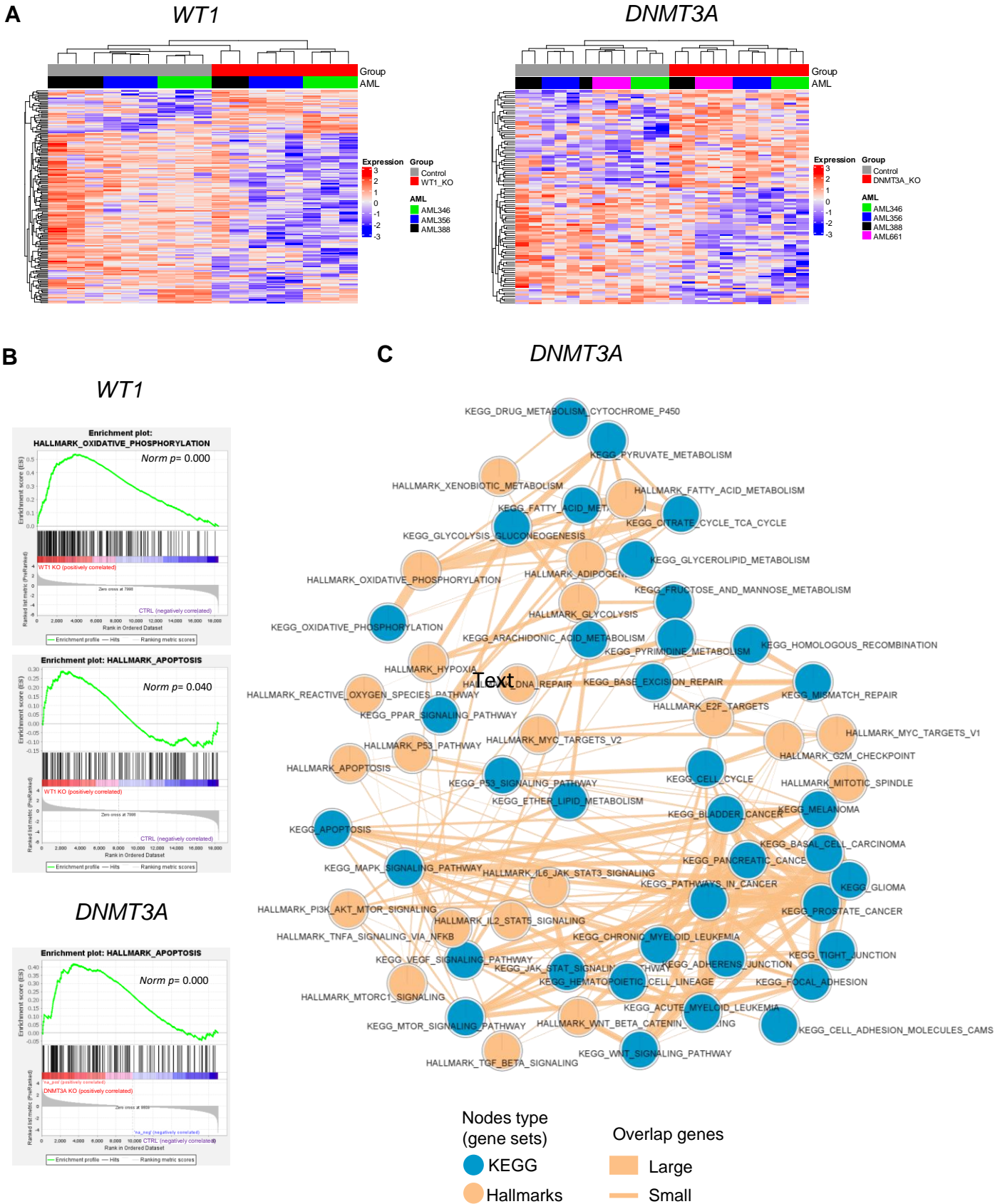


Figure S11. Knockout of *WT1* or *DNMT3A* alter gene expression in biological processes like cell death

- A** Heatmaps show different gene expression with a p -value ≤ 0.01 and log fold change > 1 , comparing *WT1* or *DNMT3A* knockouts and NT controls, in PDX models where *WT1* or *DNMT3A* knockout induced *in vivo* disadvantage (*DNMT3A*: 104 genes; *WT1*: 165 genes). For display purposes, all genes were standardized to a mean value of 0 and variance of 1.
- B** From data in A, gene enrichment plots are shown for the hallmark gene sets oxidative phosphorylation and apoptosis (*WT1* KO: Oxidative phosphorylation: NES = 2.52, p -value < 0.001 , q-value < 0.001 . Apoptosis: NES = 1.28, p -value = 0.02, q-value = 0.10; *DNMT3A* KO: Apoptosis: NES = 1.28, p -value = 0.02, q-value = 0.10).
- C** Identical data as in printed Figure 2C, here with complete annotation.

Figure S12 Knockout of *WT1* sensitizes PDX AML cells towards *in vivo* treatment with Cytarabine

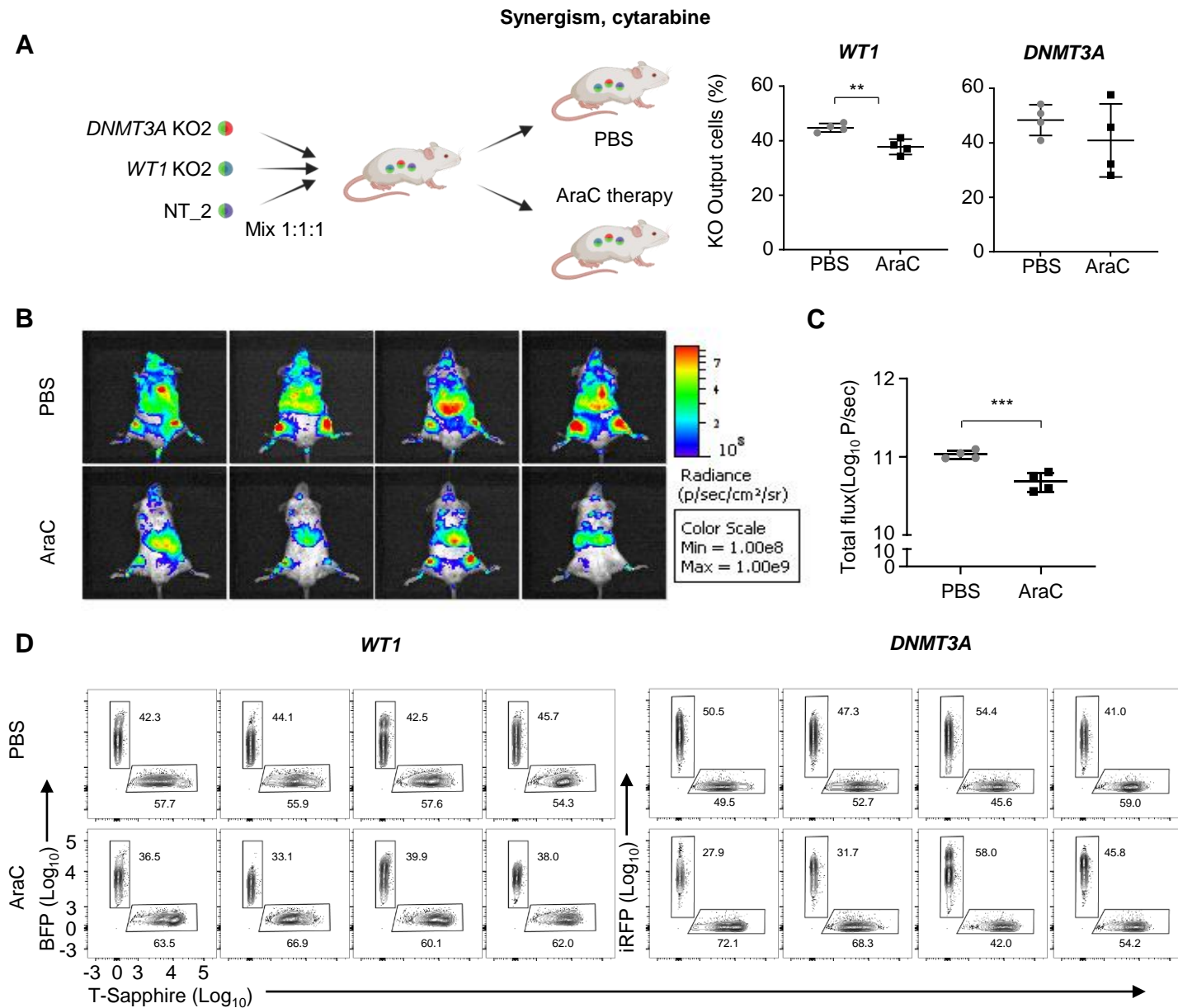


Figure S12. Knockout of *WT1* sensitizes PDX AML cells towards *in vivo* treatment with Cytarabine

- A** Synergism between *WT1* KO and chemotherapy. AML-388 cells were manipulated as in Figure 2A to gain a mixture of cells with control, *WT1* or *DNMT3A* knockout and transplanted into 8 mice. Twenty days after transplantation (AraC, 200mg/kg; 2 times per week) for 2.5 weeks. Then, cells were re-isolated and percentage of knockout cells was measured by flow cytometry. The p value was determined by unpaired two tailed t-test. (* $p < 0.05$, ** $p < 0.01$ and *** $p < 0.001$).
- B** In vivo bioluminescence images of mice treated with PBS or Cytarabine (AraC) at the end of the experiment from the experiment described in A.
- C** Quantification of the pictures shown in B; results from statistical analyses by two tailed unpaired T-test are shown if they were significant. (* $p < 0.05$, ** $p < 0.01$ and *** $p < 0.001$).
- D** Flow cytometry raw data determining the proportion of cell with *WT1* KO or *DNMT3A* KO cells versus NT control using Boolean gate strategy; raw data to A.

Figure S14 Knockout of *WT1* induces rapid disadvantage *in vivo*

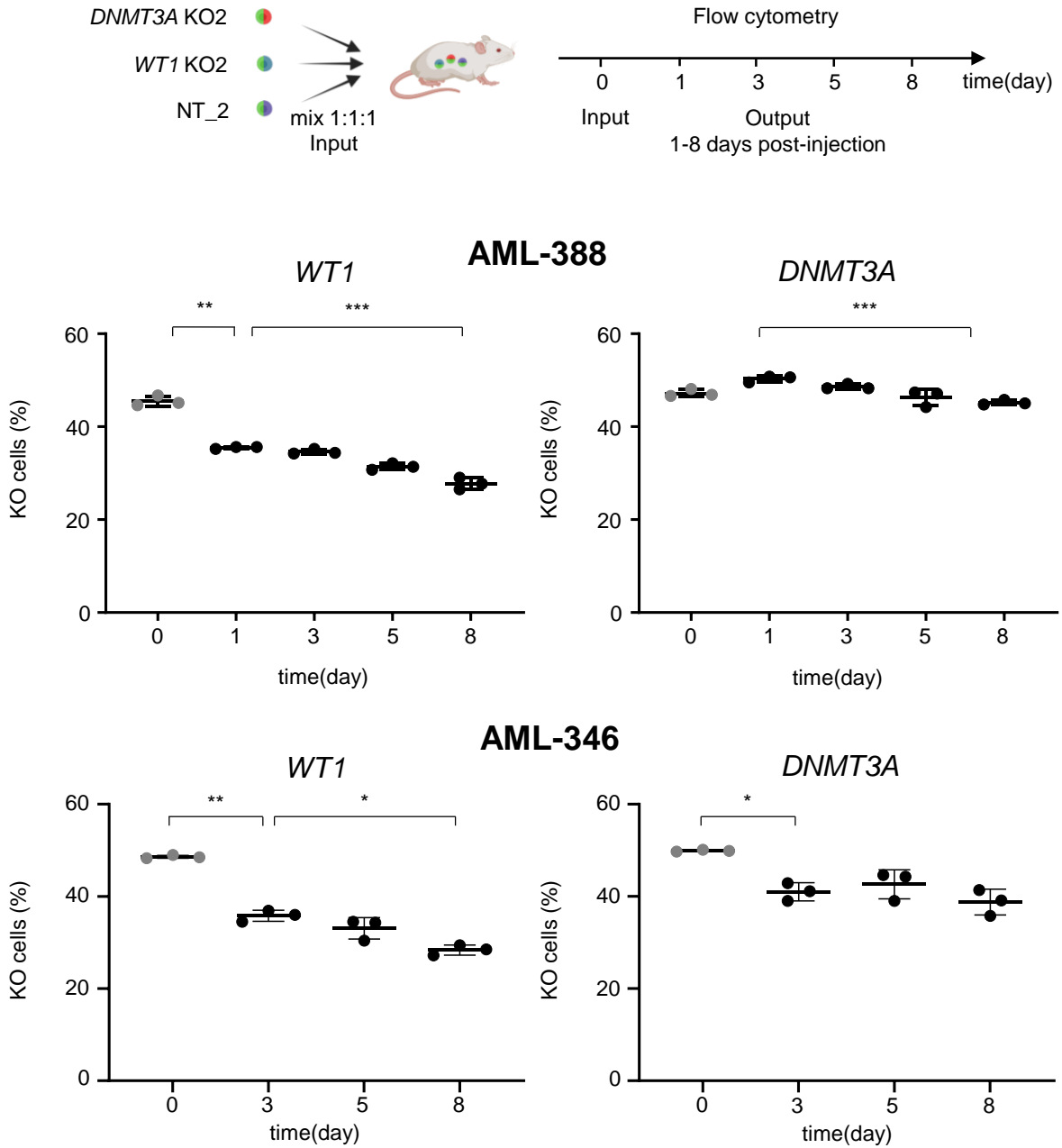


Figure S14. Knockout of *WT1* impairs the leukemia-niche interaction and induces rapid disadvantage

Competitive *in vivo* assay of AML-388 and AML-346 were performed as described in Figure 2A, except that cells were analyzed already few days after transplantation. Each dot represents a single mouse carrying one of 3 subpopulations (KO2). Day 0 represents the input samples injected into the animals that were sacrificed on day 1. Statistical analysis between day 0 and day 1 or 3, respectively was performed using paired two-tailed t-test and between day 1 and day 8 by unpaired two-tailed t-test (* $p < 0.05$; ** $p < 0.01$; *** $p < 0.001$).

Figure S15 Knockout of either *WT1* or *DNMT3A* reduces leukemia stem cells

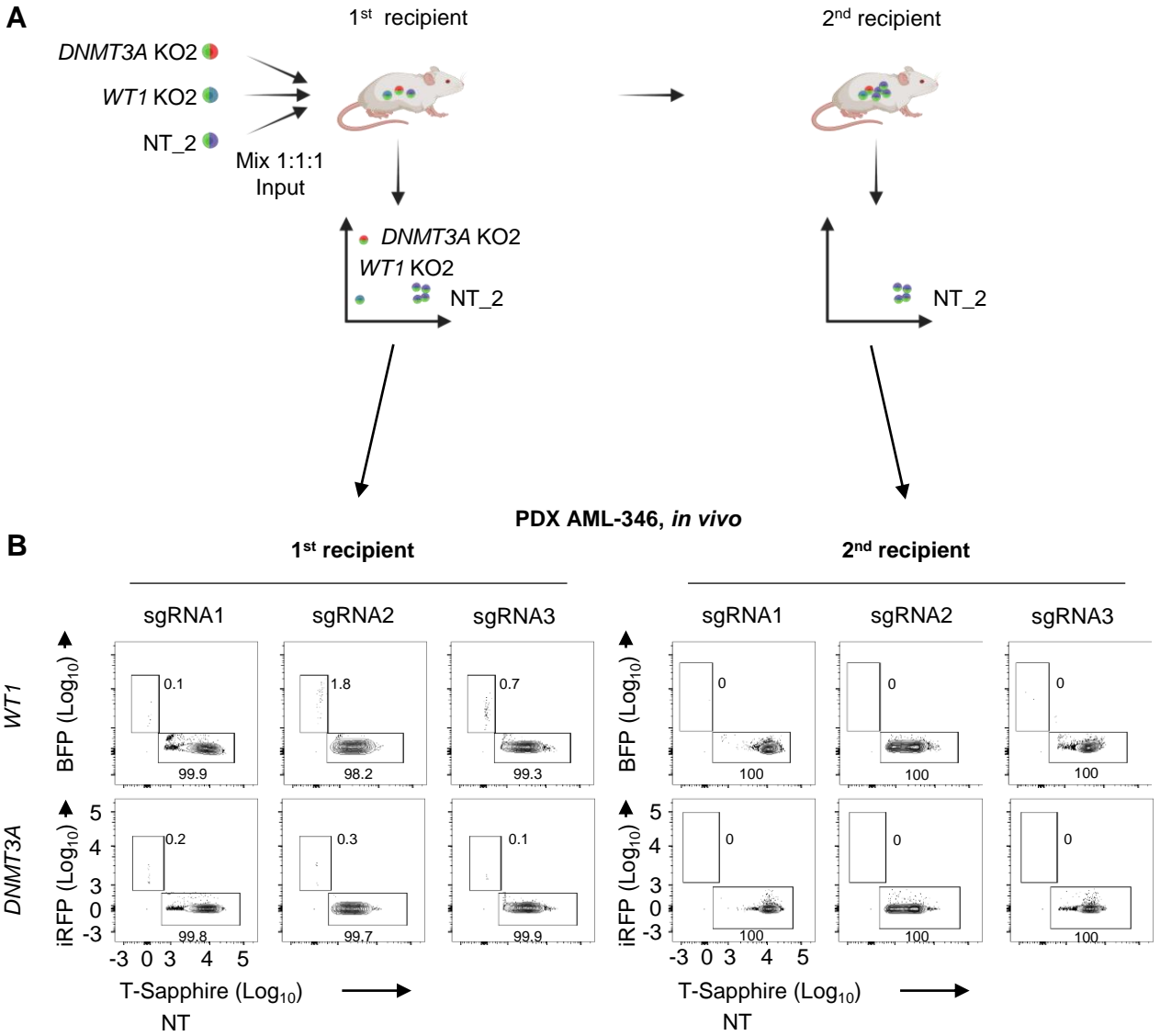


Figure S15 ff

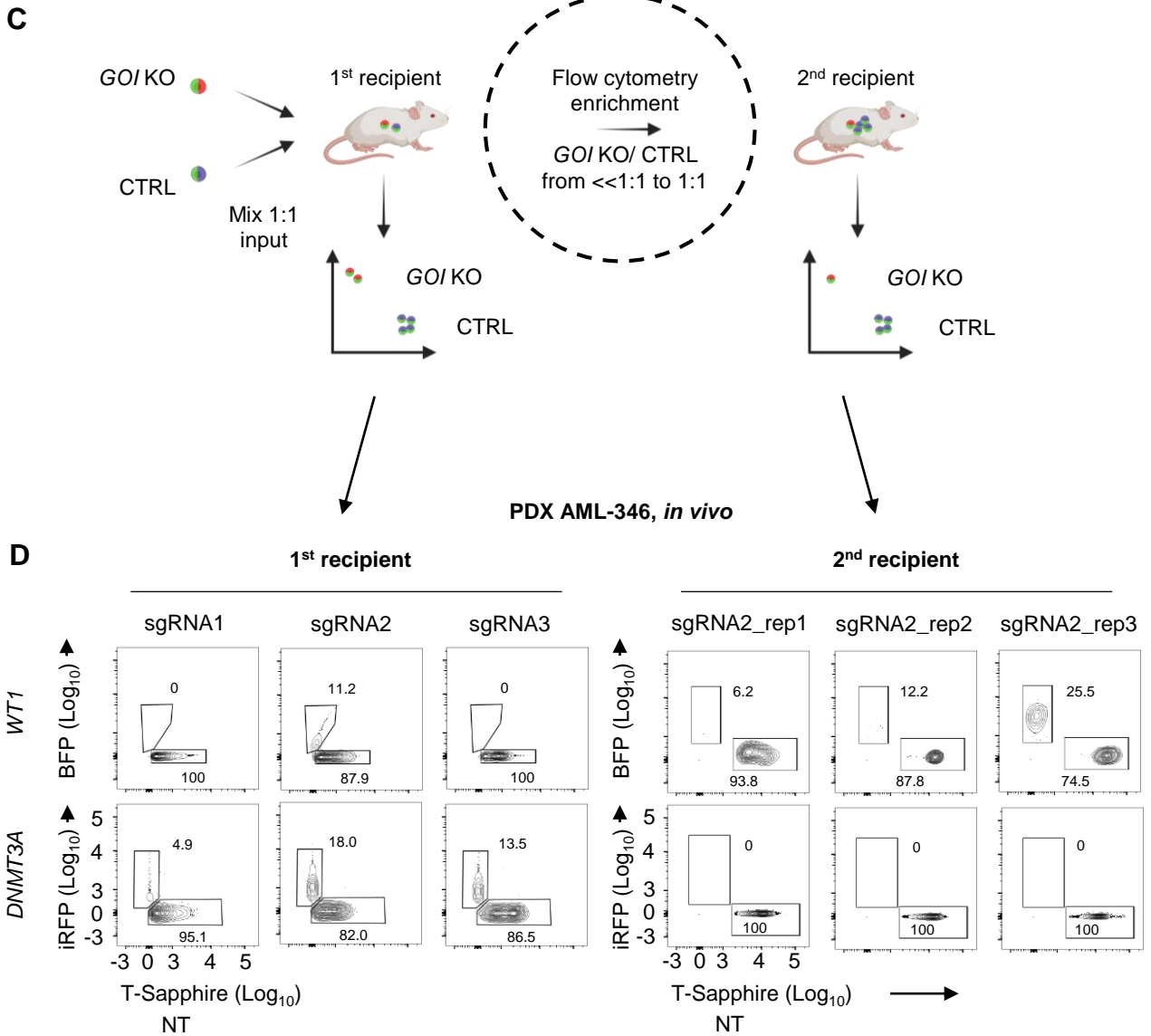


Figure S13. Knockout of either *WT1* or *DNMT3A* eliminates leukemia stem cells

A Scheme of re-transplantation assay. AML-346 cells were mixed at a 1:1:1 ratio of control, *WT1* and *DNMT3A* knockout cells, mixed and injected as Figure 2A. After an average of 2 months and upon advanced leukemic disease, output cells were re-transplanted into secondary recipient mice and grown for another 2 months, until the secondary outputs were measured.

B Flow cytometry results of outputs from both primary and secondary recipient mice are shown.

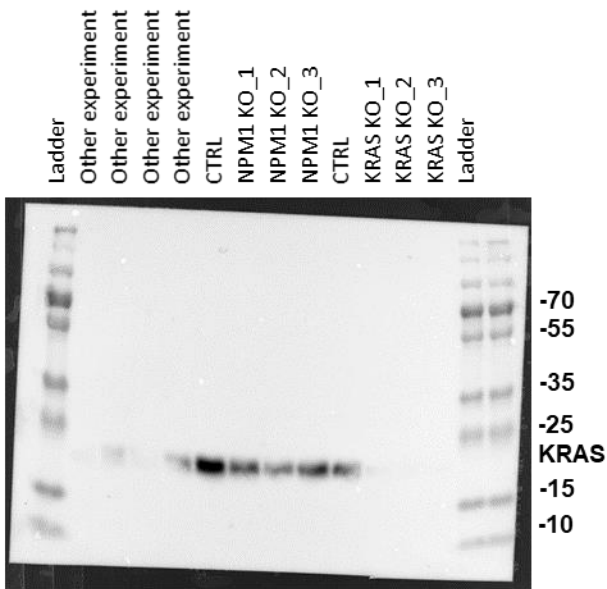
C Identical experiment as shown in A and B, except that (i) primary recipient mice were kept for a reduced period of time of 26 days to allow reisolating sufficient numbers of KO cells and that (ii) KO cells were enriched and re-injected at a 1:1 ratio into secondary recipient mice.

D Flow cytometry results of outputs from both primary and secondary recipient mice are shown, more data of secondary recipient outputs are showed in Source data.

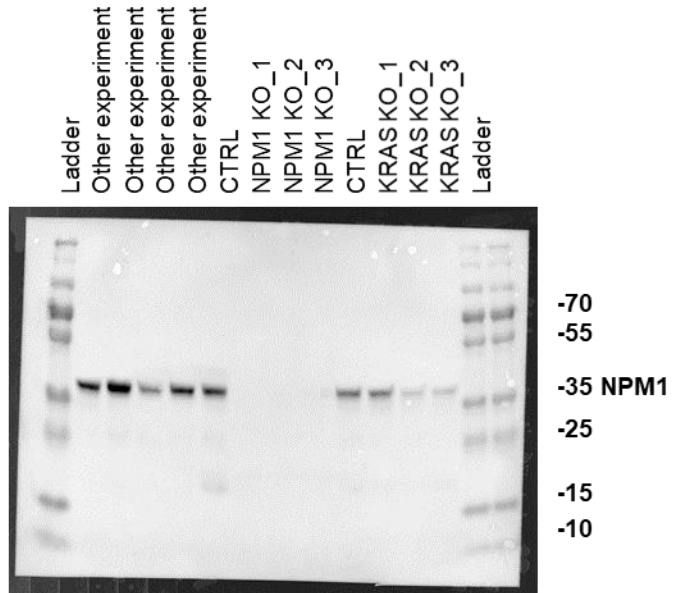
Source data_1

- Raw western blot figures for QC of KO for all genes.

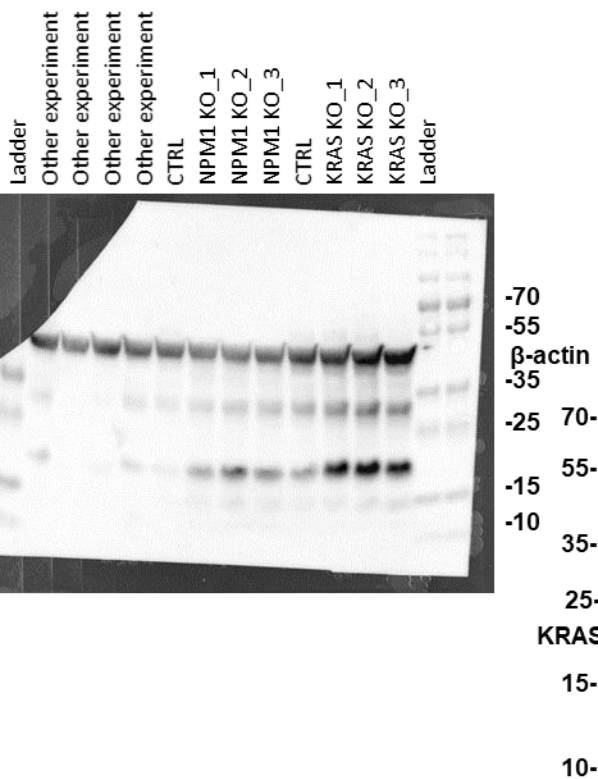
THP-1, KRAS



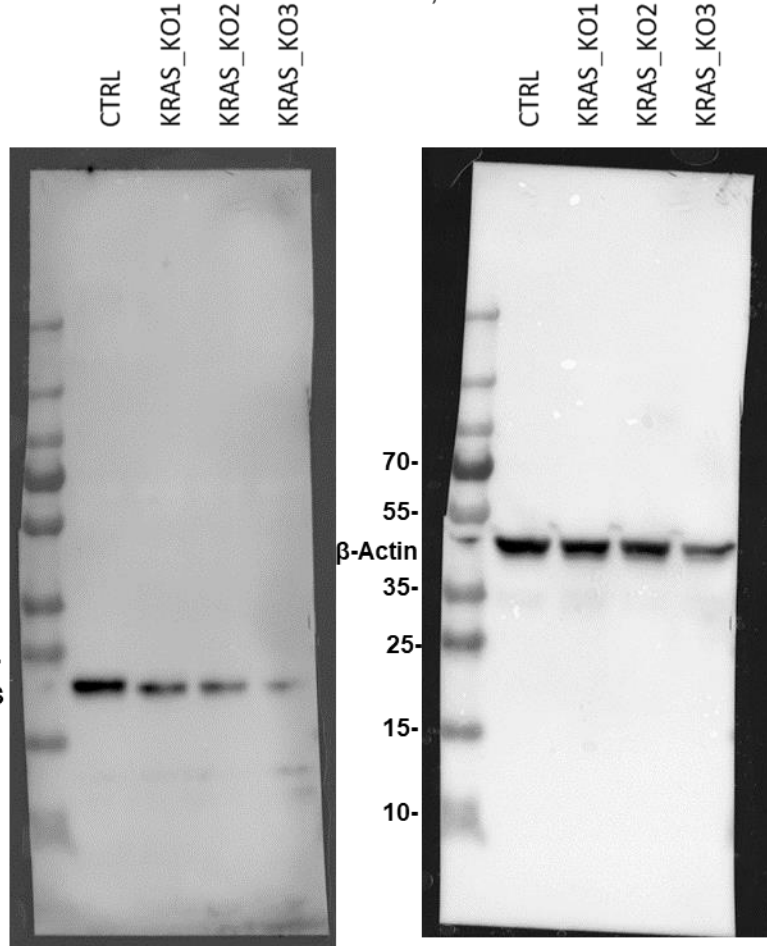
THP-1, NPM1



THP-1, β -actin



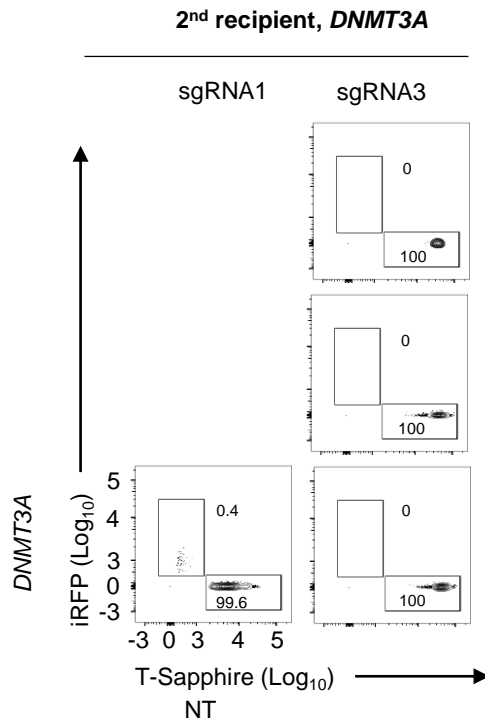
AML-388, KRAS



Source data_2











Knockout of either *WT1* or *DNMT3A* eliminates leukemia stem cells

- The rest of the flow cytometry results of outputs from secondary recipient mice are showing here. Complementary data of Figure S15.



Paper II

In vivo inducible reverse genetics in patients' tumors to identify individual therapeutic targets

Michela Carlet^{1,15}, Kerstin Völse^{1,15}, Jenny Vergalli¹, Martin Becker¹, Tobias Herold ^{1,2,3}, Anja Arner⁴, Daniela Senft¹, Vindi Jurinovic^{1,2,4}, Wen-Hsin Liu¹, Yuqiao Gao¹, Veronika Dill⁵, Boris Fehse ⁶, Claudia D. Baldus⁷, Lorenz Bastian ⁷, Lennart Lenk⁸, Denis M. Schewe ⁸, Johannes W. Bagnoli⁹, Binje Vick ^{1,3}, Jan Philipp Schmid¹, Alexander Wilhelm¹⁰, Rolf Marschalek ¹⁰, Philipp J. Jost^{3,5,11}, Cornelius Miething ^{12,13}, Kristoffer Riecken ⁶, Marc Schmidt-Supprian¹⁴, Vera Binder⁴ & Irmela Jeremias ^{1,3,4} 

High-throughput sequencing describes multiple alterations in individual tumors, but their functional relevance is often unclear. Clinic-close, individualized molecular model systems are required for functional validation and to identify therapeutic targets of high significance for each patient. Here, we establish a Cre-ER^{T2}-loxP (causes recombination, estrogen receptor mutant T2, locus of X-over P1) based inducible RNAi- (ribonucleic acid interference) mediated gene silencing system in patient-derived xenograft (PDX) models of acute leukemias in vivo. Mimicking anti-cancer therapy in patients, gene inhibition is initiated in mice harboring orthotopic tumors. In fluorochrome guided, competitive in vivo trials, silencing of the apoptosis regulator *MCL1* (myeloid cell leukemia sequence 1) correlates to pharmacological *MCL1* inhibition in patients' tumors, demonstrating the ability of the method to detect therapeutic vulnerabilities. The technique identifies a major tumor-maintaining potency of the *MLL-AF4* (mixed lineage leukemia, ALL1-fused gene from chromosome 4) fusion, restricted to samples carrying the translocation. *DUX4* (double homeobox 4) plays an essential role in patients' leukemias carrying the recently described *DUX4-IGH* (immunoglobulin heavy chain) translocation, while the downstream mediator *DDIT4L* (DNA-damage-inducible transcript 4 like) is identified as therapeutic vulnerability. By individualizing functional genomics in established tumors in vivo, our technique decisively complements the value chain of precision oncology. Being broadly applicable to tumors of all kinds, it will considerably reinforce personalizing anti-cancer treatment in the future.

Translating comprehensive cancer sequencing results into targeted therapies has been limited by shortcomings of model systems and techniques for preclinical target validation^{1,2}. The methodological gap contributes to the fact that only below 10% of drugs, successful in preclinical studies, pass early clinical evaluation and receive approval^{3,4}.

Functional genomic tools including RNA interference (RNAi) proved of utmost importance to annotate the numerous alterations detected by multi-omics profiling and significantly deepened our understanding of the merit of individual genes as drug targets^{5,6}. As limitation, functional studies have largely been restricted to cancer cell lines, which often fall short in predicting the role of alterations in individual human tumors⁷. To approximate the situation of the patient, the predictive power of primary tumor cell cultures⁸ and organoids⁹ is currently under intense investigation¹⁰.

For mirroring the clinical situation even closer, patient-derived xenograft (PDX) mouse models have been demonstrated to faithfully recapitulate the complexity of tumors in humans. PDX models are available for the vast majority of human cancers, and their preclinical value for biomarker identification and drug testing is well established^{11–15}. It is increasingly recognized that the drug development process might profit from studying PDX models with molecular techniques, routinely used in cell line models and genetically engineered mouse models (GEMM)^{16,17}. Still, RNAi techniques were only rarely applied for *in vivo* mechanistic studies in PDX, mainly due to technical challenges such as low transduction efficiencies and the need for continuous *in vivo* growth and associated high demand on resources¹⁶. As an advantage over constitutive systems, inducible gene silencing prevents overestimating *in vivo* gene function by avoiding influences from, e.g., transplantation and engraftment, and allows mimicking the treatment situation in patients with established tumors. The use of Cre-ER^{T2}-loxP combines the properties of high ligand sensitivity while maintaining tight control of shRNA expression in the un-induced state, thus minimizing leakiness, an advantage over tet-regulated systems^{16,18–20}.

Here, we report a Cre-ER^{T2} inducible RNAi in PDX models *in vivo*, using acute leukemia (AL) as prototype disease where *ex vivo* investigation on primary cells is challenging, but orthotopic PDX models are promising^{21,22}. In proof of principle studies, we demonstrated that *MCL1* silencing in acute lymphoblastic leukemia (ALL) and acute myeloid leukemia (AML) PDX models correlates to response to pharmacological *MCL1* inhibition. We confirmed a tumor-maintaining potency of the *MLL-AF4* fusion protein in PDX models *in vivo* and used the technique to identify *DDIT4L* as therapeutic targets in PDX ALL carrying the recently described *DUX4-IGH* translocation.

Results

Development of a Cre-ER^{T2} inducible shRNA knockdown approach *in vivo*. To test the suitability of the inducible knockdown system across a broad range of leukemia subtypes, primary tumor cells from 5 patients with AL (3 pediatric ALL, 1 adult ALL, 1 adult AML; clinical patient data in Table S1) were transplanted into NOD scid gamma (NSG) mice (Fig. 1a). Resulting PDX cells were genetically engineered first with a construct encoding a Tamoxifen (TAM)-inducible variant of Cre-recombinase, Cre-ER^{T2}, together with a red fluorochrome for enriching transgenic cells and Gaussia luciferase (Luc) for bioluminescence *in vivo* imaging²³ (Fig. 1a). Transduction efficiencies were typically well below 30% (Table S2), putatively indicating a single viral integration per genome according to literature²⁴, leading to homogenous expression levels of Cre-ER^{T2} (Fig. S1a), minimal toxicity and neglectable leakiness in all

samples, thus overcoming one of the challenges of TRE-based inducible expression systems¹⁶.

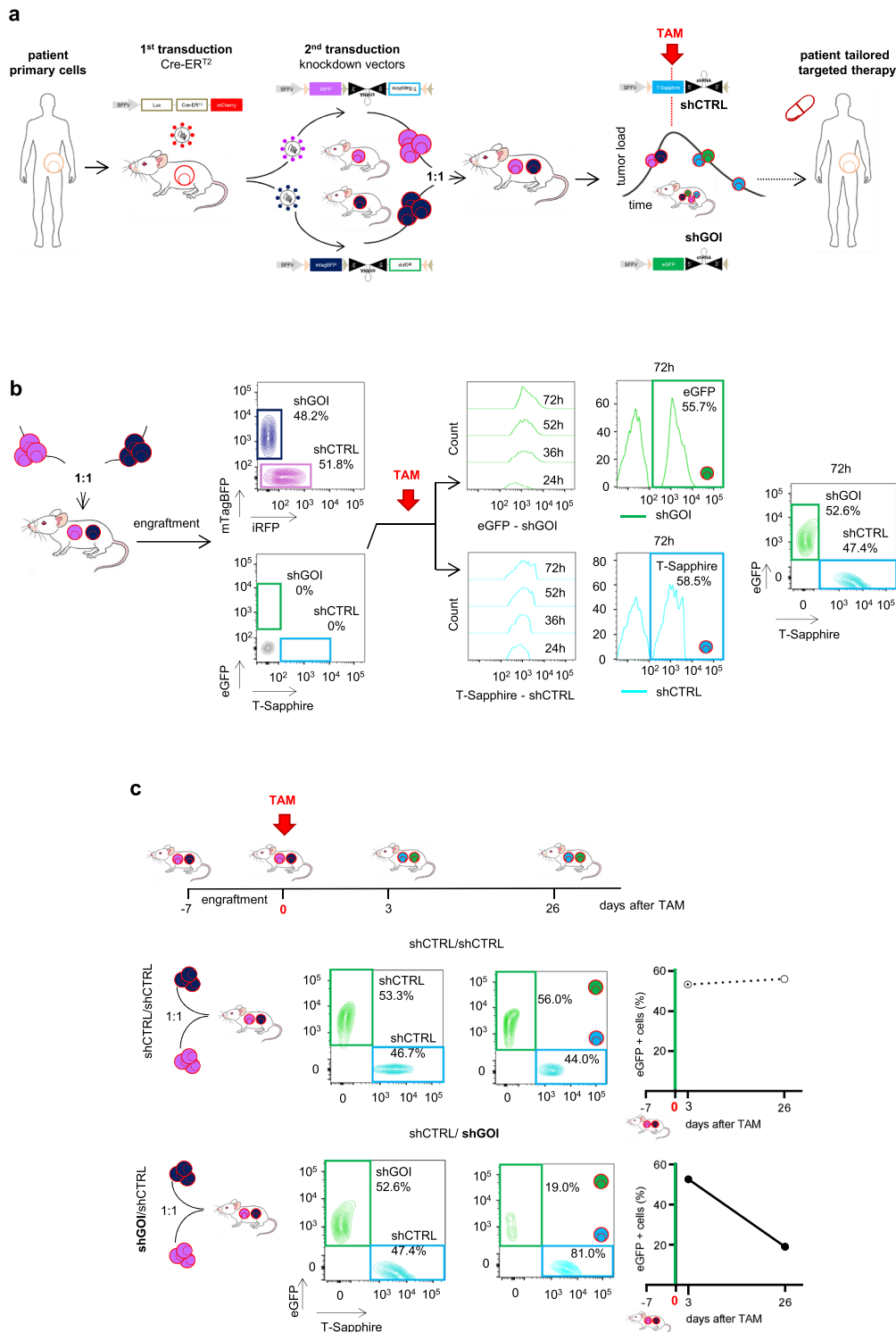
In a second step, PDX cells were transduced with the small hairpin (sh) RNA expression vectors (Figs. 1a and S1b). The miR30-based knockdown cassette was directly coupled to a fluorochrome and both were cloned in antisense orientation, flanked by two pairs of loxP sites. In the absence of TAM, neither the inducible fluorochrome nor the shRNA were expressed. TAM administration induced a two-step Cre-ER^{T2}-mediated recombination process which flipped the fluorochrome-shRNA insert into sense orientation, initiating its expression (Fig. S1b–c)^{25,26}. A set of 4 recombinant fluorochromes was used to monitor shRNA transduction and recombination and to enable competitive *in vivo* assays (Fig. S1c). Transduction efficiency was tracked by iRFP the control vector encoding an shRNA targeting Renilla luciferase (shCTRL), or by mTagBFP in the vector encoding a gene of interest (GOI)-specific shRNA (shGOI) (Table S2). Upon TAM administration, Cre-ER^{T2}-mediated recombination deleted the constitutively expressed fluorochromes iRFP and mTagBFP and induced expression of the second set of fluorochromes²⁷ (Figs. 1a and S1b–c). T-Sapphire and eGFP were chosen as inducible fluorochromes due to their high similarities in sequence and expression kinetics²⁸ and replaced iRFP and mTagBFP expression upon TAM treatment. The two knockdown vectors enabled pairwise competitive *in vivo* experiments in the same animal to increase reliability and sensitivity, while saving resources.

Mice were transplanted with a 1:1 mixture of PDX cells from the same patient expressing either of the two RNAi vectors, shCTRL or shGOI (Fig. 1a). For exemplary purposes and to describe distinct aspects of the method, the apoptosis regulator *MCL1* was chosen as GOI (Figs. 1 and S1). As quality control, expression of constitutive markers revealed equal engraftment of both populations at the time of TAM administration (Fig. 1b).

To induce gene silencing, TAM was administered to mice with pre-established leukemias when homing and initial engraftment to the murine bone marrow was achieved and PDX cells were in the exponential growth phase, mimicking treatment of patients with pre-existing tumors. Systemic TAM administration induced expression of the inducible fluorochromes T-Sapphire or eGFP, in similar amounts for both constructs, starting as early as 24 h, with highest expression levels obtained at 72 h after TAM (Fig. 1b). The functional consequences of control and GOI knockdown were monitored by quantifying each population according to their fluorochromes, using flow cytometry (Fig. 1b–c). TAM was dosed to obtain substantial Cre-ER^{T2} induced recombination in the absence of toxicity and with recombination efficiencies independent of tumor load (Fig. S1d).

Several quality controls were performed to exclude unspecific toxicities; the distribution of both populations remained stable over time after TAM treatment, if both populations expressed shCTRL (shCTRL/shCTRL mixture in Fig. 1c, upper lane) in all PDX samples analyzed (Fig. S1d). Similarly, the distribution of the shCTRL/shGOI mixture remained unchanged, if mice received the carrier solution alone (Fig. S1f–g). These results are in line with our previous studies²⁹, where we found that transduction and enrichment of PDX cells was not associated with clonal selection, and that PDX samples largely maintained their sample-specific mutational pattern.

In contrast and upon treatment with TAM, the population expressing a shRNA targeting an essential GOI (sh*MCL1*) decreased over time and was overgrown by control cells (Fig. 1c, lower lane and Fig. S1h). Loss of cells with GOI knockdown *in vivo* proved a functional importance of the GOI on the molecular level, mimicking elimination of tumor cells in patients upon treatment with a targeted drug.



Inducible silencing of *MCL1* correlates response to small molecule *MCL1* inhibitors in vivo. To test whether inducible knockdown of the GOI correlates to targeted inhibitors, we first analyzed the response of PDX samples to shRNA-mediated inhibition of *MCL1*. We selected *MCL1* as proof of principle target gene from literature as certain, but not all leukemias seem responsive to *MCL1* inhibition^{30,31}. The anti-apoptotic gene *MCL1* was chosen as it is dysregulated in numerous tumor entities³² and *MCL1* inhibitors are currently investigated in clinical trials yielding mixed results³³ (NCT03218683). Predicting treatment response for selecting patients who will profit from

MCL1 directed therapy remains a major challenge and functional in vivo assays might provide helpful insights³⁴.

We studied PDX models from three different patients with acute leukemia (AML-388, ALL-199, ALL-265). In the AML-388 PDX model, we found a clear decrease of cells with *MCL1* knockdown compared to control cells in vivo, accompanied by efficient knockdown on protein level (Fig. 2a–b), validating *MCL1* as important vulnerability. Importantly, these effects were independent of tumor load at the time of TAM administration, supporting the use of the inducible knockdown system at any disease stage (Fig. S2a). In contrast, knockdown of *MCL1* in two

Fig. 1 Establishing an inducible knockdown system in PDX acute leukemia cells in vivo. **a** Overview of the experimental setup: Primary acute leukemia (AL) cells were amplified in NSG mice and serially passaged PDX cells lentivirally transduced twice in a row; first to constitutively express Cre-ER^{T2} together with mCherry and a luciferase (Luc); second to express inducible knockdown vectors containing (i) a constitutively expressed fluorochrome marker (either iRFP or mTagBFP) and (ii), placed in antisense orientation, a miR30-based knockdown cassette coupled to a second inducible fluorochrome (either T-Sapphire or eGFP). After amplification in mice, purified transgenic PDX cells were mixed 1:1 and transplanted into next recipient mice for competitive in vivo experiments. In mice with established leukemias, TAM was administered to induce Cre-ER^{T2}-mediated recombination. Recombination inverted the knockdown cassette and induced (i) expression of the shRNA; (ii) deletion of the constitutive fluorochrome (either iRFP or mTagBFP) and (iii) expression of the inducible fluorochrome (either T-Sapphire or eGFP; see Fig. S1b for detailed description). As result, T-Sapphire positivity indicated cells expressing the shRNA targeting a control (shCTRL), while eGFP positivity indicated cells expressing the shRNA targeting the gene-of-interest (shGOI). If the GOI harbors an essential function, the eGFP-positive population gets lost over time in vivo, indicating that the patient might profit from drugs targeting the GOI. **b** Switch in fluorochrome expression upon Cre-ER^{T2}-recombination: Double transgenic PDX AML-388 cells expressing Cre-ER^{T2} together with either iRFP/shCTRL or mTagBFP/shGOI (sh*MCL1*) were mixed 1:1 and injected into the tail vein of NSG mice (3×10⁵ cells/mouse; n = 14). 7 days after injection, 2 mice were sacrificed and PDX cells analyzed by flow cytometry for all 4 fluorochromes. In the remaining mice, 50 mg/kg TAM was administered by oral gavage to induce Cre-ER^{T2}-mediated recombination. Resulting increase in T-Sapphire or eGFP expression, indicating expression of shCTRL and shGOI, respectively, was measured in PDX cells isolated from mice at the indicated time points (24, 36, 52 and 72 h after TAM; n = 3 per time point). Representative histograms and plots are shown. **c** Typical results for a GOI with essential function: Upper scheme depicts the experimental procedure: For pairwise competitive assays, mice were injected with either of two mixtures: a control mixture of iRFP/shCTRL and mTagBFP/shCTRL (short shCTRL/shCTRL) or the experimental mixture iRFP/shCTRL and mTagBFP/shGOI (short shCTRL/shGOI); as GOI, the apoptosis regulator *MCL1* was chosen (shGOI = sh*MCL1*) (3×10⁵ cells/mouse, data from 4 exemplary mice are shown). TAM was administered 7 days after injection (day 0). Mice were sacrificed 3 and 26 days after TAM and PDX cells analyzed for expression of the inducible fluorochromes T-Sapphire and eGFP. Density plots show representative results for both mixtures on day 3 (left) and day 26 (right). Right panels show quantification as percentage of [eGFP/shGOI positive cells divided by (the sum of T-Sapphire/shCTRL and eGFP/shGOI positive cells)]; the shCTRL/shCTRL mixture is analyzed and depicted, respectively.

ALL samples showed minor to no effects on growth, proving patient-individual sensitivities (Figs. 2c and S2b). Silencing *MCL1* in AML-388 induced rapid cell death, which was already detectable within the first 72 h after TAM administration (Fig. S2c–e). Gene set enrichment analysis from RNA sequencing data comparing shCTRL and sh*MCL1* PDX cells indicated that *MCL1* knockdown was associated with activation of the apoptosis pathway, verified using Annexin-V staining (Fig. S2d–e). To visualize selective loss of individual GFP-positive cells upon *MCL1* silencing, re-transplantation experiments into wildtype zebrafish (*danio rerio*) were performed, which confirmed significant and rapid depletion of PDX cells upon *MCL1* knockdown between 48 and 72 h after TAM in an independent in vivo model (Fig. S2f).

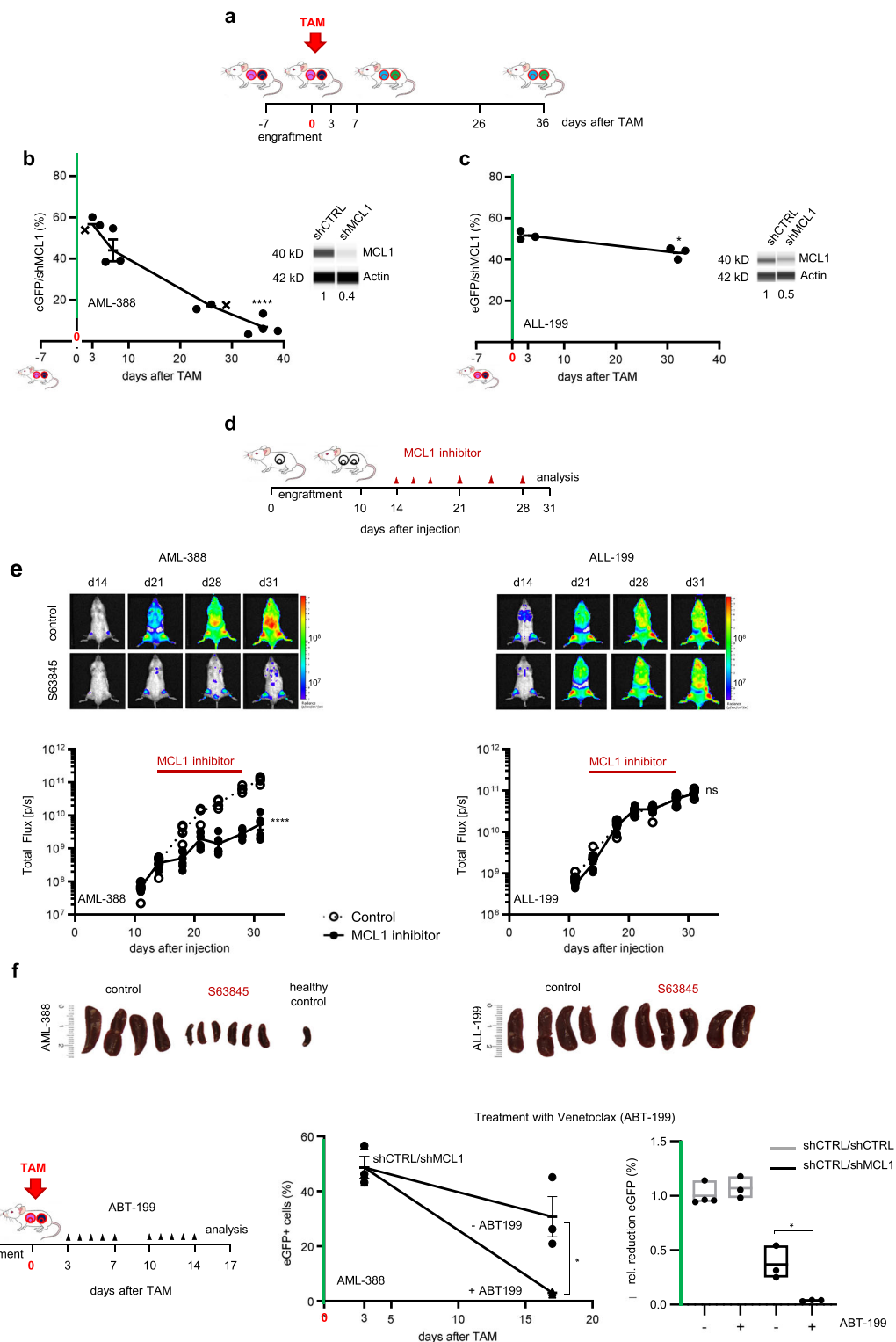
Taken together, using the inducible knockdown approach, *MCL1* could be identified as a therapeutic vulnerability in one of 3 PDX samples, for which functional relevance could not be predicted by expression levels of anti-apoptotic BCL-2 family members, highlighting the need for functional assays (Fig. S2g).

As silencing of *MCL1* induced cell death in PDX AML-388, but not in ALL-199 nor ALL-265, we next asked whether this correlates with response towards pharmacological inhibition of *MCL1*. We studied the small molecule antagonist S63845 (Fig. 2d), which has previously been shown to be effective in AML cell lines and PDX samples^{31,35,36} and is currently under clinical investigation as single agent (NCT02979366) or in combination regimens (NCT03672695). Treatment of mice bearing AML-388 significantly diminished tumor burden as monitored by in vivo bioluminescence imaging (Fig. 2e), reduced splenomegaly (Figs. 2f and S2h) and number of PDX cells (Fig. S2i) re-isolated from the murine spleens or bone marrow. In contrast, the *MCL1* inhibitor had no effect on ALL-199, recapitulating effects observed in the inducible knockdown system. Thus, the inducible knockdown system correlated to response of PDX samples to the pharmacological inhibition, confirming the use of this technique as surrogate to study sample-specific vulnerabilities on a molecular level in a highly clinically relevant setting.

Because *MCL1* has been shown to confer resistance to several anticancer drugs³⁷, we examined in a next step whether knockdown of *MCL1* strengthens the response of AML PDX

models towards drug treatment in vivo. Groups of mice were treated either with the BCL-2 inhibitor ABT-199 (Venetoclax) (Fig. 2g), or the conventional chemotherapeutic drug Cytarabine (Fig. S2j–k) at doses that do not significantly reduce tumor burden in mice. Both treatments further decreased the *MCL1* knockdown population in a synergistic way, indicating that sensitivity towards ABT-199 or Cytarabine might be increased by *MCL1* directed treatment in patients (Fig. 2g, Fig. S2j–k). Thus, using *MCL1* as exemplary target, we provide evidence that our approach enables distinguishing between subgroups of tumors in order to select patients, which might profit from therapies targeting a certain GOI, and to evaluate treatment combinations.

Specific targeting of the fusion oncogene *MLL-AF4*. To further validate the specificity of our approach, we next studied a bona fide positive control with high likelihood of harboring an essential function in established PDX tumors in vivo. The translocation t(4;11) and corresponding expression of the *MLL-AF4* fusion (KMT2A-AFF1) is present in 80% of infant B-precursor ALL patients, and is associated with poor prognosis³⁸. Several studies elucidated its role in ALL cell lines and mouse models³⁹, but up to date no molecular investigations on its function have been carried out in patient cells or established tumors growing in vivo. We designed a shRNA targeting a mRNA breakpoint shared by several patients, which significantly reduced expression of the fusion transcript (Fig. 3a). Because the shRNA sequence targeted neither of the individual wildtype genes, *MLL* or *AF4* (Figs. 3a and S3a–b), no major adverse effects on normal tissue are expected when applied in vivo, e.g., by systemic gene therapeutic approaches. Inducible knockdown of *MLL-AF4* significantly reduced ALL cells in the t(4;11)-positive PDX model tested, but not in a translocation-negative sample, proving a tumor maintaining role of *MLL-AF4* in established patient tumors in vivo (Figs. 3b and S3a). Variations between the different animals were neglectable reflecting the high reliability of our approach (Fig. 3b). Reduced tumor growth of the sh*MLL-AF4* mixture was visible using in vivo imaging, even though 50% of injected tumor cells expressed shCTRL (Fig. 3c). Gene expression analysis demonstrated that shCTRL cells expressed a set



of genes characteristic for samples with the *MLL-AF4* translocation⁴⁰, which was no longer present upon *shMLL-AF4* knockdown, where an expression signature similar to non-*MLL* rearranged samples prevailed (Fig. S3c–d).

These results prove the selectivity and operability of our technique and showed that *MLL-AF4* harbors an essential function in established patient-derived leukemias growing in vivo. We provide strong molecular evidence in a clinically relevant model that the translocation transcript represents an attractive therapeutic target for future therapies.

***DDIT4L* is a therapeutic vulnerability in *DUX4-IGH* rearranged acute lymphoblastic leukemia.** In a last step, we examined a less well studied tumor alteration, the recently discovered rearrangement t(4;14) which occurs in 7% of ALL patients and results in the *DUX4-IGH* gene fusion⁴¹. Because cells with t(4;14) display high levels of otherwise absent *DUX4*, we asked whether *DUX4* represents a vulnerability in this subgroup of ALL in vivo. Using our technique, we demonstrated an essential function for *DUX4* in t(4;14) rearranged ALL-811 (Fig. 3d). Expression of the *DUX4-IGH* translocation was reported to be associated with a defined gene expression

Fig. 2 Inducible knockdown of *MCL1* in vivo predicts response of AL PDX to pharmacological *MCL1* inhibition. **a–c** Inducible knockdown of *MCL1* in AL PDX. **a** Scheme depicting the experimental setup. Groups of mice were injected with the shCTRL/sh*MCL1* mixture for competitive in vivo assays (3×10^5 cells/mouse). TAM was administered when tumors were established; differences between eGFP-positive sh*MCL1* cells among all recombined cells were determined 3 days after TAM and at end stage leukemia to assess essentiality of *MCL1*. **b–c** Competitive experiments were set up as described in **a**; TAM (50 mg/kg) was applied once (day 0); mice bearing **(b)** AML-388 PDX cells were sacrificed 3 ($n = 3$), 7 ($n = 3$), 26 ($n = 3$) and 36 ($n = 4$) days after TAM; mice bearing ALL-199 PDX cells were sacrificed 3 ($n = 3$) and 32 ($n = 3$) days after TAM. *MCL1* protein expression was analyzed in sorted shCTRL and sh*MCL1* populations by protein immunoassay (Simple Western) 7 days after TAM (AML-388) or at the experimental endpoint (ALL-199). Mean \pm SEM of the proportion of eGFP-positive cells isolated out of all recombined cells is displayed; each dot represents one mouse; x marks mice shown in Fig. 1c. To determine significance of depletion of shGOI-expressing cells, the percentage of eGFP/shGOI cells at the experimental endpoint is compared to the percentage of eGFP/shGOI cells at 3d post TAM, as this time point is used to define the sample-specific recombination efficiency. * $p = 0.0136$, **** $p < 0.0001$, ns not significant by unpaired t-test. **d–f** Pharmacological inhibition of *MCL1* in AL PDX. **d** Scheme depicting the experimental setup. Groups of mice were injected with AML-388 (left; 3×10^5 cells/mouse, $n = 10$) or ALL-199 (right; 1×10^6 cells/mouse, $n = 10$) PDX cells expressing firefly luciferase. 14 days after injection, mice were treated with the small molecule *MCL1* antagonist S63845 (mice received 25 mg/kg three times in the first week, 12.5 mg/kg twice in the second week, and once in the third week, $n = 6$) or solvent as control ($n = 4$) and tumor growth was monitored by bioluminescence in vivo imaging until mice were sacrificed 31 days after injection. **e** Representative bioluminescence images are depicted and graph shows mean \pm SEM; **** $p < 0.0001$, ns not significant by unpaired t-test. **f** Images of spleens of control- or S63845-treated mice are displayed. One spleen of a healthy mouse without leukemia (healthy control) is shown for comparison. **g** The combinatorial effect of *MCL1* knockdown plus ABT-199 (Venetoclax) was studied by injecting mice with a 1:1 mixture of shCTRL/sh*MCL1* AML-388 cells (3×10^5 cells/mouse) and treating them with 50 mg/kg TAM, 7 days after injection (day 0). 3d after TAM administration, control mice were sacrificed ($n = 3$) and the remaining mice treated either with 100 mg/kg ABT-199 ($n = 3$) or solvent ($n = 3$) for 5 consecutive days per week, in 2 cycles. At the end of the experiment (17 days after TAM), mice were sacrificed and analyzed as in Fig. 1c. Mean \pm SEM is shown; * $p = 0.0194$ by unpaired t-test. Reduction of eGFP-positive cells in the shCTRL/sh*MCL1* mix relative to shCTRL/shCTRL (+/- ABT-199) is displayed. Each dot represents one mouse. Mean \pm SEM is shown; * $p = 0.0194$ by unpaired t-test.

signature, previously referred to as the “ERG subtype”^{42–46}. We performed gene expression analysis of sh*DUX4* and shCTRL ALL-811 cells (Fig. 3e) and performed gene set enrichment analysis (GSEA) with two published datasets^{43,45}. We found genes overexpressed in *DUX4* knockdown NALM6 cells⁴³ also enriched in our sh*DUX4* PDX sample (Figs. 3f and S3e Set 1). Accordingly, genes downregulated in *DUX4* knockdown NALM-6 cells⁴³ (Fig. S3e, Set 2) and genes highly expressed in the cluster of patients characterized by *DUX4* translocation and ERG deletion⁴⁵ (Fig. S3f, Set 3) were enriched in the shCTRL sample (Fig. S3g). These data confirm the presence of the typical *DUX4* signature in shCTRL PDX cells and demonstrate reversal of this signature upon *DUX4* knockdown in a PDX model in vivo (Figs. 3e–f and S3e–g). Our technique could thus identify *DUX4* as attractive therapeutic target to treat the recently detected subgroup of *DUX4-IGH* rearranged ALL.

To further confirm the relevance of the detected genes for tumor maintenance of *DUX4*-rearranged samples we tested the role of one gene that was downregulated upon *DUX4* silencing in PDX ALL-811 and in NALM-6 cells (Fig. 3g), the DNA-damage-inducible transcript 4-like (*DDIT4L*; also known as Redd2 or Rtp801L), which has been shown to regulate mTOR signaling and autophagy in mammalian cells. *DDIT4L* expression is induced in the presence of different types of pathological stress, suggesting a possible involvement of *DDIT4L* in stress response^{47–49}. Interestingly, we found *DDIT4L* highly expressed in *DUX4* rearranged ALL (Fig. S3h). Inducible knockdown of *DDIT4L* significantly diminished leukemic growth within 2 weeks of in vivo tumor growth (Fig. 3h–i), suggesting that downregulation of *DDIT4L* might have mediated, at least in part, the growth inhibitory effects observed in the sh*DUX4* population. Taken together, we identify *DDIT4L* as a therapeutic vulnerability in the *DUX4-IGH* subtype of B-ALL.

Discussion

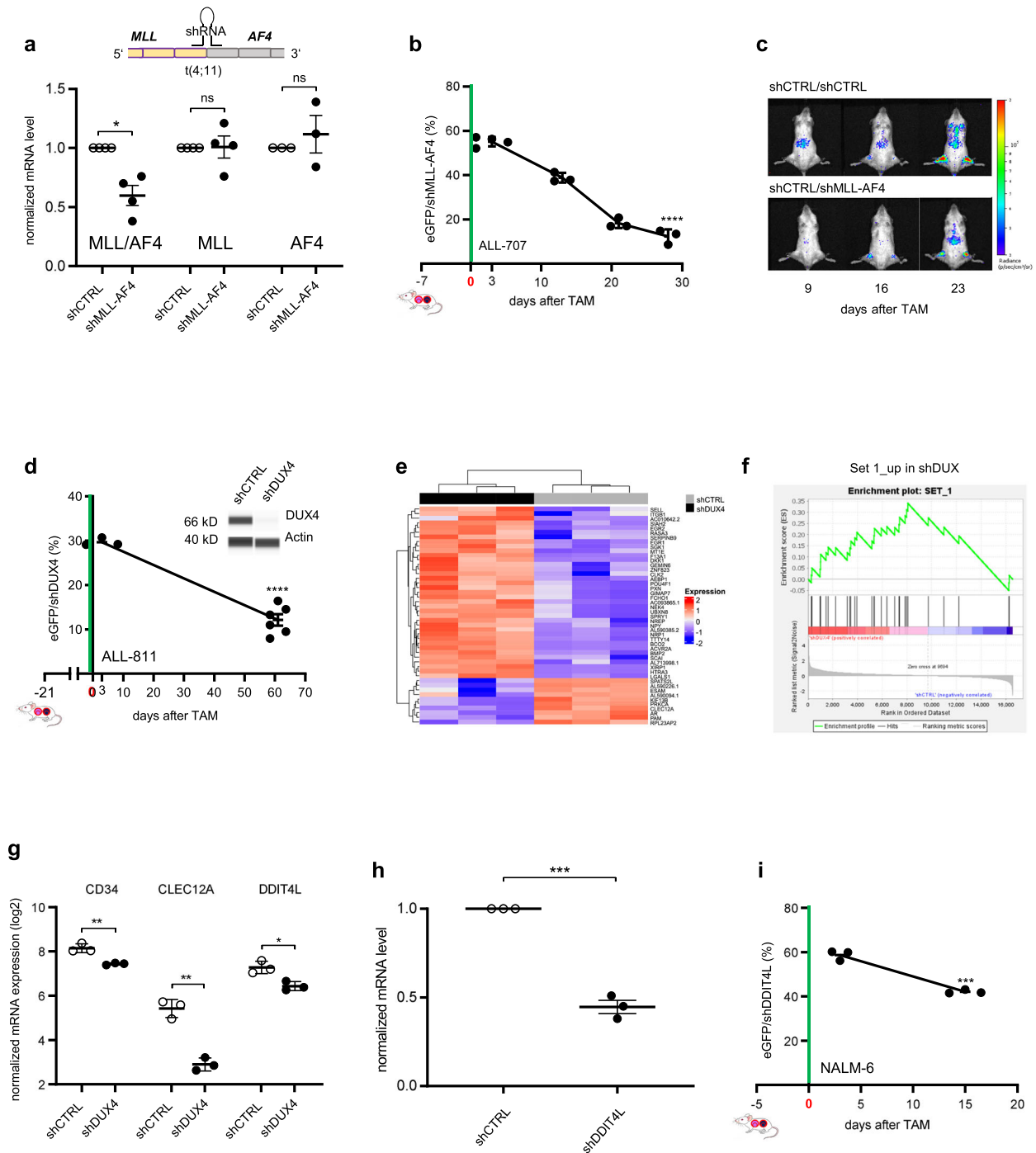
We have established a method which combines an in vivo approach with patient-derived tumor cells and pre-established tumors for inducible knockdown and allows validating vulnerabilities on an individual patient level. We established the technique, as preclinical molecular approaches are lacking which faithfully mimic the situation of treatment in patients, characterized by existence of an established tumor in vivo. Our method is capable to evaluate the functional relevance of tumor alterations (i) in the background of

individual patient tumors and their specific characteristics; (ii) in the complex in vivo environment of living beings and; (iii) in the situation of a pre-existing tumor, avoiding influences irrelevant for patients. Our molecular approach closely mimics the clinical situation and complements an important step in the evaluation chain of precision oncology. The molecular technique allows target validation, for single agent use or in combination therapies, independently from confounders such as pharmacodynamics and pharmacokinetics, toxicity and lack of specificity, inherent to drugs and compounds⁵⁰. Inducible genetically engineered mouse models (GEMM) allow studying gene function independently from, e.g., gestation-specific processes; in analogy, our approach allows studying vulnerabilities devoid of model-inherent processes like in vitro culture, transplantation, homing and engraftment. Our inducible approach closely controls for putative clonal bias as identical cells are studied, before and after induction of knockdown. Our knockdown approach might complement CRISPR/Cas9-mediated knockout approaches¹⁶, while putatively more coherently mimicking the partial, but incomplete target inhibition induced by drugs or compounds. In addition to alterations detected by sequencing efforts, our technique allows functional evaluation of targets detected by sequencing-agnostic approaches, e.g., in cell death pathways, and studying un-druggable targets, including non-coding RNAs⁵¹.

While we studied acute leukemias as model diseases, the CRE-loxP-system has been successfully used in numerous different tumor entities and our technique can easily be transferred to other cancers. We envision a major potential of our method on a proof-of-concept level, where deeper knowledge on tumor dependencies will improve drug design and the ability to interpret patient sequencing data. It might also serve as a highly clinic-related, functional biomarker to improve clinical decision making to individualize treatment. Due to its major potential to tailor drug development, improve patient care and increase the success rate of clinical trials, our technique will foster personalized oncology in the future.

Methods

Ethical statement. Written informed consent was obtained from all patients and from parents/carers in the cases where patients were minors. The study was performed in accordance with the ethical standards of the responsible committee on human experimentation (written approval by Ethikkommission des Klinikums der Ludwig-Maximilians-Universität München, Ethikkommission@med.unimuenchen.de, April 15/2008, number 068-08; September 24/2010, number 222-10; January 18/2019, number



222-10) and with the Helsinki Declaration of 1975, as revised in 2000. All animal trials were performed in compliance with the ARRIVE guidelines (<https://arriveguidelines.org>) and in accordance with the current ethical standards of the official committee on animal experimentation (written approval by Regierung von Oberbayern, tierversuche@reg-ob.bayern.de, January 15/2016, Az. ROB-55.2Vet-2532.Vet_02-16-7; Az. ROB-55.2Vet-2532.Vet_02-15-193; ROB-55.2Vet-2532.Vet_03-16-56).

Animal model. Six to 16 weeks old male and female NOD.Cg-Prkdc^{scid} IL2rg^{tm1Wjl}/SzJ (NSG) mice (The Jackson Laboratory, Bar Harbour, ME, USA) were included. Mice were kept under specified pathogen-free (SPF) conditions with a 12/12 h light cycle, temperature of 20–24 °C and 45–65% humidity according to Annex A of the European Convention 2007/526 EC. The maximum stocking density of the cages corresponds to Annex III of the 2010/63 EU. The cages were constantly filled with structural enrichment and the animals had unlimited access to food and water. During the experiment, mice were kept in individually ventilated cages (IVCs). Hygiene monitoring was carried out at least quarterly in accordance with the current FELASA recommendation.

Donor mice used for PDX cell amplification were sacrificed at advanced leukemic disease (more than 60% leukemic cells within peripheral blood) or when first clinical signs of illness appeared (rough fur, hunchback, reduced motility, paralysis). Experimental mice were sacrificed at specified time points.

Generating transgenic patient derived xenograft (PDX) models. Establishing serially passaged AML and ALL PDX models in NSG mice, re-isolating PDX cells from mice, PDX cell culture, lentiviral transduction, enrichment of transgenic cells and in vivo imaging were described previously^{29,52,53}.

Generation of AML and ALL-PDX models. Fresh primary AML or ALL cells were isolated by Ficoll gradient centrifugation from peripheral blood or bone marrow aspirates that had been obtained from leftovers of clinical routine sampling before onset of therapy and injected into 6–12 weeks old NSG mice via the tail vein. Engraftment was monitored by 2-weekly flow cytometry measurement of human cells in peripheral blood starting at week 4. Mice were sacrificed at first clinical signs of disease, as measured by quantification of human cells in peripheral blood. From engrafted mice

Fig. 3 Essential function of *MLL-AF4* and *DUX4-IGH* fusion proteins in rearranged ALL. **a–c** *MLL-AF4* plays an essential role in vivo in *MLL-AF4* rearranged ALL. **a** A shRNA targeting the *MLL-AF4* fusion mRNA was designed, according to the patient's specific breakpoint of PDX ALL-707 (Table S3). mRNA expression of *MLL-AF4*, *MLL* and *AF4* in PDX ALL-707 was analyzed by qPCR in CTRL and *MLL-AF4* knockdown cells ($n = 3$ each). Mean \pm SEM of cells isolated from mice 28 days after TAM are shown. $*p = 0.0178$ by Welch's *t*-test; ns not significant. **b** Competitive experiments were performed and analyzed as in Fig. 1c, using PDX ALL-707 cells and the shGOI targeting *MLL-AF4*. TAM was applied on two consecutive days (100 mg/kg, day $-1 + 0$). Mice were sacrificed 3 ($n = 4$), 13 ($n = 3$), 21 ($n = 3$) and 28 ($n = 3$) days after TAM; each dot represents one mouse; mean \pm SEM; $****p < 0.0001$, by unpaired *t*-test. **c** Representative in vivo bioluminescence images of mice bearing a shCTRL/shCTRL or shCTRL/sh*MLL-AF4* mixture from the experiment described in Fig. 3b, at the indicated time points after TAM administration. **d–g** *DUX4* plays an essential role in *DUX4-IGH* rearranged ALL. **d** Competitive experiments were performed and analyzed as in Fig. 2b, using ALL-811 and the shRNA targeting *DUX4* (1.4×10^6 cells/mouse). 21 days after injection, TAM (50 mg/kg) was applied once (day 0). Mice were sacrificed 3 ($n = 3$) and 61 ($n = 6$) days after TAM. Shown is mean \pm SEM. $****p < 0.0001$ by unpaired *t*-test. Protein immunoassay of *DUX4* in NALM-6 cells, after lentiviral transduction with the indicated shRNAs. β -actin was used as loading control. **e** Transcriptome analysis was performed from eGFP/shCTRL and eGFP/sh*DUX4* cells from the experiment described in panel **d** 82 days after TAM ($n = 3$ for each condition). Heatmap of 47 genes differentially expressed between the two groups is shown. All gene expressions have been scaled to a mean value of 0 and a variance of 1. **f** Enrichment plot of genes deregulated in sh*DUX4* PDX cells compared to genes upregulated two-fold (Set 1) in a published transcriptomic signature (Tanaka et al.⁴³) generated from NALM-6 cells expressing sh*DUX4*. NES = 2.19 (FDR q -value < 0.002). **g** Mean \pm SEM ($n = 3$ independent animals for shCTRL or sh*DUX4*) of three differentially expressed genes are depicted; $**p = 0.0040$ for CD34, $**p = 0.0011$ for CLEC12A and $*p = 0.0145$ for DDIT4L by unpaired *t*-test. **h, i** *DDIT4L* inhibition partially phenocopies *DUX4* silencing. **h** mRNA expression of *DDIT4L* in NALM-6 was analyzed by qPCR in CTRL and *DDIT4L* knockdown cells ($n = 3$ each). Mean \pm SEM of cells isolated 7 days after TAM are shown. $***p < 0.001$ by unpaired *t*-test. **i** Competitive experiments were performed and analyzed as in Fig. 2b, using the NALM-6 cell line and the shRNA targeting *DDIT4L* (5×10^6 cells/mouse (for day 3) and 1×10^5 cells/mouse (for day 15)). 5 days after injection, TAM (50 mg/kg) was applied once (day 0). Mice were sacrificed 3 ($n = 3$) and 15 ($n = 3$) days after TAM. Shown is mean \pm SEM. $***p = 0.0003$ by unpaired *t*-test.

(first generation), PDX AML or ALL cells were reisolated out of femurs, tibiae and spleen by mincing the tissues and filtration through a cell strainer, followed by Ficoll gradient centrifugation in case of splenic cells²⁹. PDX AML cells were identified by staining for human CD45, CD33, CD3 and CD19 (CD38 for PDX ALL) and flow cytometry analysis. Without further enrichment or manipulation, 1×10^6 – 5×10^6 total BM cells were re-injected into next recipient NSG mice for reexpansion (secondary transplantation).

Lentiviral transduction and cell enrichment. Lentiviral transduction was performed as previously described⁵². Briefly, PDX cells freshly isolated from mouse spleen or BM were re-suspended in RPMI-Medium (Life Technologies) supplemented with 20% fetal calf serum (Biochrom AG, Berlin, Germany), 5% L-Glutamine, 1% Gentamycin, 1% Penicillin/Streptomycin, 0.6% mixture of rh insulin/human transferrin/sodium selenite (Life Technologies), 1 mM sodium pyruvate, and 50 μ M 1-thioglycerol (Sigma-Aldrich, Hannover, Germany). 1×10^6 cells in 1 ml medium were transferred to a cell culture plate and were transduced overnight with lentiviral constructs in the presence of 8 μ g/ml polybrene (Sigma-Aldrich). To save one round of passaging through mice, PDX cells freshly transduced with lentiviruses were kept in culture for 4 days to allow marker expression and enrichment of transgenic cells using a FACSAria III (BD Bioscience) and the FACSDiva software 8.0.2 (BD Bioscience). Sorted cells were then re-injected into next generation recipient mice.

Bioluminescence in vivo imaging. In vivo bioluminescence imaging (BLI) BLI was performed as previously described⁵². The IVIS Lumina II Imaging System was used (Caliper Life Sciences, Mainz, Germany). Mice were anesthetized using isoflurane, placed into the imaging chamber in a supine position and fixed at the lower limbs and by the inhalation tube. Coelenterazine (Synchem OHG, Felsberg/Altenburg, Germany) was dissolved in acidified methanol (HPLC grade) at concentration 10 mg/ml and diluted shortly before injection in sterile HBG buffer (HEPES-buffered Glucose containing 20 mM HEPES at pH 7.1, 5% glucose w/v). Immediately after intravenous tail vein injection of 100 μ g of native Coelenterazine, mice were imaged for 15 s using a field of view of 12.5 cm with binning 8, *f*/stop 1 and open filter setting. To monitor tumor growth, mice were imaged once weekly; after therapy, mice were imaged every other day.

Quantification of BLI pictures. Quantification of BLI signal was performed as previously described⁵². The Living Image software 4.4 (Caliper Life Sciences, Mainz, Germany) was used for data acquisition and quantification of light emission using a scale with a minimum of 1.8×10^4 photons per second per cm² per solid angle of one steradian (sr). Different regions of interest (ROI) were defined and signals were considered positive, when light emission exceeded background in each ROI. Background was measured in mice harboring GLuc negative leukemias. A ROI covering the entire animal was used (background 4×10^6 photons per second). As an exception to determine early engraftment, a small ROI covering the femur was used (background 6×10^4 photons per second), as light emission became visible there first. Overt leukemia was considered above 10^{10} photons per second using the ROI covering the entire animal.

Cloning. For constitutive expression of the Cre-ER^{T2} recombinase, the coding sequence of the enzyme was PCR amplified from the CreERT2FrtNeoFrt cassette (gift from MSS)

using a 5' primer carrying NsiI and a 3' primer carrying P2A-NsiI and ligated into the NsiI digested pCDH-SFFV-GLuc-T2A-mCherry vector downstream of the T2A peptide (Fig. S2a) (pCDH-vector, System Bioscience). For inducible knockdown of target genes, the lentiviral FLIP vector system^{25,26} was optimized to link shRNA expression to fluorochrome expression. We used the lentiviral pCDH backbone, digested the vector with SpeI and SalI and introduced the following elements as a pre-synthesized stretch of DNA (GenScript®, Piscataway, NJ, USA): *SpeI* - SFFV - lox2272 - mTagBFP (iRFP720) - lox5171 - mir30 cassette-eGFP (T-Sapphire) - lox2272 - lox5171 - *SalI* (Fig. S2b). The shRNA sequences targeting the different genes (*MCL1*, *DUX4*, *DDIT4L*; see Table S2) were designed using the SplashRNA algorithm⁵⁴, with the exception of *MLL-AF4* where sequences were designed to directly cover the patient-specific translocation breakpoint (Table S2). As control, a shRNA targeting the Renilla luciferase was used in all experiments (shCTRL). The shRNA-sequences were introduced into the mir30 cassette of the KD vector as part of pre-synthesized and annealed, complementary single strand DNA oligos (110 bps, see Table S2; Integrated DNA Technologies, USA), having XhoI and EcoRI as 5' and 3' restriction sites, respectively. For knockdown of *MLL-AF4*, the miR-E KD cassette was used⁵⁵ and concatemerized to enhance the knockdown efficiency⁵⁶.

In vivo assays and Tamoxifen administration. For pairwise competitive in vivo experiments, PDX transduced with either the control shRNA expressing iRFP (iRFP720) or the shRNA against the GOI expressing mTagBFP were freshly isolated from a donor mouse, were mixed at a 1:1 ratio (shCTRL/shGOI mix) and cells were injected into the tail vein of recipient NSG mice. Of note, to achieve reliable and reproducible results, the use of PDX cells freshly isolated from donor mice (not frozen/thawed cells) is recommended. At best, the initial mixture should not substantially differ from a 1:1 mix. As a control, several groups of mice were injected with the shCTRL/shCTRL mix, consisting of PDX cells transduced with either the control shRNA expressing iRFP or the control shRNA expressing mTagBFP. To promote Cre-ER^{T2} translocation to the nucleus and induction of RNA interference, Tamoxifen (TAM, Cat#T5648-5G, Sigma) was resuspended in a sterile mixture of 90% corn oil (Cat#C8267-500ML, Sigma) and 10% ethanol at final concentration of 20 mg/ml; aliquots were stored for a maximum of 3 months at -20°C . Before administration to mice, the solution was heated to 37°C and applied via oral gavage. TAM concentrations were titrated to induce substantial shRNA expression and was given once at 50 mg/kg for AML-388, ALL-199, ALL-265 and ALL-811, while animals with ALL-707 received 100 mg/kg TAM on two consecutive days. TAM was given by earliest 7 days after cell transplantation and after engraftment was completed.

Flow cytometric analysis of competitive in vivo experiments. Freshly isolated PDX cells were analyzed using LSRII (BD Bioscience) to determine fluorochrome distributions. Forward/Side scatter analysis was used to gate on living cells, followed by gating on mCherry (Cre-ER^{T2}) positive PDX cells. At the beginning, the two cell populations of the mixture were distinguished by expression of either iRFP or mTagBFP. Upon Cre-ER^{T2} recombination, cells expressing shCTRL started expressing T-Sapphire (instead of iRFP), while cells expressing shGOI expressed eGFP (instead of mTagBFP) (Fig. S1b); the color switch was monitored in two separate histograms for either T-Sapphire or eGFP (Fig. 1b). The final analysis combined and compared all cells expressing either of the two shRNAs, either T-Sapphire/shCTRL or eGFP/shGOI (Fig. 1b and c).

To determine the sensitivity of different PDX samples to inhibition of selected GOI, the percentage of cells with knockdown of the GOI (eGFP-expressing cells) were compared between starting conditions (3 days after TAM) to later time points, using at least $n = 3$ data points per time point and condition. A significant depletion in the amount of eGFP/shGOI positive cells over time characterized PDX samples sensitive to the knockdown of the GOI. For target genes inducing rapid cell death upon knockdown, day 1 after TAM administration can be used for comparison. To separate shCTRL and shGOI populations for further investigations, cells were sorted using FACSAria III (BD Bioscience).

Statistical analysis. Statistical significance of pairwise competitive in vivo experiments was analyzed by comparing the percentage of eGFP-positive cells out of all recombined cells (sum of T-Sapphire positive plus eGFP positive cells) between the shCTRL/shGOI mix at 72 h after TAM administration with the shCTRL/shGOI mix at the end of each experiment. Statistical analyses were performed using GraphPad Prism 8. Student's *t*-test was used, if not differently stated in the legends. A *p*-value of ≤ 0.05 was considered significant.

In vivo drug treatment. For in vivo treatment with ABT-199 (Venetoclax, SelleckChem, USA) or Cytarabine (Cell Pharma GmbH, Bad Vilbel, Germany), mice were injected with a 1:1 mixture of shCTRL/shMCL1 AML-388 PDX cells (3×10^5 cells/mouse) and TAM was administered one week thereafter to all animals. 72 h after TAM, three mice were sacrificed to determine recombination efficiency. The remaining animals were divided into three groups and treated either with solvent ($n = 3$) or ABT-199 (100 mg/kg in Carboxymethyl cellulose (1% w/v) + DMSO (2% v/v) by oral gavage for 5 consecutive days and 2 weeks; $n = 3$) or Cytarabine (100 mg/kg in PBS by intraperitoneal injection for 4 consecutive days and 1 week; $n = 3$). At the end of the experiment, mice were sacrificed, BM processed and PDX cells analyzed by flow cytometry for subpopulations' distribution.

Synergistic effect was calculated using the fractional product method⁵⁷. Measured survival rates were 0.39 upon MCL1 KD and 1.0 upon Venetoclax; expected apoptosis induction of independent application of MCL1 knockdown and Venetoclax was calculated as [(1 minus (survival after simulation with MCL1 knockdown) times (survival after stimulation with VCR)) times 100] which resulted to be 0.61; measured apoptosis by the combination of MCL1 and Venetoclax was 0.94 and thus much higher than the expected apoptosis of 0.61, proving that the combination acted in a synergistic way.

For in vivo treatment with S63845 (Hözl Diagnostika, HY-100741-50mg), mice were injected with luciferase expressing ALL-199 (1×10^6 cells/mouse) or AML-388 PDX cells (3×10^5 cells/mouse). Tumor growth was monitored twice per week by bioluminescence imaging. Two weeks after cell injection, mice were treated with S63845 (12.5 mg/kg in 25 mM HCl + 20% 2-hydroxy propyl β -cyclo dextrin by i.v. injection; week 1: 3 doses; weeks 2 and 3: two doses). At sign of overt leukemia, mice were sacrificed, spleens weighted and the proportion of PDX cells in BM and spleen analyzed by flow cytometry.

Engraftment of PDX cells in zebrafish. For PDX cell preparation, AML-388 PDX cells expressing (i) mCherry-Cre-ER^{T2} and (ii) the knockdown construct mTagBFP/shMCL1, were amplified in a donor mouse. Mice were sacrificed, human cells isolated and treated in vitro with 50 nM TAM (Sigma-Aldrich, H7904-25G) to induce recombination and shRNA expression. To allow competitive experiments comparing cells with and without recombination, mCherry positive cells were sorted 48 h after TAM to gain a 1:1 mixture of eGFP:mTagBFP positive cells and thus 50% of cells with Cre-ER^{T2}-induced recombination.

48 h after fertilization, dechorionated, 1-phenyl 2-thiourea (PTU) treated (75 μ M) (Sigma-Aldrich, P7629) wild type zebrafish embryos (Danio rerio, AB line) were anesthetized with Tricain (Sigma-Aldrich, A5040). Embryos were injected through the Duct of Cuvier, using a Femtojet microinjector (Eppendorf, Hamburg, Germany), with 200 to 500 AML-388 PDX cells per embryo of the mTagBFP/shMCL1 mixture. Embryos were raised at 36 °C. At 4 and 28 h post transplantation (hpt), embryos were anesthetized with 750 μ M Tricain and embedded in 1.5% low melting-temperature Agarose (Lonza, MetaPhor Agarose 50185) containing 75 μ M PTU and 750 μ M Tricaine.

Each larva was imaged using a spinning disc microscope (20x magnification) and images were applied to maximal intensity projection. Using the spot detection function (LoG detector) of the Image-J plugin TrackMate⁵⁸ PDX cells were identified by mCherry-Cre-ER^{T2} expression. To quantify the subfraction of cells expressing the shRNA, the median eGFP signal was determined at 4 hpt. For each fish the percentage of eGFP positive, shRNA expressing cells was calculated at 4 hpt and 28hpt using the determined median as threshold.

Zebrafish embryos/larvae were studied exclusively within the first 5 days after fertilization, handled compliant to local animal welfare regulations and maintained according to standard protocols (www.ZFIN.org) which does not require a special permit according to German Laboratory Animal Protection Law.

Flow cytometric analysis of BH3 proteins' level and Annexin V staining. To determine intracellular expression levels of BH3 proteins, cells were fixated in 2% paraformaldehyde, permeabilized using perm/wash buffer (BD Bioscience, Franklin Lakes, NJ, USA) and subsequently stained with fluorescently labeled antibodies against

BCL-2 (clone Bcl-2/100, BD Bioscience), BCL-XL (clone 54H11, Cell Signaling, Cambridge, UK), MCL-1 (Clone D2W9E, Cell signaling) or respective isotype controls (Cat.: 556357, BD Bioscience; clone DA1E, Cell Signaling). Dead cells were excluded by Fixable Viability Dye staining. If not otherwise stated, reagents and antibodies were purchased from eBioscience. Flow cytometric analysis was performed on a BD FACS Canto II (BD Bioscience) and data were analyzed using FlowJo software (TreeStar Inc., Ashland, OR, USA).

Annexin V staining was performed on PDX AML-388, ALL-199 and ALL-265 cells isolated from the mouse BM 72 h after TAM treatment or thawed and treated in vitro, using PE/Cy7 Annexin V (BioLegend, 640949) according to the manufacturer's instruction and analyzed by flow cytometry (LSRII, BD Bioscience).

Targeted genome sequencing. The *MLL-AF4* breakpoint was sequenced at the certified laboratory for Leukemia Diagnostics, Department of Medicine III, University Hospital, LMU Munich, Munich, Germany.

Real-time quantitative PCR. Total RNA from flow cytometry enriched populations was extracted using RNeasy Mini Kit (Qiagen, Venlo, Netherlands) and reverse transcribed using the QuantiTect Reverse Transcription kit (Qiagen, Venlo, Netherlands) according to manufacturer's instruction. Quantitative PCR was performed in a LightCycler 480 (Roche, Mannheim, Germany) using the corresponding LightCycler 480 Probes Master and the pre-designed Probes of the Universal ProbeLibrary (Roche, Mannheim, Germany). The primer and probes used for qPCR are: *HPRT1_fw*: TGATAGATCCATTCTCTATGACTGTAGA, *HPRT1_rv*: CAAGACATTCTTCCAGTTAAAGTTG, UPL #22; *MLL/AF4_fw*: AAGTCCCAAAAACCACTCCTAGT, *MLL/AF4_rv*: GCCATGAATGGGTCAT TTCC, UPL #22; *MLL_fw*: AAGTCCCAAAAACCACTCCTAGT, *MLL_rv*: GATCCTGTGGACTCCATCTGC, UPL #22; *AF4_fw*: CTCCTCCAAAAG TGTTC, *AF4_rv*: TAGGCTGCTCAACTGACTGAG, UPL #84; *DDIT4L_fw*: CCCAGAGAGCCTGCTAAGTG, *DDIT4L_rev*: TTGCTTTGATTGGACAGACA, UPL #67. Relative gene expression levels were normalized to *HPRT1* using the $2^{-\Delta\Delta C_t}$ method.

Gene expression profiling. Gene expression analysis was performed by applying a bulk adjusted SCRBS-Seq protocol on sorted subpopulations from PDX samples as described previously^{59,60}. Briefly, for library preparation 2,000 cells of each individual sample were sorted and lysed in RLT Plus (Qiagen) supplemented with 1% 2-Mercaptoethanol (Sigma-Aldrich) and stored at -80 °C until processing. A modified SCRBS-Seq protocol (6, 7) was used for library preparation. Briefly, proteins in the lysate were digested by Proteinase K (Ambion), RNA was cleaned up using SPRI beads (GE, 22% PEG). In order to remove isolated DNA, samples were treated with DNase I for 15 min at RT. cDNA was generated by oligo-dT primers containing well specific (sample specific) barcodes and unique molecular identifiers (UMIs). Unincorporated barcode primers were digested using Exonuclease I (Thermo Fisher). cDNA was pre-amplified using KAPA HiFi HotStart polymerase (Roche) and pooled before Nextera libraries were constructed from 0.8 ng of pre-amplified cleaned up cDNA using Nextera XT Kit (Illumina). 3' ends were enriched with a custom P5 primer (P5NEXTPT5, IDT) and libraries were size selected using 2% E-6 Gel Agarose EX Gels (Life Technologies), cut out in the range of 300–800 bp, and extracted using the Monarch DNA Gel Extraction Kit (New England Biolabs) according to manufacturer's recommendations.

All raw fastq data was processed with zUMIs⁶¹ (2.4.5b). Mapping was performed using STAR 2.6.0a⁶² against the concatenated human (hg38) and mouse genome (mm10). Gene annotations were obtained from Ensembl (GRCh38.84/GRCh38.75). Analysis of RNA sequencing data followed standard recommendations⁶³. Statistical analysis was performed using the R 3.6.1 software package (R Core Team, 2019). In case of multiple testing, *p*-values were adjusted using the Benjamini-Hochberg procedure (FDR-cutoff < 0.05). Gene Set Enrichment Analysis (GSEA) using default settings (version 4.0.2) was used for the association of defined gene sets with different subgroups⁶⁴.

For PDX-707 Massice Analysis of cDNA Ends (MACE) was performed at GenXPro (Frankfurt am Main, Germany). Therefore, 28 days after TAM 50,000 cells eGFP/shCTRL ($n = 3$) and eGFP/shMCL1-AF4 PDX ($n = 3$) cells were sorted and sent to GenXPro for total RNA isolation, MACE library preparation and strand-specific sequencing using the HiSeq2500 (Illumina, USA), as previously described⁶⁵. The bioinformatic analysis was conducted in accordance to the analysis pipeline for MACE libraries by GenXPro GmbH. Distinct Oligo IDs and UMIs on each transcript enabled initial demultiplexing and subsequent removal of PCR-duplicates for alignment of adapter-free sequences with Bowtie 2 to the human reference genome (Genome Reference Consortium Human Build 38 patch release 13, GRCh38.p13). Considering sequencing depth and RNA composition, the sequencing data was normalized with the median of ratios method by DESeq2. GSEA was carried out to compare the effect of the *MLL-AF4* KD in the t(4;11) PDX ALL-707 with published transcriptomic data from t(4;11) leukemia patients (expression data from Stam et al.⁴⁰; GEO database: GSE19475; significant genes were selected according to Lin et al. (2016): $p \leq 0.05$, FDR ≤ 0.1 , fold change ≥ 2). The GSEA software of UC San Diego and the Broad Institute was used for analysis. Permutation testing was conducted with a gene set specific permutation test, set to 1000 permutations.

To study *DUX-4* expression in B-ALL patients we downloaded log2-FPKM values of 1988 patients with B-progenitor ALL from the publicly available St. Jude

Cloud (<https://viz.stjude.cloud/stjude/visualization/pax5-driven-subtypes-of-b-progenitor-acute-lymphoblastic-leukemia-t-sne~15>), as previously described⁶⁶.

Protein immunoassay. To quantify protein of low PDX cell numbers, the Simple Western capillary protein immunoassay (WES, ProteinSimple, San Jose, USA) was performed according to manufacturer's instructions as previously described⁶⁷. Flow cytometry enriched cell populations were incubated in lysis buffer (#9803, Cell Signaling Technology, Boston, USA) on ice for 30 min and protein concentration measured by BCA assay (#7780, New England Biolabs, Beverly, USA). Results were analyzed using the Compass software (ProteinSimple). Antibodies used were MCL1 (D3CA5, Cell Signaling Technologies), DUX4 (MAB9535, R&D system) and β -actin (NB600-501SS, Novus Biologicals). Western blot analysis of PDX ALL-265 was performed as previously described⁶⁸, using the following antibodies: MCL1 (S-19, Santa Cruz Biotechnology) and GAPDH (6C5, Merck Millipore).

Reporting summary. Further information on research design is available in the Nature Research Reporting Summary linked to this article.

Data availability

The RNA-seq data generated in this study have been deposited at the Gene Expression Omnibus under the following accession codes: [GSE182760](https://www.ncbi.nlm.nih.gov/geo/query/acc.cgi?acc=GSE182760) (MCL1), [GSE181973](https://www.ncbi.nlm.nih.gov/geo/query/acc.cgi?acc=GSE181973) (MLL-AF4), [GSE182780](https://www.ncbi.nlm.nih.gov/geo/query/acc.cgi?acc=GSE182780) (DUX4-IGH). Source data are provided with this paper.

Received: 18 June 2020; Accepted: 9 September 2021;
Published online: 27 September 2021

References

- Grobner, S. N. et al. The landscape of genomic alterations across childhood cancers. *Nature* **555**, 321–327 (2018).
- Moffat, J. G., Vincent, F., Lee, J. A., Eder, J. & Prunotto, M. Opportunities and challenges in phenotypic drug discovery: an industry perspective. *Nat. Rev. Drug Discov.* **16**, 531–543 (2017).
- Hay, M., Thomas, D. W., Craighead, J. L., Economides, C. & Rosenthal, J. Clinical development success rates for investigational drugs. *Nat. Biotechnol.* **32**, 40–51 (2014).
- Scannell, J. W. & Bosley, J. When quality beats quantity: decision theory, drug discovery, and the reproducibility crisis. *PLoS ONE* **11**, e0147215 (2016).
- Zeggini, E., Gloy, A. L., Barton, A. C. & Wain, L. V. Translational genomics and precision medicine: moving from the lab to the clinic. *Science* **365**, 1409–1413 (2019).
- Behan, F. M. et al. Prioritization of cancer therapeutic targets using CRISPR-Cas9 screens. *Nature* **568**, 511–516 (2019).
- Ben-David, U. et al. Genetic and transcriptional evolution alters cancer cell line drug response. *Nature* **560**, 325–330 (2018).
- Engle, S. J., Blaha, L. & Kleiman, R. J. Best practices for translational disease modeling using human iPSC-derived. *Neurons Neuron* **100**, 783–797 (2018).
- Driehuis, E. et al. Pancreatic cancer organoids recapitulate disease and allow personalized drug screening. *Proc. Natl Acad. Sci. USA* **116**, 26580–26590 (2019).
- Bleijs, M., van de Wetering, M., Clevers, H. & Drost, J. Xenograft and organoid model systems in cancer research. *EMBO J.* **38**, e101654 (2019).
- Townsend, E. C. et al. The public repository of xenografts enables discovery and randomized phase II-like trials in mice. *Cancer Cell* **29**, 574–586 (2016).
- Evrard, Y. A. et al. Systematic establishment of robustness and standards in patient-derived xenograft experiments and analysis. *Cancer Res.* **80**, 2286 (2020).
- Izumchenko, E. et al. Patient-derived xenografts effectively capture responses to oncology therapy in a heterogeneous cohort of patients with solid tumors. *Ann. Oncol.* **28**, 2595–2605 (2017).
- Gao, H. et al. High-throughput screening using patient-derived tumor xenografts to predict clinical trial drug response. *Nat. Med.* **21**, 1318–1325 (2015).
- Guo, S. et al. Molecular pathology of patient tumors, patient-derived xenografts, and cancer cell lines. *Cancer Res.* **76**, 4619 (2016).
- Hulton, C. H. et al. Direct genome editing of patient-derived xenografts using CRISPR-Cas9 enables rapid in vivo functional genomics. *Nat. Cancer* **1**, 359–369 (2020).
- Clohesy, J. G. & Pandolfi, P. P. The mouse hospital and its integration in ultra-precision approaches to cancer care. *Front Oncol.* **8**, 340 (2018).
- Costello, A. et al. Leaky expression of the TET-On system hinders control of endogenous miRNA abundance. *Biotechnol. J.* **14**, e1800219 (2019).
- Indra, A. K. et al. Temporally-controlled site-specific mutagenesis in the basal layer of the epidermis: comparison of the recombinase activity of the tamoxifen-inducible Cre-ER(T) and Cre-ER(T2) recombinases. *Nucleic Acids Res.* **27**, 4324–4327 (1999).
- Koo, B.-K. et al. Controlled gene expression in primary Lgr5 organoid cultures. *Nat. Methods* **9**, 81–83 (2012).
- Richter-Pechanska, P. et al. PDX models recapitulate the genetic and epigenetic landscape of pediatric T-cell leukemia. *EMBO Mol. Med.* **10**, e9443 (2018).
- Koga, Y. & Ochiai, A. Systematic review of patient-derived xenograft models for preclinical studies of anti-cancer drugs in solid tumors. *Cells* **8**, 418 (2019).
- Feil, R., Wagner, J., Metzger, D. & Chambon, P. Regulation of Cre recombinase activity by mutated estrogen receptor ligand-binding domains. *Biochem. Biophys. Res. Commun.* **237**, 752–757 (1997).
- Charrier, S. et al. Quantification of lentiviral vector copy numbers in individual hematopoietic colony-forming cells shows vector dose-dependent effects on the frequency and level of transduction. *Gene Ther.* **18**, 479–487 (2011).
- Schnutgen, F. et al. A directional strategy for monitoring Cre-mediated recombination at the cellular level in the mouse. *Nat. Biotechnol.* **21**, 562–565 (2003).
- Stegmeier, F., Hu, G., Rickles, R. J., Hannon, G. J. & Elledge, S. J. A lentiviral microRNA-based system for single-copy polymerase II-regulated RNA interference in mammalian cells. *Proc. Natl Acad. Sci. USA* **102**, 13212–13217 (2005).
- Siegel, R. W., Jain, R. & Bradbury, A. Using an in vivo phagemid system to identify non-compatible loxP sequences. *FEBS Lett.* **505**, 467–473 (2001).
- Zapata-Hommer, O. & Griesbeck, O. Efficiently folding and circularly permuted variants of the Sapphire mutant of GFP. *BMC Biotechnol.* **3**, 5 (2003).
- Vick, B. et al. An advanced preclinical mouse model for acute myeloid leukemia using patients' cells of various genetic subgroups and in vivo bioluminescence imaging. *PLoS ONE* **10**, e0120925 (2015).
- Khaw, S. L. et al. Venetoclax responses of pediatric ALL xenografts reveal sensitivity of MLL-rearranged leukemia. *Blood* **128**, 1382–1395 (2016).
- Kotschy, A. et al. The MCL1 inhibitor S63845 is tolerable and effective in diverse cancer models. *Nature* **538**, 477–482 (2016).
- Fernandez-Marrero, Y., Spinner, S., Kaufmann, T. & Jost, P. J. Survival control of malignant lymphocytes by anti-apoptotic MCL-1. *Leukemia* **30**, 2152–2159 (2016).
- Hird, A. W. & Tron, A. E. Recent advances in the development of Mcl-1 inhibitors for cancer therapy. *Pharm. Ther.* **198**, 59–67 (2019).
- Koch, R. et al. Biomarker-driven strategy for MCL1 inhibition in T-cell lymphomas. *Blood* **133**, 566–575 (2019).
- Moujalled, D. M. et al. Combining BH3-mimetics to target both BCL-2 and MCL1 has potent activity in pre-clinical models of acute myeloid leukemia. *Leukemia* **33**, 905–917 (2019).
- Bhatt, S. et al. Reduced mitochondrial apoptotic priming drives resistance to BH3 mimetics in acute myeloid leukemia. *Cancer Cell* **38**, 872–890 (2020).
- Xiang, W., Yang, C. Y. & Bai, L. MCL-1 inhibition in cancer treatment. *Oncotargets Ther.* **11**, 7301–7314 (2018).
- Hilden, J. M. et al. Analysis of prognostic factors of acute lymphoblastic leukemia in infants: report on CCG 1953 from the Children's Oncology Group. *Blood* **108**, 441–451 (2006).
- Thomas, M. et al. Targeting MLL-AF4 with short interfering RNAs inhibits clonogenicity and engraftment of t(4;11)-positive human leukemic cells. *Blood* **106**, 3559–3566 (2005).
- Stam, R. W. et al. Gene expression profiling-based dissection of MLL translocated and MLL germline acute lymphoblastic leukemia in infants. *Blood* **115**, 2835–2844 (2010).
- Yasuda, T. et al. Recurrent DUX4 fusions in B cell acute lymphoblastic leukemia of adolescents and young adults. *Nat. Genet.* **48**, 569–574 (2016).
- Schinnerl, D. et al. CD371 cell surface expression: a unique feature of DUX4-rearranged acute lymphoblastic leukemia. *Haematologica* **104**, e352–e355 (2019).
- Tanaka, Y. et al. Transcriptional activities of DUX4 fusions in B-cell acute lymphoblastic leukemia. *Haematologica* **103**, e522–e526 (2018).
- Rehn, J. A., Connor, M. J., White, D. L. & Yeung, D. T. DUX hunting—clinical features and diagnostic challenges associated with DUX4-rearranged leukaemia. *Cancers* **12**, 2815 (2020).
- Harvey, R. C. et al. Identification of novel cluster groups in pediatric high-risk B-precursor acute lymphoblastic leukemia with gene expression profiling: correlation with genome-wide DNA copy number alterations, clinical characteristics, and outcome. *Blood* **116**, 4874–4884 (2010).
- Mullighan, C. G. et al. ERG deletions define a novel subtype of B-progenitor acute lymphoblastic leukemia. *Blood* **110**, 691–691 (2007).
- Simonson, B. et al. DDIT4L promotes autophagy and inhibits pathological cardiac hypertrophy in response to stress. *Sci. Signal* **10**, eaaf5967 (2017).
- Miyazaki, M. & Esser, K. A. REDD2 is enriched in skeletal muscle and inhibits mTOR signaling in response to leucine and stretch. *Am. J. Physiol. Cell Physiol.* **296**, C583–C592 (2009).
- Corradetti, M. N., Inoki, K. & Guan, K. L. The stress-induced proteins RTP801 and RTP801L are negative regulators of the mammalian target of rapamycin pathway. *J. Biol. Chem.* **280**, 9769–9772 (2005).
- Klaeger, S. et al. The target landscape of clinical kinase drugs. *Science* **358**, eaan4368 (2017).
- Setten, R. L., Rossi, J. J. & Han, S.-P. The current state and future directions of RNAi-based therapeutics. *Nat. Rev. Drug Discov.* **18**, 421–446 (2019).
- Terziyska, N. et al. In vivo imaging enables high resolution preclinical trials on patients' leukemia cells growing in mice. *PLoS ONE* **7**, e25798 (2012).

53. Ebinger, S. et al. Characterization of rare, dormant, and therapy-resistant cells in acute lymphoblastic leukemia. *Cancer Cell* **30**, 849–862 (2016).
54. Pelossof, R. et al. Prediction of potent shRNAs with a sequential classification algorithm. *Nat. Biotechnol.* **35**, 350–353 (2017).
55. Fellmann, C. et al. An optimized microRNA backbone for effective single-copy RNAi. *Cell Rep.* **5**, 1704–1713 (2013).
56. Dow, L. E. et al. A pipeline for the generation of shRNA transgenic mice. *Nat. Protoc.* **7**, 374–393 (2012).
57. Webb J. L., Effect of more than one inhibitor. In *Enzymes and Metabolic Inhibitors* (eds. Hochster R. M. & Quastel J. H.) vol. 1, 487–512 (New York, NY; Academic Press, 1963).
58. Tinevez, J. Y. et al. TrackMate: An open and extensible platform for single-particle tracking. *Methods* **115**, 80–90 (2017).
59. Soumillon, M., Cacchiarelli, D., Semrau, S., van Oudenaarden, A. & Mikkelsen, T. S. Characterization of directed differentiation by high-throughput single-cell RNA-Seq. Preprint at <https://www.biorxiv.org/content/10.1101/003236v1> (2014).
60. Ebinger, S. et al. Plasticity in growth behavior of patients' acute myeloid leukemia stem cells growing in mice. *Haematologica* **105**, 2855–2860 (2020).
61. Parekh, S., Ziegenhain, C., Vieth, B., Enard, W. & Hellmann, I. zUMIs - A fast and flexible pipeline to process RNA sequencing data with UMIs. *Gigascience* **7**, giy059 (2018).
62. Dobin, A. et al. STAR: ultrafast universal RNA-seq aligner. *Bioinformatics* **29**, 15–21 (2013).
63. Herold, T. et al. A 29-gene and cytogenetic score for the prediction of resistance to induction treatment in acute myeloid leukemia. *Haematologica* **103**, 456–465 (2018).
64. Mootha, V. K. et al. PGC-1 α -responsive genes involved in oxidative phosphorylation are coordinately downregulated in human diabetes. *Nat. Genet.* **34**, 267–273 (2003).
65. Nold-Petry, C. A. et al. IL-37 requires the receptors IL-18R α and IL-1R8 (SIGIRR) to carry out its multifaceted anti-inflammatory program upon innate signal transduction. *Nat. Immunol.* **16**, 354–365 (2015).
66. Gu, Z. et al. PAX5-driven subtypes of B-progenitor acute lymphoblastic leukemia. *Nat. Genet.* **51**, 296–307 (2019).
67. Liu, W.-H. et al. Inducible transgene expression in PDX models in vivo identifies KLF4 as a therapeutic target for B-ALL. *Biomark. Res.* **8**, 46 (2020).
68. Ehrhardt, H. et al. Activation of DNA damage response by antitumor therapy counteracts the activity of vinca alkaloids. *Anticancer Res* **33**, 5273–5287 (2013).

Acknowledgements

We thank Liliانا Mura, Fabian Klein, Maïke Fritschle, Annette Frank and Miriam Krekel for excellent technical assistance; Markus Briemeier and team (Research Unit Comparative Medicine) for animal care services; Karsten Spiekermann and the LFL laboratory for sequencing the *MLL-*AF4** breakpoint; Wolfgang Enard and Helmut Blum for generating SCRB-seq data and Jean Pierre Bourquin and Beat Bornhäuser for providing engrafted sample ALL-265. The work was supported by the Humboldt Postdoctoral Fellowship (to M.C.), and by grants from the European Research Council Consolidator Grant 681524; a Mildred Scheel Professorship by German Cancer Aid; German Research Foundation (D.F.G.); the Collaborative Research Center 1243 "Genetic and Epigenetic Evolution of Hematopoietic Neoplasms", project A05; DFG proposal MA 1876/13-1; Bettina Bräu Stiftung and Dr. Helmut Legerlotz Stiftung (all to I.J.); by the Joint Funding project "Relapsed ALL" of the German Cancer Consortium (DKTK) (to C.B. and I.J.). T.H. was supported by the Physician Scientists Grant (G-509200-004) from the Helmholtz Zentrum München. P.J.J. was supported by the Max Eder-Program grant from the Deutsche Krebshilfe (program #111738), Deutsche José Carreras Leukämie-Stiftung

(DJCLS R 12/22 and DJCLS 21 R/2016), Else Kröner Fresenius Stiftung (2014_A185) and Deutsche Forschungsgemeinschaft (DFG FOR 2036, SFB 1335 and SFB 1371).

Author contributions

M.C. designed and performed experiments, analyzed data and wrote the manuscript, K.V. designed, performed experiments and analyzed data with contributions from J.V. (establishing the technique), M.B. (*DUX4-IGH*), D.S. (data analysis and writing the manuscript), Y.G. (PCR, MCL-1 inhibitor treatment), W.H.L. (cloning), B.V. (establishment of treatment regimens), J.P.S. (quality control experiments); J.W.B. performed and T.H. and V.J. analyzed *DUX4* SCRB-seq data; A.W. and R.M. analyzed *MLL-*AF4** RNAseq data; A.A. and V.B. performed zebrafish experiments; V.D. and P.J.J. quantified BH3 protein expression; B.F. and K.R. designed fluorochrome use; C.B., L.B., L.L. and D.M.S. provided PDX models; C.M., M.S.S. and M.B. developed cloning strategies; I.J. supervised the study, and contributed to experimental design, data analysis and writing the manuscript.

Funding

Open Access funding enabled and organized by Projekt DEAL.

Competing interests

P.J.J. has had a consulting or advisory role, received honoraria, research funding, and/or travel/accommodation expenses from: Abbvie, Bayer, Boehringer, Novartis, Pfizer, Servier, BMS and Celgene. The remaining authors declare no competing interests.

Additional information

Supplementary information The online version contains supplementary material available at <https://doi.org/10.1038/s41467-021-25963-z>.

Correspondence and requests for materials should be addressed to Irmela Jeremias.

Peer review information *Nature Communications* thanks Charles de Bock, Ross Levine and the other, anonymous, reviewer(s) for their contribution to the peer review of this work. Peer reviewer reports are available.

Reprints and permission information is available at <http://www.nature.com/reprints>

Publisher's note Springer Nature remains neutral with regard to jurisdictional claims in published maps and institutional affiliations.



Open Access This article is licensed under a Creative Commons Attribution 4.0 International License, which permits use, sharing, adaptation, distribution and reproduction in any medium or format, as long as you give appropriate credit to the original author(s) and the source, provide a link to the Creative Commons license, and indicate if changes were made. The images or other third party material in this article are included in the article's Creative Commons license, unless indicated otherwise in a credit line to the material. If material is not included in the article's Creative Commons license and your intended use is not permitted by statutory regulation or exceeds the permitted use, you will need to obtain permission directly from the copyright holder. To view a copy of this license, visit <http://creativecommons.org/licenses/by/4.0/>.

© The Author(s) 2021

¹Research Unit Apoptosis in Hematopoietic Stem Cells, Helmholtz Zentrum München, German Research Center for Environmental Health (HMGU), Munich, Germany. ²Laboratory for Leukemia Diagnostics, Department of Medicine III, University Hospital, LMU Munich, Munich, Germany. ³German Cancer Consortium (DKTK), Partnering Site Munich, Munich, Germany. ⁴Department of Pediatrics, Dr. von Hauner Children's Hospital, University Hospital, Ludwig Maximilian University (LMU), Munich, Germany. ⁵Clinic and Policlinic for Internal Medicine III, Technical University of Munich, School of Medicine, Munich, Germany. ⁶Research Department Cell and Gene Therapy, Department of Stem Cell Transplantation, University Medical Center Hamburg-Eppendorf, Hamburg, Germany. ⁷Internal Medicine II, Christian-Albrechts University Kiel and University Medical Center Schleswig-Holstein, Campus Kiel, Kiel, Germany. ⁸Department of Pediatrics I, ALL-BFM Study Group, Christian-Albrechts University Kiel and University Medical Center Schleswig-Holstein, Kiel, Germany. ⁹Anthropology and Human Genomics, Faculty of Biology, Ludwig Maximilian University (LMU), Munich, Germany. ¹⁰Institute of Pharmaceutical Biology, Diagnostic Center of Acute Leukemias (DCAL), Goethe-University, Frankfurt/Main, Germany. ¹¹Center for Translational Cancer Research (TranslaTUM), Klinikum rechts der Isar, Technical University of Munich, Munich, Germany. ¹²Department of Medicine I, Medical Center, University of Freiburg, Faculty of Medicine, Freiburg, Germany. ¹³German Cancer Consortium (DKTK), Partnering Site Freiburg, Freiburg, Germany. ¹⁴Institute of Experimental Hematology, Technical University of Munich, Munich, Germany. ¹⁵These authors contributed equally: Michela Carlet, Kerstin Völse. ✉email: Irmela.Jeremias@helmholtz-muenchen.de

Supplementary information

In vivo inducible reverse genetics in patients' tumors to identify individual therapeutic targets

Michela Carlet^{1*}, Kerstin Völse^{1*}, Jenny Vergalli¹, Martin Becker¹, Tobias Herold^{1,2,3}, Anja Arner⁴, Daniela Senft¹, Vindi Jurinovic^{1,2,4}, Wen-Hsin Liu¹, Yuqiao Gao¹, Veronika Dill⁵, Boris Fehse⁶, Claudia D. Baldus⁷, Lorenz Bastian⁷, Lennart Lenk⁸, Denis M. Schewe⁸, Johannes W. Bagnoli⁹, Binje Vick¹, Jan-Phillip Schmidt¹, Alexander Wilhelm¹⁰, Rolf Marschalek¹⁰, Philipp J. Jost^{3,5,11}, Cornelius Miething¹², Kristoffer Riecken⁶, Marc Schmidt-Supprian¹³, Vera Binder⁴, Irmela Jeremias^{1,3,4, ☆}

This file contains:

Supplementary Tables

Supplementary Figures and Legends

Supplementary Tables

Supplementary Table 1. Clinical characteristics of AML and ALL patients

sample	disease stage*	age	cytogenetics	mutations [∞]	mean passing times [§] [days]	Reference
AML-388	ID	adult	<i>KMT2A/AFDN</i>	<i>KRAS, CEBPZ</i>	47	1, 2
ALL-199	R2	child	somatic trisomy21; leukemic homozygous 9p deletion; <i>P2RY8- CRLF2</i>	N.D.	42	3, 4
ALL-265	R1	child	hyperdiploidy with additional 6,13,14,17,18,21,X chromosome	<i>KMT2D, HERC1, CSMD1, PRRT2</i>	43	3, 4
ALL-707	ID	child	t(4;11) <i>KMT2A/AFF1</i>	N.D.	50	4
ALL-811	R1	adult	<i>DUX4-IGH</i>	<i>KMT2D</i>	80	

*when the primary sample was obtained; [∞] mutations determined by panel sequencing; [§]time of passaging through mice refers to the time from injection of the sample until mice had to be sacrificed due to end stage leukemia; ID = initial diagnosis; R1 = 1st relapse; R2 = 2nd relapse; f = female; m = male; N.D. not determined.

¹ Vick et al., PLoS One 2015

² Ebinger et al., Hematologica 2020

³ Ebinger et al., Cancer Cell 2016

⁴ Heckl et al., Leuk Lymphoma 2019

Supplementary Table 2. Generation of transgenic PDX

sample	mean passaging time [§] [days]	Number of sortings *	Transduction efficiency [%]			
			Cre ^{ERT2}	shCTRL-iRFP	shCTRL-BFP	shGOI
AML-388	47	2	28.5	20.8	37.9	30.5
ALL-199	42	2	9.6	23	37	33
ALL-265	43	2	22.3	20.5	41	28
ALL-707	50	3	3.39	2.3	4.7	3.3
ALL-811	80	2	0.67	1.75	26.5	10.8

[§]time of passaging through mice refers to the time from injection of the sample until mice had to be sacrificed due to end stage leukemia; *from a blank sample to a double-transgenic (Cre and shmiR) sample

Supplementary Table 3. shRNA sequences

target	guide - 22mer
<i>MLL-AF4</i>	TGGAGTAGGTCTGCTTTTCTTT
	TAGGTCTGCTTTTCTTTTGTT *
<i>MCL1</i>	TTACACATCAATTCGTTCTGTA
	TGAAACTGAACTTTGCTTCTTT *
<i>DUX4-IGH</i>	TTCTGAAACCAAATCTGGACCC
	TTCGATTCTGAAACCAGATCTG *
<i>DDIT4L</i>	TTAGTTTGTTAGAACACTGGCT
	TAATATTTCTCATTTACTCTTA *

* For each target an additional shRNA sequence was tested.

Appendix to Supplementary Table 3.

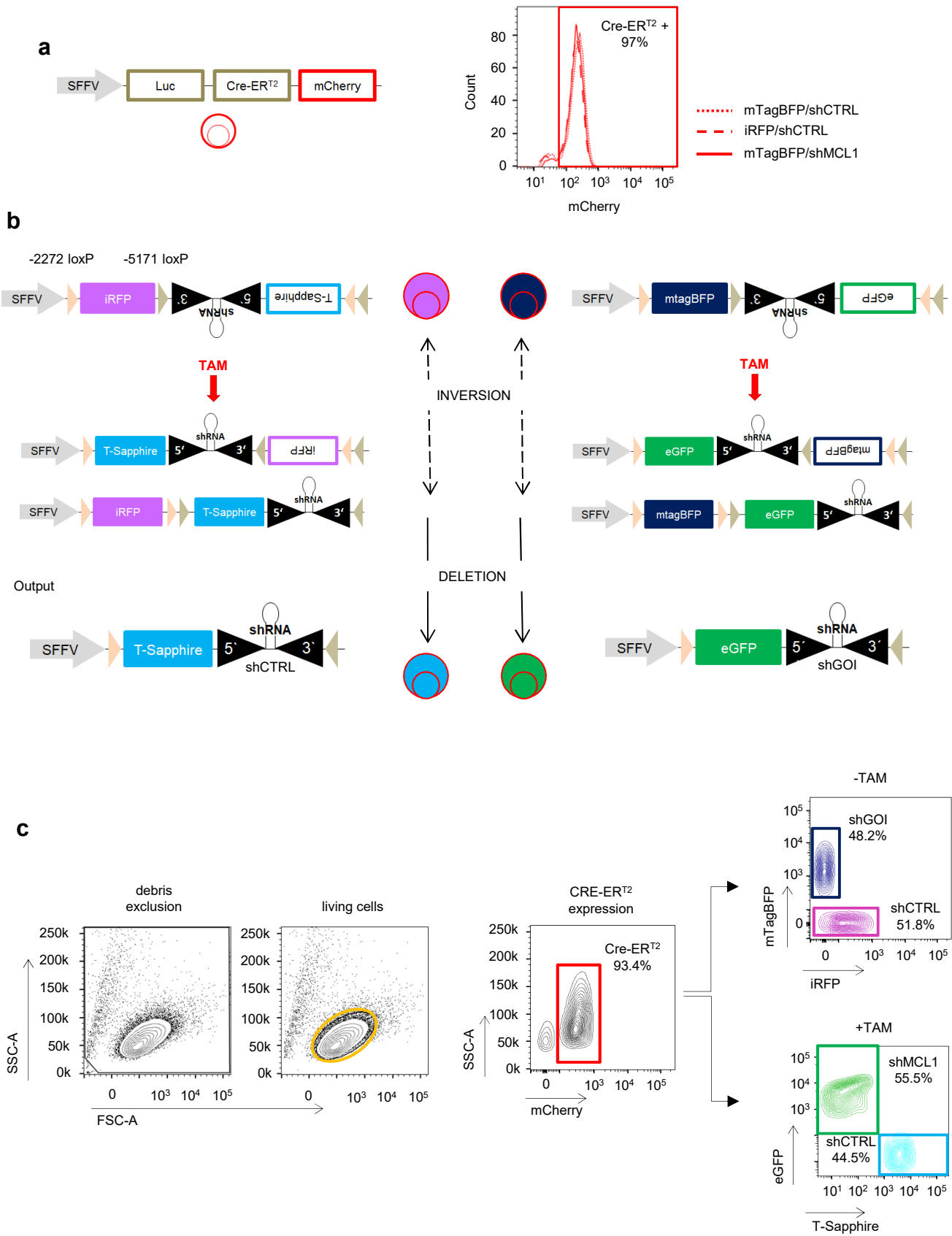
Sequence of the 110bps oligo to be cloned into the pCDH-plasmid digested with XhoI and EcoRI enzymes:

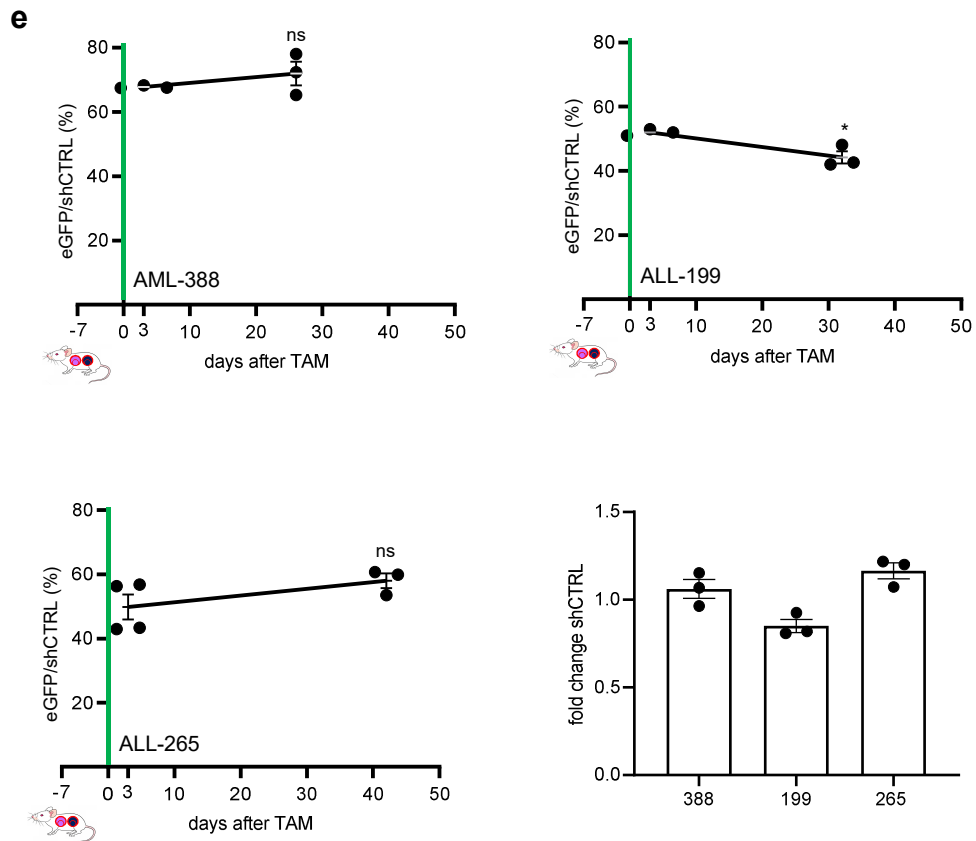
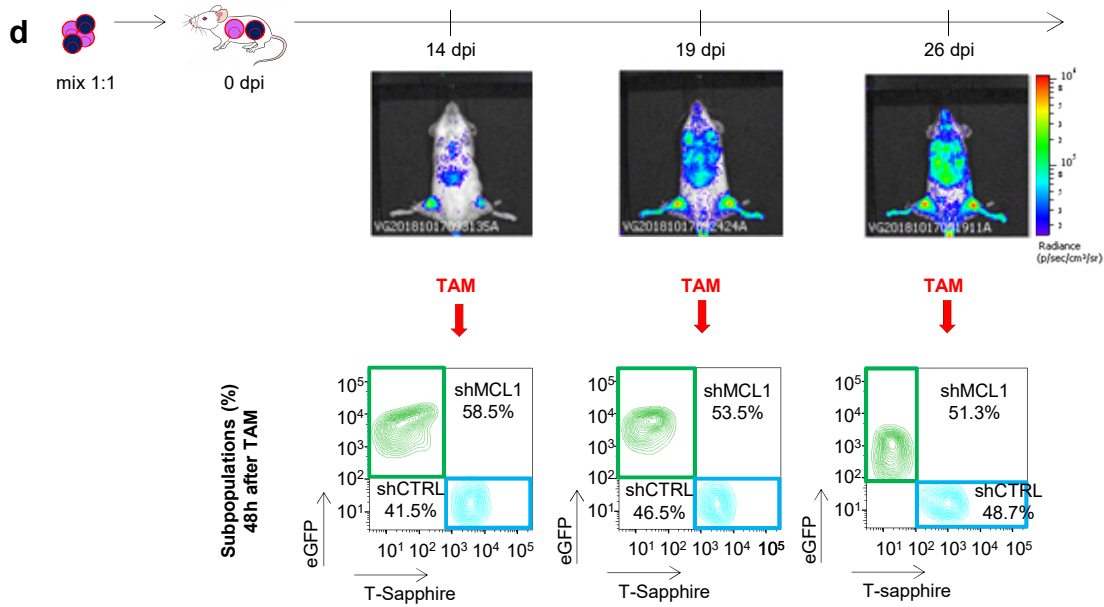
XhoI	passanger strand	guide strand	EcoRI
TCGAGAAAGGTATATTGCTGTTGACAGTGAGCGCAAGAAAAGCAGACCTACTCCATAGTGAAGCCACAGATGATGGAGTAGGTCTGCTTTTCTTTTGCCCTACTGCCTCGG			
5' common flank	loop	MLL/AF4 shRNA sequence	3' common flank

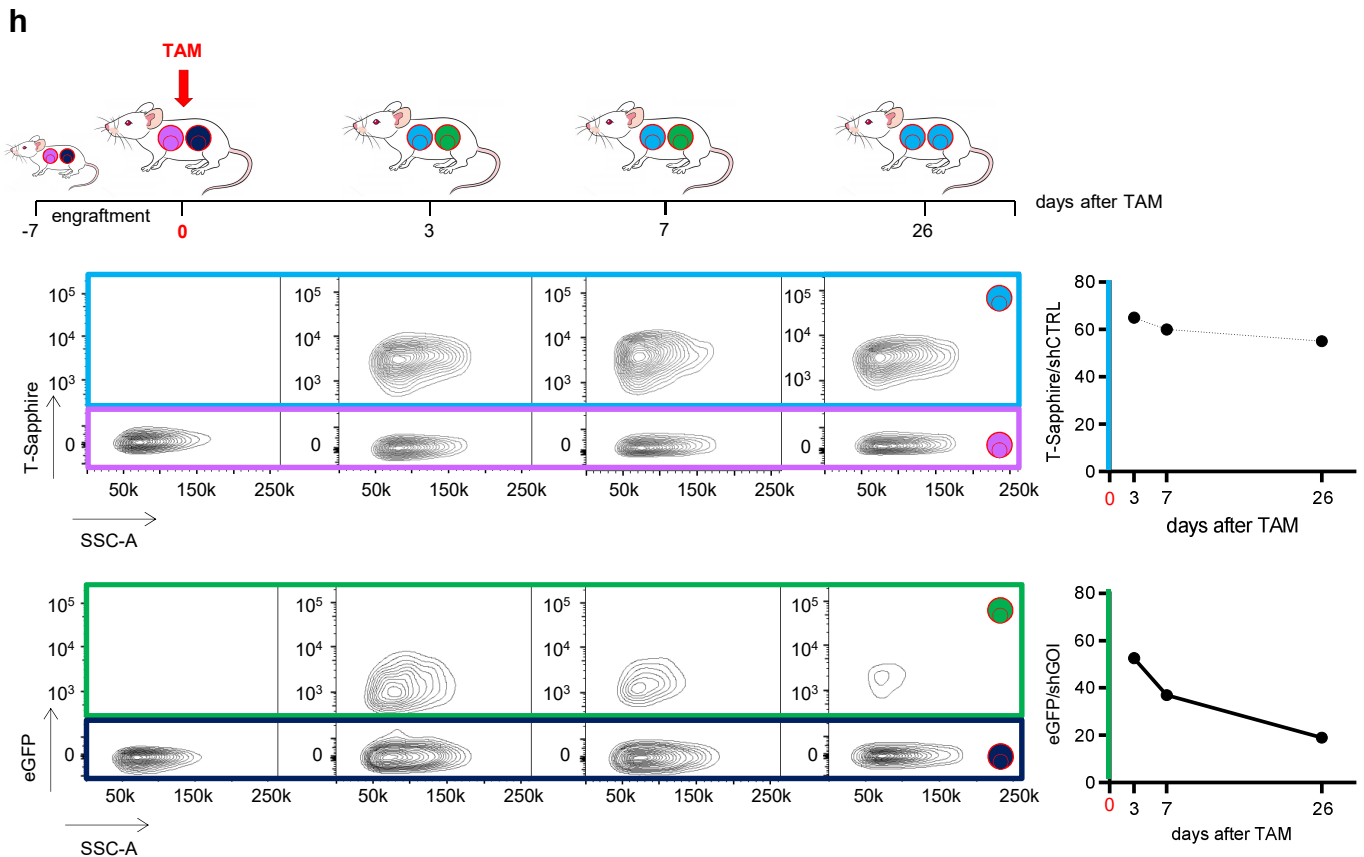
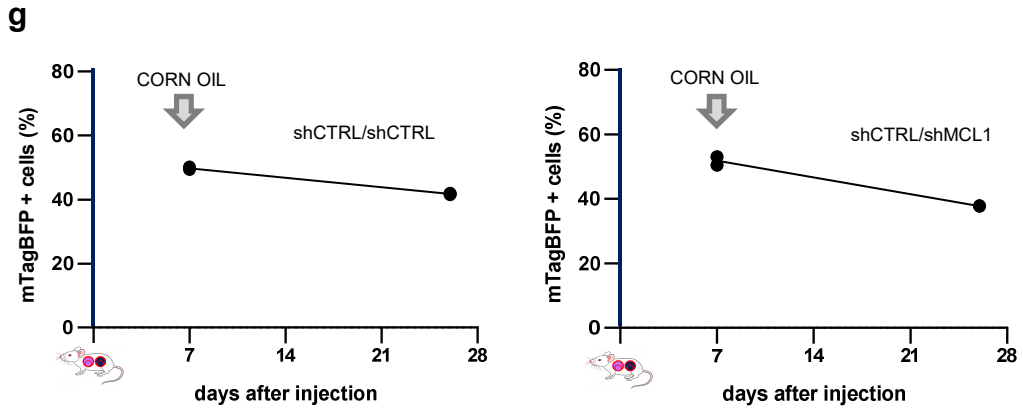
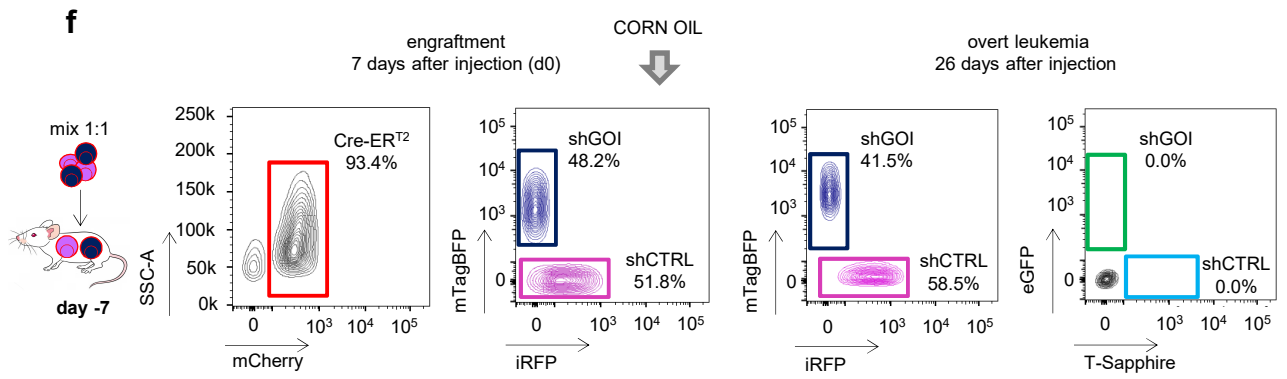
Supplementary Table 4. Primers for qPCR

target	sequence
<i>HPRT1</i>	FW_TGATAGATCCATTCCCTATGACTGTAGA RV_CAAGACATTCTTTCCAGTTAAAGTTG
<i>MLL-AF4</i>	FW_AAGTTCCCAAACCACTCCTAGT RV_GCCATGAATGGGTCATTTCC
<i>MLL</i>	FW_AAGTTCCCAAACCACTCCTAGT RV_GATCCTGTGGACTCCATCTGC
<i>AF4</i>	FW_CTCCCCTCAAAAAGTGTTGC RV_TAGGTCTGCTCAACTGACTGAG
<i>DDIT4L</i>	FW_CCCAGAGAGCCTGCTAAGTG RV_TTGCTTTGATTTGGACAGACA

Supplementary Figures







Supplementary Figure 1: Inducible knockdown system in PDX acute leukemia models in vivo and quality controls

a) Details of the Cre-ER^{T2} expression construct (left). Expression of a Gaussia luciferase (Luc) for in vivo imaging, Cre-ER^{T2} and mCherry are under the control the SFFV promoter and connected via 2A-peptides. Histogram (right) displays expression levels of mCherry in different AML-388 PDX derivatives, co-transduced with different knockdown constructs; similar data were obtained in all 5 PDX models studied.

b) The 2-steps process of Cre-ER^{T2} mediated recombination. The shRNA cassette is flanked by two different pairs of loxP sites; upon treatment of mice with TAM, Cre-ER^{T2} translocates to the nucleus and first induces a reversible inversion between either of the two pairs of loxP sites (one example is shown); this converts the out-of-frame cassette into frame so that both, the inducible fluorochrome (T-Sapphire or eGFP) and the coupled shRNA, get under control of the SFFV promoter. In a second step, Cre-ER^{T2} mediates an irreversible deletion between the second pair of loxP sites, resulting in deletion of the original fluorochrome (iRFP or mTagBFP). As end product, the constitutively expressed fluorochrome is lost, while the inducible fluorochrome is expressed in equimolar amounts together with the shRNA.

c) Gating strategy for the analysis of the competitive in vivo assays. All in vivo experiments have been analyzed following the depicted gating strategy. Debris exclusion, living cells gating (SSC-A/FSC-A), mCherry gating to analyze exclusively PDX cells expressing the CreERT2 enzyme. As last step, cells have been analyzed for the expression of mTagBFP or iRFP in the absence of TAM; or for the expression of eGFP or T-Sapphire after TAM administration.

d) Recombination efficiency is independent from tumor burden. Mice were injected with a mix of shCTRL/shMCL1 cells. Tumor growth was monitored by in vivo imaging; at the indicated time points, TAM was administered at 50 mg/kg per mouse to induce Cre-ER^{T2}-mediated inversion/deletion and consequent shRNA expression. Recombination efficiency was analyzed 48h after TAM by quantifying expression of the inducible fluorochrome markers by flow cytometry. Data from representative mice are displayed; 2 mice per time point were analyzed.

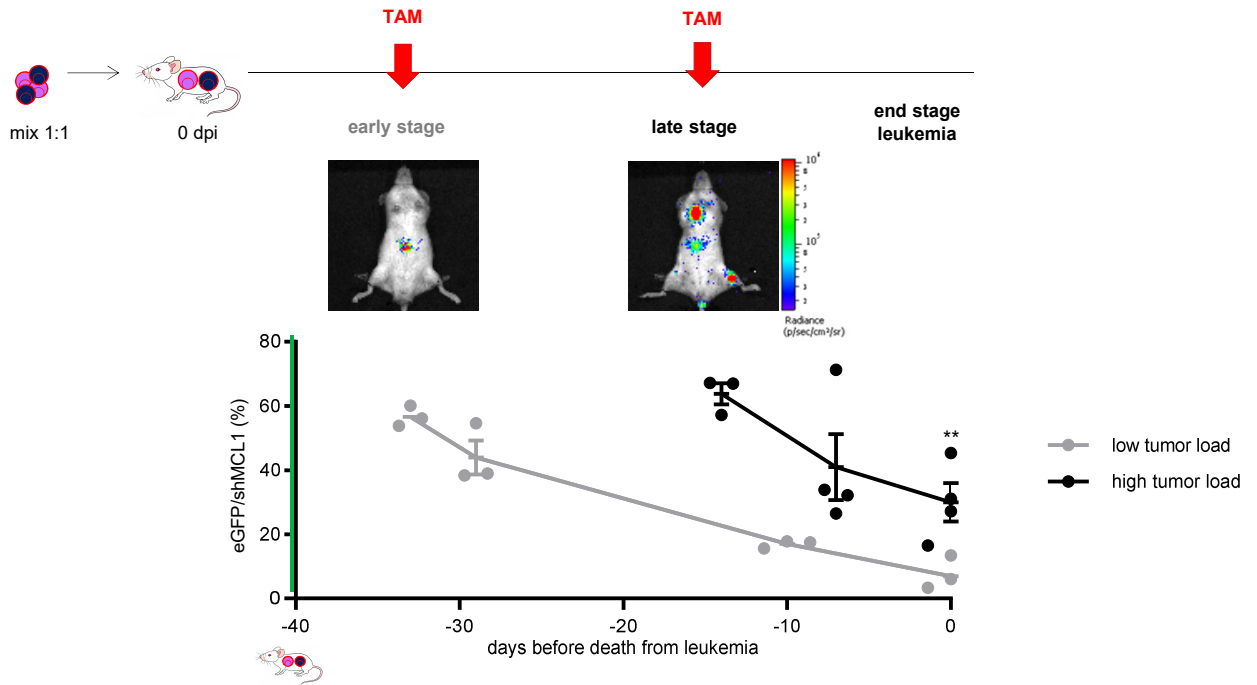
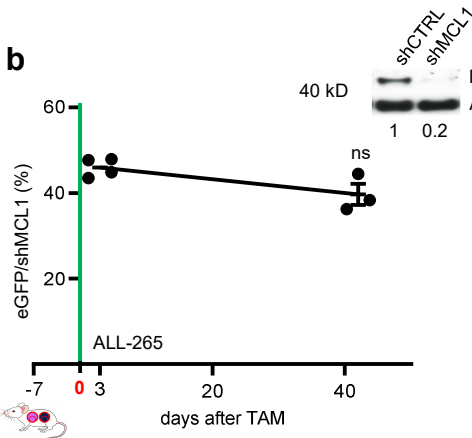
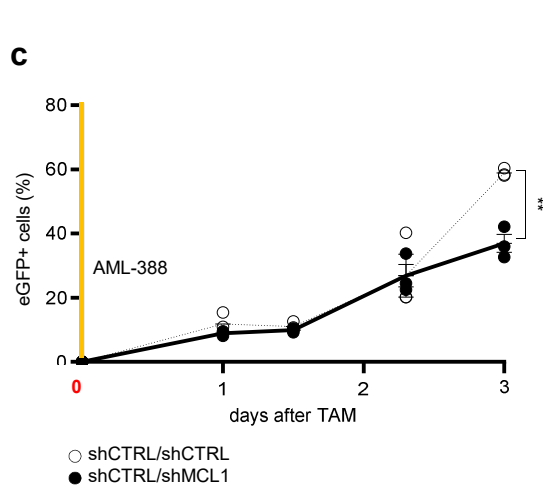
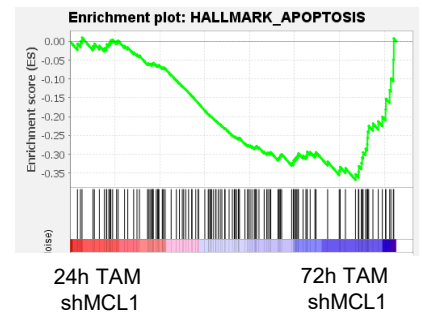
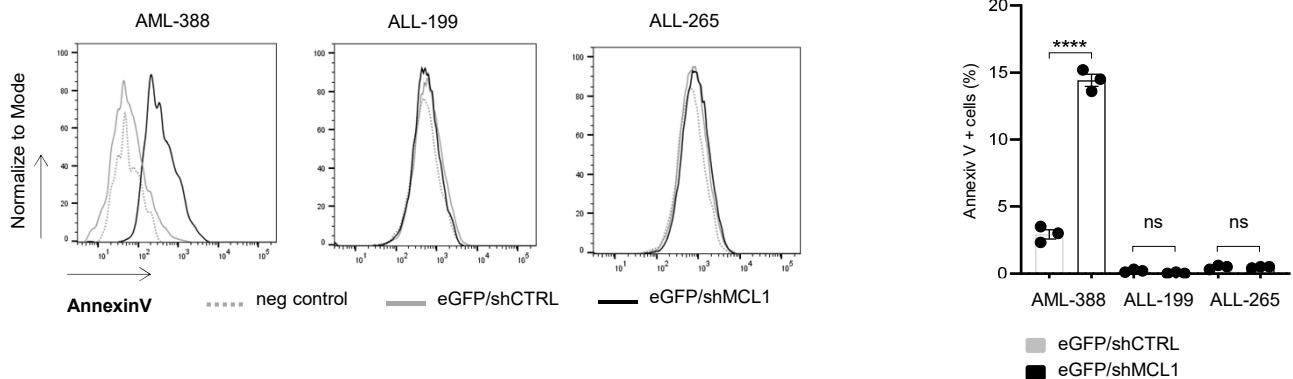
e-g) Quality control experiments:

e) Competitive in vivo experiments were set up as described in Figure 1c. The shCTRL/shCTRL mixture of AML-388 (n=6, 3*10⁵ cells/mouse), ALL-199 (n=6, 3*10⁵ cells/mouse) and ALL-265 (n=6, 3*10⁵ cells/mouse) was injected and eGFP-positive cells among all recombined cells were quantified at the indicated time points. To determine significance of depletion of eGFP-expressing cells, the percentage of eGFP cells at the experimental endpoint is compared to the percentage of eGFP cells at 3d post TAM. Mean ± SEM, * p=0.0185, ns not significant by unpaired t-test.

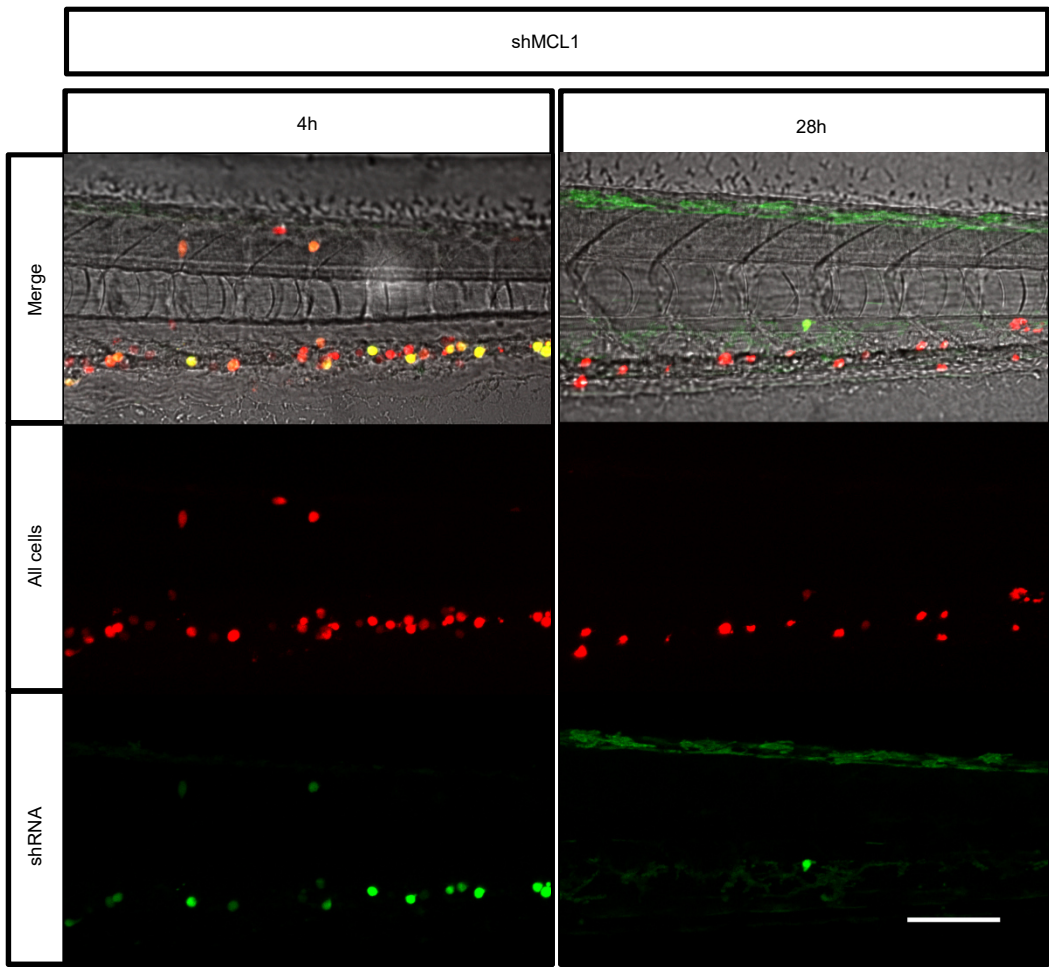
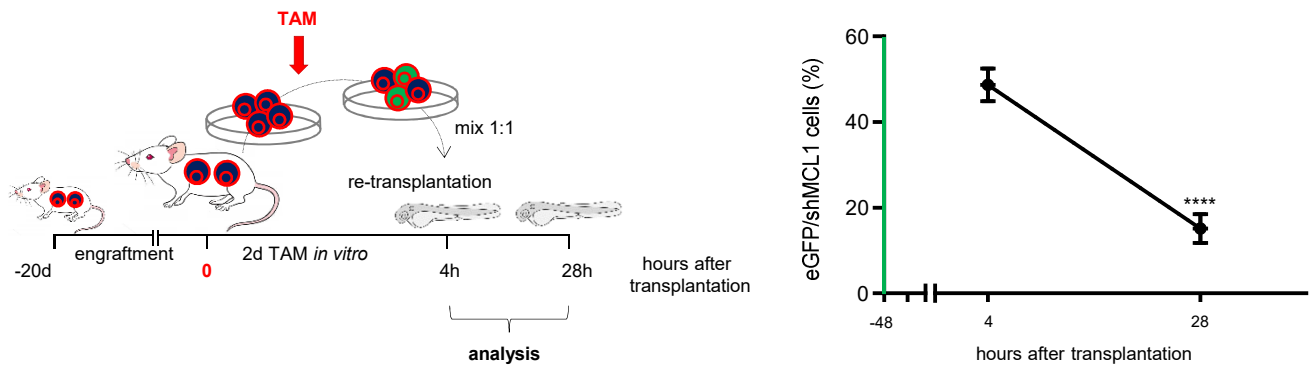
f) Competitive in vivo experiments were set up as described in Figure 1c, except that mice were injected with the solvent corn oil alone without TAM (n=4). One week after injection (day 0) two mice were sacrificed; flow cytometry plots show results from one representative mouse per time point; percentage of iRFP/shCTRL positive versus mTagBFP/shGOI (shMCL1) positive cells was determined from all mCherry-Cre-ER^{T2}-positive cells. Corn oil was administered to the remaining two mice and cells analyzed 26 days after by flow cytometry.

g) Percentage of mTagBFP positive cells was quantified from all isolated cells from the experiment described in Figure S1e, expressing either mTagBFP or iRFP, for the two different mixtures shCTRL/shCTRL or shCTRL/shMCL1.

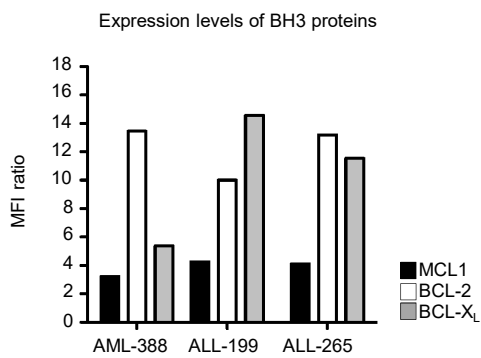
h) Data complementing Figure 1c; from the shCTRL/shMCL1 mixture, shCTRL cells and shMCL1 cells were analyzed separately and not as pairwise competitive analysis as in Figure 1c. Upper row shows cells harboring the iRFP/shCTRL construct without shCTRL expression converting upon TAM treatment into T-Sapphire/shCTRL with shCTRL expression; lower row shows cells harboring the mTagBFP/shMCL1 construct without shMCL1 expression converting into eGFP/shMCL1 with shMCL1 expression. Right panels show quantification as [eGFP/shGOI positive cells divided by (the sum of mTagBFP/shGOI positive plus eGFP/shGOI positive cells)], respectively. The reliability of this type of analysis is restricted to settings with low cell death within the first 3 days.

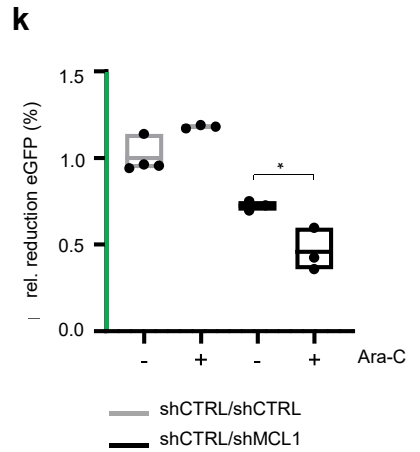
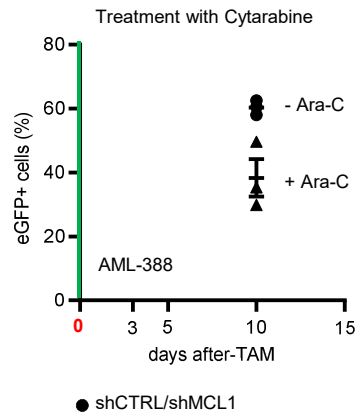
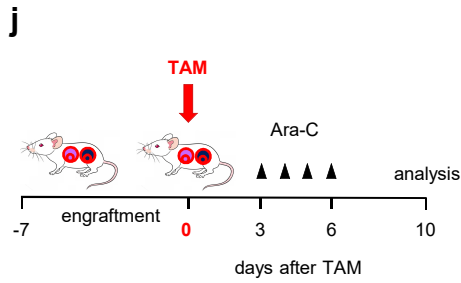
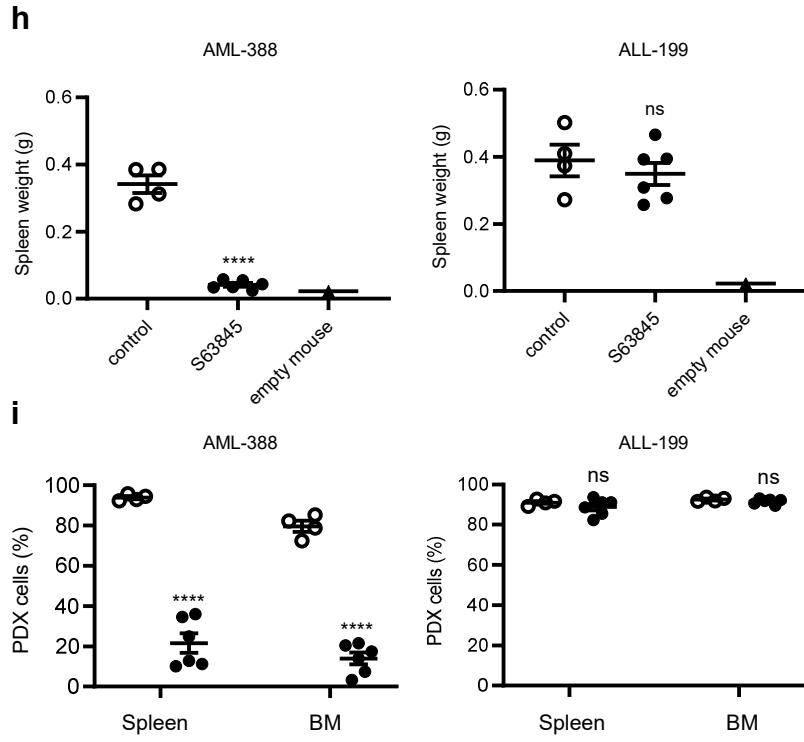
a**b****c****d****e**

f



g





Supplementary Figure 2: *MCL1* is essential in AML-388 but dispensable in two ALL-PDX

a) *MCL1* essentiality is independent from tumor burden. Experiments were set up as described in Figure 2b, except that 2×10^6 cells of the AML-388 shCTRL/sh*MCL1* mixture were injected and TAM was administered at a higher tumor burden. Mice were sacrificed 3 (n=3) and 10 (n=4) days after TAM and at end stage leukemia (n=4). Representative bioluminescence imaging pictures at the day of TAM administrations following injection of 3×10^5 (early stage; Figure 2b) and 2×10^6 (late stage) cells are shown. Graph displays mean \pm SEM of the proportion of eGFP-positive cells isolated out of all recombined cells; grey line indicates results displayed in Figure 2b for comparison. Each dot represents one mouse. ** p=0.0067 by unpaired t-test.

b) Experiment described in Figure 2b was identically performed and depicted in ALL-265 (injection of 3×10^5 cells/mouse, n=7. Mean \pm SEM of results is shown. At the end of the experiment, *MCL1* protein expression was analyzed in sorted shCTRL and sh*MCL1* populations by Western blot (ALL-256). ns not significant by unpaired t-test.

c) *MCL1* knockdown cells are depleted early after TAM induction. For a kinetic of eGFP-expression at early time points after TAM, competitive experiments were performed and each subpopulation analyzed separately as described in Figure S1g; mice were analyzed at 24, 36, 52 and 72 hours after TAM administration (n=3 each). The analysis shows quantification as [eGFP/sh*MCL1* positive cells divided by (the sum of mTagBFP/sh*MCL1*-positive plus eGFP/sh*MCL1*-positive cells)]. The same analysis was performed for the shCTRL/shCTRL mixture. Mean \pm SEM per group per time point is displayed. ** p=0.0016 by unpaired t-test.

d) Gene set enrichment analysis (GSEA) of transcriptome data from cells of experiment in Figure S2e, isolated 24 and 72 hours after TAM and sorted for eGFP/sh*MCL1* (n=3 per time point). NES= -1.52, P=0.0.

e) Knockdown of *MCL1* induces apoptosis; Annexin V staining in PDX AML-388, ALL-199 and ALL-265 3d after TAM. Representative histograms of 3 experiments are shown. Quantification of Annexin V positive eGFP/shCTRL or eGFP/sh*MCL1* cells (%) in PDX samples. Mean \pm SEM of 3 independent experiments, **** p \leq 0.0001 by unpaired t-test.

f) Zebrafish experiment. Experimental layout: mCherry-Cre-ERT2 positive PDX cells from donor mice injected with AML-388 mTagBFP/sh*MCL1* cells were isolated from the BM of mice 20 days after injection. Cells were treated *ex vivo* with 50 nM TAM to induce eGFP/shRNA expression. After 48 hours, PDX cells were sorted to adjust cells with (eGFP positive) and without recombination (mTagBFP positive) to a 1:1 ratio. Cells were re-transplanted into groups of zebrafish embryos at 48 hours after fertilization (200 to 500 PDX cells per embryo). 4 (n=19) and 28 (n=18) hours after transplantation (hpt) (52 h and 76 h after TAM, respectively), larvae were anesthetized, and a field of view of the caudal hematopoietic tissue of each larvae was imaged to quantify mCherry and eGFP-positive cells. Graph displays mean \pm SEM of the percentage of eGFP/sh*MCL1* positive cells among all transplanted, mCherry positive cells. **** p \leq 0.0001 by unpaired t-test with Welch's correction. Representative images of injected larvae with eGFP/sh*MCL1* expressing cells are displayed. Upper panel depicts merged images of the brightfield shot for anatomic orientation; mCherry positive cells are shown in red in the middle panel and eGFP/shRNA positive cells are shown in green in lower panel. Scale bar 100 μ m.

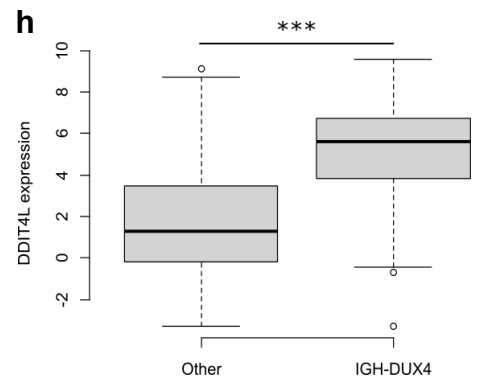
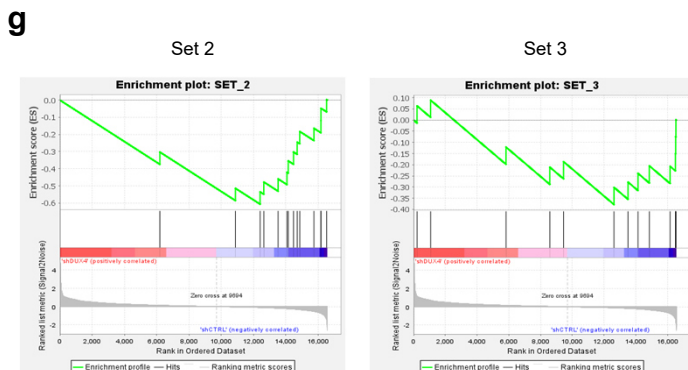
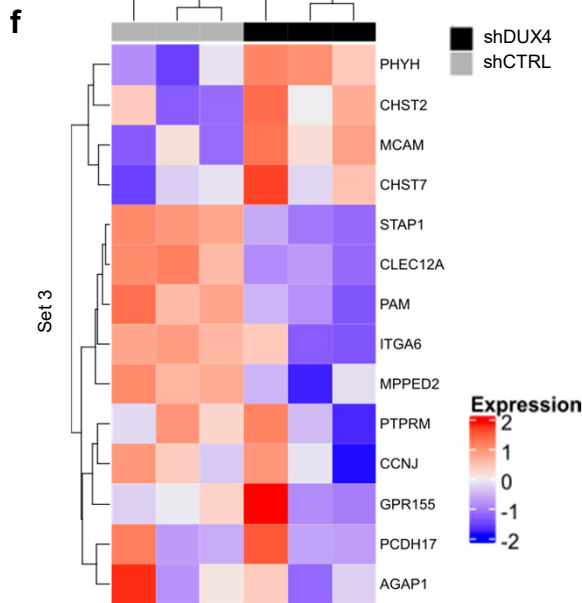
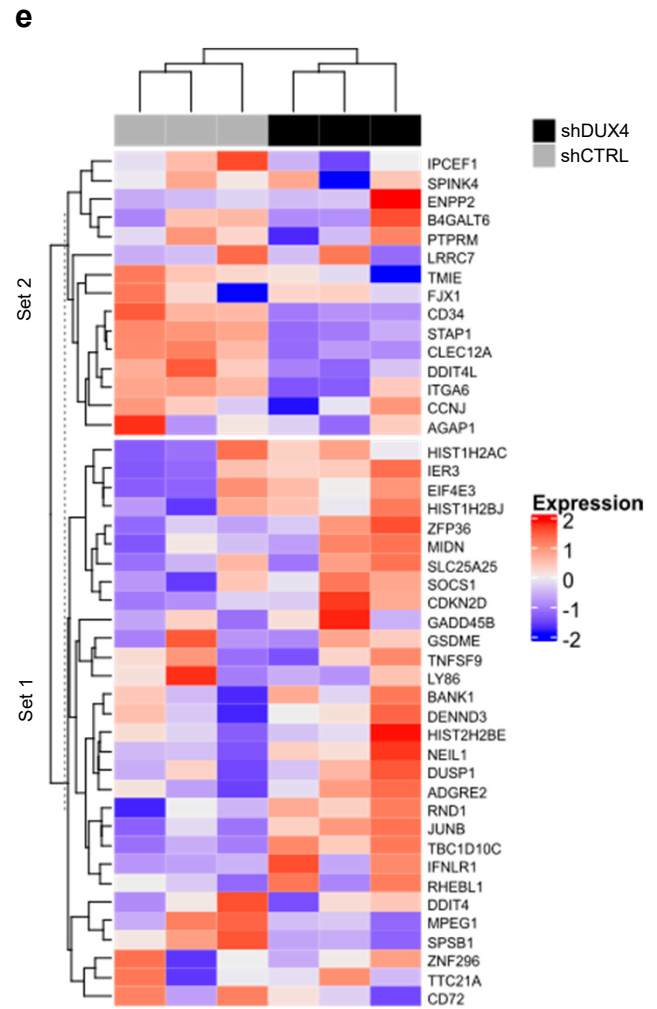
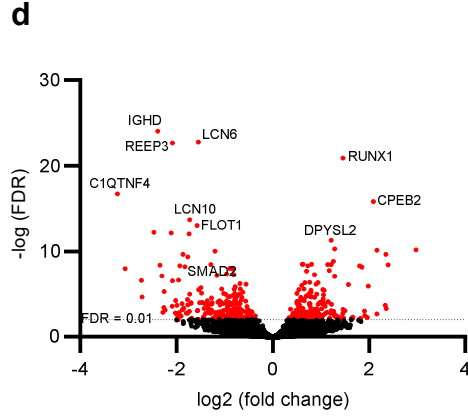
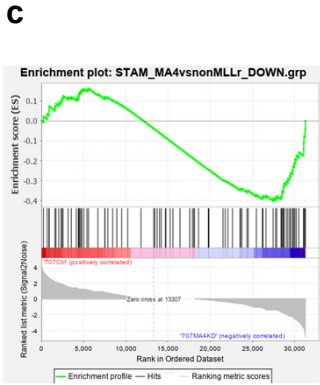
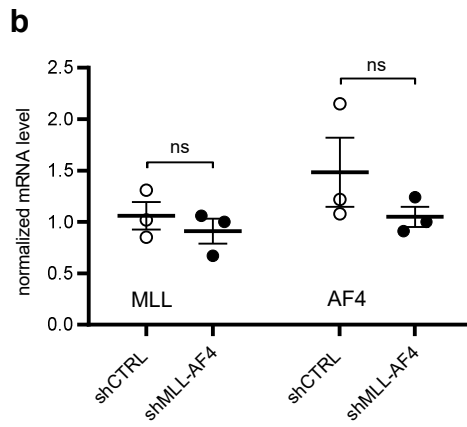
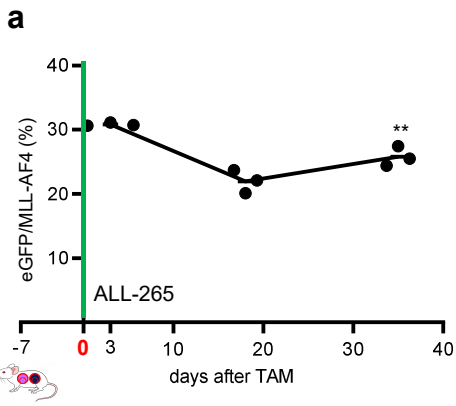
g) Intracellular expression levels of *MCL1*, BCL-2 and BCL-X_L, as measured by flow cytometry in the indicated PDX samples. Protein expression was calculated as the ratio of stained antibody mean fluorescent intensity (MFI) divided by isotype control MFI.

h-i) Pharmacological inhibition of *MCL1*. Mice from experiments in Figure 2d-f (n=4 for CTRL and n=6 for *MCL1* inhibitor) were analyzed for **(h)** spleen weight and **(i)** the percentage of PDX cells among all cells isolated from spleen and bone marrow. Mean \pm SEM, **** p \leq 0.0001, ns not significant by unpaired t-test.

j-k) Combination treatment. Experiments were set up and analyzed as described in Figure 2g except that Cytarabine (Ara-C, 100 mg/kg/per day i.p. for 4 consecutive days, n=3) or solvent (n=3) was used. At the end of the experiment (10 days after TAM), mice were analyzed as in Figure 1c.

j) Mean \pm SEM of 3 replicates per group and condition are shown. *p \leq 0.0221 by unpaired t-test.

k) Reduction of eGFP-positive cells in the shCTRL/sh*MCL1* mix relative to shCTRL/shCTRL (+/- Ara-C) is displayed. Each dot represents one mouse. Mean \pm SEM, *p \leq 0.0221 by unpaired t-test.



Supplementary Figure 3: In vivo functional validation of essential fusion genes

a-d) Selective effects of sh*MLL-AF4*.

a) Experiments described in Figures 3a-b were performed using the non *MLL-AF4* rearranged ALL-265 PDX as control; TAM was applied once (50 mg/kg) 7 days post injections (day 0). Mice were sacrificed 3, 19 and 35 days after TAM (n=3 each). Percentage of eGFP-positive cells among all recombined cells was analyzed. Each dot represents one mouse. Mean \pm SEM, ** p=0.0048 unpaired t-test.

b) mRNA expression of *MLL* and *AF4* was analyzed by qPCR in ALL-265 cells expressing shCTRL or sh*MLL-AF4*. Mean \pm SEM of cells isolated from n=3 mice, 35 days after TAM are shown. ns not significant by Welch's t-test.

c) Gene set enrichment analysis (GSEA) comparing an established *MLL-AF4* signature¹ with transcriptome data from cells of experiment in Figure 3b, isolated 28 days after TAM and sorted for eGFP/sh*MLL-AF4* and eGFP/shCTRL (n=3 per time point). NES= -1,37, P =0,031.

d) Differential expressed genes obtained from transcriptome data from experiment in Figure 3b are depicted as volcano blot (n=3). Genes with a high fold change are highly expressed shCTRL cells and low expressed in sh*MLL-AF4* cells.

e-h) Identification of therapeutic targets in *DUX4*-rearranged ALL. GSEA with two published datasets, Tanaka et al. 2018² and Harvey et al 2010³. Of 65 significant targets with a fold change of 2 in the Tanaka et al. dataset, 45 were present in our transcriptome dataset. To apply GSEA, targets were divided into upregulated (set 1) and downregulated (set 2) gene sets in *DUX4* knockdown cells. Of the Harvey et al dataset, which identified a transcriptome signature of pediatric B-precursor ALL patient samples with intragenic *ERG* deletions, 14 genes were present in our dataset (set 3).

e) Heatmap displaying expression of set 1 and set 2 between shCTRL and sh*DUX4*. All genes have been scaled to have the mean value of 0 and variance of 1.

f) Heatmap displaying expression of set 3 between shCTRL and sh*DUX4*. All genes have been scaled as described in Supplementary Figure 2e.

g) Enrichment plots for set 2 and 3. NES = -2.72 and -1.65, FDR q-value < 0.001 and q = 0.030, respectively.

h) *DDIT4L* expression values of 86 patients with an *IGH-DUX4* fusion were compared to patients without the fusion. *** p < 0.001 two-sided t-test.

Supplementary References

1. Stam, R.W. et al. Gene expression profiling-based dissection of MLL translocated and MLL germline acute lymphoblastic leukemia in infants. *Blood* **115**, 2835-2844 (2010).
2. Tanaka, Y. et al. Transcriptional activities of DUX4 fusions in B-cell acute lymphoblastic leukemia. *Haematologica* **103**, e522-e526 (2018).
3. Harvey, R.C. et al. Identification of novel cluster groups in pediatric high-risk B-precursor acute lymphoblastic leukemia with gene expression profiling: correlation with genome-wide DNA copy number alterations, clinical characteristics, and outcome. *Blood* **116**, 4874-4884 (2010).

References

1. Piller G. Leukaemia - a brief historical review from ancient times to 1950. *Br J Haematol* 2001; **112**(2): 282-92.
2. Chennamadhavuni A LV, Mukkamalla SKR, et al. Leukemia. 2023. <https://www.ncbi.nlm.nih.gov/books/NBK560490/>.
3. Whiteley AE, Price TT, Cantelli G, Sipkins DA. Leukaemia: a model metastatic disease. *Nat Rev Cancer* 2021; **21**(7): 461-75.
4. Weinberg OK, Arber DA. How I Diagnose Acute Leukemia of Ambiguous Lineage. *Am J Clin Pathol* 2022; **158**(1): 27-34.
5. Newell LF, Cook RJ. Advances in acute myeloid leukemia. *BMJ* 2021; **375**: n2026.
6. De Kouchkovsky I, Abdul-Hay M. 'Acute myeloid leukemia: a comprehensive review and 2016 update'. *Blood Cancer J* 2016; **6**(7): e441.
7. DiNardo CD, Erba HP, Freeman SD, Wei AH. Acute myeloid leukaemia. *Lancet* 2023; **401**(10393): 2073-86.
8. Pollyea DA, Bixby D, Perl A, et al. NCCN Guidelines Insights: Acute Myeloid Leukemia, Version 2.2021. *J Natl Compr Canc Netw* 2021; **19**(1): 16-27.
9. Hunger SP, Mullighan CG. Acute Lymphoblastic Leukemia in Children. *N Engl J Med* 2015; **373**(16): 1541-52.
10. Malard F, Mohty M. Acute lymphoblastic leukaemia. *Lancet* 2020; **395**(10230): 1146-62.
11. Terwilliger T, Abdul-Hay M. Acute lymphoblastic leukemia: a comprehensive review and 2017 update. *Blood Cancer J* 2017; **7**(6): e577.
12. Khoury JD, Solary E, Abla O, et al. The 5th edition of the World Health Organization Classification of Haematolymphoid Tumours: Myeloid and Histiocytic/Dendritic Neoplasms. *Leukemia* 2022; **36**(7): 1703-19.
13. Dohner H, Estey E, Grimwade D, et al. Diagnosis and management of AML in adults: 2017 ELN recommendations from an international expert panel. *Blood* 2017; **129**(4): 424-47.
14. Shimony S, Stahl M, Stone RM. Acute myeloid leukemia: 2023 update on diagnosis, risk-stratification, and management. *Am J Hematol* 2023; **98**(3): 502-26.
15. Rai KR, Holland JF, Glidewell OJ, et al. Treatment of acute myelocytic leukemia: a study by cancer and leukemia group B. *Blood* 1981; **58**(6): 1203-12.
16. Lusk MR, Lee JW, Fernandez HF, et al. Benefit of high-dose daunorubicin in AML induction extends across cytogenetic and molecular groups. *Blood* 2016; **127**(12): 1551-8.
17. Alfayez M, Kantarjian H, Kadia T, Ravandi-Kashani F, Daver N. CPX-351 (vyxeos) in AML. *Leuk Lymphoma* 2020; **61**(2): 288-97.
18. Lancet JE, Uy GL, Cortes JE, et al. CPX-351 (cytarabine and daunorubicin) Liposome for Injection Versus Conventional Cytarabine Plus Daunorubicin in Older Patients With Newly Diagnosed Secondary Acute Myeloid Leukemia. *J Clin Oncol* 2018; **36**(26): 2684-92.
19. Swaminathan M, Cortes JE. Update on the role of gemtuzumab-ozogamicin in the treatment of acute myeloid leukemia. *Ther Adv Hematol* 2023; **14**: 20406207231154708.
20. Hills RK, Castaigne S, Appelbaum FR, et al. Addition of gemtuzumab ozogamicin to induction chemotherapy in adult patients with acute myeloid leukaemia: a meta-analysis of individual patient data from randomised controlled trials. *Lancet Oncol* 2014; **15**(9): 986-96.

References

21. Heuser M, Freeman SD, Ossenkoppele GJ, et al. 2021 Update on MRD in acute myeloid leukemia: a consensus document from the European LeukemiaNet MRD Working Party. *Blood* 2021; **138**(26): 2753-67.
22. Cornelissen JJ, Blaise D. Hematopoietic stem cell transplantation for patients with AML in first complete remission. *Blood* 2016; **127**(1): 62-70.
23. Jimenez-Chillon C, Dillon R, Russell N. Optimal post-remission consolidation therapy in patients with AML. *Acta Haematol* 2023.
24. Bhansali RS, Pratz KW, Lai C. Recent advances in targeted therapies in acute myeloid leukemia. *J Hematol Oncol* 2023; **16**(1): 29.
25. Derissen EJ, Beijnen JH, Schellens JH. Concise drug review: azacitidine and decitabine. *Oncologist* 2013; **18**(5): 619-24.
26. Cang S, Iragavarapu C, Savooji J, Song Y, Liu D. ABT-199 (venetoclax) and BCL-2 inhibitors in clinical development. *J Hematol Oncol* 2015; **8**: 129.
27. Lachowiec CA, Atluri H, DiNardo CD. Advancing the standard: venetoclax combined with intensive induction and consolidation therapy for acute myeloid leukemia. *Ther Adv Hematol* 2022; **13**: 20406207221093964.
28. Garciaz S, Saillard C, Hicheri Y, Hospital MA, Vey N. Venetoclax in Acute Myeloid Leukemia: Molecular Basis, Evidences for Preclinical and Clinical Efficacy and Strategies to Target Resistance. *Cancers (Basel)* 2021; **13**(22).
29. Stone RM, Mandrekar SJ, Sanford BL, et al. Midostaurin plus Chemotherapy for Acute Myeloid Leukemia with a FLT3 Mutation. *N Engl J Med* 2017; **377**(5): 454-64.
30. Dohner K, Thiede C, Jahn N, et al. Impact of NPM1/FLT3-ITD genotypes defined by the 2017 European LeukemiaNet in patients with acute myeloid leukemia. *Blood* 2020; **135**(5): 371-80.
31. Perl AE, Larson RA, Podoltsev NA, et al. Outcomes in Patients with FLT3-Mutated Relapsed/Refractory Acute Myelogenous Leukemia Who Underwent Transplantation in the Phase 3 ADMIRAL Trial of Gilteritinib versus Salvage Chemotherapy. *Transplant Cell Ther* 2023; **29**(4): 265 e1- e10.
32. Thol F, Ganser A. Treatment of Relapsed Acute Myeloid Leukemia. *Curr Treat Options Oncol* 2020; **21**(8): 66.
33. Thol F, Heuser M. Treatment for Relapsed/Refractory Acute Myeloid Leukemia. *Hemasphere* 2021; **5**(6): e572.
34. Guy DG, Uy GL. Bispecific Antibodies for the Treatment of Acute Myeloid Leukemia. *Curr Hematol Malig Rep* 2018; **13**(6): 417-25.
35. Mardiana S, Gill S. CAR T Cells for Acute Myeloid Leukemia: State of the Art and Future Directions. *Front Oncol* 2020; **10**: 697.
36. Kim MY, Yu KR, Kenderian SS, et al. Genetic Inactivation of CD33 in Hematopoietic Stem Cells to Enable CAR T Cell Immunotherapy for Acute Myeloid Leukemia. *Cell* 2018; **173**(6): 1439-53 e19.
37. Kulkarni U, Arunachalam AK, Palani HK, et al. Haploidentical Natural Killer Cell Therapy as an Adjunct to Stem Cell Transplantation for Treatment of Refractory Acute Myeloid Leukemia. *Cell Transplant* 2023; **32**: 9636897231198178.
38. Silva RAM, de Mendonca RMH, Dos Santos Aguiar S, et al. Induction therapy for acute lymphoblastic leukemia: incidence and risk factors for bloodstream infections. *Support Care Cancer* 2022; **30**(1): 695-702.
39. Pui CH, Mullighan CG, Evans WE, Relling MV. Pediatric acute lymphoblastic leukemia: where are we going and how do we get there? *Blood* 2012; **120**(6): 1165-74.
40. Blade J, Rosinol L, Sureda A, et al. High-dose therapy intensification compared with continued standard chemotherapy in multiple myeloma patients responding to the initial chemotherapy: long-term results from a prospective randomized trial from the Spanish cooperative group PETHEMA. *Blood* 2005; **106**(12): 3755-9.

References

41. Kato M, Manabe A. Treatment and biology of pediatric acute lymphoblastic leukemia. *Pediatr Int* 2018; **60**(1): 4-12.
42. Kato M, Ishimaru S, Seki M, et al. Long-term outcome of 6-month maintenance chemotherapy for acute lymphoblastic leukemia in children. *Leukemia* 2017; **31**(3): 580-4.
43. Giebel S, Krawczyk-Kulis M, Adamczyk-Cioch M, et al. Prophylaxis and therapy of central nervous system involvement in adult acute lymphoblastic leukemia: recommendations of the Polish Adult Leukemia Group. *Pol Arch Med Wewn* 2008; **118**(6): 356-61.
44. Wu SY, Short NJ, Nasr L, Dabaja BS, Fang PQ. Central Nervous System Prophylaxis and Treatment in Acute Leukemias. *Curr Treat Options Oncol* 2022; **23**(12): 1829-44.
45. Pui CH. Central nervous system disease in acute lymphoblastic leukemia: prophylaxis and treatment. *Hematology Am Soc Hematol Educ Program* 2006: 142-6.
46. Giralt S, Bishop MR. Principles and overview of allogeneic hematopoietic stem cell transplantation. *Cancer Treat Res* 2009; **144**: 1-21.
47. Leung W, Pui CH, Coustan-Smith E, et al. Detectable minimal residual disease before hematopoietic cell transplantation is prognostic but does not preclude cure for children with very-high-risk leukemia. *Blood* 2012; **120**(2): 468-72.
48. Giebel S, Marks DI, Boissel N, et al. Hematopoietic stem cell transplantation for adults with Philadelphia chromosome-negative acute lymphoblastic leukemia in first remission: a position statement of the European Working Group for Adult Acute Lymphoblastic Leukemia (EWALL) and the Acute Leukemia Working Party of the European Society for Blood and Marrow Transplantation (EBMT). *Bone Marrow Transplant* 2019; **54**(6): 798-809.
49. Brivio E, Baruchel A, Beishuizen A, et al. Targeted inhibitors and antibody immunotherapies: Novel therapies for paediatric leukaemia and lymphoma. *Eur J Cancer* 2022; **164**: 1-17.
50. Huang YH, Wan CL, Dai HP, Xue SL. Targeted therapy and immunotherapy for T cell acute lymphoblastic leukemia/lymphoma. *Ann Hematol* 2023; **102**(8): 2001-13.
51. Ottmann OG, Wassmann B, Pfeifer H, et al. Imatinib compared with chemotherapy as front-line treatment of elderly patients with Philadelphia chromosome-positive acute lymphoblastic leukemia (Ph+ALL). *Cancer* 2007; **109**(10): 2068-76.
52. Ohno R, Japan Adult Leukemia Study G. Treatment of Philadelphia-chromosome-positive acute lymphoblastic leukemia with imatinib in combination with chemotherapy. *Curr Hematol Malig Rep* 2006; **1**(3): 180-7.
53. Lim SN, Joo YD, Lee KH, et al. Long-term follow-up of imatinib plus combination chemotherapy in patients with newly diagnosed Philadelphia chromosome-positive acute lymphoblastic leukemia. *Am J Hematol* 2015; **90**(11): 1013-20.
54. Mathisen MS, O'Brien S, Thomas D, Cortes J, Kantarjian H, Ravandi F. Role of tyrosine kinase inhibitors in the management of Philadelphia chromosome-positive acute lymphoblastic leukemia. *Curr Hematol Malig Rep* 2011; **6**(3): 187-94.
55. Aumann S, Shaulov A, Haran A, Gross Even-Zohar N, Vainstein V, Nachmias B. The Emerging Role of Venetoclax-Based Treatments in Acute Lymphoblastic Leukemia. *Int J Mol Sci* 2022; **23**(18).
56. Jain N, Stevenson KE, Winer ES, et al. A Multicenter Phase I Study Combining Venetoclax with Mini-Hyper-CVD in Older Adults with Untreated and Relapsed/Refractory Acute Lymphoblastic Leukemia. *Blood* 2019; **134**(Supplement_1): 3867-.
57. Suzuki S, Hourai S, Uozumi K, et al. Gamma-secretase inhibitor does not induce cytotoxicity in adult T-cell leukemia cell lines despite NOTCH1 expression. *BMC Cancer* 2022; **22**(1): 1065.
58. Menne T, Slade D, Savage J, et al. Selumetinib in combination with dexamethasone for the treatment of relapsed/refractory RAS-pathway mutated paediatric and adult acute lymphoblastic leukaemia (SeluDex): study protocol for an international, parallel-group, dose-finding with expansion phase I/II trial. *BMJ Open* 2022; **12**(3): e059872.
59. Thomas DA, O'Brien S, Jorgensen JL, et al. Prognostic significance of CD20 expression in adults with de novo precursor B-lineage acute lymphoblastic leukemia. *Blood* 2009; **113**(25): 6330-7.

References

60. Thomas DA, O'Brien S, Faderl S, et al. Chemoimmunotherapy with a modified hyper-CVAD and rituximab regimen improves outcome in de novo Philadelphia chromosome-negative precursor B-lineage acute lymphoblastic leukemia. *J Clin Oncol* 2010; **28**(24): 3880-9.
61. Maury S, Chevret S, Thomas X, et al. Rituximab in B-Lineage Adult Acute Lymphoblastic Leukemia. *N Engl J Med* 2016; **375**(11): 1044-53.
62. Topp MS, Gokbuget N, Stein AS, et al. Safety and activity of blinatumomab for adult patients with relapsed or refractory B-precursor acute lymphoblastic leukaemia: a multicentre, single-arm, phase 2 study. *Lancet Oncol* 2015; **16**(1): 57-66.
63. Topp MS, Gokbuget N, Zugmaier G, et al. Long-term follow-up of hematologic relapse-free survival in a phase 2 study of blinatumomab in patients with MRD in B-lineage ALL. *Blood* 2012; **120**(26): 5185-7.
64. Kantarjian H, Thomas D, Jorgensen J, et al. Results of inotuzumab ozogamicin, a CD22 monoclonal antibody, in refractory and relapsed acute lymphocytic leukemia. *Cancer* 2013; **119**(15): 2728-36.
65. Kantarjian HM, DeAngelo DJ, Stelljes M, et al. Inotuzumab Ozogamicin versus Standard Therapy for Acute Lymphoblastic Leukemia. *N Engl J Med* 2016; **375**(8): 740-53.
66. Maude SL, Frey N, Shaw PA, et al. Chimeric antigen receptor T cells for sustained remissions in leukemia. *N Engl J Med* 2014; **371**(16): 1507-17.
67. Spiegel JY, Patel S, Muffly L, et al. CAR T cells with dual targeting of CD19 and CD22 in adult patients with recurrent or refractory B cell malignancies: a phase 1 trial. *Nat Med* 2021; **27**(8): 1419-31.
68. Hu Y, Zhou Y, Zhang M, et al. Genetically modified CD7-targeting allogeneic CAR-T cell therapy with enhanced efficacy for relapsed/refractory CD7-positive hematological malignancies: a phase I clinical study. *Cell Res* 2022; **32**(11): 995-1007.
69. Xie L, Gu R, Yang X, et al. Universal Anti-CD7 CAR-T Cells Targeting T-ALL and Functional Analysis of CD7 Antigen on T/CAR-T Cells. *Hum Gene Ther* 2023; **34**(23-24): 1257-72.
70. Mamonkin M, Rouce RH, Tashiro H, Brenner MK. A T-cell-directed chimeric antigen receptor for the selective treatment of T-cell malignancies. *Blood* 2015; **126**(8): 983-92.
71. Tyner JW, Tognon CE, Bottomly D, et al. Functional genomic landscape of acute myeloid leukaemia. *Nature* 2018; **562**(7728): 526-31.
72. Conneely SE, Rau RE. The genomics of acute myeloid leukemia in children. *Cancer Metastasis Rev* 2020; **39**(1): 189-209.
73. Kumar CC. Genetic abnormalities and challenges in the treatment of acute myeloid leukemia. *Genes Cancer* 2011; **2**(2): 95-107.
74. Funk L, Su KC, Ly J, et al. The phenotypic landscape of essential human genes. *Cell* 2022; **185**(24): 4634-53 e22.
75. Chang L, Ruiz P, Ito T, Sellers WR. Targeting pan-essential genes in cancer: Challenges and opportunities. *Cancer Cell* 2021; **39**(4): 466-79.
76. Lin A, Sheltzer JM. Discovering and validating cancer genetic dependencies: approaches and pitfalls. *Nat Rev Genet* 2020; **21**(11): 671-82.
77. Valent P, Orfao A, Kubicek S, et al. Precision Medicine in Hematology 2021: Definitions, Tools, Perspectives, and Open Questions. *Hemasphere* 2021; **5**(3): e536.
78. Tsherniak A, Vazquez F, Montgomery PG, et al. Defining a Cancer Dependency Map. *Cell* 2017; **170**(3): 564-76 e16.
79. Wang T, Yu H, Hughes NW, et al. Gene Essentiality Profiling Reveals Gene Networks and Synthetic Lethal Interactions with Oncogenic Ras. *Cell* 2017; **168**(5): 890-903 e15.
80. Verma D, Kantarjian HM, Jones D, et al. Chronic myeloid leukemia (CML) with P190 BCR-ABL: analysis of characteristics, outcomes, and prognostic significance. *Blood* 2009; **114**(11): 2232-5.
81. Ben-Neriah Y, Daley GQ, Mes-Masson AM, Witte ON, Baltimore D. The chronic myelogenous leukemia-specific P210 protein is the product of the bcr/abl hybrid gene. *Science* 1986; **233**(4760): 212-4.

References

82. Huang X, Cortes J, Kantarjian H. Estimations of the increasing prevalence and plateau prevalence of chronic myeloid leukemia in the era of tyrosine kinase inhibitor therapy. *Cancer* 2012; **118**(12): 3123-7.
83. Hochhaus A, Larson RA, Guilhot F, et al. Long-Term Outcomes of Imatinib Treatment for Chronic Myeloid Leukemia. *N Engl J Med* 2017; **376**(10): 917-27.
84. Warren CFA, Wong-Brown MW, Bowden NA. BCL-2 family isoforms in apoptosis and cancer. *Cell Death Dis* 2019; **10**(3): 177.
85. Mato AR, Roeker LE, Eyre TA, et al. A retrospective comparison of venetoclax alone or in combination with an anti-CD20 monoclonal antibody in R/R CLL. *Blood Adv* 2019; **3**(10): 1568-73.
86. Gaj T, Sirk SJ, Shui SL, Liu J. Genome-Editing Technologies: Principles and Applications. *Cold Spring Harb Perspect Biol* 2016; **8**(12).
87. Ferreira P, Choupina AB. CRISPR/Cas9 a simple, inexpensive and effective technique for gene editing. *Mol Biol Rep* 2022; **49**(7): 7079-86.
88. Agrawal N, Dasaradhi PV, Mohmmmed A, Malhotra P, Bhatnagar RK, Mukherjee SK. RNA interference: biology, mechanism, and applications. *Microbiol Mol Biol Rev* 2003; **67**(4): 657-85.
89. Krill-Burger JM, Dempster JM, Borah AA, et al. Partial gene suppression improves identification of cancer vulnerabilities when CRISPR-Cas9 knockout is pan-lethal. *Genome Biol* 2023; **24**(1): 192.
90. Ishino Y, Shinagawa H, Makino K, Amemura M, Nakata A. Nucleotide sequence of the iap gene, responsible for alkaline phosphatase isozyme conversion in Escherichia coli, and identification of the gene product. *J Bacteriol* 1987; **169**(12): 5429-33.
91. Jansen R, Embden JD, Gaastra W, Schouls LM. Identification of genes that are associated with DNA repeats in prokaryotes. *Mol Microbiol* 2002; **43**(6): 1565-75.
92. Dupuis ME, Villion M, Magadan AH, Moineau S. CRISPR-Cas and restriction-modification systems are compatible and increase phage resistance. *Nat Commun* 2013; **4**: 2087.
93. Makarova KS, Koonin EV. Annotation and Classification of CRISPR-Cas Systems. *Methods Mol Biol* 2015; **1311**: 47-75.
94. Xu Y, Li Z. CRISPR-Cas systems: Overview, innovations and applications in human disease research and gene therapy. *Comput Struct Biotechnol J* 2020; **18**: 2401-15.
95. Ran FA, Hsu PD, Wright J, Agarwala V, Scott DA, Zhang F. Genome engineering using the CRISPR-Cas9 system. *Nat Protoc* 2013; **8**(11): 2281-308.
96. Chen H, Choi J, Bailey S. Cut site selection by the two nuclease domains of the Cas9 RNA-guided endonuclease. *J Biol Chem* 2014; **289**(19): 13284-94.
97. Ceccaldi R, Rondinelli B, D'Andrea AD. Repair Pathway Choices and Consequences at the Double-Strand Break. *Trends Cell Biol* 2016; **26**(1): 52-64.
98. San Filippo J, Sung P, Klein H. Mechanism of eukaryotic homologous recombination. *Annu Rev Biochem* 2008; **77**: 229-57.
99. Lieber MR. The mechanism of double-strand DNA break repair by the nonhomologous DNA end-joining pathway. *Annu Rev Biochem* 2010; **79**: 181-211.
100. Cong L, Ran FA, Cox D, et al. Multiplex genome engineering using CRISPR/Cas systems. *Science* 2013; **339**(6121): 819-23.
101. Jinek M, Chylinski K, Fonfara I, Hauer M, Doudna JA, Charpentier E. A programmable dual-RNA-guided DNA endonuclease in adaptive bacterial immunity. *Science* 2012; **337**(6096): 816-21.
102. Shalem O, Sanjana NE, Hartenian E, et al. Genome-scale CRISPR-Cas9 knockout screening in human cells. *Science* 2014; **343**(6166): 84-7.
103. Bahrami E, Schmid JP, Jurinovic V, et al. Combined proteomics and CRISPR-Cas9 screens in PDX identify ADAM10 as essential for leukemia in vivo. *Mol Cancer* 2023; **22**(1): 107.
104. Becker M, Noll-Puchta H, Amend D, et al. CLUE: a bioinformatic and wet-lab pipeline for multiplexed cloning of custom sgRNA libraries. *Nucleic Acids Res* 2020; **48**(13): e78.

References

105. Galaxy C. The Galaxy platform for accessible, reproducible and collaborative biomedical analyses: 2022 update. *Nucleic Acids Res* 2022; **50**(W1): W345-W51.
106. Razeghian E, Nasution MKM, Rahman HS, et al. A deep insight into CRISPR/Cas9 application in CAR-T cell-based tumor immunotherapies. *Stem Cell Res Ther* 2021; **12**(1): 428.
107. Stadtmayer EA, Fraietta JA, Davis MM, et al. CRISPR-engineered T cells in patients with refractory cancer. *Science* 2020; **367**(6481).
108. Kuscü C, Arslan S, Singh R, Thorpe J, Adli M. Genome-wide analysis reveals characteristics of off-target sites bound by the Cas9 endonuclease. *Nat Biotechnol* 2014; **32**(7): 677-83.
109. Caplen NJ. Gene therapy progress and prospects. Downregulating gene expression: the impact of RNA interference. *Gene Ther* 2004; **11**(16): 1241-8.
110. Lee Y, Ahn C, Han J, et al. The nuclear RNase III Drosha initiates microRNA processing. *Nature* 2003; **425**(6956): 415-9.
111. Lund E, Guttinger S, Calado A, Dahlberg JE, Kutay U. Nuclear export of microRNA precursors. *Science* 2004; **303**(5654): 95-8.
112. Ketting RF, Fischer SE, Bernstein E, Sijen T, Hannon GJ, Plasterk RH. Dicer functions in RNA interference and in synthesis of small RNA involved in developmental timing in *C. elegans*. *Genes Dev* 2001; **15**(20): 2654-9.
113. Elbashir SM, Lendeckel W, Tuschl T. RNA interference is mediated by 21- and 22-nucleotide RNAs. *Genes Dev* 2001; **15**(2): 188-200.
114. Mocellin S, Provenzano M. RNA interference: learning gene knock-down from cell physiology. *J Transl Med* 2004; **2**(1): 39.
115. Fellmann C, Hoffmann T, Sridhar V, et al. An optimized microRNA backbone for effective single-copy RNAi. *Cell Rep* 2013; **5**(6): 1704-13.
116. Ventura A, Meissner A, Dillon CP, et al. Cre-lox-regulated conditional RNA interference from transgenes. *Proc Natl Acad Sci U S A* 2004; **101**(28): 10380-5.
117. Guo F, Gopaul DN, van Duyn GD. Structure of Cre recombinase complexed with DNA in a site-specific recombination synapse. *Nature* 1997; **389**(6646): 40-6.
118. Hoess RH, Abremski K. Interaction of the bacteriophage P1 recombinase Cre with the recombining site loxP. *Proc Natl Acad Sci U S A* 1984; **81**(4): 1026-9.
119. Zhang Y, Riesterer C, Ayrall AM, Sablitzky F, Littlewood TD, Reth M. Inducible site-directed recombination in mouse embryonic stem cells. *Nucleic Acids Res* 1996; **24**(4): 543-8.
120. Mattioni T, Louvion JF, Picard D. Regulation of protein activities by fusion to steroid binding domains. *Methods Cell Biol* 1994; **43 Pt A**: 335-52.
121. Feil R, Wagner J, Metzger D, Chambon P. Regulation of Cre recombinase activity by mutated estrogen receptor ligand-binding domains. *Biochem Biophys Res Commun* 1997; **237**(3): 752-7.
122. Stern P, Astrof S, Erkeland SJ, Schustak J, Sharp PA, Hynes RO. A system for Cre-regulated RNA interference in vivo. *Proc Natl Acad Sci U S A* 2008; **105**(37): 13895-900.
123. Abdolahi S, Ghazvinian Z, Muhammadnejad S, Saleh M, Asadzadeh Aghdai H, Baghaei K. Patient-derived xenograft (PDX) models, applications and challenges in cancer research. *J Transl Med* 2022; **20**(1): 206.
124. Gillet JP, Varma S, Gottesman MM. The clinical relevance of cancer cell lines. *J Natl Cancer Inst* 2013; **105**(7): 452-8.
125. Porter RJ, Murray GI, McLean MH. Current concepts in tumour-derived organoids. *Br J Cancer* 2020; **123**(8): 1209-18.
126. Kersten K, de Visser KE, van Miltenburg MH, Jonkers J. Genetically engineered mouse models in oncology research and cancer medicine. *EMBO Mol Med* 2017; **9**(2): 137-53.
127. Liu Y, Wu W, Cai C, Zhang H, Shen H, Han Y. Patient-derived xenograft models in cancer therapy: technologies and applications. *Signal Transduct Target Ther* 2023; **8**(1): 160.

References

128. Ito M, Hiramatsu H, Kobayashi K, et al. NOD/SCID/gamma(c)(null) mouse: an excellent recipient mouse model for engraftment of human cells. *Blood* 2002; **100**(9): 3175-82.
129. Heckl BC, Carlet M, Vick B, et al. Frequent and reliable engraftment of certain adult primary acute lymphoblastic leukemias in mice. *Leuk Lymphoma* 2019; **60**(3): 848-51.
130. Senft D, Jeremias I. A rare subgroup of leukemia stem cells harbors relapse-inducing potential in acute lymphoblastic leukemia. *Exp Hematol* 2019; **69**: 1-10.
131. Castro Alves C, Terziyska N, Grunert M, et al. Leukemia-initiating cells of patient-derived acute lymphoblastic leukemia xenografts are sensitive toward TRAIL. *Blood* 2012; **119**(18): 4224-7.
132. Ebinger S, Zeller C, Carlet M, et al. Plasticity in growth behavior of patients' acute myeloid leukemia stem cells growing in mice. *Haematologica* 2020; **105**(12): 2855-60.
133. Liu WH, Mrozek-Gorska P, Wirth AK, et al. Inducible transgene expression in PDX models in vivo identifies KLF4 as a therapeutic target for B-ALL. *Biomark Res* 2020; **8**: 46.
134. Carlet M, Vorse K, Vergalli J, et al. In vivo inducible reverse genetics in patients' tumors to identify individual therapeutic targets. *Nat Commun* 2021; **12**(1): 5655.
135. Carlet M, Schmelz K, Vergalli J, et al. X-linked inhibitor of apoptosis protein represents a promising therapeutic target for relapsed/refractory ALL. *EMBO Mol Med* 2023; **15**(1): e14557.
136. Wirth AK, Wange L, Vosberg S, et al. In vivo PDX CRISPR/Cas9 screens reveal mutual therapeutic targets to overcome heterogeneous acquired chemo-resistance. *Leukemia* 2022; **36**(12): 2863-74.
137. Zeller C, Richter D, Jurinovic V, et al. Adverse stem cell clones within a single patient's tumor predict clinical outcome in AML patients. *J Hematol Oncol* 2022; **15**(1): 25.
138. Klco JM, Spencer DH, Miller CA, et al. Functional heterogeneity of genetically defined subclones in acute myeloid leukemia. *Cancer Cell* 2014; **25**(3): 379-92.
139. Terziyska N, Castro Alves C, Groiss V, et al. In vivo imaging enables high resolution preclinical trials on patients' leukemia cells growing in mice. *PLoS One* 2012; **7**(12): e52798.
140. Vick B, Rothenberg M, Sandhofer N, et al. An advanced preclinical mouse model for acute myeloid leukemia using patients' cells of various genetic subgroups and in vivo bioluminescence imaging. *PLoS One* 2015; **10**(3): e0120925.
141. Jancik S, Drabek J, Radzioch D, Hajduch M. Clinical relevance of KRAS in human cancers. *J Biomed Biotechnol* 2010; **2010**: 150960.
142. McBride OW, Swan DC, Tronick SR, et al. Regional chromosomal localization of N-ras, K-ras-1, K-ras-2 and myb oncogenes in human cells. *Nucleic Acids Res* 1983; **11**(23): 8221-36.
143. Pantsar T. The current understanding of KRAS protein structure and dynamics. *Comput Struct Biotechnol J* 2020; **18**: 189-98.
144. Lavoie H, Therrien M. Regulation of RAF protein kinases in ERK signalling. *Nat Rev Mol Cell Biol* 2015; **16**(5): 281-98.
145. Barbacid M. ras genes. *Annu Rev Biochem* 1987; **56**: 779-827.
146. Giri B, Sethi V, Dudeja V, Banerjee S, Livingstone A, Saluja A. Genetics of pancreatic cyst-cancer progression: standing on the shoulders of giants. *Curr Opin Gastroenterol* 2017; **33**(5): 404-10.
147. Dinu D, Dobre M, Panaitescu E, et al. Prognostic significance of KRAS gene mutations in colorectal cancer--preliminary study. *J Med Life* 2014; **7**(4): 581-7.
148. Liang DC, Shih LY, Fu JF, et al. K-Ras mutations and N-Ras mutations in childhood acute leukemias with or without mixed-lineage leukemia gene rearrangements. *Cancer* 2006; **106**(4): 950-6.
149. Zhu C, Guan X, Zhang X, et al. Targeting KRAS mutant cancers: from druggable therapy to drug resistance. *Mol Cancer* 2022; **21**(1): 159.
150. Kim D, Xue JY, Lito P. Targeting KRAS(G12C): From Inhibitory Mechanism to Modulation of Antitumor Effects in Patients. *Cell* 2020; **183**(4): 850-9.
151. Severi C, Van Cutsem E. KRAS G12C inhibition with sotorasib in metastatic colorectal cancer. *Ann Palliat Med* 2022; **11**(8): 2792-5.

References

152. Matsuo H, Yoshida K, Nakatani K, et al. Fusion partner-specific mutation profiles and KRAS mutations as adverse prognostic factors in MLL-rearranged AML. *Blood Adv* 2020; **4**(19): 4623-31.
153. Chang JH, Olson MO. Structure of the gene for rat nucleolar protein B23. *J Biol Chem* 1990; **265**(30): 18227-33.
154. Borer RA, Lehner CF, Eppenberger HM, Nigg EA. Major nucleolar proteins shuttle between nucleus and cytoplasm. *Cell* 1989; **56**(3): 379-90.
155. Negi SS, Olson MO. Effects of interphase and mitotic phosphorylation on the mobility and location of nucleolar protein B23. *J Cell Sci* 2006; **119**(Pt 17): 3676-85.
156. Maggi LB, Jr., Kuchenruether M, Dadey DY, et al. Nucleophosmin serves as a rate-limiting nuclear export chaperone for the Mammalian ribosome. *Mol Cell Biol* 2008; **28**(23): 7050-65.
157. Brunetti L, Gundry MC, Sorcini D, et al. Mutant NPM1 Maintains the Leukemic State through HOX Expression. *Cancer Cell* 2018; **34**(3): 499-512 e9.
158. Mahipal A, Malafa M. Importins and exportins as therapeutic targets in cancer. *Pharmacol Ther* 2016; **164**: 135-43.
159. Federici L, Falini B. Nucleophosmin mutations in acute myeloid leukemia: a tale of protein unfolding and mislocalization. *Protein Sci* 2013; **22**(5): 545-56.
160. Ranieri R, Pianigiani G, Sciabolacci S, et al. Current status and future perspectives in targeted therapy of NPM1-mutated AML. *Leukemia* 2022; **36**(10): 2351-67.
161. Hindley A, Catherwood MA, McMullin MF, Mills KI. Significance of NPM1 Gene Mutations in AML. *Int J Mol Sci* 2021; **22**(18).
162. Patel SS, Kluk MJ, Weinberg OK. NPM1 Biology in Myeloid Neoplasia. *Curr Hematol Malig Rep* 2020; **15**(4): 350-9.
163. Garzon R, Savona M, Baz R, et al. A phase 1 clinical trial of single-agent selinexor in acute myeloid leukemia. *Blood* 2017; **129**(24): 3165-74.
164. Falini B, Brunetti L, Martelli MP. How I diagnose and treat NPM1-mutated AML. *Blood* 2021; **137**(5): 589-99.
165. Mason EF, Hasserjian RP, Aggarwal N, Seegmiller AC, Pozdnyakova O. Blast phenotype and comutations in acute myeloid leukemia with mutated NPM1 influence disease biology and outcome. *Blood Adv* 2019; **3**(21): 3322-32.
166. Issa GC, Bidikian A, Venugopal S, et al. Clinical outcomes associated with NPM1 mutations in patients with relapsed or refractory AML. *Blood Adv* 2023; **7**(6): 933-42.
167. Chen BF, Chan WY. The de novo DNA methyltransferase DNMT3A in development and cancer. *Epigenetics* 2014; **9**(5): 669-77.
168. Brunetti L, Gundry MC, Goodell MA. DNMT3A in Leukemia. *Cold Spring Harb Perspect Med* 2017; **7**(2).
169. Gaidzik VI, Schlenk RF, Paschka P, et al. Clinical impact of DNMT3A mutations in younger adult patients with acute myeloid leukemia: results of the AML Study Group (AMLSG). *Blood* 2013; **121**(23): 4769-77.
170. Celik H, Kramer A, Challen GA. DNA methylation in normal and malignant hematopoiesis. *Int J Hematol* 2016; **103**(6): 617-26.
171. Nguyen TV, Yao S, Wang Y, et al. The R882H DNMT3A hot spot mutation stabilizes the formation of large DNMT3A oligomers with low DNA methyltransferase activity. *J Biol Chem* 2019; **294**(45): 16966-77.
172. Challen GA, Sun D, Jeong M, et al. Dnmt3a is essential for hematopoietic stem cell differentiation. *Nat Genet* 2011; **44**(1): 23-31.
173. Ahn JS, Kim HJ, Kim YK, et al. DNMT3A R882 Mutation with FLT3-ITD Positivity Is an Extremely Poor Prognostic Factor in Patients with Normal-Karyotype Acute Myeloid Leukemia after Allogeneic Hematopoietic Cell Transplantation. *Biol Blood Marrow Transplant* 2016; **22**(1): 61-70.

References

174. Dunlap JB, Leonard J, Rosenberg M, et al. The combination of NPM1, DNMT3A, and IDH1/2 mutations leads to inferior overall survival in AML. *Am J Hematol* 2019; **94**(8): 913-20.
175. Kantarjian H. Acute myeloid leukemia--major progress over four decades and glimpses into the future. *Am J Hematol* 2016; **91**(1): 131-45.
176. Kadia TM, Cortes J, Ravandi F, et al. Cladribine and low-dose cytarabine alternating with decitabine as front-line therapy for elderly patients with acute myeloid leukaemia: a phase 2 single-arm trial. *Lancet Haematol* 2018; **5**(9): e411-e21.
177. Venugopal K, Feng Y, Shabashvili D, Guryanova OA. Alterations to DNMT3A in Hematologic Malignancies. *Cancer Res* 2021; **81**(2): 254-63.
178. Hastie ND. Wilms' tumour 1 (WT1) in development, homeostasis and disease. *Development* 2017; **144**(16): 2862-72.
179. Dallosso AR, Hancock AL, Brown KW, Williams AC, Jackson S, Malik K. Genomic imprinting at the WT1 gene involves a novel coding transcript (AWT1) that shows deregulation in Wilms' tumours. *Hum Mol Genet* 2004; **13**(4): 405-15.
180. Ullmark T, Montano G, Gullberg U. DNA and RNA binding by the Wilms' tumour gene 1 (WT1) protein +KTS and -KTS isoforms-From initial observations to recent global genomic analyses. *Eur J Haematol* 2018; **100**(3): 229-40.
181. Bor YC, Swartz J, Morrison A, Rekosh D, Ladomery M, Hammarskjold ML. The Wilms' tumor 1 (WT1) gene (+KTS isoform) functions with a CTE to enhance translation from an unspliced RNA with a retained intron. *Genes Dev* 2006; **20**(12): 1597-608.
182. Luna I, Such E, Cervera J, et al. WT1 isoform expression pattern in acute myeloid leukemia. *Leuk Res* 2013; **37**(12): 1744-9.
183. Li H, Oka Y, Tsuboi A, et al. The lck promoter-driven expression of the Wilms tumor gene WT1 blocks intrathymic differentiation of T-lineage cells. *Int J Hematol* 2003; **77**(5): 463-70.
184. Loeb DM, Evron E, Patel CB, et al. Wilms' tumor suppressor gene (WT1) is expressed in primary breast tumors despite tumor-specific promoter methylation. *Cancer Res* 2001; **61**(3): 921-5.
185. Shandilya J, Roberts SG. A role of WT1 in cell division and genomic stability. *Cell Cycle* 2015; **14**(9): 1358-64.
186. Baird PN, Simmons PJ. Expression of the Wilms' tumor gene (WT1) in normal hemopoiesis. *Exp Hematol* 1997; **25**(4): 312-20.
187. Rampal R, Figueroa ME. Wilms tumor 1 mutations in the pathogenesis of acute myeloid leukemia. *Haematologica* 2016; **101**(6): 672-9.
188. Niktoreh N, Walter C, Zimmermann M, et al. Mutated WT1, FLT3-ITD, and NUP98-NSD1 Fusion in Various Combinations Define a Poor Prognostic Group in Pediatric Acute Myeloid Leukemia. *J Oncol* 2019; **2019**: 1609128.
189. King-Underwood L, Renshaw J, Pritchard-Jones K. Mutations in the Wilms' tumor gene WT1 in leukemias. *Blood* 1996; **87**(6): 2171-9.
190. Hou HA, Huang TC, Lin LI, et al. WT1 mutation in 470 adult patients with acute myeloid leukemia: stability during disease evolution and implication of its incorporation into a survival scoring system. *Blood* 2010; **115**(25): 5222-31.
191. Gaidzik VI, Schlenk RF, Moschny S, et al. Prognostic impact of WT1 mutations in cytogenetically normal acute myeloid leukemia: a study of the German-Austrian AML Study Group. *Blood* 2009; **113**(19): 4505-11.
192. Schmied S, Gostick E, Price DA, Abken H, Assenmacher M, Richter A. Analysis of the functional WT1-specific T-cell repertoire in healthy donors reveals a discrepancy between CD4(+) and CD8(+) memory formation. *Immunology* 2015; **145**(4): 558-69.
193. Augsberger C, Hanel G, Xu W, et al. Targeting intracellular WT1 in AML with a novel RMF-peptide-MHC-specific T-cell bispecific antibody. *Blood* 2021; **138**(25): 2655-69.

References

- 194.Jagannathan S. The evolution of DUX4 gene regulation and its implication for facioscapulohumeral muscular dystrophy. *Biochim Biophys Acta Mol Basis Dis* 2022; **1868**(5): 166367.
- 195.Dumbovic G, Forcales SV, Perucho M. Emerging roles of macrosatellite repeats in genome organization and disease development. *Epigenetics* 2017; **12**(7): 515-26.
- 196.Hamm DC, Paatela EM, Bennett SR, et al. The transcription factor DUX4 orchestrates translational reprogramming by broadly suppressing translation efficiency and promoting expression of DUX4-induced mRNAs. *PLoS Biol* 2023; **21**(9): e3002317.
- 197.Dong X, Zhang W, Wu H, et al. Structural basis of DUX4/IGH-driven transactivation. *Leukemia* 2018; **32**(6): 1466-76.
- 198.Jones TI, Chen JC, Rahimov F, et al. Facioscapulohumeral muscular dystrophy family studies of DUX4 expression: evidence for disease modifiers and a quantitative model of pathogenesis. *Hum Mol Genet* 2012; **21**(20): 4419-30.
- 199.Rehn JA, O'Connor MJ, White DL, Yeung DT. DUX Hunting-Clinical Features and Diagnostic Challenges Associated with DUX4-Rearranged Leukaemia. *Cancers (Basel)* 2020; **12**(10).
- 200.Zhang J, McCastlain K, Yoshihara H, et al. Deregulation of DUX4 and ERG in acute lymphoblastic leukemia. *Nat Genet* 2016; **48**(12): 1481-9.
- 201.Tian L, Shao Y, Nance S, et al. Long-read sequencing unveils IGH-DUX4 translocation into the silenced IGH allele in B-cell acute lymphoblastic leukemia. *Nat Commun* 2019; **10**(1): 2789.
- 202.Zaliova M, Stuchly J, Winkowska L, et al. Genomic landscape of pediatric B-other acute lymphoblastic leukemia in a consecutive European cohort. *Haematologica* 2019; **104**(7): 1396-406.
- 203.Schwab C, Cranston RE, Ryan SL, et al. Integrative genomic analysis of childhood acute lymphoblastic leukaemia lacking a genetic biomarker in the UKALL2003 clinical trial. *Leukemia* 2023; **37**(3): 529-38.
- 204.Migita NA, Jotta PY, Nascimento NPD, et al. Classification and genetics of pediatric B-other acute lymphoblastic leukemia by targeted RNA sequencing. *Blood Adv* 2023; **7**(13): 2957-71.
- 205.Simonson B, Subramanya V, Chan MC, et al. DDIT4L promotes autophagy and inhibits pathological cardiac hypertrophy in response to stress. *Sci Signal* 2017; **10**(468).
- 206.Gupta M, Rath PC. Interferon regulatory factor-1 (IRF-1) interacts with regulated in development and DNA damage response 2 (REDD2) in the cytoplasm of mouse bone marrow cells. *Int J Biol Macromol* 2014; **65**: 41-50.
- 207.Garcia J, Schneider MF. Calcium transients and calcium release in rat fast-twitch skeletal muscle fibres. *J Physiol* 1993; **463**: 709-28.
- 208.Koga Y, Pelizzola M, Cheng E, et al. Genome-wide screen of promoter methylation identifies novel markers in melanoma. *Genome Res* 2009; **19**(8): 1462-70

Acknowledgements

First, I would like to express my sincere thanks to my supervisor, Prof. Dr. Irmela Jeremias, for her great support of my doctoral study. In the past three years, I have been impressed by her personality, way of thinking, and attitude to scientific research. I appreciate all our deep conversations. To make a long story short, I will follow her path and try my best to be a charming and excellent female scientist like her.

Second, I would like to thank the other two professors in my Thesis Advisory Committee, Priv. Doz. Dr. Ursula Zimmer-Strobl and Prof. Dr. Oliver Gires. Both are so kind and warm in supporting all my requests. I will always remember that Prof. Dr. Oliver Gires always came to me to sign all the documents, even though he was busy working in the clinic. I shed tears of gratitude when Priv. Doz. Dr. Ursula Zimmer-Strobl came and found our lab just to sign an urgent document because I lost contact with her at that time. I really appreciate all their efforts and suggestions during my study.

Moreover, I would like to thank Kerstin Völse and Maryam Ghalandary. I am grateful that I gained all the scientific skills in our lab under both of their patient guidance and became an independent doctoral student within one year. Furthermore, I would like to thank all our group members, including Ehsan Bahrami, Jan Philipp Schmid, Katharina Hunt, Romina Ludwig, and Diana Amend, but not limited to those. I appreciate that we could openly have a lively scientific discussion at any time needed, support each other's experiments with double, and share ideas about various topics. I enjoy the time with all of you and will keep these precious memories in mind.

Additionally, I would like to thank my beloved family and my friends. Thanks to my parents for unconditional respect and support in all my decisions, and thanks to all my friends for sharing the joys of life.

To this end, I wish all of you who have ever appeared in my life a wonderful and fruitful future!